On the Interplay of Superconductivity and Magnetism

Benjamin James Powell

A thesis submitted to the University of Bristol in accordance with the requirements of the degree of Doctor of Philosophy in the Faculty of Science.

September 2002

Abstract

We explore the exchange field dependence of the Hubbard model with a attractive, effective, pairwise, nearest neighbour interaction via the Hartree–Fock–Gorkov approximation. We derive a Ginzburg–Landau theory of spin triplet superconductivity in an exchange field. For microscopic parameters which lead to ABM phase superconductivity in zero field, the Ginzburg–Landau theory allows both an axial (A, A_1 or A_2) solution with the vector order parameter, $\mathbf{d}(\mathbf{k})$, perpendicular to the field, $\mathbf{H}$, and an A phase solution with $\mathbf{d}(\mathbf{k})$ parallel to $\mathbf{H}$.

We study the spin-generalised Bogoliubov–de Gennes (BdG) equations for this model with parameters suitable for strontium ruthenate (Sr_2RuO_4). The A_2 phase is found to be stable in a magnetic field. However, in the real material, spin-orbit coupling could pin the order parameter to the crystallographic c-axis which would favour the A phase for fields parallel to the c-axis. We show that the low temperature thermodynamic behaviour in a magnetic field could experimentally differentiate between these two possible behaviours. Further we show that this pinning could cause a Freedericksz (Frederiks) transition in bulk Sr_2RuO_4. (Freedericksz transitions have only previously been seen in confined geometries.)

We calculate the superconducting critical temperature, T_C, of $ZrZn_2$ in the presence of non-magnetic impurity scattering from the Abrikosov–Gorkov formula. Residual resistivity experiments indicate that the transition temperature in the absence of impurity scattering, $T_{C0} = 1.15 \pm 0.15$ K, while de Haas–van Alphen experiments give $T_{C0} \sim 3$ K. We discuss this disagreement and conclude that the former estimate is the more reliable.

We derive the equal spin pairing (ESP) gap equations for a ferromagnetic superconductor, which we solve for parameters chosen for $ZrZn_2$. We show that for ESP states in a ferromagnetic superconductor, in the absence of spin flip processes, the two spin states are separate subsystems due to exchange splitting. This unique property of a ferromagnetic superconductor allows us to calculate not only T_C, but also the temperature of the transition from the A_1 phase to the A_2 phase from the linearised gap equations. We account for scattering from non-magnetic impurities. Our results show that the observed pressure dependence of T_C in $ZrZn_2$ is consistent with ESP superconductivity mediated by a pressure independent potential in the presence of impurity scattering.

For my family.

Acknowledgements

I would like to begin by thanking my wonderful family, especially my parents, my brother Luke and my sister Susanna. Without their love and support, throughout my life, and particularly in the last three years, none of this would have been possible.

Of course most of the credit for this work must go to my two supervisors Balasz Györffy and James Annett. I know that I have tried their patience to the limit at times. It is no wonder that the task of supervising me has taken both of them! I thank them both for their patience and insight. Giles Santi has also been a great help to me. None of the work on $ZrZn_2$ would have been possible without his collaboration and his door has always been open. I am also indebted to Steve Yates for the many hours we have spent discussing this bizarre ferromagnetic superconductor and for the his willingness to discuss his work with me. I would also like to thank the other members of the theory group for creating such an inquisitive and interesting environment in which to work and study.

I have benefited greatly from using the computational facilities of the of the the Laboratory for Advanced Computation in the Mathematical Sciences (LACMS). In particular Jason Hogan–O'Neill has been a great help to me.

It is a great pleasure to thank all of the other students in my year: Dan Collins. And the other students and postdocs in the theory group Roland, Mariusz, Jason, Murtaz, Jorge, Markus, Sam, Hussain, Joe, Mark, Rostam, Denzil, Andy, Danny and Jamie who have made the last three years so enjoyable, for so many interesting discussions (about almost anything, but often physics) and who have also encouraged, consoled and cajoled me.

I would also like thank the members of the Low Temperature Group, Tony Carrington, Stephen Hayden, Nigel Hussey, Phil Meeson and Mike Springford who have all taken an interest in my work and made insightful comments about it. I would also like to thank the students and postdocs of that group for Friday lunchtimes at Micawbers in particular Fran, for always being so interested in everything and Steve (again), Alex, Matt, Jon, Anthony and Pierre for their friendship and explaining a little of experimental physics to me.

How could I forget those who've put up with me at home for the last three years? I'd like to acknowledge Mat - he exists, and thank(?) Dan for providing that joke (one of his better - unfortunately) as well as Steve (yes, again), Wig and Tim.

Finally, I am extremely grateful to Balasz, James, Danny and Steve (I know, I know, this is getting silly) who have proofread sections of this thesis.

Author's declaration

I declare that the work in this thesis was carried out in accordance with the regulations of the University of Bristol. No part of this work has been submitted previously for a degree at this or any other university either in the United Kingdom or overseas. The research reported herein is the result of my own investigation except where special reference is made to the work of others. All research was carried out under the guidance of Prof. B.L. Györffy and James F. Annett, at the University of Bristol between October 1999 and September 2002.

B.J. Powell

October 29, 2002

If we knew what we were doing it wouldn't be research.

A. Stein and J. Mitton [199]

Contents

List of Figures

List of Tables

Chapter 1

Introduction

Superconductivity and magnetism are often thought of as antagonistic phenomena. If one places a superconductor in a large enough magnetic field then it will stop superconducting. (The strength of magnetic field required to completely eradicate superconductivity is known as the (upper) critical field.) If one places a superconductor above a magnet that produces a field smaller than the critical field then the superconductor will levitate above the magnet (see figure 1.1). In fact this effect is so strong that it has even been used to levitate a Sumo wrestler (see figure 1.2). The superconductor levitates because it will not allow the magnetic field to penetrate into its interior, a phenomena known as the Meissner effect, so to avoid the field it must move away from the magnet.

This traditional view of antagonism between superconductivity and magnetism has come under threat recently. First superconductors with enormous upper critical fields were discovered. These include the so called heavy fermion compounds UPt_3 [185] and UNi_2Al_3 [101], the

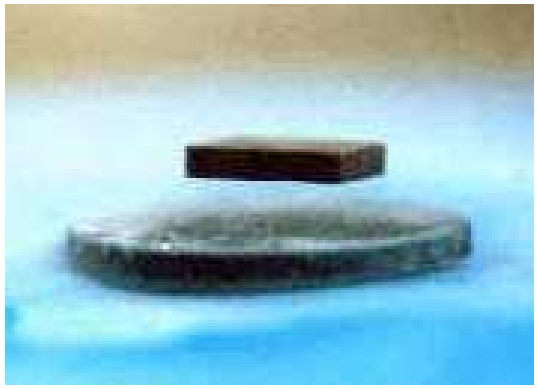

Figure 1.1: A magnet levitating over a superconductor from reference [173].

Figure 1.2: A sumo wrestler stood on a piece of magnetic material levitated over a superconductor, taken from the Asian Technology Information Program (ATIP) website [20].

Bechgaard salts ($(TMTSF)_2X$ where X = PF_6 [49, 121], ClO_4 [122]) and Sr_2RuO_4 (strontium ruthenate or 'struthenate' to its friends) [137]. We study the latter in chapter 5 of this thesis. But recently three even more remarkable materials have been discovered which are (ferro)magnetic and superconducting at the same time. Even more surprisingly it appears that the *same* electrons are responsible for both the superconductivity and the ferromagnetism. These materials are UGe_2 [98], URhGe [15] and $ZrZn_2$ [166] the last of which we will study in chapter 6 of this thesis.

1.1 A brief history of superconductivity

The beginning of the twentieth century saw a revolution in theoretical physics. The new physics, and in particular quantum mechanics, met with success after success, it explained the ultraviolet catastrophe, the photoelectric effect, the Compton effect, the structure of the atom (and hence physical chemistry) and even made the prediction of antimatter. 'This advance on all fronts was stopped by the two phenomena of superfluidity of helium and superconductivity of metals which stood like cites under siege resisting qualitative explanation.'[1]

The phenomena of superconductivity was discovered in 1911 by Kammerlingh Onnes who observed an enormous drop in the d.c. resistance of mercury at 4.2 K. It soon emerged that the resistance of a superconductor (as this new state of matter was named) does not merely become much smaller, it actually vanishes. Superfluidity is just as strange as superconductivity, the viscosity of helium completely disappears at 2.17 K. The superfluid exhibits remarkable effects like the ability to flow through tiny holes and the so called fountain effect where superfluid helium will actually climb out of a beaker!

One important result from elementary quantum mechanics is the particles have an intrinsic angular momentum which is known as the spin of a particle. (Although this intrinsic angular momentum is not related to the particles rotating on their axes as even point particles have this spin.) In units of $\hbar$ (Planks constant divided by 2π, the fundamental unit of quantum mechanics) this spin must either be an integer (0,1,2,...) or half-integer ($\frac{1}{2}$, $\frac{3}{2}$, $\frac{5}{2}$,...). The distinction between particles with integer spin and those with half-integer spin is extremely important in the quantum world (although this distinction is lost as the energy of the particles is increased and we return to the classical world). Particles with integer spin obey Bose–Einstein statistics and are known as Bosons. While particles with a half-integer spin obey Fermi–Dirac statistics and are called

[1] This quotation is taken from Richard Feynman [73] writing in the conference proceedings of the 1958 Kammerlingh Onnes conference.

Fermions. This distinction is far from academic: Fermions obey the Pauli exclusion principle (only one Fermion is allowed in each state) while Bosons do not (many Bosons are allowed in any given state).

Examples of Bosons are the quantised particles of light (photons) and sound (phonons) (both of these particles have spin 1). Examples of Fermions are electrons, protons and neutrons (all three of these particles have spin $\frac{1}{2}$). However, composite particles are also separated into Bosons and Fermions. For example helium, the second lightest element has two isotopes ^{3}He and ^{4}He. ^{3}He is made up of seven Fermions (2 protons, 1 neutron and 2 electrons) and so has total spin $\frac{7}{2}$, thus ^{3}He is a Fermion. On the other hand ^{4}He is made up of eight Fermions (2 protons, 2 neutrons and 2 electrons) and has total spin 4, therefore ^{4}He is a Boson. This leads to very different behaviours in the two isotopes at low temperatures. This is an excellent example of how materials physics gives us a window on the quantum world, the wide range of materials in nature providing a seemingly infinite variety of quantum behaviours.

The last paragraph begs the question "why at low temperatures?" In fact, this question could be asked of this entire thesis. Temperature is a measure of the average kinetic energy of a system of a large number of particles. Therefore, high temperatures mean that quantum mechanical effects are lost and we return to our usual, classical world. But at low temperatures quantum mechanical behaviour returns, thus if we want to study many body quantum mechanics we must look to low temperatures. To quote Feynman [73] again 'low temperatures exhibit the strange quantum mechanical effects because of the very small number of states excited. So that low temperature physics will continue to be a technique for exhibiting the interesting consequences of quantum mechanics on large scale systems.'

At high temperatures (like room temperature) thermal energy means that Bosons choose their state more or less at random. Albert Einstein showed [61] that as Bosons do not obey the Pauli exclusion principle a system of Bosons cooled towards absolute zero will all congregate in the lowest energy state. This process is known as Bose-Einstein condensation.

Superfluidity of helium is closely related to Bose–Einstein condensation. Although interactions play a very important role in the superfluidity of helium where as the theory of Bose–Einstein condensation is based on non interacting particles, this leads to some important effects. This idea was lent further support by the fact that superfluidity was observed in ^{4}He and not ^{3}He. (Superfluidity in ^{3}He was eventually discovered in the 1970s and finds its explanation in the BCS theory.)

The first real progress in understanding superconductivity came when Ogg [161] suggested

that there may be a link between superconductivity and Bose–Einstein condensation. This would require that the electrons formed pairs, which could be shown to explain the Meissner effect (as Schafroth [188, 189] had already shown that a charged superfluid would display the Meissner effect), but pairs of electrons appeared impossible because of the repulsion of electrons due to the Coulomb force. Eventually a phenomenological theory was proposed by Ginzburg and Landau [79] working in the U.S.S.R. but, at the height of the cold war, western scientists remained unaware of this development. This ignorance only serves to heighten achievements of Bardeen, Cooper and Schrieffer (BCS) who constructed a microscopic theory which explained the phenomena of superconductivity and superfluidity in ^{3}He. As well as explaining many experimental facts BCS theory can also be used to derive the Ginzburg–Landau theory.

1.1.1 BCS theory

The road to a full microscopic theory of superconductivity began when Leon Cooper considered the problem (now known as the Cooper problem) of two electrons (or more strictly two of the quasiparticles in Landaus theory from Fermi liquids) interacting above a filled Fermi sea. He showed that, in the presence of an arbitrarily weak attractive interaction between the two quasiparticles, the quasiparticles form a bound state [52] known as a Cooper pair.

This bound state is reminiscent of the suggestion that superconductivity is related to Bose–Einstein condensation. Indeed BCS [25] were able to derive a mean-field theory of the full many body state (as opposed to the effectively two body Cooper problem). In this theory every electron is effectively paired with every other electron rather than one specific electron, so in this sense the idea of a Cooper pair is somewhat misleading as it can lead to thoughts of diatomic (or perhaps 'dielectronic') molecules, which are not the case. Further, the coherence length (the effective radius of a Cooper pair in BCS theory) is very large, which explains how the Coulomb force is overcome. However, the integer spin of the paired electronic states is enough to allow them to form a condensate, which is not entirely dissimilar to a Bose–Einstein condensate.

BCS theory contains an effective potential, so the question remained of what provided the attractive potential to cause the formation of Cooper pairs or, put another way, what is the pairing mechanism? Frölich [74] had already shown that phonons could lead to a weak attraction between electrons, and indeed in BCS theory the attractive potential is cut off at the Debye frequency which is clearly an implication that phonons are involved. Eliashberg was able to derive a full treatment of the pairing interaction [62, 63] and show that phonons do indeed provide the glue which binds a Cooper pair together (at least in a conventional superconductor).

It was found that as the strength of the coupling interaction in Eliashberg theory tends to zero BCS theory is recovered. BCS theory is therefore often referred to as the weak coupling limit.

In the original version of BCS theory there is no angular momentum between the quasiparticles, further Cooper pairs are spin 0 objects. However, it was found that in ^{3}He the Cooper pairs have an orbital angular momentum and spin 1. Spin 0 objects have only one projection ($S_z = 0$), spin 1 objects have three projections ($S_z = -1, 0$ or 1). Superconductivity with spin 0 Cooper pairs is therefore called singlet superconductivity and superconductivity with spin 1 Cooper pairs is called triplet superconductivity.

As we will see throughout this thesis much attention has been focused on non-phononic pairing mechanisms which can give various forms of unconventional pairing. The best understood example of non-phononic pairing is ^{3}He which we will explore in chapter 3. However there has also been much attention focused on spin fluctuation pairing mechanisms particularly in Sr_2RuO_4 and $ZrZn_2$.

In this thesis however we will not focus mechanism of superconductivity. Instead we employ an effective interaction and a generalised form of BCS theory to study some of the fascinating phenomenology found in triplet superconductors. We focus in particular on the strange effects of magnetic fields and ferromagnetism on triplet superconductivity.

1.2 A brief outline of this thesis

Before we can study the complex phenomena observed in Sr_2RuO_4 in an external magnetic field and $ZrZn_2$ because of its own (internal) magnetic field, we must understand a great deal of previous work. To this end we review some of the basics of many-body theory in chapter 2. In particular we introduce the basic notions of the many body problem, the tight binding model, second quantisation and Green's functions.

We introduce the phenomena of superconductivity in general and triplet superconductivity in particular by discussing superfluid ^{3}He in chapter 3. We begin by introducing the Ginzburg–Landau and BCS theories for conventional superconductors. We then compare and contrast the nature of singlet and triplet states in both two body and many body quantum mechanics. We then generalise BCS to finite angular momentum states and either spin singlet or spin triplet pairing. We are now in a position to discuss superfluidity in ^{3}He. This discussion includes theoretical (Ginzburg–Landau) and experimental descriptions of the triplet phases observed in superfluid ^{3}He (especially those observed in a magnetic field). We also discuss

phases which have been found (theoretically) to be stable in other regions of phase space.

Chapter 4 sees the introduction of the Hubbard model, which we explore by considering the phenomena of ferromagnetism. We then use an extended Hubbard model to derive a BCS like theory which is valid for either singlet or triplet superconductivity in the presence of a magnetic field. We explore the analytic properties of both the singlet and triplet solutions, in addition we study the singlet solution numerically. Some unexpected consequences are found highlights include a p-wave state with a Clogston–Chandrasekhar limit and the discovery that some triplet and all singlet states are unaffected by the application of a spin-only magnetic field at zero temperature.

In chapter 5 we study the triplet solutions of our model in two dimensions: these results are applied to strontium ruthenate. Our study begins with a review of other work of Sr_2RuO_4, we then derive a Ginzburg–Landau theory from our microscopic Hamiltonian. The results of our Ginzburg–Landau theory are compared with numerical solutions of the microscopic Hamiltonian in the (mean field) Hartree–Fock–Gorkov approximation. We find two solutions with very different thermodynamic properties. We speculate that the higher energy solution may be observed in Sr_2RuO_4 when an external magnetic field is aligned with the c-axis and that this may lead to a Freedericksz transition in Sr_2RuO_4.

In chapter 6 we study our model in three dimensions, applying our results to $ZrZn_2$. We begin by studying the work of others on this system. We then calculate the critical temperature of $ZrZn_2$ on the basis of residual resistivity and de Haas–van Alphen experiments. We derive the equal spin pairing gap equations for a ferromagnetic superconductor. These show that, for equal spin pairing states in the absence of spin flip processes, the two spin states are separate subsystems in a ferromagnetic superconductor due to exchange splitting. This allows the calculation of the critical temperature for each spin state from a linearised gap equation. The higher of these transition temperatures is the global T_C, while, remarkably, the linearised equation giving the lower transition temperature remains valid and predicts the temperature of a transition from one superconducting phase to another. We then introduce a new model for superconductivity in $ZrZn_2$ in which the attractive, effective pairing interaction is independent of pressure. We show that this leads to a theory in qualitative agreement with current experimental results and make potentially falsifiable predictions from our model.

We draw our conclusions from this work in chapter 7 and then suggest some directions for further work.

Chapter 2

Some mathematical and physical preliminaries

In this chapter we introduce a number of concepts which are required to understand the following chapters. This chapter can either be read as a coherent whole, or 'dipped' into as is desired. To facilitate this, as far as is possible, each section is self-contained. Of course, all of the topics have been covered in far more detail elsewhere. References to some of the many excellent textbooks on the subjects covered here are therefore given.

We begin this chapter by describing the nature of the many body problem. To study this we introduce the tight binding model. As an example a tight binding fit for Sr_2RuO_4 is presented in section 2.2.1. This fit is used as the basis for calculations which are presented in chapter 5. We examine the second quantisation technique and derive the tight binding Hamiltonian from a second quantisation Hamiltonian to demonstrate the power of the method. We then, briefly, discuss the use of Green's functions in many body physics.

2.1 The many body problem

The time independent Schrödinger equation (TISE) for a single particle is

$$\hat{\mathcal{H}}\psi(\mathbf{r}) = E\psi(\mathbf{r}). \tag{2.1.1}$$

The Hamiltonian, $\hat{\mathcal{H}}$, is

$$\hat{\mathcal{H}} = \hat{\mathcal{T}} + \hat{\mathcal{V}} \tag{2.1.2}$$

where, the kinetic energy term is

$$\hat{\mathcal{T}} = -\frac{\hbar^2}{2m}\nabla^2 \tag{2.1.3}$$

and an external potential depends only on the position of the particle:

$$\hat{\mathcal{V}} = V(\mathbf{r}). \tag{2.1.4}$$

For more than one particle the TISE is

$$\hat{\mathcal{H}}\Psi(\mathbf{r}_1\sigma_1, \mathbf{r}_2\sigma_2, ..., \mathbf{r}_n\sigma_n, ...) = E\Psi(\mathbf{r}_1\sigma_1, \mathbf{r}_2\sigma_2, ..., \mathbf{r}_n\sigma_2, ...). \tag{2.1.5}$$

$\Psi(\mathbf{r}_1\sigma_1, \mathbf{r}_2\sigma_2, ..., \mathbf{r}_n\sigma_n, ...)$ is the many body wave-function. The Hamiltonian is still of the form detailed in equation 2.1.1, but now the kinetic energy term is

$$\hat{\mathcal{T}} = -\frac{\hbar^2}{2m}\left(\nabla_1^2 + \nabla_2^2 + ... + \nabla_n^2 + ...\right), \tag{2.1.6}$$

and the potential energy term is a function of all of the particle coordinates

$$\hat{\mathcal{V}} = V(\mathbf{r}_1, \mathbf{r}_2, ..., \mathbf{r}_n, ...) \tag{2.1.7}$$

and in general includes interactions between the particles as well as the effect of an external potential.

The problems of superconductivity and magnetism, aspects of which will be considered in this thesis, are both intrinsically many body problems as the interactions between the conduction electrons determine the ground state of the many body system. However, it is not possible, in general, to solve the full many body TISE, so approximations must be made.

It is clearly pragmatic to 'integrate out' quark and nucleon degrees of freedom. In this work we will not consider the majority of the electronic degrees of freedom either. Instead, we will consider a system of 'ions' and 'conduction' electrons.

Landau's theory of Fermi liquids [3] is one of the most important tools for studying the system of conduction electrons interacting in an ionic potential. Landau's theory is also very important for studying ^{3}He, the normal state of which is very well described by Landau Fermi liquid theory. Landau showed [115, 116] that the system of interacting electrons can be mapped onto a system of 'quasiparticles'. The quasiparticles can either be particle-like ($\varepsilon_{\mathbf{k}} > \varepsilon_F$) or hole-like ($\varepsilon_{\mathbf{k}} < \varepsilon_F$) excitations, but importantly quasiparticles retain the labels of the non-interacting electron gas i.e. the momentum, $\mathbf{k}$, and spin, σ, are good quantum numbers of both the non-interacting and the interacting systems. The quasiparticles can often be thought of as a particle surrounded by a polarisation cloud of other particles.

2.2 The tight binding approximation

One of the simplest models of electrons in solids is the tight binding approximation. The tight binding approximation is therefore described in many elementary textbooks (particularly recommended are the discussions in the books by Ziman [225] and Ashcroft and Mermin [19]).

It is possible to expand the single particle eigenstates, $\Psi(\mathbf{r})$, of any system as a linear sum of any other complete set of states, $\psi_n(\mathbf{r})$, as follows

$$\Psi(\mathbf{r}) \quad = \quad \sum_n a_n \psi_n(\mathbf{r}). \tag{2.2.1}$$

Solids are made up of atoms, so a natural (and complete) set of states in which to expand the eigenstates of the system is the eigenfunctions of an isolated atom - the atomic orbitals, $\phi_n(\mathbf{r})$. Which are the eigenstates of the atomic Hamiltonian, $\hat{\mathcal{H}}_{at}$, i.e.

$$\hat{\mathcal{H}}_{at}\phi_n(\mathbf{r}) = E_n\phi_n(\mathbf{r}) \tag{2.2.2}$$

Of course, while the electrons retain much of the localised character of the free atom, the fact that we are dealing with a solid changes the Hamiltonian (and hence the eigenstates) of the system. However, we can write the perturbed Hamiltonian as

$$\hat{\mathcal{H}} = \hat{\mathcal{H}}_{at} + \mathcal{V}(\mathbf{r} - \mathbf{R}_i). \tag{2.2.3}$$

The $\mathbf{R}_i = i \times \mathbf{a}$ (where $\mathbf{a}$ is a basis vector of the crystal and $i \in \mathbb{I}$) are the locations of the lattice sites. $\mathcal{V}(\mathbf{r} - \mathbf{R}_i)$ is the difference between the potential felt by an electron at $\mathbf{r} - \mathbf{R}_i$ in a free atom with its nucleus at the origin and the potential felt by an electron at $\mathbf{r}$ in an orbital arising from atom at the location $\mathbf{R}_i$. The energy of the system, $\varepsilon(\mathbf{k})$, is the given by the expectation value of the Hamiltonian,

$$\varepsilon(\mathbf{k}) = \frac{\int \Psi^*(\mathbf{r})\hat{\mathcal{H}}\Psi(\mathbf{r})\mathrm{d}\mathbf{r}}{\int \Psi^*(\mathbf{r})\Psi(\mathbf{r})\mathrm{d}\mathbf{r}}. \tag{2.2.4}$$

If the atoms are sufficiently separated from one another then only a few occupied orbitals will significantly overlap with one another.

Recall that Bloch's theorem states that

$$\Psi(\mathbf{r} + \mathbf{a}) = e^{\mathrm{i}\mathbf{k}\cdot\mathbf{a}}\Psi(\mathbf{r}). \tag{2.2.5}$$

Hence, when only one orbital at each site has a significant overlap with it's neighbours we find that

$$\varepsilon(\mathbf{k}) = \sum_i t_i e^{\mathrm{i}\mathbf{k}\cdot\mathbf{R}_i} \tag{2.2.6}$$

The coefficients, t_i, are given by

$$t_i = \int \mathrm{d}r \phi^*(\mathbf{r}) \mathcal{V}(\mathbf{r}) \phi(\mathbf{r} - \mathbf{R}_i), \tag{2.2.7}$$

and are known as hopping integrals as they correspond to the amplitude for a quasiparticle to move from an orbital around the atom at the origin to an orbital on the atom at $\mathbf{R}_i$. Hence, t_0 is an *on site* term, t_1 describes *nearest neighbour* hopping, t_2 describes *next nearest neighbour* hopping and t_n describes n^{th} nearest neighbour hopping.

We now assume that only the first few terms in the series have no-zero coefficients. For example, if only $t_0 = \varepsilon_0$ and $t_1 = -t$ are non-zero, then the quasiparticle dispersion relation for a simple cubic lattice is

$$\varepsilon(\mathbf{k}) = \varepsilon_0 - 2t\big(\cos(k_x a) + \cos(k_y a) + \cos(k_z a)\big) \tag{2.2.8}$$

where a is the lattice spacing. Thus by carefully choosing a complete set of states we have been able to write down a simple approximation for the dispersion relation of a cubic lattice. If more than one orbital has a significant overlap with it's neighbours then the effect is simply to introduce more hopping integrals. Higher order hopping terms can be included to give the approximation greater accuracy.

2.2.1 Example: A tight binding fit to the band structure of Sr_2RuO_4 as determined by quantum oscillations.

By way of an illustration of what has been described above, we will now examine an application of the tight binding approximation. We will show how tight binding parameters can be fitted to experimental data obtained from de Haas–van Alphen measurements [30].

As will be examined in greater detail in chapter 5, Sr_2RuO_4 is a quasi two dimensional metal with a perovskite crystal structure (see figure 5.1). Both first principles band structure calculations [147] and experiment [30, 130, 220] indicate that there are three Fermi surface sheets. These arise from the overlap of the Ru-d_{xy}, -d_{xz} and -d_{yz} orbitals, one can therefore fit the experimental parameters with a tight binding model. This means that each order we expand to

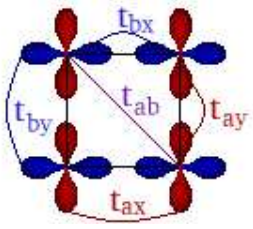

Figure 2.1: Sketch of the hopping integrals in equations 2.2.10, 2.2.11 and 2.2.12 and the symmetry of the relevant orbitals.

will give us nine hopping integrals. Therefore to second order we have twenty seven free parameters.

Twenty seven free parameters make this model a gross over-specification. Therefore we must introduce some reasonable approximations. To do this we consider the two dimensional (2D) nature of the Ru-d orbitals of which of which the bands are composed.

As both band structure and experiments indicate that Sr_2RuO_4 is highly 2D, that is to say that, to the first approximation, the Fermi surface is independent of the z coordinate[1]. We will limit our fit to the basal plane in which, the d_{xz} and d_{yz} orbitals are one dimensional.

Our model can be further simplified as the band structure calculations indicate that there is little hybridisation between the d_{xy} orbital and the two 1D orbitals. We will therefore fit the d_{xy} orbital separately from the 1D bands. To second order the tight binding model for a 2D band is

$$\varepsilon_\gamma(\mathbf{k}) = \varepsilon_c - 2t(\cos k_x + \cos k_y) - t' \cos k_x \cos k_y, \tag{2.2.9}$$

in units where the lattice spacing equals one.

The two 1D bands are slightly more complex as there is significant hybridisation between them. We will therefore fit these orbitals to the functions $\varepsilon_\alpha, \varepsilon_\beta$ and $\varepsilon_{\alpha\beta}$ where

$$\varepsilon_\alpha(\mathbf{k}) = \varepsilon_a - 2t_{ax}\cos k_x - 2t_{ay}\cos k_y, \tag{2.2.10}$$

$$\varepsilon_\beta(\mathbf{k}) = \varepsilon_b - 2t_{ax}\cos k_x - 2t_{ay}\cos k_y, \tag{2.2.11}$$

$$\varepsilon_{\alpha\beta}(\mathbf{k}) = -4t_{ab}\sin k_x \sin k_y. \tag{2.2.12}$$

[1]The 'warping' of the Fermi in the third direction (along the c-axis) has also been studied [30] by de Haas-van Alphen experiments and was found to be minimal.

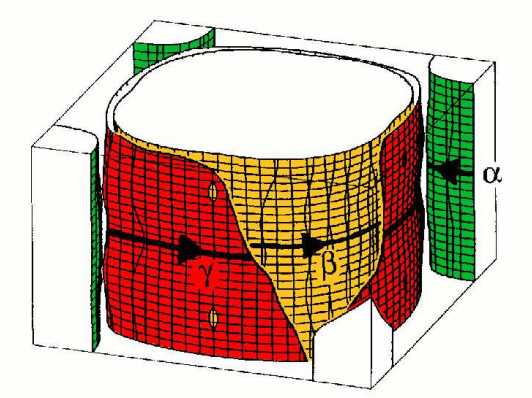

Figure 2.2: The experimental Fermi surface of Sr_2RuO_4 taken from Mackenzie *et al*. [136].

Figure 2.1 shows the nature of hopping integrals and the orbitals which they represent hopping between. For example, t_{ax} describes hopping between a (d_{xz}) orbitals in the x-direction. t_{ab} corresponds to hopping between the a and b (d_{yz}) orbitals. Because of $x - y$ symmetry

$$\varepsilon_a = \varepsilon_b \tag{2.2.13}$$

$$t_{ax} = t_{by} \tag{2.2.14}$$

$$t_{bx} = t_{ay}. \tag{2.2.15}$$

We are now left with only seven free parameters. Three parameters for the d_{xy} orbital[2] and four parameters for the hybridised d_{xz}/d_{yz} system.

Experimentally [30] it is found that there are three bands, canonically[3] labelled α, β and γ (see figure 2.2). Mazin and Singh associate the α and β sheets with the bands arising from the hybridisation of the d_{xz} and d_{yz} orbitals and the γ sheet with the d_{xy} orbital. We therefore assume this in our fit.

For each band we have two experimentally measured parameters, the cyclotron mass, m, and the angularly averaged Fermi wavevector, k_F. These are detailed in table 2.1. However, for the theorist the fundamental parameter is the area enclosed by the Fermi surface, A, as this is simple to calculate numerically from the tight binding approximation and encapsulates both the

[2]We should note that this is still a slight over-specification as for the γ sheet we will fit three free parameters to only two measured quantities, however this is far more justifiable than our original twenty seven free parameters.

[3]Confusingly some early works do not follow this convention, in particular Mazin and Singh [147] use $\alpha_c = \beta_{MS}$, $\beta_c = \alpha_{MS}$, $\gamma_c = \gamma_{MS}$, where the subscript c corresponds to the canonical labels (which we will use throughout this thesis) and the subscript MS corresponds to Mazin and Singh's labels.

Sheet	α	β	γ
k_F (Å)	0.305	0.623	0.754
m/m_e	3.4	7.5	14.6

Table 2.1: Experimental parameters from Mackenzie *et al.* [135] used to determine the tight binding fit for Sr_2RuO_4.

t	0.08162 eV
t'	$0.45t$
ε_c	-1.615t
$t_{ax} = t_{by}$	1.34t
$t_{ay} = t_{bx}$	0.08t
t_{ab}	0.11t
$\varepsilon_a = \varepsilon_b$	-1.42t

Table 2.2: Tight binding parameters fitted to de Haas-van Alphen experiments performed on Sr_2RuO_4.

measured quantities as

$$\pi k_F^2 = A \tag{2.2.16}$$

and

$$m = \frac{\hbar^2}{2\pi}\frac{\partial A}{\partial \varepsilon}. \tag{2.2.17}$$

Based on the experimental data a fit, detailed in table 2.2, was constructed. The cyclotron masses and Fermi wavevectors calculated from this fit are shown in table 2.3 and are in excellent agreement with the experimental parameters, while the Fermi surface for this model is shown in figure 2.3 this compares favourably with the experimentally measured Fermi surface (figure 2.2).

Sheet	α	β	γ
k_F (Å)	0.305	0.623	0.754
m/m_e	3.368	7.560	14.60

Table 2.3: Tight binding cyclotron masses and Fermi wavevectors c.f. table 2.1.

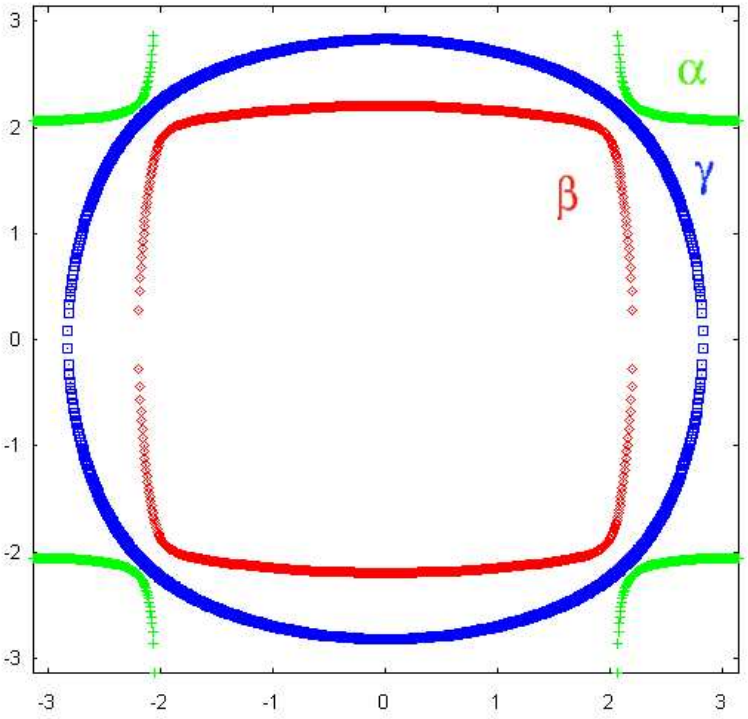

Figure 2.3: The Fermi surface of Sr_2RuO_4 calculated from a tight binding fit.

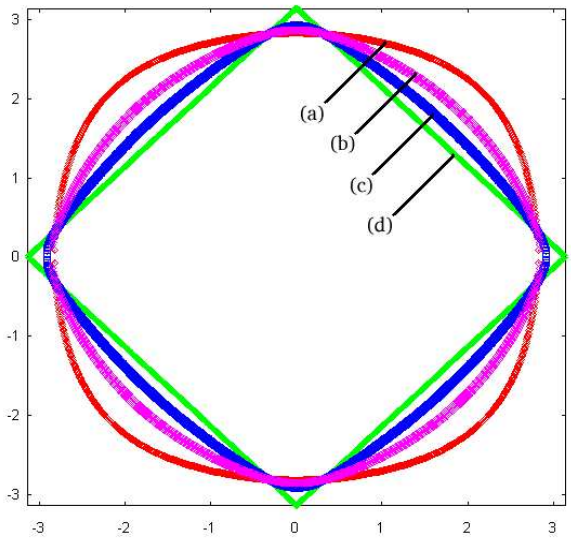

Figure 2.4: The Fermi surface of a tight binding model with on-site, nearest neighbour and next nearest neighbour terms for various values of the hopping integrals. The parameters are as follows: (a) $t_0/t_1 = -1.615$, $t_2/t_1 = 0.45$ (b) $t_0/t_1 = -1.077$, $t_2/t_1 = 0.30$ (c) $t_0/t_1 = -0.538$, $t_2/t_1 = 0.15$ (d) $t_0/t_1 = 0$, $t_2/t_1 = 0$.

To show a little more of the possible range of the tight binding approximation, we briefly examine a model of the d_{xy} orbital/γ band of Sr_4RuO_4. In figures 2.4 and 2.5 we plot the Fermi surface of the tight binding model corresponding to equation 2.2.9 with various choices of the parameters ε_c and t'. And in figure 2.6 we show the well know Fermi surfaces of the nearest neighbour Hubbard model in two dimensions at various fillings.

2.2.2 The tight binding density of states

Another important feature of the electronic structure in the density of states (DOS). For practical purposes (when working close to experiment) we often only require that the DOS is correct near the Fermi level. For example, in our tight binding fit (above) we ensured that the gradient of the DOS at the Fermi energy was correct my fitting to cyclotron mass.

We have numerically calculated the DOS, $D(\varepsilon)$, for our tight binding models by two methods. (i) Direct evaluation of the formula

$$D(\varepsilon) = \sum_{\mathbf{k}} \delta(\varepsilon - \varepsilon_{\mathbf{k}}), \tag{2.2.18}$$

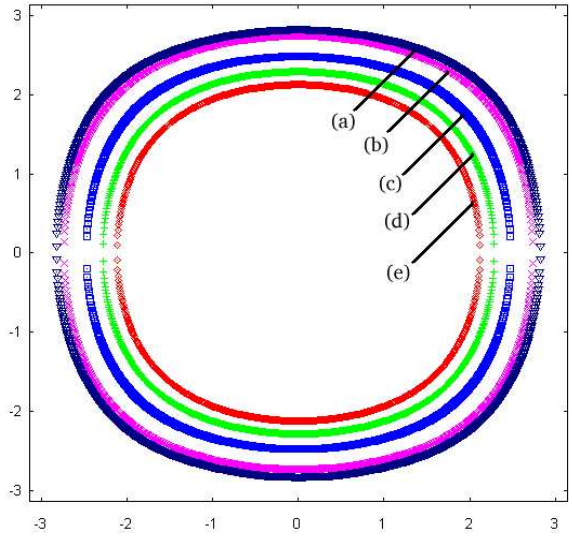

Figure 2.5: The Fermi surface of a tight binding model with on-site, nearest neighbour and next nearest neighbour terms for various fillings. The parameters are as follows: (a) $t_0/t_1 = -1.615$, $t_2/t_1 = 0.45$ (b) $t_0/t_1 = -1.5$, $t_2/t_1 = 0.45$ (c) $t_0/t_1 = -1.0$, $t_2/t_1 = 0.45$ (d) $t_0/t_1 = -0.5$, $t_2/t_1 = 0.45$ (e) $t_0/t_1 = 0.0$, $t_2/t_1 = 0.45$.

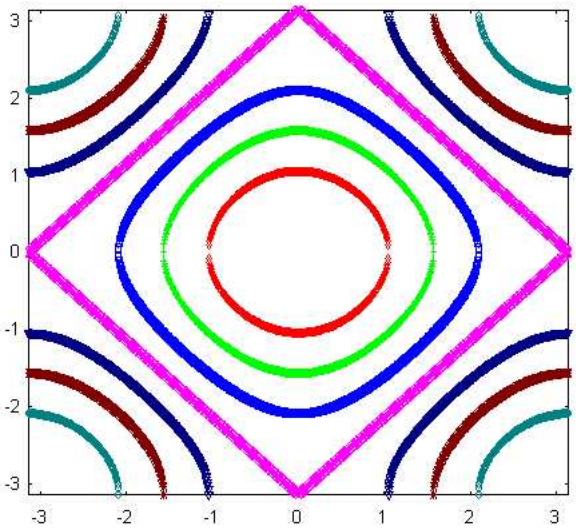

Figure 2.6: The Fermi surface of a tight binding model with nearest neighbour hopping only for various fillings. The chemical potential is (from the centre out): $t_0/t_1 = -3$, $t_0/t_1 = -2$, $t_0/t_1 = -1$, $t_0/t_1 = 0$, $t_0/t_1 = 1$, $t_0/t_1 = 2$ and $t_0/t_1 = 3$.

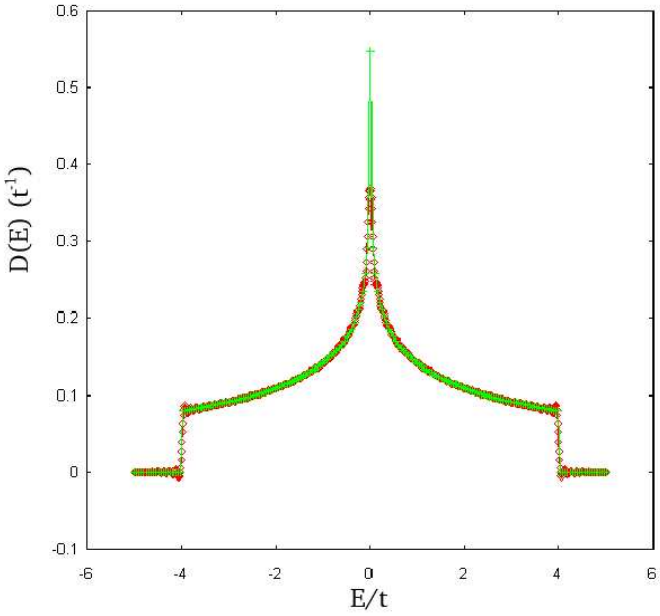

Figure 2.7: The density of states for a tight binding model with nearest neighbour hopping only in two dimensions, calculated both by direct evaluation of equation 2.2.18 and by the Bessel function method.

(which requires certain subtleties discussed in appendix A.2) and (ii) by expanding the solution in terms of Bessel functions as discussed in appendix A.1. These two calculations are in good agreement. The well known DOS for a nearest neighbour, tight binding model (i.e. for the Hamiltonian given in equation 2.2.8) is shown in figure 2.7. Particular features to notice are that the bandwidth is $8t$ (as can clearly be seen from equation 2.2.8) and that there is a van Hove singularity at half filling (one electron per cite, $E/t = 0$).

Also shown are the DOS for the tight binding fit to the γ band of Sr_2RuO_4 (figure 2.8) and the full three orbital fit to Sr_2RuO_4 (figure 2.9). Note that the next nearest neighbour terms break the symmetry about half filling. The γ band has two van Hove singularities, both above the Fermi energy, while the van Hove singularities on the α and β bands are shifted to very high and very low energies respectively because of their one dimensionality. Both the α and β bands are relatively smooth at the Fermi level, the gradient of the DOS at the Fermi level is therefore dominated by the γ band. This indicates that the γ band will play a leading role in determining the physics of Sr_2RuO_4.

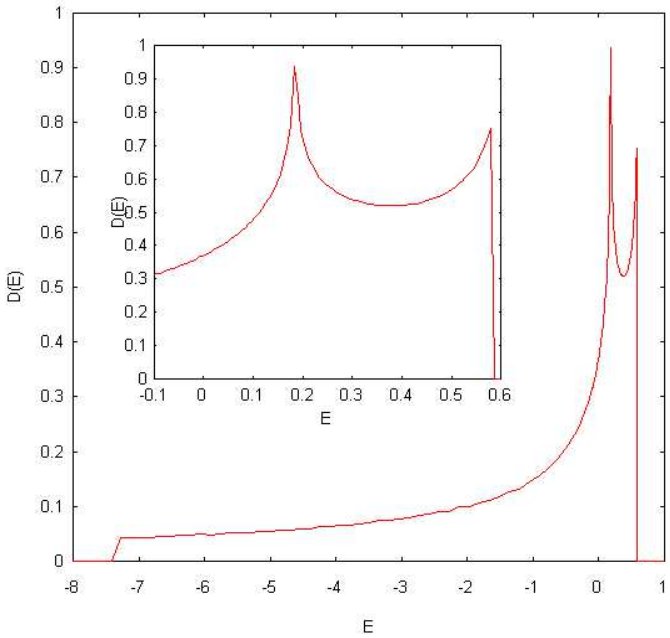

Figure 2.8: The density of states for the tight binding fit to the γ sheet of Sr_2RuO_4, calculated by direct evaluation of equation 2.2.18. Inset, detail of region near the Fermi level and the van Hove singularities.

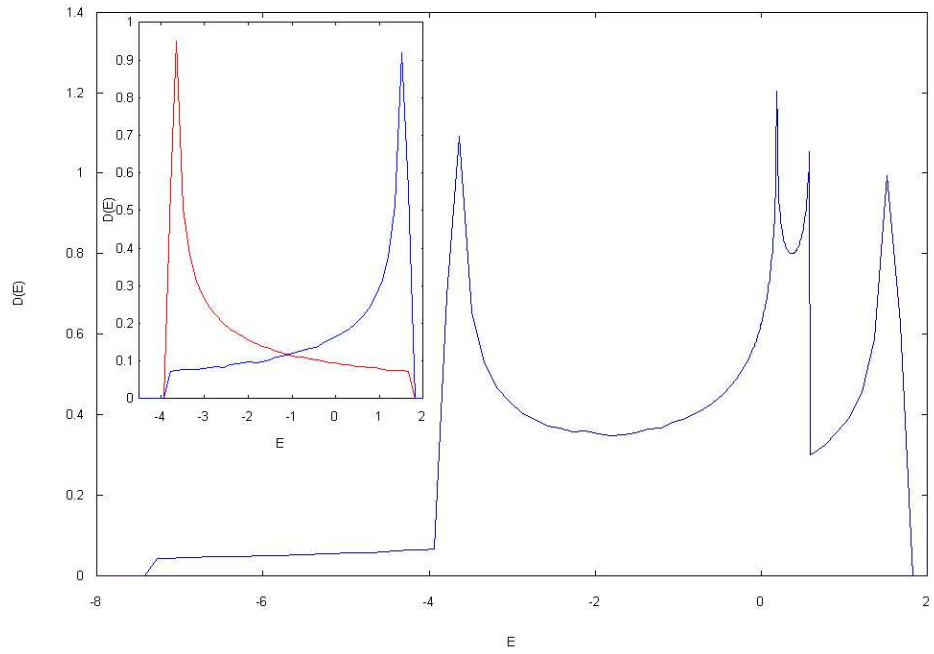

Figure 2.9: The density of states for the tight binding fit to the three band model Sr_2RuO_4, calculated by direct evaluation of equation 2.2.18. Inset, density of states of the α and β bands calculated by the same method.

2.3 Second quantisation

We now consider a mathematical technique that is central to this thesis, namely that of second quantisation. Second quantisation is in fact, the basic building block of all quantum field theories, and as such is one of the most important tools in the theoretical physicists armoury.

Consider the wavefunction, $|\Psi\rangle$, of a many body system. In the occupation number representation $|\Psi\rangle$ has the generic form

$$|\Psi\rangle = |..., n_{\lambda-1}, n_\lambda, n_{\lambda+1}, ...\rangle. \tag{2.3.1}$$

We now introduce two operators, $\hat{c}_\lambda$ and $\hat{c}^\dagger_\lambda$, which we define to have the following effects of $|\Psi\rangle$

$$\hat{c}^\dagger_\lambda|\Psi\rangle = \hat{c}^\dagger_\lambda|..., n_\lambda..., \rangle = (\pm 1)^{(\sum_{\lambda'}^{\lambda'<\lambda} n_{\lambda'})}(1-n_\lambda)^{\frac{1}{2}}|..., (n_\lambda+1), ...\rangle, \tag{2.3.2}$$

$$\hat{c}_\lambda|\Psi\rangle = \hat{c}_\lambda|..., n_\lambda, ...\rangle = (\pm 1)^{(\sum_{\lambda'}^{\lambda'<\lambda} n_{\lambda'})}(n_\lambda)^{\frac{1}{2}}|..., (n_\lambda-1), ...\rangle, \tag{2.3.3}$$

where the $+$ corresponds to Bosons and the $-$ corresponds to Fermions. Thus $\hat{c}^\dagger_\lambda$ increases the number of particles, n_λ, in the state λ by one. $\hat{c}^\dagger_\lambda$ is therefore known as a creation operator. Similarly, $\hat{c}_\lambda$ decreases n_λ by one and is therefore known as an annihilation operator. To fully specify the operators we must also specify their commutation relations. For Fermions the commutation relations are:

$$\hat{c}_\lambda\hat{c}^\dagger_{\lambda'} + \hat{c}^\dagger_{\lambda'}\hat{c}_\lambda = \delta_{\lambda\lambda'} \tag{2.3.4}$$

$$\hat{c}^\dagger_{\lambda'}\hat{c}^\dagger_\lambda + \hat{c}^\dagger_\lambda\hat{c}^\dagger_{\lambda'} = 0 \tag{2.3.5}$$

$$\hat{c}_{\lambda'}\hat{c}_\lambda + \hat{c}_\lambda\hat{c}_{\lambda'} = 0. \tag{2.3.6}$$

While the Bosons commutation relations are:

$$\hat{c}_\lambda\hat{c}^\dagger_{\lambda'} - \hat{c}^\dagger_{\lambda'}\hat{c}_\lambda = \delta_{\lambda\lambda'} \tag{2.3.7}$$

$$\hat{c}^\dagger_{\lambda'}\hat{c}^\dagger_\lambda - \hat{c}^\dagger_\lambda\hat{c}^\dagger_{\lambda'} = 0 \tag{2.3.8}$$

$$\hat{c}_{\lambda'}\hat{c}_\lambda - \hat{c}_\lambda\hat{c}_{\lambda'} = 0. \tag{2.3.9}$$

We now define the field operators, $\hat{\psi}^\dagger_\sigma(\mathbf{r})$ and $\hat{\psi}_\sigma(\mathbf{r})$, by

$$\hat{\psi}^\dagger_\sigma(\mathbf{r}) = \sum_\lambda \hat{c}^\dagger_\lambda \phi^*_\lambda(\mathbf{r}) \tag{2.3.10}$$

$$\hat{\psi}_\sigma(\mathbf{r}) = \sum_\lambda \hat{c}_\lambda \phi_\lambda(\mathbf{r}) \tag{2.3.11}$$

where $\phi_\lambda(\mathbf{r})$ is the wavefunction of a particle in the state λ at the position $\mathbf{r}$. $\hat{\psi}^\dagger_\sigma(\mathbf{r})$ therefore creates a particle with spin σ at position $\mathbf{r}$ and $\hat{\psi}_\sigma(\mathbf{r})$ annihilates a particle with spin σ at position $\mathbf{r}$.

We can use the field operators to define composite operators. For example the density operator:

$$\hat{\rho}_\sigma(\mathbf{r}) = m\hat{\psi}^\dagger_\sigma(\mathbf{r})\hat{\psi}_\sigma(\mathbf{r}) \tag{2.3.12}$$

the expectation value of which is the density:

$$\rho_\sigma(\mathbf{r}) = m\big\langle \psi_0 \big| \hat{\psi}^\dagger_\sigma(\mathbf{r})\hat{\psi}_\sigma(\mathbf{r}) \big| \psi_0 \big\rangle \tag{2.3.13}$$

or the (particle) current operator:

$$\hat{\mathbf{j}}_\sigma(\mathbf{r}) = \hat{\psi}^\dagger_\sigma(\mathbf{r}) \frac{\hbar}{\mathtt{i}m} \nabla \hat{\psi}_\sigma(\mathbf{r}) + \text{h.c.}, \tag{2.3.14}$$

where h.c. indicates the Hermitian conjugate, the expectation value of which is the (particle) current :

$$\mathbf{j}_\sigma(\mathbf{r}) = \Big\langle \psi_0 \Big| \hat{\psi}^\dagger_\sigma(\mathbf{r}) \frac{\hbar}{\mathtt{i}m} \nabla \hat{\psi}_\sigma(\mathbf{r}) + \text{h.c.} \Big| \psi_0 \Big\rangle. \tag{2.3.15}$$

As the Hamiltonian is an operator we can of course write the Hamiltonian in terms of the field operators. For example the single particle Hamiltonian, $\hat{\mathcal{H}}_0$, is given by

$$\hat{\mathcal{H}}_0 = \sum_\sigma \int \mathrm{d}\mathbf{r} \hat{\psi}^\dagger_\sigma(\mathbf{r}) \left(-\frac{\hbar^2}{2m}\nabla^2 + V^{ext}(\mathbf{r}) \right) \hat{\psi}_\sigma(\mathbf{r}). \tag{2.3.16}$$

For two body interactions the Hamiltonian, $\hat{\mathcal{H}}_{int}$, is

$$\hat{\mathcal{H}}_{int} = \frac{1}{2} \sum_{\sigma\sigma'} \int \mathrm{d}\mathbf{r} \int \mathrm{d}\mathbf{r}' \hat{\psi}^\dagger_\sigma(\mathbf{r}) \hat{\psi}^\dagger_{\sigma'}(\mathbf{r}') V(|\mathbf{r} - \mathbf{r}'|) \hat{\psi}_{\sigma'}(\mathbf{r}') \hat{\psi}_\sigma(\mathbf{r}). \tag{2.3.17}$$

2.3.1 Example: The tight binding Hamiltonian

We will now derive the tight binding Hamiltonian from equation 2.3.16. We begin by substituting (2.3.10) and (2.3.11) into the single particle Hamiltonian. This gives

$$\hat{\mathcal{H}}_0 = \sum_{\mathbf{k}\sigma} \int \mathrm{d}\mathbf{r} \hat{c}^\dagger_{\mathbf{k}\sigma} \phi^*_{\mathbf{k}\sigma}(\mathbf{r}) \left(-\frac{\hbar^2}{2m}\nabla^2 + V^{ext}(\mathbf{r}) \right) \phi_{\mathbf{k}\sigma}(\mathbf{r}) \hat{c}_{\mathbf{k}\sigma}. \tag{2.3.18}$$

where we have identified $\mathbf{k}$ and σ as the state labels λ. Recall that $\phi_{\mathbf{k}\sigma}(\mathbf{r})$ is the solution of the single particle TISE so

$$\left(-\frac{\hbar^2}{2m}\nabla^2 + V^{ext}(\mathbf{r}) \right) \phi_{\mathbf{k}\sigma}(\mathbf{r}) = \varepsilon_{\mathbf{k}\sigma} \phi_{\mathbf{k}\sigma}(\mathbf{r}). \tag{2.3.19}$$

Substituting this into (2.3.18) we find that

$$\hat{\mathcal{H}}_0 = \sum_{\mathbf{k}\sigma} \varepsilon_{\mathbf{k}\sigma} \hat{c}^\dagger_{\mathbf{k}\sigma} \hat{c}_{\mathbf{k}\sigma}. \tag{2.3.20}$$

We now introduce the number operator, $\hat{n}_{\mathbf{k}\sigma}$, which is defined as

$$\hat{n}_{\mathbf{k}\sigma} = \hat{c}^\dagger_{\mathbf{k}\sigma} \hat{c}_{\mathbf{k}\sigma}. \tag{2.3.21}$$

Clearly, the number operator simply counts[4] the number of particles in the state $|\mathbf{k}, \sigma\rangle$. The single particle Hamiltonian then becomes

$$\hat{\mathcal{H}}_0 = \sum_{\mathbf{k}\sigma} \varepsilon_{\mathbf{k}\sigma} \hat{n}_{\mathbf{k}\sigma}. \tag{2.3.22}$$

Thus the energy of the non-interacting system is given by the product of the energy of a given state and the number of particles in the that state summed over all states.

We now introduce the (lattice) Fourier transformations of the second quantisation operators.

$$\hat{c}_{i\sigma} = \frac{1}{\sqrt{N}} \sum_{\mathbf{k}} e^{i\mathbf{k}\cdot\mathbf{R}_i} \hat{c}_{\mathbf{k}\sigma} \tag{2.3.23}$$

$$\hat{c}^\dagger_{i\sigma} = \frac{1}{\sqrt{N}} \sum_{\mathbf{k}} e^{-i\mathbf{k}\cdot\mathbf{R}_i} \hat{c}^\dagger_{\mathbf{k}\sigma} \tag{2.3.24}$$

[4] This is easily seen, $\hat{c}^\dagger_{\mathbf{k}\sigma}\hat{c}_{\mathbf{k}\sigma}|0\rangle = 0 = 0.|0\rangle$ as the annihilation operator acting on the vacuum state gives 0, while $\hat{c}^\dagger_{\mathbf{k}\sigma}\hat{c}_{\mathbf{k}\sigma}|1\rangle = \hat{c}^\dagger_{\mathbf{k}\sigma}|0\rangle = |1\rangle = 1.|1\rangle$.

for a lattice with N sites. $\hat{c}_{i\sigma}^{(\dagger)}$ annihilates (creates) a particle in an orbital centred on the lattice site i. Substituting the inverse Fourier transforms into equation 2.3.20 we find that

$$\hat{\mathcal{H}}_0 = \sum_{ij\sigma} t_{ij} \hat{c}_{i\sigma}^{\dagger} \hat{c}_{j\sigma} \tag{2.3.25}$$

where the hopping integral, t_{ij}, must clearly be the Fourier transform of the state energy, $\varepsilon_{\mathbf{k}\sigma}$. Thus

$$\varepsilon_{\mathbf{k}\sigma} = \sum_{j} t_{ij} e^{i\mathbf{k}\cdot(\mathbf{R}_i - \mathbf{R}_j)}. \tag{2.3.26}$$

If we assume a simple cubic lattice with on site and nearest neighbour[5] hopping only, we find that

$$\varepsilon_{\mathbf{k}\sigma} = t_0 + 2t_1\big(cos(k_x a) + cos(k_y a) + cos(k_z a)\big) \tag{2.3.27}$$

and we have therefore regained (2.2.8) as required.

2.4 Green's functions

Only a brief use of Green's functions is made in this work. But due to their great importance in many areas of physics, and because some readers may not be familiar with the generalised form of the Green's function (as opposed to the Green's as used in the theory of linear differential equations[6]) a brief discussion will be given below. For a more detailed discussion see one of the many excellent textbooks on the subject [3, 72].

To describe the Green's function at finite temperature we must introduce two new concepts. The first of these is *imaginary time*, $\tau = \mathtt{i}t$. Secondly we introduce the 'Heisenberg' field operators, $\widetilde{\psi}_\alpha(\mathbf{r},\tau)$ and $\widetilde{\overline{\psi}}_\alpha(\mathbf{r},\tau)$, which depend on the 'time' τ, and are defined by

$$\widetilde{\psi}_\alpha(\mathbf{r},\tau) = e^{(\hat{H}-\mu\hat{N})\tau}\psi_\alpha(\mathbf{r})e^{-(\hat{H}-\mu\hat{N})\tau}, \tag{2.4.1}$$

$$\widetilde{\overline{\psi}}_\alpha(\mathbf{r},\tau) = e^{(\hat{H}-\mu\hat{N})\tau}\psi_\alpha^{\dagger}(\mathbf{r})e^{-(\hat{H}-\mu\hat{N})\tau}. \tag{2.4.2}$$

In units where $\hbar = 1$.

[5] Of course the simple cubic structure has six nearest neighbours, located at $\pm a$ in each of the $\hat{\mathbf{x}}$, $\hat{\mathbf{y}}$ and $\hat{\mathbf{z}}$ directions. This leads to the three cosines in the dispersion relation (2.3.27).

[6] The name 'Green's function' is derived from the fact that the free particle 'Green's function' is the appropriate Green's function of the linear equations for $\psi(\mathbf{r},t)$.

The finite temperature (single particle) Green's function $\mathcal{G}_{\alpha\beta}(\mathbf{r}_1,\tau_1;\mathbf{r}_2,\tau_2)$ is then defined by

$$\mathcal{G}_{\alpha\beta}(\mathbf{r}_1,\tau_1;\mathbf{r}_2,\tau_2) = -\Big\langle T_\tau\Big(\widetilde{\psi}_\alpha(\mathbf{r}_1,\tau_1)\widetilde{\overline{\psi}}_\alpha(\mathbf{r}_2,\tau_2)\Big)\Big\rangle. \tag{2.4.3}$$

T_τ is the time ordering operator[7] (which of course generates the appropriate sign if it commutes the operators) i.e.

$$T_\tau\Big(\widetilde{\psi}_\alpha(\mathbf{r},\tau)\widetilde{\overline{\psi}}_\alpha(\mathbf{r},\tau)\Big) = \begin{cases} \widetilde{\psi}_\alpha(\mathbf{r},\tau)\widetilde{\overline{\psi}}_\alpha(\mathbf{r},\tau) & \text{for } \tau_1 > \tau_2 \\ -\widetilde{\overline{\psi}}_\alpha(\mathbf{r},\tau)\widetilde{\psi}_\alpha(\mathbf{r},\tau) & \text{for } \tau_2 > \tau_1 \end{cases} \tag{2.4.4}$$

As with the second quantisation operators (equation 2.3.21) we can easily define many observable quantities in terms of Green's functions, for example the number operator is given by,

$$\hat{n} = \int \mathrm{d}^3\mathbf{r}\, \mathcal{G}_{\alpha\alpha}(\mathbf{r},\tau;\mathbf{r},\tau+0). \tag{2.4.5}$$

($\tau' = \tau + 0$ is standard shorthand for the limit of $\tau' = \tau + \tau''$ as $\tau'' \to 0$ from above.)

We can Fourier transform the Green's function into momentum space by

$$\mathcal{G}_{\alpha\beta}(\mathbf{k},\tau_1-\tau_2) = \int \mathrm{d}^3\mathbf{r}\; \mathcal{G}_{\alpha\beta}(\mathbf{r}_1,\tau_1;\mathbf{r}_2,\tau_2)e^{-\mathbf{k}\cdot(\mathbf{r}_1-\mathbf{r}_2)}. \tag{2.4.6}$$

The Green's function can also be expanded as a Fourier series of τ,

$$\mathcal{G}_{\alpha\beta}(\mathbf{k},\tau) = T\sum_n e^{-\mathrm{i}\omega_n\tau}\mathcal{G}_{\alpha\beta}(\mathbf{k},\omega_n), \tag{2.4.7}$$

$$\mathcal{G}_{\alpha\beta}(\mathbf{k},\omega_n) = \frac{1}{2}\int_{-1/T}^{1/T} \mathrm{d}\tau\; e^{\mathrm{i}\omega_n\tau}\mathcal{G}_{\alpha\beta}(\mathbf{k},\tau), \qquad \omega_n = n\pi T. \tag{2.4.8}$$

The ω_n are known as the Matsubara frequencies.

It can be shown that for Fermions only the Fourier components of 'odd' frequencies, $\omega_n = (2n+1)\pi T$, are non zero, and only for Bosons only the Fourier components of 'even' frequencies, $\omega_n = 2n\pi T$, are finite. This leads to the result [3] that for Fermions

$$\mathcal{G}_{\alpha\beta}(\mathbf{k},\omega_n) = \delta_{\alpha\beta}\frac{1}{\mathrm{i}\omega_n - \varepsilon(\mathbf{k}) + \mu}, \qquad \omega_n = (2n+1)\pi T. \tag{2.4.9}$$

A similar result is found for Bosons, it is therefore usual to drop the spin labels and write

[7] The subscript τ is included here to distinguish the time ordering operator from the temperature, T, but is often dropped.

$$\mathcal{G}(\mathbf{k},\omega_n) = \frac{1}{\mathtt{i}\omega_n - \varepsilon(\mathbf{k}) + \mu}, \qquad \begin{cases} \omega_n = (2n+1)\pi T & \text{for Fermions} \\ \omega_n = 2n\pi T & \text{for Bosons.} \end{cases} \tag{2.4.10}$$

These results are particularly useful as they allow the calculation of Green's functions to become automatic. It is, in part, this automatic calculation that makes the Green's function technique so powerful.

Chapter 3

The Ginzburg–Landau and BCS theories: applications to triplet superfluidity in ^{3}He

In this chapter we introduce the Ginzburg–Landau and Bardeen–Cooper–Schrieffer (BCS) theories of superconductivity are introduced in the correct form for singlet (s-wave) superconductivity. The relationship between the triplet state of two Fermions and triplet pairing is explored. This motivates the generalisation the BCS theory to allow for finite angular momentum pairing states and for either spin singlet or spin triplet pairing.

We discuss the properties of ^{3}He at some length. We consider the phase diagram of ^{3}He, the generalisations of Ginzburg–Landau theory that are required to describe ^{3}He and give a mathematical and physical description of all of the phases seen experimentally in ^{3}He and some phases that are not seen experimentally, but which are stable in some region of parameter space. Once again we attempt to provide as many references as possible to the extensive literature as possible

3.1 The Ginzburg–Landau theory of superconductivity

The Ginzburg–Landau theory of superconductivity was first developed as a phenomenological theory [79, 108]. However, as will be seen in section 5.2, Ginzburg–Landau theories can readily be derived from a microscopic (BCS) theory. In this section we will discuss the Ginzburg–Landau theory for a singlet superconductor and in section 3.8 we will describe the

Ginzburg–Landau theory for triplet pairing.

Ginzburg–Landau theory is the appropriate Landau theory [117, 174] for superconductivity and as such it has much in common with any other Landau theory. In particular, the theory characterises the emergence of superconductivity by the appearance of an order parameter. In zero field the superconducting transition is second order, so the order parameter goes continuously to zero at the transition temperature (T_C). In a magnetic field the superconducting transition is first order and the order parameter is a discontinuous at T_C.

To construct their order parameter Ginzburg and Landau assumed the existence of some macroscopic 'wavefunction', ψ. The order parameter must be $|\psi|^2$, as wavefunctions are intrinsically complex while the free energy is, by definition, real. As with all Landau theories the difference in free energy between the low temperature and high temperature states is calculated by expanding in terms of the order parameter. Thus to fourth order the free energy is

$$F_{SC} - F_N = \alpha|\psi|^2 + \beta|\psi|^4, \tag{3.1.1}$$

where the subscripts SC and N refer to the superconducting and normal states respectively. In general other terms may also be included. For example, gradient terms can be introduced to account for the cost to the free energy of spatial distortions of the order parameter. Gradient terms also allow the effect of an external magnetic field to enter via minimal coupling, however, it should be remembered that the charge included in the minimal coupling term is the charge of the Cooper pair, $2e$, rather than the charge of the electron. In a field we must also include the contribution of the magnetic field to the free energy density, giving us

$$F_{SC} - F_N = \int \mathrm{d}^3\mathbf{r} \left(\alpha|\psi(\mathbf{r})|^2 + \beta|\psi(\mathbf{r})|^4 + \frac{\hbar^2}{2m^*} \left| \left(\nabla - \frac{\mathrm{i}2e}{\hbar c}\mathbf{A}(\mathbf{r}) \right) \psi(\mathbf{r}) \right|^2 + \widetilde{\alpha}\frac{H^2(\mathbf{r})}{8\pi} \right). \tag{3.1.2}$$

However, in this thesis we will not consider the effects of gradient terms or the spatial variation of magnetic fields, and will therefore limit ourselves to generalisations of equation 3.1.1.

3.2 The BCS theory of superconductivity

We now briefly outline the microscopic theory of superconductivity due to Bardeen, Cooper and Schrieffer (BCS). This is built on the proof by Cooper [52] that, in the presence of a filled Fermi sea, two quasiparticles are unstable with respect to the formation of a bound state if

there is an arbitrarily weak potential between them. The full BCS theory [25] is the solution of a closely related many body problem in the mean field approximation. BCS theory has a number of properties that are necessary to explain the phenomena observed in the superconducting state. In the BCS theory the superconducting state contains both normal and superconducting quasiparticles, all the quasiparticles which participate in superconducting are in a single quantum state and, probably most importantly, there is an energy gap between the superconducting ground state and the low lying excited states.

BCS considered the Hamiltonian

$$\mathcal{H}_{BCS} = \sum_{\mathbf{k}\sigma} \varepsilon_{\mathbf{k}} \hat{c}^{\dagger}_{\mathbf{k}\sigma} \hat{c}_{\mathbf{k}\sigma} + V \sum_{\mathbf{k}} \hat{c}^{\dagger}_{\mathbf{k}\uparrow} \hat{c}^{\dagger}_{-\mathbf{k}\downarrow} \hat{c}_{-\mathbf{k}\downarrow} \hat{c}_{\mathbf{k}\uparrow}, \tag{3.2.1}$$

where V is the attractive, on site, (pairing) potential. In BCS theory the 'anomalous averages' $\langle \hat{c}_{\mathbf{k}\uparrow} \hat{c}_{-\mathbf{k}\downarrow} \rangle$ and $\langle \hat{c}^{\dagger}_{\mathbf{k}\uparrow} \hat{c}^{\dagger}_{-\mathbf{k}\downarrow} \rangle$, which are zero in a normal metal, become finite in the superconducting state. It is therefore natural to define the order parameter of the superconducting state, Δ, as

$$\Delta = V \sum_{\mathbf{k}} \langle \hat{c}_{\mathbf{k}\uparrow} \hat{c}_{-\mathbf{k}\downarrow} \rangle \tag{3.2.2}$$

It can be shown [108] that the gap between the superconducting ground state and the excited states is given by $2|\Delta|$. (We will explore some of the consequences of this gap in section 3.5.)

The BCS wavefunction is

$$|\Psi_{BCS}\rangle = \prod_{\mathbf{k}} \left(u(\mathbf{k}) + v(\mathbf{k}) \hat{c}^{\dagger}_{\mathbf{k}\uparrow} \hat{c}^{\dagger}_{-\mathbf{k}\downarrow} \right) |0\rangle \tag{3.2.3}$$

where $|0\rangle$ is the vacuum state. The quantities $u(\mathbf{k})$ and $v(\mathbf{k})$ must be chosen to minimise the free energy and are not independent, but are fixed by the normalisation of the BCS wavefunction which yields

$$|u(\mathbf{k})|^2 + |v(\mathbf{k})|^2 = 1. \tag{3.2.4}$$

Note that the BCS state is not an eigenstate of the number operator. This means that in the BCS state the number of particles, N, is not fixed. However, as a consequence of the N, θ, uncertainty relation the phase, θ, of the order parameter is fixed. Therefore the BCS ground state spontaneously breaks gauge symmetry. This has many interesting consequences, most notably

the Josephson effect (which we will not discuss here, see, for example, Ketterson and Song [108] for details).

BCS theory can also be cast in terms of Green's functions. To do so it is necessary to define the so called anomalous Greens's functions, $\mathcal{F}(\mathbf{r}_1,\tau_1;\mathbf{r}_2,\tau_2)$ and $\mathcal{F}^\dagger(\mathbf{r}_1,\tau_1;\mathbf{r}_2,\tau_2)$, by

$$\mathcal{F}(\mathbf{r}_1,\tau_1;\mathbf{r}_2,\tau_2) = -\Big\langle T_\tau\Big(\widetilde{\psi}_\uparrow(\mathbf{r}_1,\tau_1)\widetilde{\psi}_\downarrow(\mathbf{r}_2,\tau_2)\Big)\Big\rangle \tag{3.2.5}$$

$$\mathcal{F}^\dagger(\mathbf{r}_1,\tau_1;\mathbf{r}_2,\tau_2) = -\Big\langle T_\tau\Big(\widetilde{\overline{\psi}}_\uparrow(\mathbf{r}_1,\tau_1)\widetilde{\overline{\psi}}_\downarrow(\mathbf{r}_2,\tau_2)\Big)\Big\rangle \tag{3.2.6}$$

We can derive equations equivalent to (2.4.10) for the automatic computation of the Green's functions in the superconducting state (we will merely state these here, for details of the derivation see, for example, Abrikosov, Gorkov and Dzyaloshinski [3]). They are

$$\mathcal{G}(\mathbf{k},\omega_n) = -\frac{\mathtt{i}\omega_n + \varepsilon(\mathbf{k}) + \mu}{\omega_n^2 + \varepsilon(\mathbf{k})^2 + |\Delta|^2}, \tag{3.2.7}$$

$$\mathcal{F}(\mathbf{k},\omega_n) = \frac{\Delta}{\omega_n^2 + \varepsilon(\mathbf{k})^2 + |\Delta|^2}, \tag{3.2.8}$$

Clearly as we are only considering Fermions here $\omega_n = (2n+1)\pi T$.

Once the microscopic (BCS) theory of superconductivity had been invented, Gorkov [81] was able to derive the Ginzburg–Landau theory from BCS theory and, in the process, show that $\Delta \propto \psi$. We will undertake a similar procedure in section 5.2.

Further details of BCS theory can be found in many texts, particularly notable examples are the classics by Abrikosov, Gorkov and Dzyaloshinski [3] and de Gennes [56], while for a more modern treatment see Ketterson and Song [108]. In chapter 4 we derive a generalised form of BCS theory from a tight binding model due to Hubbard, conventional BCS theory is recovered from this and some standard results are explored.

3.3 The triplet state its relation to triplet superconductivity

It is well known that the wavefunction of a two body Fermionic system is antisymmetric under the exchange of all labels i.e.

$$\Psi_{\sigma_1\sigma_2}(\mathbf{r}_1,\mathbf{r}_2) = -\Psi_{\sigma_2\sigma_1}(\mathbf{r}_2,\mathbf{r}_1). \tag{3.3.1}$$

By writing the wavefunction as the product of spatial and spin parts,

$$\Psi_{\sigma_1\sigma_2}(\mathbf{r}_1,\mathbf{r}_2) = \phi(\mathbf{r}_1,\mathbf{r}_2)\chi_{\sigma_1\sigma_2} \tag{3.3.2}$$

we arrive at the conclusion that either the spatial part, $\phi(\mathbf{r}_1,\mathbf{r}_2)$, is symmetric and the spin part, $\chi_{\sigma_1\sigma_2}$, is antisymmetric, or the spatial part is antisymmetric while to spin part is symmetric. That is to say,

$$\text{either} \quad \phi(\mathbf{r}_1,\mathbf{r}_2) = \phi(\mathbf{r}_2,\mathbf{r}_1) \quad \text{and} \quad \chi_{\sigma_1\sigma_2} = -\chi_{\sigma_2\sigma_1}, \tag{3.3.3}$$

$$\text{or} \quad \phi(\mathbf{r}_1,\mathbf{r}_2) = -\phi(\mathbf{r}_2,\mathbf{r}_1) \quad \text{and} \quad \chi_{\sigma_1\sigma_2} = \chi_{\sigma_2\sigma_1}. \tag{3.3.4}$$

If the spatial part of the wavefunction is symmetric the spin part must be

$$\frac{1}{\sqrt{2}}\left(|\uparrow\downarrow\rangle - |\downarrow\uparrow\rangle\right). \tag{3.3.5}$$

For an antisymmetric spatial part of the wavefunction there are three possible spin parts:

$$|\uparrow\uparrow\rangle \tag{3.3.6}$$

$$\frac{1}{\sqrt{2}}\left(|\uparrow\downarrow\rangle + |\downarrow\uparrow\rangle\right) \tag{3.3.7}$$

$$|\downarrow\downarrow\rangle. \tag{3.3.8}$$

Thus wavefunctions with an antisymmetric spin part of the wavefunction are known as spin singlet states, while states with a symmetric spin part of the wavefunction are known as spin triplet states. This nomenclature is often generalised from the two body system to the many body system as is appropriate to the behaviour of the many body wavefunction under the exchange of two particles.

In the original formulation of BCS theory of superconductivity the superconducting order parameter, Δ, is defined by (3.2.2). However, in the most general formulation of BCS theory, the order parameter is dependent on the spin of the quasiparticles forming the Cooper pair, the difference in their wavevectors or both. Therefore, in general one must consider a complex, $\mathbf{k}$-dependent, 2×2 matrix order parameter,

$$\underline{\underline{\Delta}}_{\mathbf{k}} = \begin{pmatrix} \Delta_{\uparrow\uparrow}(\mathbf{k}) & \Delta_{\uparrow\downarrow}(\mathbf{k}) \\ \Delta_{\downarrow\uparrow}(\mathbf{k}) & \Delta_{\downarrow\downarrow}(\mathbf{k}) \end{pmatrix} \tag{3.3.9}$$

where,

$$\Delta_{\alpha\beta}(\mathbf{k}) = \sum_{\mathbf{q}} V(\mathbf{k}-\mathbf{q})\langle \hat{c}_{\mathbf{q}\alpha}\hat{c}_{-\mathbf{q}\beta}\rangle. \tag{3.3.10}$$

We can now generalise [12, 23] BCS theory to allow for pairing in a finite angular momentum. This is most simply done by now expand the order parameter[1] in terms of the spherical harmonics, $Y_{lm}(\mathbf{k})$,

$$\Delta(\mathbf{k}) = \sum_{l=0}^{\infty}\sum_{m=-l}^{l} \Delta_{l,m}(\mathbf{k})Y_{l,m}(\hat{\mathbf{k}}). \tag{3.3.11}$$

It is easy to show (see, for example, chapter 1 of Mineev and Samokhin [154] for details) that each value of the orbital angular momentum, l, corresponds to a specific eigenstate of the gap equation[2]. One therefore speaks of superconductivity in a given 'channel', that is to say superconductivity caused by the attraction of a particular $V_l(\mathbf{k},\mathbf{k}')$. By analogy with atomic orbitals the channels are labelled s, p, d, f, g,... corresponding to $l = 0, 1, 2, 3, 4, ...$

It is easy to see from the symmetry of the spherical harmonics that even l superconductors (s, d, g,...) are even under parity inversion[3], these superconductors are therefore labelled singlet superconductors by analogy with the even parity case of the two electron problem. The odd l superconductors (p, f,...) are odd under parity and are therefore labelled triplet superconductors by the same analogy. This also leads to a rather nice picture of the Cooper pairs. One can view the Cooper pair as isolated two electron system, the singlet Cooper pair being in the spin state (3.3.5), while a triplet Cooper pair can be viewed as being in a linear superposition of (3.3.6), (3.3.7) and (3.3.8). Of course it should be remembered that the true many body wavefunction is far more complicated than it is portrayed in the above picture, but the picture can be a powerful aid to intuition.

Keeping in mind what we have said above we now introduce a notation due to Balian and Werthamer [23]. We rewrite the matrix order parameter as

[1] Equivalently we can expand the interaction potential, rather than the order parameter

$$V(\mathbf{k}-\mathbf{k}') = \sum_{l=0}^{\infty} V_l(\mathbf{k},\mathbf{k}') \sum_{m=-l}^{l} Y_{lm}(\mathbf{k})Y^*_{lm}(\mathbf{k}').$$

For examples of this approach see [58, 213].

[2] The gap equation self consistently determines $\Delta_{\alpha\beta}(\mathbf{k})$, as we will see in chapter 4.

[3] Parity inversion is the operation defined to take $\mathbf{r}$ to $-\mathbf{r}$ and hence this operation takes $\mathbf{k}$ to $-\mathbf{k}$.

$$\underline{\underline{\Delta}}_{\mathbf{k}} = \sum_{\mu=0}^{3} d_{\mu}(\mathbf{k}) \underline{\underline{\sigma}}_{\mu} \mathrm{i} \underline{\underline{\sigma}}_{2} \tag{3.3.12}$$

where the $\underline{\underline{\sigma}}_{\mu}$ are the Pauli matrices (including the 2×2 identity matrix, $\underline{\underline{\sigma}}_{0}$.)

We will now prove that $d_0(\mathbf{k})$ transforms as a scalar under rotation, and therefore is the order parameter for singlet superconductivity. Furthermore we will show that

$$\mathbf{d}(\mathbf{k}) \equiv (d_1(\mathbf{k}), d_2(\mathbf{k}), d_3(\mathbf{k})) \tag{3.3.13}$$

transforms as a vector under rotation, and is therefore the order parameter for triplet superconductivity.

We begin by considering rotation about the $\hat{\mathbf{z}}$-axis. When $\underline{\underline{\Delta}}_{\mathbf{k}}$ is rotated through the angle α it becomes [207]

$$\underline{\underline{\Delta}}'_{\mathbf{k}} = \underline{\underline{\widehat{\theta}}}_{\alpha} \underline{\underline{\Delta}}_{\mathbf{k}} \underline{\underline{\widehat{\theta}}}^{\dagger}_{\alpha} \tag{3.3.14}$$

where

$$\underline{\underline{\widehat{\theta}}}_{\alpha} = \begin{pmatrix} e^{-\mathrm{i}\alpha/2} & 0 \\ 0 & e^{\mathrm{i}\alpha/2} \end{pmatrix}. \tag{3.3.15}$$

Hence,

$$\underline{\underline{\Delta}}'_{\mathbf{k}} = \begin{pmatrix} -d'_1(\mathbf{k}) + \mathrm{i}d'_2(\mathbf{k}) & d_0(\mathbf{k}) + \mathrm{i}d'_3(\mathbf{k}) \\ -d_0(\mathbf{k}) + \mathrm{i}d'_3(\mathbf{k}) & d'_1(\mathbf{k}) + \mathrm{i}d'_2(\mathbf{k}) \end{pmatrix} \tag{3.3.16}$$

where

$$\begin{pmatrix} d'_1(\mathbf{k}) \\ d'_2(\mathbf{k}) \\ d'_3(\mathbf{k}) \end{pmatrix} = \begin{pmatrix} \cos\alpha & -\sin\alpha & 0 \\ \sin\alpha & \cos\alpha & 0 \\ 0 & 0 & 1 \end{pmatrix} \begin{pmatrix} d_1(\mathbf{k}) \\ d_2(\mathbf{k}) \\ d_3(\mathbf{k}) \end{pmatrix}. \tag{3.3.17}$$

Similarly, the rotation of a 2×2 matrix through the angle β about the $\hat{\mathbf{y}}$-axis gives

$$\underline{\underline{\Delta}}'_{\mathbf{k}} = \underline{\underline{\widehat{\theta}}}_{\beta} \underline{\underline{\Delta}}_{\mathbf{k}} \underline{\underline{\widehat{\theta}}}^{\dagger}_{\beta} \tag{3.3.18}$$

where

$$\underline{\underline{\widehat{\theta}}}_{\beta} = \begin{pmatrix} \cos\frac{\beta}{2} & -\sin\frac{\beta}{2} \\ \sin\frac{\beta}{2} & \cos\frac{\beta}{2} \end{pmatrix}. \tag{3.3.19}$$

Which gives

$$\underline{\underline{\Delta}}'_{\mathbf{k}} = \begin{pmatrix} -d'_1(\mathbf{k}) + \mathtt{i}d'_2(\mathbf{k}) & d_0(\mathbf{k}) + \mathtt{i}d'_3(\mathbf{k}) \\ -d_0(\mathbf{k}) + \mathtt{i}d'_3(\mathbf{k}) & d'_1(\mathbf{k}) + \mathtt{i}d'_2(\mathbf{k}) \end{pmatrix} \tag{3.3.20}$$

where

$$\begin{pmatrix} d'_1(\mathbf{k}) \\ d'_2(\mathbf{k}) \\ d'_3(\mathbf{k}) \end{pmatrix} = \begin{pmatrix} \cos\beta & 0 & \sin\beta \\ 0 & 1 & 0 \\ -\sin\beta & 0 & \cos\beta \end{pmatrix} \begin{pmatrix} d_1(\mathbf{k}) \\ d_2(\mathbf{k}) \\ d_3(\mathbf{k}) \end{pmatrix}. \tag{3.3.21}$$

There is no need to rotate about the $\hat{\mathbf{x}}$-axis, as any rotation about the $\hat{\mathbf{x}}$-axis can be decomposed into rotations about the $\hat{\mathbf{y}}$ and $\hat{\mathbf{z}}$-axes. Note that in (3.3.16) and (3.3.20) $d_0(\mathbf{k})$ is unchanged by the rotation. Thus $d_0(\mathbf{k})$ transforms as a scalar under rotation. We also note that $\mathbf{d}'(\mathbf{k})$ as defined by (3.3.17) and (3.3.21) is simply what one would find if a vector were rotated by the relevant angles about the relevant axes. Thus, $\mathbf{d}(\mathbf{k})$ transforms as a vector under rotation. The exchange of the spatial labels of a two body system is, of course, equivalent to rotation by π about any axis. Therefore a scalar is even under the exchange of spatial labels and a vector is odd under the same operation.

To further illustrate the relation between the two particle triplet state and triplet superconductivity we note that from 3.3.12 we have

$$d_0(\mathbf{k}) = \frac{1}{2}\Big(\Delta_{\uparrow\downarrow}(\mathbf{k}) - \Delta_{\downarrow\uparrow}(\mathbf{k})\Big) \tag{3.3.22}$$

$$d_1(\mathbf{k}) = \frac{1}{2}\Big(\Delta_{\downarrow\downarrow}(\mathbf{k}) - \Delta_{\uparrow\uparrow}(\mathbf{k})\Big) \tag{3.3.23}$$

$$d_2(\mathbf{k}) = -\frac{\mathtt{i}}{2}\Big(\Delta_{\downarrow\downarrow}(\mathbf{k}) + \Delta_{\uparrow\uparrow}(\mathbf{k})\Big) \tag{3.3.24}$$

$$d_3(\mathbf{k}) = \frac{1}{2}\Big(\Delta_{\uparrow\downarrow}(\mathbf{k}) + \Delta_{\downarrow\uparrow}(\mathbf{k})\Big). \tag{3.3.25}$$

Comparing (3.3.22) and (3.3.25) with (3.3.5) and (3.3.7) respectively we see that $d_0(\mathbf{k})$ is the analogue of the singlet state, where as $d_3(\mathbf{k})$ is analogous to the $S_z = 0$ projection of the spin triplet state. We also note that $d_1(\mathbf{k})$ and $d_2(\mathbf{k})$ are simply linear superpositions of the two equal

spin pairing states (3.3.6) and (3.3.8). Clearly then the singlet state is antisymmetric under exchange of spin labels while the triplet state is symmetric.

Hence, we have shown that the order parameter of a singlet superconductor is symmetric under parity inversion and antisymmetric under the exchange of spin labels. We have also shown that the order parameter of a triplet superconductor is antisymmetric under parity inversion and symmetric under the exchange of spin labels. The states behaviour is therefore the same as that of their two body namesakes under the same operations.

3.4 Unconventional pairing and spin-generalised BCS theory

Many of the qualitative features of BCS theory are the same regardless of whether the pairing state is singlet or triplet. In the rest of this chapter we will explore some of the special features of triplet pairing by considering the prototypical BCS triplet state: superfluid ^{3}He. Further, it is legitimate to consider the rest of this thesis as an exploration of the differences in the behaviour of the singlet and triplet BCS states in an exchange field.

The BCS wavefunction can be extended to allow for either singlet or triplet pairing. (We will describe this formulation of BCS theory as spin-generalised.) The spin-generalised BCS (SGBCS) Hamiltonian is

$$\mathcal{H}_{SGBCS} = \sum_{\mathbf{k}\sigma} \varepsilon_{\mathbf{k}} \hat{c}^{\dagger}_{\mathbf{k}\sigma} \hat{c}_{\mathbf{k}\sigma} + \sum_{\mathbf{k}\mathbf{k}'\alpha\beta} V_{\alpha\beta}(\mathbf{k}-\mathbf{k}') \hat{c}^{\dagger}_{\mathbf{k}\alpha} \hat{c}^{\dagger}_{-\mathbf{k}\beta} \hat{c}_{-\mathbf{k}\beta} \hat{c}_{\mathbf{k}\alpha}, \tag{3.4.1}$$

While the SGBCS wavefunction [213] is

$$|\Psi_{SGBCS}\rangle = \prod_{\mathbf{k}} \prod_{\alpha} \left(u_{\alpha\alpha}(\mathbf{k}) + \sum_{\beta} v_{\alpha\beta}(\mathbf{k}) \hat{c}^{\dagger}_{\mathbf{k}\alpha} \hat{c}^{\dagger}_{-\mathbf{k}\beta} \right) |0\rangle. \tag{3.4.2}$$

The requirement that the SGBCS wavefunction is properly normalised yields

$$\sum_{\alpha\beta} |u_{\alpha\beta}(\mathbf{k})|^2 + |v_{\alpha\beta}(\mathbf{k})|^2 = 1. \tag{3.4.3}$$

It is also useful to extend the definition of anomalous Green's functions so that they can be used to describe the spin-generalised state. To this end we define

$$\mathcal{F}_{\alpha\beta}(\mathbf{r}_1,\tau_1;\mathbf{r}_2,\tau_2) = -\Big\langle T_\tau\Big(\widetilde{\psi}_\alpha(\mathbf{r}_1,\tau_1)\widetilde{\psi}_\beta(\mathbf{r}_2,\tau_2)\Big)\Big\rangle \tag{3.4.4}$$

$$\mathcal{F}^\dagger_{\alpha\beta}(\mathbf{r}_1,\tau_1;\mathbf{r}_2,\tau_2) = -\Big\langle T_\tau\Big(\widetilde{\overline{\psi}}_\alpha(\mathbf{r}_1,\tau_1)\widetilde{\overline{\psi}}_\beta(\mathbf{r}_2,\tau_2)\Big)\Big\rangle \tag{3.4.5}$$

Again we can compute the Green's functions automatically. For a singlet or unitary[4] triplet state

$$\mathcal{G}_{\alpha\beta}(\mathbf{k},\omega_n) = -\frac{\mathtt{i}\omega_n + \varepsilon(\mathbf{k}) + \mu}{\omega_n^2 + \varepsilon(\mathbf{k})^2 + \left|\left|\underline{\underline{\Delta}}_{\mathbf{k}}\right|\right|^2}\delta_{\alpha\beta}, \tag{3.4.6}$$

$$\mathcal{F}_{\alpha\beta}(\mathbf{k},\omega_n) = \frac{\Delta_{\alpha\beta}(\mathbf{k})}{\omega_n^2 + \varepsilon(\mathbf{k})^2 + \left|\left|\underline{\underline{\Delta}}_{\mathbf{k}}\right|\right|^2}. \tag{3.4.7}$$

The generalisation to non-unitary states and other details of the properties of the anomalous Green's functions for the spin-generalised BCS theory are given in Mineev and Samokhin [154] and Sigrist and Ueda [193]. In chapter 4 for we will derive the spin-generalised BCS theory in an exchange field.

3.5 Thermodynamics of the BCS state

As was described above, conventional BCS theory introduces an order parameter, Δ. This order parameter describes the opening of a gap of $2|\Delta|$ at the Fermi level. This means that only elementary excitations with an energy greater than $2|\Delta|$ can exist in the superconducting state. In zero field the superconducting transition is second order, therefore the gap grows from zero at T_C to some maximum value $\big(2\Delta(T=0)\big)$ at absolute zero. However, at the same time the energy available to form excitations (k_BT) decreases as the temperature is lowered. It can be shown [154] that this leads to an exponential decay of thermodynamic quantities at low temperature. For example, at low temperatures specific heat goes as,

$$C_V^{SC} \sim C_V^N \left(\frac{T_C}{T}\right)^{5/2} e^{-|\Delta(0)|/T}. \tag{3.5.1}$$

where C_V^{SC} is the heat capacity in the superconducting state, C_V^N is the heat capacity in the normal state and $\Delta(0)$ is the order parameter at $T=0$.

[4] For a unitary state $\mathbf{d}(\mathbf{k}) \times \mathbf{d}(\mathbf{k})^* = 0$, see section 3.9.6 for details.

The above assumes an isotropic gap, however, as we saw in section 3.4, for states with non-zero angular momentum the order parameter may vary within with $\mathbf{k}$. Thus it is quite possible for the order parameter to go to zero at some point in the Brillouin zone. If this point lies on the Fermi surface it of course means that the gap goes to zero at that point, such a point is known as a node. It is also perfectly possible for there to be lines of nodes on the Fermi surface[5]. The gap going to zero has a profound effect on thermodynamics of the superconductor, as now arbitrary small excitations are allowed at the node. This leads to power law behaviours at low temperatures. Again using specific heat as an example for an isolated point node it can be shown [154] that

$$C_V^{SC} \sim C_V^N \left(\frac{T}{T_C}\right)^3. \tag{3.5.2}$$

While, for a line of nodes

$$C_V^{SC} \sim C_V^N \left(\frac{T}{T_C}\right)^2. \tag{3.5.3}$$

We summarise other the equivalent results for other thermodynamic properties in table 3.1.

3.6 Some properties of superfluid ^{3}He.

Superconductivity and superfluidity are essentially the same phenomena as a superconductor can be viewed is simply a superfluid of electrons. The zero viscosity of the superfluid leads to zero resistivity in a superconductor because of the charge on the electrons.

The first known superfluid was ^{4}He, which has one important difference from a superconductor. ^{4}He is composed of 2 protons, 2 neutrons and 2 electrons are is therefore a Boson. This means that the superfluidity in ^{4}He is much more closely related to Bose–Einstein condensation than BCS superconductivity [160]. On the other hand, ^{3}He is composed of 2 protons, 1 neutron and 2 electrons and is therefore a Fermion. This is of course reminiscent of the electrons in a superconductor. The advent of the BCS theory of superconductivity led to the suggestion [65, 206, 39] that a BCS like mechanism could cause the ^{3}He atoms form Cooper pairs and thus condense into a superfluid.

One obvious difference between a the electrons in a BCS superconductor and the atoms in ^{3}He is the background potential in which they move. The BCS theory of superconductivity

[5] In fact, it is even possible to have gapless superconductivity [193, 108] however, we will not discuss this possibility here.

		nodeless gap	point nodes	line nodes
Specific heat [154, 193]	$C_V^{SC}/C_V^N \sim$	$e^{-\lvert\Delta(0)\rvert/T}$	T^3	T^2
Thermal conductivity[a] [21, 187]	$\kappa/\kappa_N \sim$	$e^{-\lvert\Delta(0)\rvert/T}$	T^2	T
NMR relaxation rate [193]	$\frac{1/T_1^{SC}}{1/T_1^N} \sim$	$e^{-\lvert\Delta(0)\rvert/T}$	T^5	T^3
Penetration depth[a,b][14]	$\frac{\lambda(0)-\lambda(T)}{\lambda(0)} \sim$	$e^{-\lvert\Delta(0)\rvert/T}$	T^2	T
Normal fluid density[b][213]	$\rho_N \sim$			
Magnetic susceptibility[b][213, 154]	$\chi^{SC}/\chi^N \sim$	$e^{-\lvert\Delta(0)\rvert/T}$	T^2	T

Table 3.1: The temperature dependence of various thermodynamic and transport properties at low temperatures.

[a] In a polycrystalline sample: in a single crystal thermal conductivity and penetration depth can be used to investigate the location of the nodes as they are *directional probes*.

[b] For a singlet superconductor. For an anisotropic triplet superconductor the situation is somewhat more complicated. However, the normal fluid density tensor and the magnetic susceptibility tensor can be expressed in terms of the Yosida function (which we will discuss in section 3.9 in the context of magnetic susceptibity, however, the treatment of the normal density tensor is broadly similar [213] to that of the magnetic susceptibility). The anisotropy in the normal fluid density was important in the identification of the phases of ^{3}He and thus many books on the subject of ^{3}He deal with the normal fluid density in far greater detail than space permits here.

introduces an effective attractive potential which causes the conduction electrons to form Cooper pairs. Frölich suggested [74] that this attraction arises from the electron–phonon interaction[7]. Hence, in ^{3}He where there is no crystal lattice, and hence no phonons another pairing mechanism must be at work.

The interatomic potential in ^{3}He is well described by van der Waals theory. Thus the main features of the potential are the strong 'hard core' repulsion at short distances and the weak attraction at medium separations. It is therefore clear that the quasiparticles be spatially separated to avoid the hard core repulsion and hence, that the Cooper pairs must have non-zero angular momentum. Pitaevskii [169] calculated the transition temperature of ^{3}He based on the van der Waals potential, but found that T_C was unfeasibly low. This is because the Cooper pairs in ^{3}He are not formed from bare ^{3}He atoms but from the quasiparticles of Landau's Fermi liquid theory.

[7] This suggestion was latter made into a quantitative theory by Eliashberg [62, 63]. In fact BCS theory emerges as the week coupling limit of Eliashberg theory and as such one can calculate the BCS effective potential, V, in terms of the electron phonon coupling constant, λ. It turns out that $D(\varepsilon_F)V = \lambda$ where $D(\varepsilon_F)$ is the density of states at the Fermi level. For an excellent discussion of Eliashberg theory see [214], or for a discussion within the tight binding model see [22].

The effective mass of the quasiparticles in ^{3}He can have as much as six times that of the unrenormalised mass of a ^{3}He atom. This large renormalisation effect is largely due to ferromagnetic spin–fluctuation effects. (This can be seen from the qualitative agreement of the thermodynamic and transport properties calculated from spin–fluctuation theory with experiment [31, 59, 34, 35, 176, 177, 37, 179].) Emery [64] showed that ferromagnetic spin–fluctuations favour spin–triplet states over spin–singlet states and it indeed turns out that ^{3}He is a triplet superfluid. ^{3}He therefore became the first known superconducting/superfluid system in which the order parameter does not have an s-wave symmetry. ^{3}He is therefore the prototypical triplet system and as such will often be referred to in this thesis.

In 1975 Leggett published one of the most influential papers [123] in the story of triplet superfluidity/superconductivity. In this review he summarised much of what had been done before and laid the groundwork of the unambiguous identification of the superfluid phases of ^{3}He. Although Leggett's article is highly readable and an excellent place to learn about triplet superfluidity/superconductivity, ^{3}He (along with its isotopic cousin ^{4}He) is one of the best characterised materials in nature and much has been discovered about ^{3}He since 1975. There are some excellent textbooks on the physics of helium at low temperatures, among the best are the classic text by Vollhardt and Wölfle [213], the compilation edited by Bennemann and Ketterson [28] and a more recent and comprehensive text has been written by Dobbs [58].

3.7 The (experimental) phase diagram of superfluid ^{3}He

One strong indication of triplet superconductivity/superfludity is the existence of multiple superconducting/superfluid phases. We will begin by considering the phase diagram of ^{3}He in zero field (figure 3.1). At ambient pressure ^{3}He is superfluid down to the very lowest temperatures, only becoming a solid at pressures greater than 3.44 MPa (at $T = 0$)[8]. The critical temperature, T_C, varies from 0.929 mK at $P = 0$ to 2.49 mK at the point labelled T_A in figure 3.1. However, at the so-called polycritical point, P ($T = 2.273$ mK, $P = 2.122$ MPa), there is a line, T_{AB}, of first order transitions which terminates at $T_{B'}$ (1.93 mK). This phase transition thus occurs entirely within the superfluid region i.e. it is a transition between two superfluid phases. The two phases where labelled the A and B phases as shown in the diagram.

We now consider the phase diagram of ^{3}He in a finite magnetic field (see figure 3.2). The most important feature to notice is the appearance of a phase transition within the A phase. The

[8] All data in this paragraph is taken from Dobbs [58].

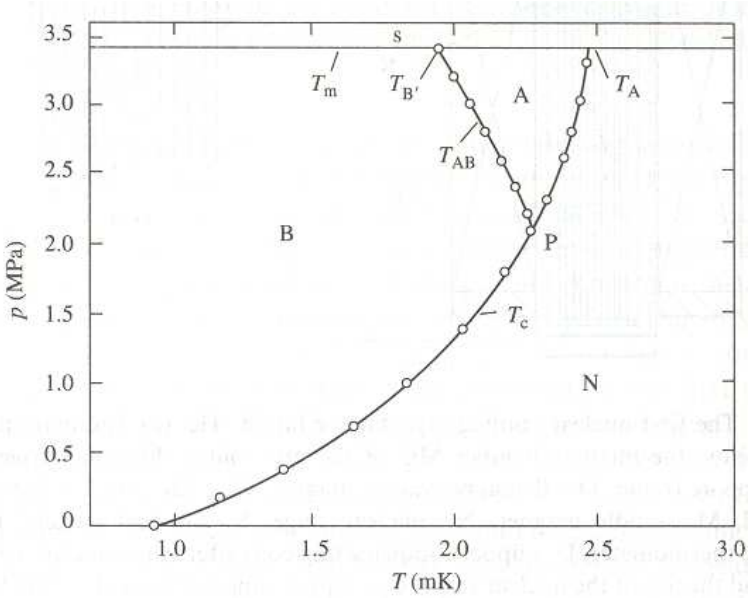

Figure 3.1: The experimentally determined phase diagram (P, T) of ^{3}He in zero magnetic field, taken from Dobbs [58].

two new phases we will label (with the advantage of hindsight) the A_1 and A_2 phases as indicated in figure 3.2. The higher temperature A_1 phase is therefore separated from the A phase by a phase transition, where as there is no phase transition between the A and A_2 phases. The fact that there is a crossover between the A and A_2 means that the A_2 phase is often mislabelled the A phase or described as the 'A phase in a magnetic field' [213]. However, there are many important differences between the A phase and the A_2 phase. We shall introduce some of these differences in section 3.8 before discussing them in more detail in chapter 5. We should also note that in a magnetic field the B phase crosses over to the B_2 phase. We will discuss the nature of these phases in section 3.9.

3.8 The Ginzburg-Landau theory of superfluidity in ^{3}He

In section 3.1 we saw that a superconductor is described by a single, complex order parameter. This is the appropriate theory for a singlet (s-wave) superconductor. To describe a triplet superconductor we will need to introduce more degrees of freedom. Firstly, there are three spin projections, therefore we must have an order parameter for each. However, the order parameter of a triplet superconductor must transform as a vector under rotation (see section 3.3 for details) and so, the order parameter must have a (linear - in the p-wave case) k-dependence.

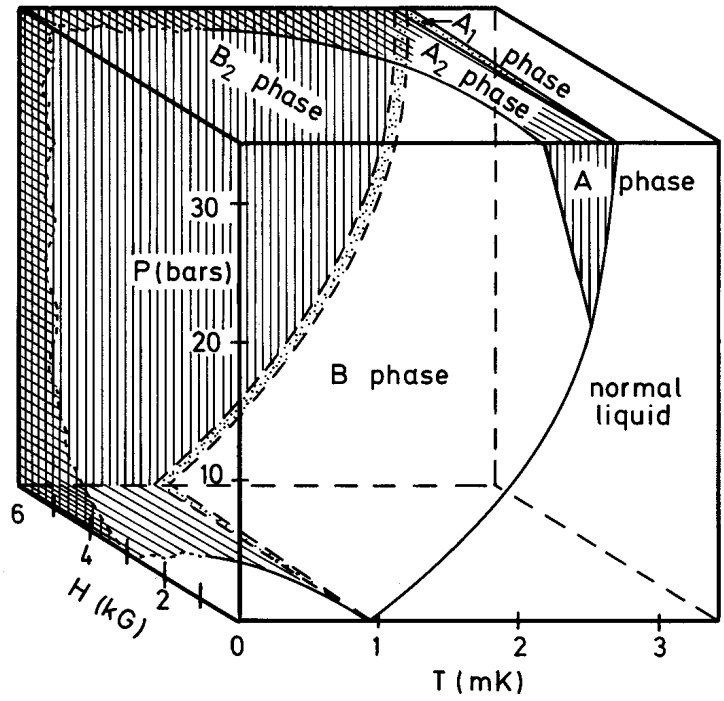

Figure 3.2: The experimentally determined phase diagram (P, T, H) of ^{3}He in a finite magnetic field, taken from Vollhardt and Wölfle [213].

(In three dimensions) there are three linearly independent k variables and therefore each spin projection has three degrees of freedom. To describe a p-wave superconductor or superfluid we therefore require a three by three matrix order parameter, $\underline{\underline{A}}$, which is related to the microscopic order parameter, $\mathbf{d}(\mathbf{k})$ by

$$\mathbf{d}(\mathbf{k}) = \underline{\underline{A}}\,\hat{\mathbf{k}}. \tag{3.8.1}$$

Barton and Moore [26] considered superfluids with non-zero angular momentum, l. They showed that a singlet superconductor/superfluid is described by $(1+l)$ fourth order (β) Ginzburg–Landau terms and that a triplet superconductor is described by $(3l+2)$ fourth order Ginzburg–Landau terms. This means that a p-wave superconductor/superfluid such as ^{3}He has five fourth order terms. The free energy of condensation is given by,

$$\begin{aligned} F_{SC} - F_N &= \alpha\,\mathrm{tr}(\underline{\underline{A}}\,\underline{\underline{A}}^\dagger) + \beta_1|\mathrm{tr}(\underline{\underline{A}}\,\underline{\underline{A}}^T)|^2 + \beta_2\left[\mathrm{tr}(\underline{\underline{A}}\,\underline{\underline{A}}^\dagger)\right]^2 + \beta_3\mathrm{tr}\left[(\underline{\underline{A}}\,\underline{\underline{A}}^T)(\underline{\underline{A}}\,\underline{\underline{A}}^T)^*\right] \\ &\quad +\beta_4\mathrm{tr}\left[(\underline{\underline{A}}\,\underline{\underline{A}}^\dagger)^2\right] + \beta_5\mathrm{tr}\left[(\underline{\underline{A}}\,\underline{\underline{A}}^\dagger)(\underline{\underline{A}}\,\underline{\underline{A}}^\dagger)^*\right]. \end{aligned} \tag{3.8.2}$$

This is commonly rewritten as

$$F_{SC} - F_N = \alpha\, tr(\underline{\underline{A}}\,\underline{\underline{A}}^\dagger) + \sum_{i=1}^{5}\beta_i I_i \tag{3.8.3}$$

where

$$I_1 = |tr(\underline{\underline{A}}\,\underline{\underline{A}}^T)|^2, \tag{3.8.4}$$

$$I_2 = \left[tr(\underline{\underline{A}}\,\underline{\underline{A}}^\dagger)\right]^2, \tag{3.8.5}$$

$$I_3 = tr\left[(\underline{\underline{A}}\,\underline{\underline{A}}^T)(\underline{\underline{A}}\,\underline{\underline{A}}^T)^*\right], \tag{3.8.6}$$

$$I_4 = tr\left[(\underline{\underline{A}}\,\underline{\underline{A}}^\dagger)^2\right], \tag{3.8.7}$$

$$I_5 = tr\left[(\underline{\underline{A}}\,\underline{\underline{A}}^\dagger)(\underline{\underline{A}}\,\underline{\underline{A}}^\dagger)^*\right]. \tag{3.8.8}$$

In the (BCS) weak coupling limit the Ginzburg–Landau coefficients take the following values,

$$\alpha(T) = -D(\varepsilon_F)\left(1 - \frac{T}{T_C}\right) \tag{3.8.9}$$

$$\beta_2 = \beta_3 = \beta_4 = -\beta_5 = -2\beta_1 = 2\beta_0 \tag{3.8.10}$$

where

$$\beta_0 = \frac{21}{40}\zeta(3)D(\varepsilon_F)(\pi k_B T_C)^{-2} \tag{3.8.11}$$

and $D(\varepsilon_F)$ is the density of states at the Fermi level.

In section 3.9.4 we will explore the validity of the weak coupling approximation for superfluid ^{3}He.

3.9 The superfluid phases of ^{3}He

The first theoretical investigations [12, 23] of triplet superfluid/superconducting phases where carried out before the experimental discovery of superfluidity in ^{3}He. After superfluidity had been observed in ^{3}He more systematic searches for the superfluid phases that are stable in different regions of parameter (β) space were conducted [27, 43]. We shall now proceed to discuss some of the more important phases in a quasi-historical order, beginning with ABM and BW states in zero field. We shall then discuss the phases which are stable in a magnetic field and give some details of some other (theoretically) possible phases.

3.9.1 The ABM phase

The first people to investigate triplet superconductivity where Anderson, Brinkman and Morel (ABM) [12, 10]. They chose 'more or less by chance' [11] to consider the state

$$\underline{\underline{A}} = \frac{1}{\sqrt{2}}\begin{pmatrix} 1 & \mathtt{i} & 0 \\ 0 & 0 & 0 \\ 0 & 0 & 0 \end{pmatrix}, \tag{3.9.1}$$

$$\mathbf{d}(\mathbf{k}) \sim (k_x + \mathtt{i}k_y, 0, 0). \tag{3.9.2}$$

This state has nodes (zeros of the order parameter at the Fermi energy) at $k_x = k_y = 0$ i.e. at the north and south poles of a spherical Fermi surface, see figure 3.3.

The ABM state breaks time reversal symmetry (TRS) due to the complex nature of the order parameter. To see the breaking of TRS consider the operation $\mathcal{T}$ which maps T to $-T$,

$$\mathcal{T}\mathbf{k} \;=\; -\mathbf{k} \tag{3.9.3}$$

Figure 3.3: The gap of the ABM state.

and

$$\mathcal{T}\sigma \;=\; -\sigma. \tag{3.9.4}$$

Therefore by (3.3.12),

$$\mathcal{T}\mathbf{d}(\mathbf{k}) = -\mathbf{d}^*(-\mathbf{k}). \tag{3.9.5}$$

Hence the ABM phase breaks TRS.

The ABM state has equal pairing amplitudes in the two equal spin pairing (ESP) states $\big(|\uparrow\uparrow\rangle$ and $|\downarrow\downarrow\rangle\big)$ and no pairing in the $S_z = 0$ projection $\Big(\frac{1}{\sqrt{2}}\big(|\uparrow\downarrow\rangle + |\downarrow\uparrow\rangle\big)\Big)$. Thus we see that vector order parameter, $\mathbf{d}(\mathbf{k})$ points perpendicular to the spin of the Cooper pair.

3.9.2 The BW phase

Balian and Werthamer (BW) showed [23] that, in the weak coupling limit, the state which gives the absolute minimum of free energy is

$$\underline{\underline{A}} = \frac{1}{\sqrt{3}} \begin{pmatrix} 1 & 0 & 0 \\ 0 & 1 & 0 \\ 0 & 0 & 1 \end{pmatrix}, \tag{3.9.6}$$

$$\mathbf{d}(\mathbf{k}) \sim (k_x, k_y, k_z). \tag{3.9.7}$$

Figure 3.4: The gap of the BW state.

The BW state is clearly isotropic (see figure 3.4). Therefore it is thermodynamically indistinguishable from the s-wave (BCS) state. As, modulo a complex phase, the BW is real it does not break TRS. The BW state has equal pairing amplitudes for all three of the triplet pairing states.

3.9.3 The Yosida function and the identification of the superfluid states of the experimental (A and B) phases

For a singlet superconductor, the magnetic susceptibility, $\chi \to 0$ as $T \to 0$ (see table 3.1 for details). This is because as $T \to 0$, the number of quasiparticles that have formed Cooper pairs increases, until at $T = 0$ there are no unpaired quasiparticles. Singlet Cooper pairs have zero spin, therefore electrons that are paired up do not contribute to (the dominant Pauli term of) the magnetic susceptibility.

The ABM phase is has ESP only i.e. the spin 1 Cooper pairs are in the $S_z = 1$ and $S_z = -1$ projections for $\mathbf{H} \parallel \hat{z}$. This means that the Cooper pair contribute fully to the susceptibility and, in the weak coupling limit,

$$\chi_{SC} = \chi_N. \tag{3.9.8}$$

The BW phase contains all three projections. The $S_z = \pm 1$ pairs contribute to the magnetic susceptibility as in the ABM phase. Where as the $S_z = 0$ pairs do not contribute to the susceptibility for the same reasons as singlet pairs do not. As one third of the pairs are in the $S_z = 0$ projection

$$\chi_{SC} = \frac{2}{3}\chi_N. \tag{3.9.9}$$

at $T = 0$ in the weak coupling limit.

The magnetic susceptibility of a superconductor/superfluid was first studied by Yosida[9] [222], who introduced the function $Y(T)$. For a singlet superconductor the Yosida function is defined by

$$\chi_{SC}(T) = Y(T)\chi_N(T). \tag{3.9.10}$$

This can of course be generalised to triplet superconductivity. The temperature dependence of the Yosida function depends on the node structure of the gap (table 3.1). As we have seen in the weak coupling limit Cooper pairs with their spin (anti)parallel to the magnetic field do not contribute to the magnetic susceptibility. Thus we define

$$\chi_{SC}(T) = \left(\frac{N_\parallel}{N_{SC}} + \frac{N_\perp}{N_{SC}}Y(T)\right)\chi_N(T). \tag{3.9.11}$$

Which clearly regains (3.9.10) for a singlet superconductor/superfluid. For the two phases we are discussing here we have

$$\chi_{ABM}(T) = \chi_N(T) \qquad \|\mathbf{d}(\mathbf{k}), \tag{3.9.12}$$

$$\chi_{ABM}(T) = \chi_N(T)Y(T), \qquad \perp \mathbf{d}(\mathbf{k}), \tag{3.9.13}$$

$$\chi_{BW}(T) = \chi_N(T)\left(\frac{2}{3} + \frac{1}{3}Y(T)\right). \tag{3.9.14}$$

The magnetic susceptibility as measured [217] by the NMR Knight [123] shift and other thermodynamic measurements [123, 217] which determined the nodal structure allowed the identification [123, 148] of the theoretical ABM and BW phases, with the experimental A and B phases respectively[10]. From now on we will use the terms A phase and ABM phase interchangeably. Similarly, the term B phase is synonymous with the term BW phase.

[9] Prof. Yosida's name is often confused with the more common Japanese name Yoshida.

[10] It is worth noting the felicity of this coincidence as the experimental phases were named before this identification was made. One can easily imagine the level of confusion if the naming convention had been the reverse! One might also recall that in the past physicists have been particularly unlucky when choosing seemingly arbitrary conventions, for example the charge on the electron (or equivalently the direction of conventional current) or the strangeness of the strange quark.

	BW	ABM
κ_{BCS}	1	1.2
κ_{SC}, 1.2MPa	0.829	0.916
κ_{SC}, 2.4MPa	0.759	0.783
κ_{SC}, 3.44MPa	0.716	0.678

Table 3.2: Values of $\kappa(\propto F$ for $T \lesssim T_C)$ at various pressures from Sauls and Serine [186] and in the BCS limit after Leggett [123].

3.9.4 Strong coupling corrections and the stabilisation of the A phase

We stated above that the B phase is the ground state in the weak coupling limit. This begs the question, why is the A phase also seen experimentally in ^{3}He? The obvious answer turns out to be correct, strong coupling corrections, in particular paramagnon effects [123, 10, 148], are important in ^{3}He .

The strong coupling corrections are pressure dependent, which allows different phases to be stable in different regions of the phase diagram, as is observed. To quantify this we introduce the variable κ defined by

$$\kappa = \frac{3}{5}\sum_{i=1}^{5}\beta_i I_i. \tag{3.9.15}$$

It can be shown [58] that near T_C

$$F \propto \kappa. \tag{3.9.16}$$

Table 3.2 shows the values of κ at various pressures after Sauls and Serine [186]. Also shown are the weak coupling (BCS) values after Leggett [123]. It can clearly be seen that at the highest pressure shown the A phase has the lowest free energy near T_C, where as at the lower pressures the B phase is stable.

3.9.5 The $\mathbf{A_1}$ phase

We have stated above that the A and B phases are not stable in a magnetic field so we will now consider the phases observed in a magnetic field.

We begin by introducing the A_1 phase, which has the order parameter,

$$\underline{\underline{A}} = \frac{1}{\sqrt{2}} \begin{pmatrix} 1 & \mathtt{i} & 0 \\ \mathtt{i} & -1 & 0 \\ 0 & 0 & 0 \end{pmatrix}, \tag{3.9.17}$$

$$\mathbf{d}(\mathbf{k}) \sim (k_x + \mathtt{i}k_y, \mathtt{i}(k_x + \mathtt{i}k_y), 0)\,. \tag{3.9.18}$$

It is interesting to note that in the A_1 phase

$$\mathbf{d}(\mathbf{k}) \times \mathbf{d}^*(\mathbf{k}) = (0, 0, -2i(|k_x|^2 + |k_y|^2)) \tag{3.9.19}$$

and

$$\underline{\underline{\Delta}}_{\mathbf{k}} \underline{\underline{\Delta}}^{\dagger}_{\mathbf{k}} \sim \begin{pmatrix} k_x^2 + k_y^2 & 0 \\ 0 & 0 \end{pmatrix}. \tag{3.9.20}$$

Because $\underline{\underline{\Delta}}_{\mathbf{k}}$ is not unitary, the A_1 phase is described as a *non-unitary phase*. In general any phase for which $\mathbf{d}(\mathbf{k}) \times \mathbf{d}^*(\mathbf{k}) \neq 0$ is non-unitary. The *only possible* unitary phases are the BW, ABM, planar and polar states. (See table 3.3.)

Note that $\mathbf{d}(\mathbf{k}) \times \mathbf{d}^*(\mathbf{k})$ is purely imaginary, which is easily verified as

$$\begin{aligned} [\mathbf{d}(\mathbf{k}) \times \mathbf{d}^*(\mathbf{k})]^* &= \mathbf{d}(\mathbf{k})^* \times \mathbf{d}(\mathbf{k}) \\ &= -\mathbf{d}(\mathbf{k}) \times \mathbf{d}^*(\mathbf{k}). \end{aligned} \tag{3.9.21}$$

The A_1 phase has zero pairing amplitude in the $|\downarrow\downarrow\rangle$ and $\frac{1}{\sqrt{2}}(|\uparrow\downarrow\rangle + |\downarrow\uparrow\rangle)$ states and so only has finite pairing in the $|\uparrow\uparrow\rangle$ state. The A_1 has the same nodal structure as the A phase, that is point nodes at the north and south poles ($k_x = k_y = 0$, see figure 3.3). We can of course construct the state

$$\mathbf{d}(\mathbf{k}) \sim (k_x + \mathtt{i}k_y, -\mathtt{i}(k_x + \mathtt{i}k_y), 0)\,. \tag{3.9.22}$$

This is also an A_1 phase. However, in this case we have pairing in the $|\downarrow\downarrow\rangle$ channel but none in the $|\uparrow\uparrow\rangle$ or $\frac{1}{\sqrt{2}}(|\uparrow\downarrow\rangle + |\downarrow\uparrow\rangle)$ channels.

3.9.6 The A_2 phase

The order parameter of the A_2 phase is

$$\underline{\underline{A}} = \frac{1}{\sqrt{2}} \begin{pmatrix} 1 & \mathtt{i} & 0 \\ \mathtt{i}\kappa & -\kappa & 0 \\ 0 & 0 & 0 \end{pmatrix}, \tag{3.9.23}$$

$$\mathbf{d}(\mathbf{k}) \sim (k_x + \mathtt{i}k_y, \mathtt{i}\kappa(k_x + \mathtt{i}k_y), 0) \tag{3.9.24}$$

where

$$\kappa = \frac{\Delta_{\downarrow\downarrow} - \Delta_{\uparrow\uparrow}}{\Delta_{\downarrow\downarrow} + \Delta_{\uparrow\uparrow}} \sim -\frac{N_\uparrow - N_\downarrow}{N_\uparrow + N_\downarrow}. \tag{3.9.25}$$

Clearly the A_2 is non-unitary and has the same nodal structure as the A and A_1 phases.

The A_2 phase is described by the parameter κ, which is a function of H and T. Phases whose order parameters depend on the state variables where named *non-inert* by Barton and Moore [27]. All the other phases considered above are *inert* that is, they are independent of the state variables.

We now see that where as the A phase corresponds to equal pairing amplitudes in the $|\uparrow\uparrow\rangle$ and the $|\downarrow\downarrow\rangle$ channels and the A_1 phase corresponds to a finite pairing amplitude in one spin state only, the A_2 phase has finite, but different, pairing amplitudes in the $|\uparrow\uparrow\rangle$ and $|\downarrow\downarrow\rangle$ channels. Thus when $\kappa = 0$ the A_2 becomes the A phase, this is a crossover because it is simply two pairing amplitudes becoming equal. Experimentally this is observed as $|\mathbf{H}| \to 0$ and no phase transition is seen. When $\kappa = \pm 1$ the A_2 phase becomes the A_1 phase, which means that the pairing amplitude for one spin state goes to zero. Clearly this is a phase transition. Experimentally the boundary between the A_1 and A_2 phases is a phase transition, so our description of the physics is in agreement with experiment.

An analogy may be drawn between the A phases of ^{3}He and the description of elliptically polarised light in optics [33]. One can think of the three axial (A, A_1 or A_2) phases as being described by an ellipse of eccentricity $\sqrt{1-\kappa^2}$. The A phase is the special case of linear polarisation when the ellipse reduces to a line parallel to $\mathbf{d}(\mathbf{k})$. The A_1 phase is the special case of circularly polarised light a circle which lies in the x,y-plane. The A_2 phase corresponds to any ellipse between these two extremes.

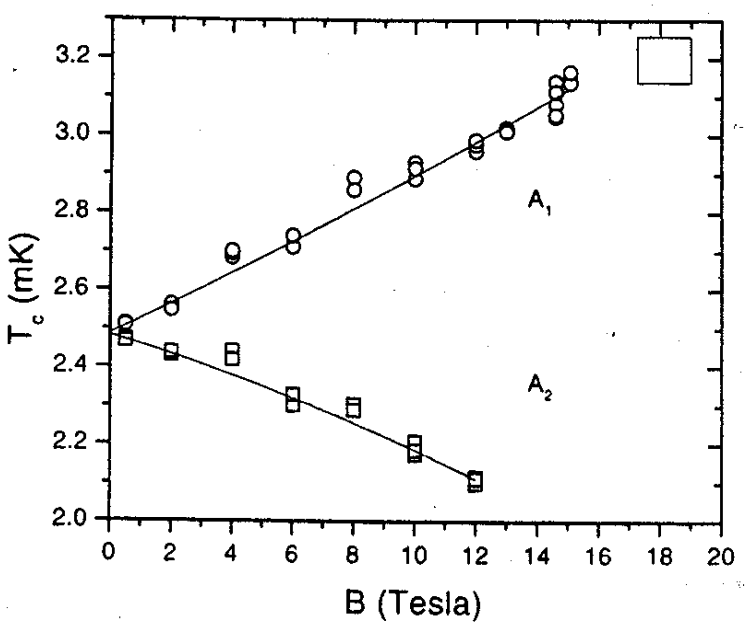

Figure 3.5: The splitting of the A_1 and A_2 phases by a magnetic field as measured by Remeijer *et al*. [175].

3.9.7 Splitting of the A_1 and A_2 phases by a magnetic field

In magnetic field there are three phase transitions (see figure 3.2). We will now focus on the transition from the normal state to the A_1 phase which we will call T_{A_1}, and the transition from the A_1 phase to the A_2 phase which we call T_{A_2}.

It is observed experimentally [175] that, at a constant pressure, T_{A_1} increases and conversely T_{A_2} decreases with an applied field (see figure 3.5). This is in qualitative agreement with the results of Ginzburg–Landau theory when the calculations include strong coupling corrections [104].

In a magnetic field, the coefficient of the quadratic term, α, of the Ginzburg–Landau expansion (3.8.2) becomes [175]

$$\alpha_{\uparrow,\downarrow} = -D(\varepsilon_F)\left(1 - \frac{T}{T_C}\right) \pm \eta|\mathbf{H}|. \tag{3.9.26}$$

As in Ginzburg–Landau theory T_C is the temperature at which $\alpha = 0$, a magnetic field clearly splits the transition temperature on the two (spin) sheets of the Fermi surface. In the BCS theory the transition temperature is given by [214]

$$T_C \sim e^{-1/VD(\varepsilon_F)}. \tag{3.9.27}$$

For ESP states in a magnetic field this becomes [213]

$$T_C^{\uparrow,\downarrow} \sim e^{-1/\lambda^{\uparrow,\downarrow}} \tag{3.9.28}$$

where, to first order in $\mathbf{H}$,

$$\lambda^{\uparrow,\downarrow} = VD(\varepsilon_F) \pm \mu_B |\mathbf{H}| V \frac{\partial D(\varepsilon_F)}{\partial \varepsilon_F}. \tag{3.9.29}$$

Thus, the splitting of T_{A_1} and T_{A_2} is equivalent to a splitting in the $|\uparrow\uparrow\rangle$ and $|\downarrow\downarrow\rangle$ transition temperatures. Which to first order in $\mathbf{H}$ split linearly with the applied field, in good agreement with experiment.

3.9.8 The B_2 phase

In a magnetic field the B phase is unstable with respect to the B_2 phase whose order parameter is

$$\underline{\underline{A}} = \frac{1}{\sqrt{3}} \begin{pmatrix} 1 & \mathrm{i}\kappa & 0 \\ -\mathrm{i}\kappa & 1 & 0 \\ 0 & 0 & 1 \end{pmatrix}, \tag{3.9.30}$$

$$\mathbf{d}(\mathbf{k}) \sim (k_x + \mathrm{i}\kappa k_y, k_y - \mathrm{i}\kappa k_x, k_z)\,. \tag{3.9.31}$$

where κ is given by equation 3.9.25. It is clear from the above discussion that the B_2 phase in non-unitary and non-inert.

3.9.9 Other stable phases of triplet superconductors/superfluids

We have now discussed all of the phases which have been observed in ^{3}He . We will conclude this section by detailing some phases which have been found to be stable in certain regions of phase space, both in zero field and in a finite magnetic field. The results in this tables 3.3 and 3.4 summarise Vollhardt and Wölfle [213] and Barton and Moore [27].

Polar	$\begin{pmatrix} 1 & 0 & 0 \\ 0 & 0 & 0 \\ 0 & 0 & 0 \end{pmatrix}$	$(k_x, 0, 0)$	inert unitary
α	$\frac{1}{\sqrt{3}} \begin{pmatrix} 1 & 0 & 0 \\ 0 & e^{-\mathrm{i}2\pi/3} & 0 \\ 0 & 0 & e^{\mathrm{i}2\pi/3} \end{pmatrix}$	$\left(k_x, k_y e^{-\mathrm{i}2\pi/3}, k_z e^{\mathrm{i}2\pi/3}\right)$	inert non-unitary
β	$\begin{pmatrix} 1 & 0 & 0 \\ \mathrm{i} & 0 & 0 \\ 0 & 0 & 0 \end{pmatrix}$	$(k_x, \mathrm{i}k_x, 0)$	inert non-unitary
Axi-planar	$\begin{pmatrix} 0 & \sin\theta\sin\phi & 0 \\ -\cos\theta & 0 & \mathrm{i}\sin\theta\cos\phi \\ 0 & 0 & 0 \end{pmatrix}$	$\begin{pmatrix} \sin\theta\sin\phi k_y, \\ -\cos\theta k_x + \mathrm{i}\sin\theta\cos\phi k_z, \\ 0 \end{pmatrix}$	non-inert non-unitary
δ	$\begin{pmatrix} 0 & -\cos\theta & 0 \\ \sin\theta\sin\phi & 0 & 0 \\ 0 & \mathrm{i}\sin\theta\cos\phi & 0 \end{pmatrix}$	$\begin{pmatrix} -\cos\theta k_y, \\ \sin\theta\sin\phi k_x, \\ \mathrm{i}\sin\theta\cos\phi k_y \end{pmatrix}$	non-inert non-unitary
ϵ	$\begin{pmatrix} 0 & 0 & \cos\theta \\ 0 & 0 & \mathrm{i}\cos\theta \\ \sin\theta & \mathrm{i}\sin\theta & 0 \end{pmatrix}$	$\begin{pmatrix} \cos\theta k_z, \\ \mathrm{i}\cos\theta k_z, \\ \sin\theta k_x + \mathrm{i}\sin\theta k_y \end{pmatrix}$	non-inert non-unitary
ζ	$\begin{pmatrix} -\sin\theta\cos\phi & -\mathrm{i}\sin\theta\sin\phi & 0 \\ -\mathrm{i}\sin\theta\sin\phi & \sin\theta\cos\phi & 0 \\ 0 & 0 & \sqrt{2}\cos\theta \end{pmatrix}$	$\begin{pmatrix} -\sin\theta\cos\phi k_x - \mathrm{i}\sin\theta\sin\phi k_y, \\ -\mathrm{i}\sin\theta\sin\phi k_x + \sin\theta\cos\phi k_y, \\ \sqrt{2}\cos\theta k_z \end{pmatrix}$	non-inert non-unitary

Table 3.3: The order parameters of some triplet phases, after Vollhardt and Wölfle [213] and Barton and Moore [27].

Phase	$\underline{\underline{A}}$	$\mathbf{d}(\mathbf{k})$	
A (ABM, axial)	$\frac{1}{\sqrt{2}}\begin{pmatrix} 1 & \mathtt{i} & 0 \\ 0 & 0 & 0 \\ 0 & 0 & 0 \end{pmatrix}$	$(k_x + \mathtt{i}k_y, 0, 0)$	inert unitary
A_1 (γ, axial)	$\frac{1}{2}\begin{pmatrix} 1 & \mathtt{i} & 0 \\ \mathtt{i} & -1 & 0 \\ 0 & 0 & 0 \end{pmatrix}$	$(k_x + \mathtt{i}k_y, \mathtt{i}(k_x + \mathtt{i}k_y), 0)$	inert non-unitary
A_2 (axial)	$\frac{1}{\sqrt{2\kappa}}\begin{pmatrix} 1 & \mathtt{i} & 0 \\ \mathtt{i}\kappa & -\kappa & 0 \\ 0 & 0 & 0 \end{pmatrix}$	$(k_x + \mathtt{i}k_y, \mathtt{i}\kappa(k_x + \mathtt{i}k_y), 0)$	non-inert non-unitary
B (BW, isotropic)	$\frac{1}{\sqrt{3}}\begin{pmatrix} 1 & 0 & 0 \\ 0 & 1 & 0 \\ 0 & 0 & 1 \end{pmatrix}$	(k_x, k_y, k_z)	inert unitary
B_2 (oblate)	$\frac{1}{\sqrt{3}}\begin{pmatrix} 1 & \mathtt{i}\kappa & 0 \\ -\mathtt{i}\kappa & 1 & 0 \\ 0 & 0 & 1 \end{pmatrix}$	$(k_x + \mathtt{i}\kappa k_y, k_y - \mathtt{i}\kappa k_x, k_z)$	non-inert non-unitary
Bipolar	$\frac{1}{\sqrt{2}}\begin{pmatrix} 1 & 0 & 0 \\ 0 & i & 0 \\ 0 & 0 & 0 \end{pmatrix}$	$(k_x, \mathtt{i}k_y, 0)$	inert non-unitary
Planar (B_1)	$\frac{1}{\sqrt{2}}\begin{pmatrix} 1 & 0 & 0 \\ 0 & 1 & 0 \\ 0 & 0 & 0 \end{pmatrix}$	$(k_x, k_y, 0)$	inert unitary

Phase	Synonyms	I_1	I_2	I_3	I_4	I_5	stable region
A	ABM, axial	0	1	0	1	1	$\beta_1, \beta_3 > 0; \beta_3\beta_4 < 0$
A_1	γ, axial	0	1	0	1	0	$\beta_3, \beta_5 > 0; \beta_4 < 0$
B	BW, isotropic	1	1	$\frac{1}{3}$	$\frac{1}{3}$	$\frac{1}{3}$	weak coupling, $-\beta_1, \beta_4 \to \infty$
Bipolar		0	1	$\frac{1}{2}$	$\frac{1}{2}$	$\frac{1}{2}$	No simple criteria
Planar	B_1	1	1	$\frac{1}{2}$	$\frac{1}{2}$	$\frac{1}{2}$	No simple criteria
Polar		1	1	1	1	1	$\beta_1, \beta_3, \beta_4, \beta_5 < 0$
α		0	1	$\frac{1}{3}$	$\frac{1}{3}$	$\frac{1}{3}$	$\beta_1, \beta_4 \to \infty$
β		0	1	1	1	0	$\beta_1, \beta_5 > 0; \beta_3, \beta_4 < 0$

Table 3.4: Some inert triplet superfluid/superconducting phases, after Vollhardt and Wölfle [213] and Barton and Moore [27].

Chapter 4

The Hubbard model

In this chapter we will introduce the Hubbard model. After a brief survey of the development and uses of the Hubbard model we will examine the phenomenon of ferromagnetism - the context in which the Hubbard model was first studied. We then derive the spin-generalised Hartree–Fock–Gorkov Hamiltonian which will form the basis of this thesis from an extended Hubbard model. From this Hamiltonian we derive a spin-generalised Bogoliubov–de Gennes (BdG) equations. The spin dependent order parameter is then separated into triplet and singlet parts and the BdG equations are thus separated into equations for singlet (even–parity) and for triplet (odd–parity) superconductivity. These two cases are then studied independently. Analytical results for the spectrum of the elementary excitations and various thermodynamic quantities are derived for both cases and the singlet case is, briefly, studied numerically. We reproduce several well know results for singlet superconductors in zero field and describe the effect of an exchange field on a s-wave superconductor. We examine the Clogston–Chandrasekhar limit in singlet superconductors both analytically and numerically and we show analytically that a similar phenomena can occur (in certain circumstances) in a triplet superconductor.

Some of the results presented in this chapter have previously been published in reference [172].

4.1 Historical development

In 1963 Hubbard begin a series of papers [92, 93, 94, 95, 96, 97] in which he developed a model of 'Electron Correlations in Narrow Energy Bands.' Although Gutzwiller [86] and

Kanamori [105] considered similar models at about the same time, this paradigm of condensed matter physics is universally known as the Hubbard model.

In his original paper [92] Hubbard postulates a Hamiltonian for the electrons in a band and then, by introducing the Wannier functions, derives his Hamiltonian. However, from the perspective of tight binding theory - which is the perspective we predominantly take in this thesis - the correct thing to do is to postulate the Hubbard Hamiltonian and proceed from there. We will therefore take the later approach.

Within the tight binding approximation it is natural to consider a lattice of 'sites'. Each site represents a single orbital of a single atom which can accommodate, at most, two electrons (one of each spin.) The canonical Hubbard Hamiltonian is:

$$\hat{\mathcal{H}} = -\sum_{ij\sigma} t_{ij}\hat{c}^{\dagger}_{i\sigma}\hat{c}_{j\sigma} + U\sum_{i}\hat{n}_{i\uparrow}\hat{n}_{i\downarrow}. \tag{4.1.1}$$

t_{ij} is the usual hoping integral i.e. the amplitude of an electron on site i 'hoping' to site j. $\hat{c}^{(\dagger)}_{i\sigma}$ annihilates (creates) an electron with spin σ on site i. The number operator, $\hat{n}_{i\sigma} \equiv \hat{c}^{\dagger}_{i\sigma}\hat{c}_{i\sigma}$, counts the number of electrons with spin σ on site i, and clearly can only take the values 0 or 1. U is the potential between an electron on site i and an electron with the opposite spin[1] on the same site. U is therefore described as an 'on-site' potential. (The terms introduced above are discussed in greater detail in chapter 2.)

There are many ways in which the Hubbard model can be extended and in its various formulations many solutions have been found. With $U > 0$ paramagnetic-metallic [86, 128], ferromagnetic-metallic [92] and antiferromagnetic-insulating [128, 8] solutions have been found. For $U < 0$ there are normal Fermi liquid [212], insulating charge density wave [111], insulating normal Bose liquid [150], Bose-Einstein type (bipolaron) superfluids [150] and superconducting [128] solutions. There are also have been several attempts to explain the exotic high temperature superconductivity of the cuprates [9] such as the t-J model [223], which is derived from the Hubbard model. Yet even this is far from exhaustive list, as virtually every imaginably condensed matter system has been studied, at one time or another, in the context of the Hubbard model.

[1] As there are only two states on each site (one corresponding to each spin state) the Pauli exclusion principle ensures that only electrons with opposite spin to one another can occupy the same site simultaneously.

4.2 Ferromagnetism from the Hubbard model

We will now consider one of the solutions presented in the paper in which Hubbard first introduced the Hubbard model [92]. We will study the Hubbard model with $U > 0$ and as, for arbitrary U, in an arbitrary number of dimensions and in the thermodynamic limit, we do not know how to solve this model exactly we will use a mean field approximation.

4.2.1 Wicks theorem and the Hartree-Fock approximation

Wick's theorem [56, 83] states that for non interacting particles

$$\langle \hat{\psi}_1^\dagger \hat{\psi}_2^\dagger \hat{\psi}_3 \hat{\psi}_4 \rangle = \langle \hat{\psi}_1^\dagger \hat{\psi}_4 \rangle \langle \hat{\psi}_2^\dagger \hat{\psi}_3 \rangle - \langle \hat{\psi}_1^\dagger \hat{\psi}_3 \rangle \langle \hat{\psi}_2^\dagger \hat{\psi}_4 \rangle + \langle \hat{\psi}_1^\dagger \hat{\psi}_2^\dagger \rangle \langle \hat{\psi}_3 \hat{\psi}_4 \rangle. \tag{4.2.1}$$

It should be noted that this is an exact result and no approximation has been made. For the case of interacting particles Wicks theorem is no longer valid. But, we can progress using Wick's theorem as the basis for approximations.

We cannot apply Wick's theorem to an interacting system, but the Hartree–Fock approximation, which has the same mathematical form, can be used. We begin by noting that if the wavefunction is an eigenstate of the number operator, then

$$\langle \hat{c}_{i\uparrow} \hat{c}_{i\downarrow} \rangle = \langle \hat{c}_{i\uparrow}^\dagger \hat{c}_{i\downarrow}^\dagger \rangle = 0. \tag{4.2.2}$$

and we assume that spin flip processes and negligible, that is that

$$\left\langle \hat{c}_{i\uparrow}^\dagger \hat{c}_{i\downarrow} \right\rangle = \left\langle \hat{c}_{i\downarrow}^\dagger \hat{c}_{i\uparrow} \right\rangle = 0. \tag{4.2.3}$$

To derive the Hartree–Fock approximation, we write the interaction term of the Hubbard Hamiltonian 4.1.1 in terms of the fluctuations about the mean values of the number operators.

$$\begin{aligned}
\hat{\mathcal{H}}_{int} &= U \sum_i \hat{n}_{i\uparrow} \hat{n}_{i\downarrow} && (4.2.4)\\
&= U \sum_i \hat{c}_{i\uparrow}^\dagger \hat{c}_{i\uparrow} \hat{c}_{i\downarrow}^\dagger \hat{c}_{i\downarrow} && (4.2.5)\\
&= U \sum_i \left(\hat{c}_{i\uparrow}^\dagger \hat{c}_{i\uparrow} - \left\langle \hat{c}_{i\uparrow}^\dagger \hat{c}_{i\uparrow} \right\rangle + \left\langle \hat{c}_{i\uparrow}^\dagger \hat{c}_{i\uparrow} \right\rangle \right) \left(\hat{c}_{i\downarrow}^\dagger \hat{c}_{i\downarrow} - \left\langle \hat{c}_{i\downarrow}^\dagger \hat{c}_{i\downarrow} \right\rangle + \left\langle \hat{c}_{i\downarrow}^\dagger \hat{c}_{i\downarrow} \right\rangle \right). && (4.2.6)
\end{aligned}$$

Clearly, $\left\langle \hat{c}_{i\sigma}^\dagger \hat{c}_{i\sigma} \right\rangle$ is the mean of $\hat{n}_{i\sigma}$ and the fluctuations about the mean are given by $\hat{c}_{i\sigma}^\dagger \hat{c}_{i\sigma} - \left\langle \hat{c}_{i\sigma}^\dagger \hat{c}_{i\sigma} \right\rangle$. Thus we find that,

$$\begin{aligned}\hat{\mathcal{H}}_{int} &= U\sum_i \Big[\left(\hat{c}^\dagger_{i\uparrow}\hat{c}_{i\uparrow} - \left\langle \hat{c}^\dagger_{i\uparrow}\hat{c}_{i\uparrow}\right\rangle\right)\left(\hat{c}^\dagger_{i\downarrow}\hat{c}_{i\downarrow} - \left\langle \hat{c}^\dagger_{i\downarrow}\hat{c}_{i\downarrow}\right\rangle\right) \\ &\quad + \left(\hat{c}^\dagger_{i\uparrow}\hat{c}_{i\uparrow} - \left\langle \hat{c}^\dagger_{i\uparrow}\hat{c}_{i\uparrow}\right\rangle\right)\left\langle \hat{c}^\dagger_{i\downarrow}\hat{c}_{i\downarrow}\right\rangle \\ &\quad + \left\langle \hat{c}^\dagger_{i\uparrow}\hat{c}_{i\uparrow}\right\rangle\left(\hat{c}^\dagger_{i\downarrow}\hat{c}_{i\downarrow} - \left\langle \hat{c}^\dagger_{i\downarrow}\hat{c}_{i\downarrow}\right\rangle\right) + \left\langle \hat{c}^\dagger_{i\uparrow}\hat{c}_{i\uparrow}\right\rangle\left\langle \hat{c}^\dagger_{i\downarrow}\hat{c}_{i\downarrow}\right\rangle \Big]. \qquad (4.2.7)\end{aligned}$$

So to first order in the fluctuations we have

$$\begin{aligned}\hat{\mathcal{H}}_{int} &\approx U\sum_i \Big[\left(\hat{c}^\dagger_{i\uparrow}\hat{c}_{i\uparrow} - \left\langle \hat{c}^\dagger_{i\uparrow}\hat{c}_{i\uparrow}\right\rangle\right)\left\langle \hat{c}^\dagger_{i\downarrow}\hat{c}_{i\downarrow}\right\rangle \\ &\quad + \left\langle \hat{c}^\dagger_{i\uparrow}\hat{c}_{i\uparrow}\right\rangle\left(\hat{c}^\dagger_{i\downarrow}\hat{c}_{i\downarrow} - \left\langle \hat{c}^\dagger_{i\downarrow}\hat{c}_{i\downarrow}\right\rangle\right) + \left\langle \hat{c}^\dagger_{i\uparrow}\hat{c}_{i\uparrow}\right\rangle\left\langle \hat{c}^\dagger_{i\downarrow}\hat{c}_{i\downarrow}\right\rangle \Big] \qquad (4.2.8) \\ &= U\sum_i \Big[\left\langle \hat{c}^\dagger_{i\downarrow}\hat{c}_{i\downarrow}\right\rangle \hat{c}^\dagger_{i\uparrow}\hat{c}_{i\uparrow} + \left\langle \hat{c}^\dagger_{i\uparrow}\hat{c}_{i\uparrow}\right\rangle \hat{c}^\dagger_{i\downarrow}\hat{c}_{i\downarrow} - \left\langle \hat{c}^\dagger_{i\uparrow}\hat{c}_{i\uparrow}\right\rangle\left\langle \hat{c}^\dagger_{i\downarrow}\hat{c}_{i\downarrow}\right\rangle \Big]. \qquad (4.2.9)\end{aligned}$$

Transforming away the last term of the right hand side of equation 4.2.10 which is a constant we arrive at the Hartree–Fock approximation,

$$\hat{\mathcal{H}}_{int} \approx U\sum_i \Big[\left\langle \hat{c}^\dagger_{i\downarrow}\hat{c}_{i\downarrow}\right\rangle \hat{c}^\dagger_{i\uparrow}\hat{c}_{i\uparrow} + \left\langle \hat{c}^\dagger_{i\uparrow}\hat{c}_{i\uparrow}\right\rangle \hat{c}^\dagger_{i\downarrow}\hat{c}_{i\downarrow} \Big]. \qquad (4.2.10)$$

We now assume that our system is homogeneous

$$\begin{aligned}\left\langle \hat{c}^\dagger_{i\sigma}\hat{c}_{i\sigma}\right\rangle &\equiv \left\langle \hat{n}_{i\sigma}\right\rangle \qquad (4.2.11) \\ &= n_{i\sigma} \qquad (4.2.12) \\ &\simeq \overline{n}_\sigma, \qquad (4.2.13)\end{aligned}$$

Thus equation 4.1.1 is approximated by

$$\hat{\mathcal{H}}^{HF} = \sum_{ij\sigma} t_{ij}\hat{c}^\dagger_{i\sigma}\hat{c}_{j\sigma} + U\sum_{i\sigma}\overline{n}_{-\sigma}\hat{c}^\dagger_{i\sigma}\hat{c}_{i\sigma}. \qquad (4.2.14)$$

which is a single electron Hamiltonian, and therefore much easier to solve. This approximation is equivalent to calculating the expectation value with respect to a *mean field* wavefunction.

4.2.2 Solution of the mean field Hamiltonian

We can solve the Hartree–Fock Hamiltonian exactly in arbitrary dimension. We begin by noting that for $U = 0$ we regain the tight binding Hamiltonian (2.3.26) but writing the Hartree–Fock–Hubbard Hamiltonian in the form

$$\hat{\mathcal{H}}^{HF} = \sum_{ij\sigma} \left(t_{ij} + U\overline{n}_{-\sigma}\delta_{ij}\right) \hat{c}^{\dagger}_{i\sigma}\hat{c}_{j\sigma}, \tag{4.2.15}$$

it is clear (from the arguments given in section 2.3.1) that

$$\varepsilon^{HF}_{\mathbf{k}\sigma} = \varepsilon^{0}_{\mathbf{k}\sigma} + U\overline{n}_{-\sigma}, \tag{4.2.16}$$

where $\varepsilon^{0}_{\mathbf{k}\sigma}$ is the dispersion relation found from the tight binding model (or, indeed, the Hubbard model with $U = 0$). If we define

$$\overline{n} = \overline{n}_{\uparrow} + \overline{n}_{\downarrow} \tag{4.2.17}$$

$$m = \overline{n}_{\uparrow} - \overline{n}_{\downarrow} \tag{4.2.18}$$

then we have

$$\varepsilon^{HF}_{\mathbf{k}\uparrow} = \varepsilon^{0}_{\mathbf{k}\sigma} + \frac{1}{2}U\overline{n} + \frac{1}{2}Um \tag{4.2.19}$$

$$\varepsilon^{HF}_{\mathbf{k}\downarrow} = \varepsilon^{0}_{\mathbf{k}\sigma} + \frac{1}{2}U\overline{n} - \frac{1}{2}Um. \tag{4.2.20}$$

The exchange splitting[2], E_{ex}, is given by

$$E_{ex} = \varepsilon^{HF}_{\mathbf{k}\uparrow} - \varepsilon^{HF}_{\mathbf{k}\downarrow} = Um. \tag{4.2.21}$$

The effect of a finite E_{ex} is to split the spectrum into two branches - one for each of the spin states. This is sketched in figure 4.1.

It is not immediately clear why an on site interaction should lead to ferromagnetism. However, one should realise that we are dealing with metallic magnetism. This means that we have itinerant electrons which spend a short time on any given site compared with the lifetime of

[2]The exchange splitting is often denoted Δ, however we will not use this notation in this thesis to avoid confusion with the superconducting order parameter, which is also usually denoted Δ.

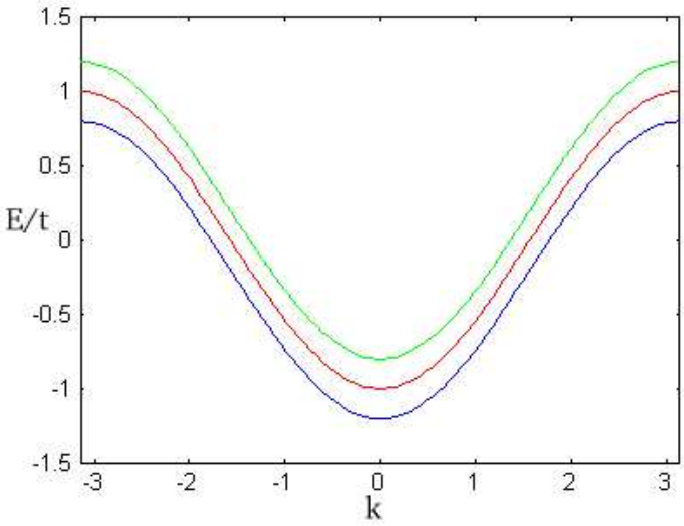

Figure 4.1: Sketch of the effect of exchange splitting on the spectrum of a one dimensional Hubbard model. The upper curve is $\varepsilon_{\mathbf{k}} + E_{ex}$, the middle curve is $\varepsilon_{\mathbf{k}}$ and the lower curve is $\varepsilon_{\mathbf{k}} - E_{ex}$.

the magnetic moment on that site. The positive U implies that there is an energy penalty for doubly occupied sites, but, the Pauli exclusion principle ensures that electrons of the same spin cannot be on the same site. Which means that electrons of the same spin have lower energy and thus drives ferromagnetism.

4.3 Derivation of the spin–generalised Bogoliubov–de Gennes equations in the presence of a magnetic field

We will now use the Hubbard model to study superconductivity. Cooper showed that [52], in the presence of an arbitrarily weak, attractive interaction two electrons near to the Fermi level are always unstable with respect to the formation of a bound state (a Cooper pair). BCS theory extends this simple model to deal with the full many body problem within mean field theory. Thus, as we want to study superconductivity, it is natural to consider effective attractive pairwise potentials i.e. negative U models.

In real materials, interactions are not only on site. We can take account of this by introducing inter-site interaction constants, $U_{ij\sigma\sigma'}$, which will in general depend on the spin of the two electrons. These new interaction constants still describe two body interactions, so our generalised Hubbard Hamiltonian is

$$\hat{\mathcal{H}} = \sum_{ij\sigma} t_{ij} \hat{c}^{\dagger}_{i\sigma} \hat{c}_{j\sigma} + \frac{1}{2} \sum_{ij\sigma\sigma'} U_{ij\sigma\sigma'} \hat{n}_{i\sigma} \hat{n}_{j\sigma'}. \tag{4.3.1}$$

It is simple to see that on site potentials cannot give triplet superconductivity. As only one electron of each spin can occupy each site the equal spin pairing (ESP) states will clearly not arise from on site potentials. However, one can see that no triplet states can arise from an on site potential as all triplet states must have odd parity and on site potentials cannot give a k dependent order parameter, which means that the order parameter is, trivially, even.[3]

In general two new terms are introduced into the Schrödinger equation by a magnetic field: the minimal coupling term $\left(\hat{\mathbf{p}} = -\mathrm{i}\hbar\nabla \mapsto -\mathrm{i}\hbar\nabla - \frac{e}{c}\mathbf{A}\right)$ and the Zeeman term $\left(\frac{1}{2}\mu_B \sigma H\right)$. The vector potential enters via minimal coupling and thus only effects the kinetic energy terms, t_{ij}. It can be shown [151, 152] that in a magnetic field

$$t_{ij} \mapsto t_{ij} \exp\left(\frac{-\mathrm{i}e}{\hbar} \int_{\mathbf{R}_i}^{\mathbf{R}_j} \mathbf{A}(\mathbf{r}) \cdot \mathrm{d}\mathbf{r}\right) = t_{ij} e^{-\mathrm{i}A_{ij}}. \tag{4.3.2}$$

Thus the Hamiltonian for the Hubbard model generalised to include n^{th} nearest neighbour interactions in the presence of a magnetic field is

$$\hat{\mathcal{H}} = -\sum_{ij\sigma} t_{ij} e^{-\mathrm{i}A_{ij}} \hat{c}^{\dagger}_{i\sigma} \hat{c}_{j\sigma} + \frac{1}{2} \sum_{ij\sigma\sigma'} U_{ij\sigma\sigma'} \hat{n}_{i\sigma} \hat{n}_{j\sigma'} + \mu_B \sum_{i\sigma\sigma'} \hat{c}^{\dagger}_{i\sigma} (\sigma_{\sigma\sigma'} \cdot \mathbf{H}) \hat{c}_{i\sigma} \tag{4.3.3}$$

where the $\sigma_{\sigma\sigma'}$ are the components of the vector of Pauli matrices

$$\underline{\underline{\sigma}} = (\underline{\underline{\sigma}}_1, \underline{\underline{\sigma}}_2, \underline{\underline{\sigma}}_3). \tag{4.3.4}$$

However, in this thesis we do not attempt to solve this Hamiltonian. Instead we neglect the vector potential. The differences between singlet and triplet superconductors are caused by the spin of the Cooper pairs. Thus, the most interesting new physics observed in a triplet superconductor is likely to be due to the interaction of the Cooper pairs with a magnetic field via the Zeeman term.

In chapter 5 we consider the triplet superconductor Sr_2RuO_4 in a magnetic field. The upper critical field, H_{C2} is determined by the interaction with the vector potential, so we will be unable to comment on H_{C2}. But, away from H_{C2} it is plausible that many effects are dominated

[3] This is not strictly true, Spalek and co-workers [198] have considered on site potentials in multiple orbital models and have found triplet solutions. However, for single orbital models the above discussion is correct.

by the Zeeman term particularly in light of the large Stoner enhancement in Sr_2RuO_4 (see section 5.1.1). In chapter 6 we consider the weak Stoner ferromagnet $ZrZn_2$. For this system the Zeeman term is likely to be the dominant interaction between ferromagnetism and superconductivity.

Neglecting the effect of the vector potential our Hamiltonian becomes

$$\hat{\mathcal{H}} = -\sum_{ij\sigma} t_{ij}\hat{c}^{\dagger}_{i\sigma}\hat{c}_{j\sigma} + \frac{1}{2}\sum_{ij\sigma\sigma'} U_{ij\sigma\sigma'}\hat{n}_{i\sigma}\hat{n}_{j\sigma'} + \mu_B \sum_{i\sigma\sigma'} \hat{c}^{\dagger}_{i\sigma}(\sigma_{\sigma\sigma'}\cdot\mathbf{H})\hat{c}_{i\sigma} \tag{4.3.5}$$

This model has a very rich set of solutions, so much so that the remainder of this thesis will almost entirely consist of solutions of this Hamiltonian.

4.3.1 The Hartree–Fock–Gorkov approximation

The BCS wavefunction is a coherent state. This means that it is not an eigenstate of the number operator, but it is an eigenstate of the annihilation/creation operator. Therefore,

$$\langle\hat{\psi}^{\dagger}_1\hat{\psi}^{\dagger}_2\rangle, \langle\hat{\psi}_3\hat{\psi}_4\rangle \quad \neq \quad 0. \tag{4.3.6}$$

The Hartree–Fock–Gorkov approximation treats these terms in the same way as the Hartree–Fock approximation treats the 'number operator terms'. That is one introduces a mean field order parameter, $\Delta_{ij\sigma\sigma'}$ and its Hermitian conjugate, which are defined by,

$$\Delta_{ij\sigma\sigma'} = -U_{ij\sigma\sigma'}\langle\hat{c}_{i\sigma}\hat{c}_{j\sigma'}\rangle \tag{4.3.7}$$

$$\Delta^{\dagger}_{ij\sigma\sigma'} = -U_{ij\sigma\sigma'}\langle\hat{c}^{\dagger}_{j\sigma'}\hat{c}^{\dagger}_{i\sigma}\rangle \tag{4.3.8}$$

The Hartree–Fock–Gorkov Hamiltonian is therefore,

$$\hat{\mathcal{H}}^{HFG} = \sum_{ij\sigma\sigma'}\left\{t_{ij}\delta_{\sigma\sigma'}\hat{c}^{\dagger}_{i\sigma}\hat{c}_{j\sigma} + \frac{1}{2}\Delta_{ij\sigma\sigma'}\hat{c}^{\dagger}_{i\sigma}\hat{c}^{\dagger}_{j\sigma'} - \frac{1}{2}\Delta^{\dagger}_{ij\sigma\sigma'}\hat{c}_{i\sigma}\hat{c}_{j\sigma'} + \mu_B\delta_{ij}\hat{c}^{\dagger}_{i\sigma}(\sigma_{\sigma\sigma'}\cdot\mathbf{H})\hat{c}_{i\sigma}\right\} \tag{4.3.9}$$

4.3.2 The Bogoliubov-de Gennes equations

Famously the Hartree–Fock–Gorkov Hamiltonian is diagonalised by the Bogoliubov–Valatin transformation [56]

$$\hat{c}_{i\uparrow} = \sum_{\mathbf{k}} u_{\mathbf{k}}(\mathbf{R}_i)\hat{\gamma}_{\mathbf{k}\uparrow} - v^*_{\mathbf{k}}(\mathbf{R}_i)\hat{\gamma}^\dagger_{\mathbf{k}\downarrow} \tag{4.3.10}$$

$$\hat{c}_{i\downarrow} = \sum_{\mathbf{k}} u_{\mathbf{k}}(\mathbf{R}_i)\hat{\gamma}_{\mathbf{k}\downarrow} + v^*_{\mathbf{k}}(\mathbf{R}_i)\hat{\gamma}^\dagger_{\mathbf{k}\uparrow} \tag{4.3.11}$$

where

$$u_{\mathbf{k}}(\mathbf{R}_i)u^*_{\mathbf{k}}(\mathbf{R}_j) + v_{\mathbf{k}}(\mathbf{R}_i)v^*_{\mathbf{k}}(\mathbf{R}_j) = \delta_{ij}. \tag{4.3.12}$$

This can be extended for the spin-generalised situation when the transformations are

$$\hat{c}_{i\sigma} = \sum_{\mathbf{k}\sigma'} u_{\mathbf{k}\sigma\sigma'}(\mathbf{R}_i)\hat{\gamma}_{\mathbf{k}\sigma'} + v^*_{\mathbf{k}\sigma\sigma'}(\mathbf{R}_i)\hat{\gamma}^\dagger_{\mathbf{k}\sigma'} \tag{4.3.13}$$

and the completeness relation is

$$\sum_{\mathbf{k}\sigma} \left(u^*_{\mathbf{k}\alpha\sigma}(\mathbf{R}_i)u_{\mathbf{k}\beta\sigma}(\mathbf{R}_j) + v_{\mathbf{k}\alpha\sigma}(\mathbf{R}_i)v^*_{\mathbf{k}\beta\sigma}(\mathbf{R}_j)\right) = \delta_{ij}\delta_{\alpha\beta}. \tag{4.3.14}$$

The completeness relation follows from the fact that both the $\hat{c}$ and $\hat{\gamma}$ operators are Fermionic operators and as such obey

$$\left\{\hat{c}^\dagger_{i\sigma}, \hat{c}_{j\sigma'}\right\} = \delta_{ij}\delta_{\sigma\sigma'}, \tag{4.3.15}$$

$$\left\{\hat{\gamma}^\dagger_{\mathbf{k}\sigma}, \hat{\gamma}_{\mathbf{k}'\sigma'}\right\} = \delta(\mathbf{k}-\mathbf{k}')\delta_{\sigma\sigma'}. \tag{4.3.16}$$

We must now choose our Bogoliubov-Valatin transformation so that it diagonalises the Hamiltonian, or equivalently so that

$$\hat{\mathcal{H}} = \sum_{\mathbf{k}\sigma} E_{\mathbf{k}\sigma}\gamma^\dagger_{\mathbf{k}\sigma}\gamma_{\mathbf{k}\sigma}. \tag{4.3.17}$$

Now, from equation 4.3.9 we have

$$\left[\hat{\mathcal{H}}, \hat{c}_{i\sigma}\right] = \sum_{\mathbf{k}j\alpha\beta} \Big(\left(t_{ij}\delta_{\sigma\alpha} - \mu_B(\sigma_{\sigma\alpha}\cdot\mathbf{H})\delta_{ij}\right)\left(u_{\mathbf{k}\alpha\beta}(\mathbf{R}_j)\gamma_{\mathbf{k}\beta} + v^*_{\mathbf{k}\alpha\beta}(\mathbf{R}_j)\gamma^\dagger_{\mathbf{k}\beta}\right) - \Delta_{ij\sigma\alpha}\left(u^*_{\mathbf{k}\alpha\beta}(\mathbf{R}_j)\gamma^\dagger_{\mathbf{k}\beta} + v_{\mathbf{k}\alpha\beta}(\mathbf{R}_j)\gamma_{\mathbf{k}\beta}\right)\Big). \tag{4.3.18}$$

But, from equation 4.3.17 we have

$$\Big[\hat{\mathcal{H}}, \hat{c}_{i\sigma}\Big] = \Big[\hat{\mathcal{H}}, \sum_{\mathbf{k}\beta} \big(u_{\mathbf{k}\sigma\beta}(\mathbf{R}_i)\gamma_{\mathbf{k}\beta} + v^*_{\mathbf{k}\sigma\beta}(\mathbf{R}_i)\gamma^\dagger_{\mathbf{k}\beta}\big)\Big] \tag{4.3.19}$$

$$= \sum_{\mathbf{k}\beta} \big(- E_{\mathbf{k}\beta} u_{\mathbf{k}\sigma\beta}(\mathbf{R}_i)\gamma_{\mathbf{k}\beta} + E_{\mathbf{k}\beta} v^*_{\mathbf{k}\sigma\beta}(\mathbf{R}_i)\gamma^\dagger_{\mathbf{k}\beta}\big). \tag{4.3.20}$$

So, equating coefficients of $\gamma_{\mathbf{k}\beta}$ we find that

$$\sum_{j\beta} \big(t_{ij}\delta_{\alpha\beta} + \mu_B(\sigma_{\alpha\beta}\cdot\mathbf{H})u_{\mathbf{k}\beta\sigma}(\mathbf{R}_j) + \Delta_{ij\alpha\beta} v_{\mathbf{k}\beta\sigma}(\mathbf{R}_j) = E_{\mathbf{k}\sigma} u_{\mathbf{k}\alpha\sigma}(\mathbf{R}_i), \tag{4.3.21}$$

while equating coefficients of $\gamma^\dagger_{\mathbf{k}\beta}$ gives

$$\sum_{j\beta} \big(- t_{ij}\delta_{\alpha\beta} - \mu_B(\sigma^*_{\alpha\beta}\cdot\mathbf{H})\delta_{ij}\big)v_{\mathbf{k}\beta\sigma}(\mathbf{R}_j) - \Delta^*_{ij\alpha\beta} u_{\mathbf{k}\beta\sigma}(\mathbf{R}_j) = E_{\mathbf{k}\sigma} v_{\mathbf{k}\alpha\sigma}(\mathbf{R}_i). \tag{4.3.22}$$

(4.3.21) and (4.3.22) are the spin generalised Bogoliubov–de Gennes (BdG) equations in real space. In principle we could solve these but the sum over (infinitely many) lattice sites (in thermodynamic limit) makes this impossible in practice. Fortunately we can avoid this problem by Fourier transforming the BdG equations, which gives

$$\sum_{\beta} \big(\varepsilon_{\mathbf{k}}\delta_{\alpha\beta} + \mu_B(\sigma_{\alpha\beta}\cdot\mathbf{H})\big)u_{\mathbf{k}\beta\sigma} + \Delta_{\alpha\beta}(\mathbf{k})v_{\mathbf{k}\beta\sigma} = E_{\mathbf{k}\sigma}u_{\mathbf{k}\alpha\sigma}, \tag{4.3.23}$$

$$\sum_{\beta} \big(- \varepsilon_{\mathbf{k}}\delta_{\alpha\beta} - \mu_B(\sigma^*_{\alpha\beta}\cdot\mathbf{H})\big)v_{\mathbf{k}\beta\sigma} - \Delta^*_{\alpha\beta}(\mathbf{k})u_{\mathbf{k}\beta\sigma} = E_{\mathbf{k}\sigma}v_{\mathbf{k}\alpha\sigma} \tag{4.3.24}$$

or, in their, more familiar, matrix form

$$\begin{pmatrix} \varepsilon_{\mathbf{k}} + \mu_B H_3 & \mu_B(H_1 - \mathrm{i}H_2) & \Delta_{\uparrow\uparrow}(\mathbf{k}) & \Delta_{\uparrow\downarrow}(\mathbf{k}) \\ \mu_B(H_1 + \mathrm{i}H_2) & \varepsilon_{\mathbf{k}} - \mu_B H_3 & \Delta_{\downarrow\uparrow}(\mathbf{k}) & \Delta_{\downarrow\downarrow}(\mathbf{k}) \\ -\Delta^*_{\uparrow\uparrow}(-\mathbf{k}) & -\Delta^*_{\uparrow\downarrow}(-\mathbf{k}) & -\varepsilon_{-\mathbf{k}} - \mu_B H_3 & \mu_B(-H_1 - \mathrm{i}H_2) \\ -\Delta^*_{\downarrow\uparrow}(-\mathbf{k}) & -\Delta^*_{\downarrow\downarrow}(-\mathbf{k}) & \mu_B(-H_1 + \mathrm{i}H_2) & -\varepsilon_{-\mathbf{k}} + \mu_B H_3 \end{pmatrix} \begin{pmatrix} u_{\uparrow\sigma}(\mathbf{k}) \\ u_{\downarrow\sigma}(\mathbf{k}) \\ v_{\uparrow\sigma}(\mathbf{k}) \\ v_{\downarrow\sigma}(\mathbf{k}) \end{pmatrix}$$

$$= E_\sigma(\mathbf{k}) \begin{pmatrix} u_{\uparrow\sigma}(\mathbf{k}) \\ u_{\downarrow\sigma}(\mathbf{k}) \\ v_{\uparrow\sigma}(\mathbf{k}) \\ v_{\downarrow\sigma}(\mathbf{k}) \end{pmatrix}. \tag{4.3.25}$$

4.3.3 The self consistency conditions

Recall that we defined the order parameter by

$$\Delta_{ij\sigma\sigma'} = -U_{ij\sigma\sigma'}\langle \hat{c}_{i\sigma}\hat{c}_{j\sigma'}\rangle \tag{4.3.26}$$

substituting the Bogoliubov–Valatin transformation (4.3.13) into this we find that

$$\Delta_{ij\sigma\sigma'} = -U_{ij\sigma\sigma'}\sum_{\mathbf{q}\sigma''}\Big(u_{\mathbf{q}\sigma\sigma''}(\mathbf{R}_i)v^*_{\mathbf{q}\sigma'\sigma''}(\mathbf{R}_j)\big(1-f_{E_{\mathbf{q}\sigma}}\big) + v^*_{\mathbf{q}\sigma\sigma''}(\mathbf{R}_i)u_{\mathbf{q}\sigma'\sigma''}(\mathbf{R}_j)f_{E_{\mathbf{q}\sigma}}\Big) \tag{4.3.27}$$

as $\langle\hat{\gamma}_{\mathbf{q}\sigma}\hat{\gamma}^\dagger_{\mathbf{q}\sigma}\rangle = (1-f_{E_{\mathbf{q}\sigma}})$ and $\langle\hat{\gamma}^\dagger_{\mathbf{q}\sigma}\hat{\gamma}_{\mathbf{q}\sigma}\rangle = f_{E_{\mathbf{q}\sigma}}$. However, the total wavefunction, and thus the order parameter by 4.3.26 must be antisymmetric under the exchange of spin and coordinate labels. Hence,

$$\begin{aligned}\Delta_{ij\sigma\sigma'} &= -\Delta_{ji\sigma'\sigma} \qquad (4.3.28)\\ &= U_{ij\sigma\sigma'}\sum_{\mathbf{q}\sigma''}\Big(u_{\mathbf{q}\sigma'\sigma''}(\mathbf{R}_j)v^*_{\mathbf{q}\sigma\sigma''}(\mathbf{R}_i)\big(1-f_{E_{\mathbf{q}\sigma}}\big) + v^*_{\mathbf{q}\sigma'\sigma''}(\mathbf{R}_j)u_{\mathbf{q}\sigma\sigma''}(\mathbf{R}_i)f_{E_{\mathbf{q}\sigma}}\Big).\end{aligned}$$

Subtracting (4.3.28) from (4.3.27) gives

$$\Delta_{ij\sigma\sigma'} = -\frac{1}{2}U_{ij\sigma\sigma'}\sum_{\mathbf{q}\sigma''}\Big(u_{\mathbf{q}\sigma\sigma''}(\mathbf{R}_i)v^*_{\mathbf{q}\sigma'\sigma''}(\mathbf{R}_j) - v^*_{\mathbf{q}\sigma\sigma''}(\mathbf{R}_i)u_{\mathbf{q}\sigma'\sigma''}(\mathbf{R}_j)\Big)\Big(1-2f_{E_{\mathbf{q}\sigma''}}\Big) \tag{4.3.29}$$

Fourier transforming we find that the order parameters $\Delta_{\sigma\sigma'}(\mathbf{k})$ are determined self consistently by

$$\Delta_{\sigma\sigma'}(\mathbf{k}) = -\frac{1}{2}\sum_{\mathbf{q}\sigma''}U_{\sigma\sigma'}(\mathbf{k}-\mathbf{q})\Big(u_{\sigma\sigma''}(-\mathbf{q})v^*_{\sigma'\sigma''}(-\mathbf{q}) - v^*_{\sigma\sigma''}(\mathbf{q})u_{\sigma'\sigma''}(\mathbf{q})\Big)(1-2f_{E_{\mathbf{q}\sigma''}}) \tag{4.3.30}$$

where $U_{\sigma\sigma'}(\mathbf{k}-\mathbf{q})$ is the lattice Fourier transform of $U_{ij\sigma\sigma'}$. We note that if only the on site term is finite then $U_{\sigma\sigma'}(\mathbf{k}-\mathbf{q})$ must be spin dependent because to the Pauli exclusion principle.

Similarly we can calculate the Hartree–Fock terms, $\left\langle\hat{c}^\dagger_{i\alpha}\hat{c}_{j\beta}\right\rangle$, by substituting in the Bogoliubov–Valatin transformations. This gives additional terms in the normal state energy, $\epsilon'_{\alpha\beta}(\mathbf{k})$, where

$$\epsilon'_{\alpha\beta}(\mathbf{k}) = \sum_{\mathbf{q}\sigma} U_{\alpha\beta}(\mathbf{k}-\mathbf{q})\Big(u^*_{\alpha\sigma}(\mathbf{q})u_{\beta\sigma}(\mathbf{q})f_{E_{\mathbf{q}\sigma}} + v_{\alpha\sigma}(-\mathbf{q})v^*_{\beta\sigma}(-\mathbf{q})\big(1-f_{E_{\mathbf{q}\sigma}}\big)\Big). \quad (4.3.31)$$

4.3.4 Singlet-triplet separation

It is natural to separate the spin-generalised BdG equation into triplet and singlet parts. In the BW notation [23] (see section 3.3 for an introduction):

$$\underline{\underline{\Delta}}(\mathbf{k}) \equiv \begin{pmatrix} \Delta_{\uparrow\uparrow}(\mathbf{k}) & \Delta_{\uparrow\downarrow}(\mathbf{k}) \\ \Delta_{\downarrow\uparrow}(\mathbf{k}) & \Delta_{\downarrow\downarrow}(\mathbf{k}) \end{pmatrix} = (d_0(\mathbf{k}) + \underline{\sigma}\cdot\mathbf{d}(\mathbf{k}))\mathtt{i}\underline{\underline{\sigma_2}}. \quad (4.3.32)$$

$d_0(\mathbf{k})$ is the (scalar) singlet order parameter and $\mathbf{d}(\mathbf{k})$ is the (vector) triplet order parameter[4]. The singlet order parameter is symmetric under spatial inversion while the triplet order parameter in anti-symmetric under spatial inversion. Hence, the BdG equation can be rewritten as

$$\begin{pmatrix} \varepsilon_{\mathbf{k}}+\mu_B H_3 & \mu_B(H_1-\mathtt{i}H_2) & -d_1(\mathbf{k})+\mathtt{i}d_2(\mathbf{k}) & d_0(\mathbf{k})+d_3(\mathbf{k}) \\ \mu_B(H_1+\mathtt{i}H_2) & \varepsilon_{\mathbf{k}}-\mu_B H_3 & -d_0(\mathbf{k})+d_3(\mathbf{k}) & d_1(\mathbf{k})+\mathtt{i}d_2(\mathbf{k}) \\ -d^*_1(\mathbf{k})-\mathtt{i}d^*_2(\mathbf{k}) & -d^*_0(\mathbf{k})+d^*_3(\mathbf{k}) & -\varepsilon_{\mathbf{k}}-\mu_B H_3 & \mu_B(-H_1-\mathtt{i}H_2) \\ d^*_0(\mathbf{k})+d^*_3(\mathbf{k}) & d^*_1(\mathbf{k})-\mathtt{i}d^*_2(\mathbf{k}) & \mu_B(-H_1+\mathtt{i}H_2) & -\varepsilon_{\mathbf{k}}+\mu_B H_3 \end{pmatrix} \begin{pmatrix} u_{\uparrow\sigma}(\mathbf{k}) \\ u_{\downarrow\sigma}(\mathbf{k}) \\ v_{\uparrow\sigma}(\mathbf{k}) \\ v_{\downarrow\sigma}(\mathbf{k}) \end{pmatrix}$$
$$= E_\sigma(\mathbf{k}) \begin{pmatrix} u_{\uparrow\sigma}(\mathbf{k}) \\ u_{\downarrow\sigma}(\mathbf{k}) \\ v_{\uparrow\sigma}(\mathbf{k}) \\ v_{\downarrow\sigma}(\mathbf{k}) \end{pmatrix}. \quad (4.3.34)$$

4.4 Regaining BCS (singlet) superconductivity from the spin–generalised Bogoliubov–de Gennes equations

If there is no superconductivity in the triplet channel the BdG equations are

[4] We note that we have separated the singlet and triplet parts using the quaternion group [46]

$$\{\sigma_0\mathtt{i}\sigma_2, \sigma_1\mathtt{i}\sigma_2, \sigma_2\mathtt{i}\sigma_2, \sigma_3\mathtt{i}\sigma_2\} \quad (4.3.33)$$

Quaternions were first introduced by Hamilton [88] as a generalisation to complex numbers, and interestingly enough, are where the letters i, j and k as commonly used for the unit vectors in Cartesian space originate.

$$\begin{pmatrix} \varepsilon_{\mathbf{k}} + \mu_B H_3 & \mu_B(H_1 - \mathtt{i}H_2) & 0 & d_0(\mathbf{k}) \\ \mu_B(H_1 + \mathtt{i}H_2) & \varepsilon_{\mathbf{k}} - \mu_B H_3 & -d_0(\mathbf{k}) & 0 \\ 0 & -d_0^*(\mathbf{k}) & -\varepsilon_{\mathbf{k}} - \mu_B H_3 & \mu_B(-H_1 - \mathtt{i}H_2) \\ d_0^*(\mathbf{k}) & 0 & \mu_B(-H_1 + \mathtt{i}H_2) & -\varepsilon_{\mathbf{k}} + \mu_B H_3 \end{pmatrix} \begin{pmatrix} u_{\uparrow\sigma}(\mathbf{k}) \\ u_{\downarrow\sigma}(\mathbf{k}) \\ v_{\uparrow\sigma}(\mathbf{k}) \\ v_{\downarrow\sigma}(\mathbf{k}) \end{pmatrix} = E_\sigma(\mathbf{k}) \begin{pmatrix} u_{\uparrow\sigma}(\mathbf{k}) \\ u_{\downarrow\sigma}(\mathbf{k}) \\ v_{\uparrow\sigma}(\mathbf{k}) \\ v_{\downarrow\sigma}(\mathbf{k}) \end{pmatrix}. \quad (4.4.1)$$

In section 3.3 we saw that $d_0(\mathbf{k})$ transforms as a scalar under rotation. This means that we can always rotate the system so that $\mathbf{H}$ is parallel to $\hat{z}$. The BdG equations then become

$$\begin{pmatrix} \varepsilon_{\mathbf{k}} + \mu_B|\mathbf{H}| & 0 & 0 & d_0(\mathbf{k}) \\ 0 & \varepsilon_{\mathbf{k}} - \mu_B|\mathbf{H}| & -d_0(\mathbf{k}) & 0 \\ 0 & -d_0^*(\mathbf{k}) & -\varepsilon_{\mathbf{k}} - \mu_B|\mathbf{H}| & 0 \\ d_0^*(\mathbf{k}) & 0 & 0 & -\varepsilon_{\mathbf{k}} + \mu_B|\mathbf{H}| \end{pmatrix} \begin{pmatrix} u_{\uparrow\sigma}(\mathbf{k}) \\ u_{\downarrow\sigma}(\mathbf{k}) \\ v_{\uparrow\sigma}(\mathbf{k}) \\ v_{\downarrow\sigma}(\mathbf{k}) \end{pmatrix}$$

$$= E_\sigma(\mathbf{k}) \begin{pmatrix} u_{\uparrow\sigma}(\mathbf{k}) \\ u_{\downarrow\sigma}(\mathbf{k}) \\ v_{\uparrow\sigma}(\mathbf{k}) \\ v_{\downarrow\sigma}(\mathbf{k}) \end{pmatrix}. \quad (4.4.2)$$

Which can be separated into sets of BdG equations, so we have

$$\begin{pmatrix} \varepsilon_{\mathbf{k}} + \mu_B|\mathbf{H}| & d_0(\mathbf{k}) \\ d_0^*(\mathbf{k}) & -\varepsilon_{\mathbf{k}} + \mu_B|\mathbf{H}| \end{pmatrix} \begin{pmatrix} u_{\uparrow\uparrow}(\mathbf{k}) \\ v_{\downarrow\uparrow}(\mathbf{k}) \end{pmatrix} = E_\uparrow(\mathbf{k}) \begin{pmatrix} u_{\uparrow\uparrow}(\mathbf{k}) \\ v_{\downarrow\uparrow}(\mathbf{k}) \end{pmatrix} \quad (4.4.3)$$

and

$$\begin{pmatrix} \varepsilon_{\mathbf{k}} - \mu_B|\mathbf{H}| & -d_0(\mathbf{k}) \\ -d_0^*(\mathbf{k}) & -\varepsilon_{\mathbf{k}} - \mu_B|\mathbf{H}| \end{pmatrix} \begin{pmatrix} u_{\downarrow\downarrow}(\mathbf{k}) \\ v_{\uparrow\downarrow}(\mathbf{k}) \end{pmatrix} = E_\downarrow(\mathbf{k}) \begin{pmatrix} u_{\downarrow\downarrow}(\mathbf{k}) \\ v_{\uparrow\downarrow}(\mathbf{k}) \end{pmatrix}. \quad (4.4.4)$$

It is now a simple matter to regain the standard result [154] for the spectrum of a singlet superconductor in a spin only magnetic field:

$$E_\sigma(\mathbf{k}) = \sqrt{\varepsilon_{\mathbf{k}}^2 + |d_0(\mathbf{k})|^2} + \sigma\mu_B|\mathbf{H}|, \tag{4.4.5}$$

with $\sigma = \uparrow \equiv 1$ and $\sigma = \downarrow \equiv -1$. Equation 4.4.5 clearly reduces to the standard BCS expression for the spectrum of a singlet superconductor in zero field as $H \to 0$. Also, when $H = 0$ equations 4.4.3 and 4.4.4 reduce to the usual BdG equations [56] and we see that we are justified in associating $d_0(\mathbf{k})$ with the usual singlet superconducting order parameter $\Delta(\mathbf{k})$.

4.4.1 The peculiar independence of the gap of a singlet superconductor on H at T = 0

It is clear from equation 4.4.2 that

$$u_{\sigma-\sigma}(\mathbf{k}) = v_{\sigma\sigma}(\mathbf{k}) = 0. \tag{4.4.6}$$

While it is trivial to show that

$$u_{\sigma\sigma}(\mathbf{k}) = \frac{d_0(\mathbf{k})}{\sqrt{(E_0(\mathbf{k}) - \varepsilon_{\mathbf{k}})^2 + |d_3(\mathbf{k})|^2}} \tag{4.4.7}$$

and

$$v_{\sigma-\sigma}(\mathbf{k}) = \frac{E_0(\mathbf{k}) - \varepsilon_{\mathbf{k}}}{\sqrt{(E_0(\mathbf{k}) - \varepsilon_{\mathbf{k}})^2 + |d_3(\mathbf{k})|^2}} \tag{4.4.8}$$

where

$$E_0(\mathbf{k}) = \sqrt{\varepsilon_{\mathbf{k}} + |d_0(\mathbf{k})|^2}. \tag{4.4.9}$$

$E_0(\mathbf{k})$ is, of course, of the same mathematical form as the spectrum of a singlet superconductor in zero field. However, it is *not* correct to say that $E_0(\mathbf{k})$ *is* the spectrum of a singlet superconductor in zero magnetic field as the value of $d_0(\mathbf{k})$ (although, importantly, not the value of $\varepsilon(\mathbf{k})$) depends on $|\mathbf{H}|$ in general.

Substituting our expressions for the eigenvectors of the BdG into the self-consistency condition (4.3.30) we find that the gap equation is

$$d_0(\mathbf{k}) = -\frac{1}{4}\sum_{\mathbf{k}\sigma} U_{\sigma-\sigma}(\mathbf{k})\frac{d_0(\mathbf{k})}{E_0(\mathbf{k})}\tanh\left(\frac{E_0(\mathbf{k}) + \sigma\mu_B H}{2k_B T}\right). \tag{4.4.10}$$

In zero field the gap equation regains its familiar BCS form [108]. However, we note that surprisingly the field dependence of the gap only enters via the Fermi ($\tanh$) term. This means that when $T = 0$ the gap equation becomes

$$d_0(\mathbf{k}) = -\frac{1}{4}\sum_{\mathbf{k}\sigma} U_{\sigma-\sigma}(\mathbf{k})\frac{d_0(\mathbf{k})}{E_0(\mathbf{k})}. \tag{4.4.11}$$

which is independent of $\mathbf{H}$.

We must now ask what this result means physically, as, thus far, we have considered the gap equation purely as a mathematical exercise. The most obvious conclusion is that, at zero temperature, the gap in independent of field strength. This is true but with one corollary, which we will discuss below.

The gap equation is a non-linear integral equation. And, as such, has, in general, more than one solution. (For example the trivial solution $d_0(\mathbf{k}) = 0$ is always a solution.) All that we have actually shown is that for any given solution $d_0(\mathbf{k})$ is independent $\mathbf{H}$ at $T = 0$. To find the ground state we must consider all possible solutions and calculate the free energy of each solution. In zero field the gap equation can be derived by minimising the free energy with respect to the superconducting order parameter [87]. This leads to the conclusion that the trivial solution is only the ground state when no other solution exists. However, no such proof exists for a superconductor in a finite field. This means that it is perfectly possible there to be a phase transition from the superconducting to normal states as the magnetic field is increased at zero temperature. Any such phase transition will be 'perfectly' first order in the sense that the order parameter will jump from zero (above the critical field, H_C) to some finite value (below H_C) and remain at that value for all $|\mathbf{H}| \leq H_C$. The order parameter as a function of magnetic field strength will therefore resemble a Heaviside step function.

Such a phase transition was first studied independently by Clogston [50] and Chandrasekhar [48] who in fact tacitly assumed the independence what we have shown above. According to the BCS theory, in the absence of a Meissner effect, the difference between the normal state free energy, F_N, and the free energy of the superconducting state, F_{SC}, would be

$$F_N - F_{SC} = \frac{1}{2}\chi_P H^2 \tag{4.4.12}$$

at absolute zero. In the absence of any orbital paramagnetism[5] the paramagnetic susceptibility, χ_P, is given by

$$\chi_P = 2\mu_B^2 D(\varepsilon_F). \tag{4.4.13}$$

(Assuming a g factor of 2.) Where $D(\varepsilon_F)$ is the density of states at the Fermi level.

[5] Or if the orbital paramagnetism is the same in both the normal and superconducting states.

BCS theory also states that in zero field the difference between the energy of the superconducting state relative to the normal state is

$$F_N - F_{SC} = \frac{1}{2}D(\varepsilon_F)|\Delta(0)|^2 \tag{4.4.14}$$

where $\Delta(0)$ is the superconducting order parameter at $T = 0$. Equating (4.4.12) with (4.4.14) we find that

$$(\mu_B H)^2 = \frac{1}{2}|\Delta(0)|^2. \tag{4.4.15}$$

Equation 4.4.15 clearly gives us a criterion for the field at which the free energy of the normal state becomes lower than that of the superconducting state. The limiting field H_P is given by

$$H_P = \frac{|\Delta(0)|}{\sqrt{2}\mu_B}. \tag{4.4.16}$$

This is known both of as Clogston–Chandrasekhar limiting and as Pauli-paramagnetic limiting. Clogston–Chandrasekhar limiting clearly applies to all singlet states, but does not necessarily apply to triplet states. In most superconducting materials $H_{C2} < H_P$. Therefore, if a superconductor has a large upper critical field (in comparison to the Clogston–Chandrasekhar limit) this is good evidence for triplet superconductivity[6].

[6] $H_{C2} > H_P$ is in no way proof of triplet superconductivity as other scenarios are possible. The most well known of these in the Fulde–Ferrell–Larkin–Ovchinnikov (FFLO) state [75, 119, 181]. In the BCS (singlet) state Cooper pairs are formed not only with no net spin, but also with no net angular momentum as an electron in the state $|\mathbf{k}, \sigma\rangle$ pairs with and electron in the state $|-\mathbf{k}, -\sigma\rangle$. In the FFLO state Cooper pairs are formed with finite momentum. In a exchange field the Fermi surface splits into up and down parts. Thus the only way for a Cooper pair to form is for an electron in the state $|\mathbf{k} + \mathbf{q}/2, \sigma\rangle$ to pair with an electron in the state $|-\mathbf{k} + \mathbf{q}/2, -\sigma\rangle$. Meaning that the Cooper pair will have net momentum $\mathbf{q}$.

We will not find FFLO in our calculations because our self consistency relation (4.3.30) does not allow for finite momentum pairing. To find an FFLO state one must define the order parameter by

$$\Delta_{\sigma\sigma'}(\mathbf{k}, \mathbf{k}') = \sum_{\mathbf{q}} -U_{\sigma\sigma'}(\mathbf{k}' - \mathbf{q})\langle \hat{c}_{\mathbf{k}+\mathbf{q}\sigma}\hat{c}_{-\mathbf{k}+\mathbf{q}\sigma'}\rangle. \tag{4.4.17}$$

and then minimise the free energy with respect to $\mathbf{k}$ to find the ground state solution. (Of course $\mathbf{k} = \mathbf{0}$ corresponds to BCS superconductivity.)

The FFLO state is believed to occur in the organic superconductors κ-(BEDT-TTF)$_2$Cu(NCS)$_2$ [196], λ-(BETS)$_2$FeCl$_4$ [209] and λ-(BETS)$_2$GaCl$_4$ [203] (see Singleton and Mielke [195] for a review) and in (very clean samples of) the high κ superconductors, UPd$_2$Al$_3$ [80], CeRu$_2$ [155] and V$_3$Si [76]. There has also been speculation

4.4.2 Thermodynamic quantities of a singlet superconductor in a spin only magnetic field

One of the great successes of BCS theory was that it correctly predicted the behaviour of wide variety of measurable quantities. Some of the simplest quantities (either to calculate or to measure) are the thermodynamic properties of a superconductor. We will now describe such calculations for our model.

Specific heat

Recall from thermodynamics that the specific heat is given by

$$C_V = \frac{\partial^2}{\partial T^2} F = T \frac{\partial^2 S}{\partial T^2}. \tag{4.4.18}$$

And for a Fermionic system

$$S = -k_B \sum_{\mathbf{k}\sigma} \Big[f_{\mathbf{k}\sigma} \ln f_{\mathbf{k}\sigma} + \big(1 - f_{\mathbf{k}\sigma}\big) \ln \big(1 - f_{\mathbf{k}\sigma}\big) \Big]. \tag{4.4.19}$$

Hence we have

$$C_V = -k_B T \sum_{\mathbf{k}\sigma} \frac{\partial}{\partial f_{\mathbf{k}\sigma}} \Big[f_{\mathbf{k}\sigma} \ln f_{\mathbf{k}\sigma} + \big(1 - f_{\mathbf{k}\sigma}\big) \ln \big(1 - f_{\mathbf{k}\sigma}\big) \Big] \frac{\partial f_{\mathbf{k}\sigma}}{\partial T}. \tag{4.4.20}$$

It is straightforward to show that

$$\frac{\partial}{\partial f_{\mathbf{k}\sigma}} \Big[f_{\mathbf{k}\sigma} \ln f_{\mathbf{k}\sigma} + \big(1 - f_{\mathbf{k}\sigma}\big) \ln \big(1 - f_{\mathbf{k}\sigma}\big) \Big] = -\frac{E_{\mathbf{k}\sigma}}{k_B T} \tag{4.4.21}$$

and

$$\frac{\partial f_{\mathbf{k}\sigma}}{\partial T} = f_{\mathbf{k}\sigma}\big(1 - f_{\mathbf{k}\sigma}\big) \left(\frac{E_{\mathbf{k}\sigma}}{k_B T^2} - \frac{1}{k_B T} \frac{\partial E_{\mathbf{k}\sigma}}{\partial T} \right). \tag{4.4.22}$$

From (4.4.5) we have

$$\frac{\partial E_{\mathbf{k}\sigma}}{\partial T} = \frac{1}{\sqrt{\varepsilon_{\mathbf{k}}^2 + |\Delta(\mathbf{k})|^2}} \frac{\partial |\Delta(\mathbf{k})|^2}{\partial T}. \tag{4.4.23}$$

that an FFLO state may occur in ^{3}He/^{4}He mixtures [125], the rutheno-cuprate $RuSr_2GdCu_2O_8$ [192] which is a layered ferromagnetic superconductor and in ferromagnetic, superconductor hetrostructures [103, 112].

We can therefore view the FFLO state as, in a rather loose sense, an intermediate between the singlet and triplet states as it has neither even or odd parity, but it can be expressed as a mixture of the two.

So we have

$$C_V = \sum_{\mathbf{k}\sigma} \frac{1}{k_B T^2} f_{\mathbf{k}\sigma}(1 - f_{\mathbf{k}\sigma}) \left(E_{\mathbf{k}\sigma}^2 - \frac{1}{E_{\mathbf{k}\sigma} - \sigma\mu_B H} \frac{\partial |\Delta(\mathbf{k})|^2}{\partial T} \right). \tag{4.4.24}$$

Magnetisation

The magnetisation, M, of a singlet superconductor must come solely from the elementary excitations, as the Cooper pairs are spin zero and therefore do not contribute to the magnetisation. Thus the magnetisation is given by

$$M = \mu_B \sum_{\mathbf{k}} \Big(f_{\mathbf{k}\uparrow} - f_{\mathbf{k}\downarrow} \Big). \tag{4.4.25}$$

For small $H (= |\mathbf{H}|)$

$$\frac{\partial f_{\mathbf{k}0}}{\partial E} \simeq \frac{f_{\mathbf{k}\uparrow} - f_{\mathbf{k}\downarrow}}{2\mu_B} \tag{4.4.26}$$

where $f_{\mathbf{k}0}$ is the Fermi function of the zero field spectrum, $E_{\mathbf{k}0} = \sqrt{\varepsilon_{\mathbf{k}}^2 + |\Delta(\mathbf{k})|^2}$.

Hence we have

$$\begin{aligned} M &\simeq -2\mu_B^2 H \sum_{\mathbf{k}} \frac{\partial f_{\mathbf{k}0}}{\partial E} && (4.4.27)\\ &\simeq -2\mu_B^2 H \frac{V}{(2\pi^3)} \int \frac{\mathrm{d}\Omega}{4\pi} \int \mathrm{d}k \frac{\partial f_{\mathbf{k}0}}{\partial E} && (4.4.28)\\ &\simeq -2\mu_B^2 H \frac{V}{(2\pi^3)} \int \frac{\mathrm{d}\Omega}{4\pi} \int \mathrm{d}\varepsilon\, D(\varepsilon_F) \frac{\partial f_{\mathbf{k}0}}{\partial E} && (4.4.29)\\ &= 2\mu_B H D(\varepsilon_F) \int \frac{\mathrm{d}\Omega}{4\pi} \int \mathrm{d}\varepsilon \frac{\beta}{4} \mathrm{sech}^2(\beta E_{\mathbf{k}0}/2). && (4.4.30) \end{aligned}$$

where $\beta = \frac{1}{k_B T}$.

Magnetic susceptibility

The magnetic susceptibility, χ, is given by

$$\chi = \frac{\partial M}{\partial H}. \tag{4.4.31}$$

So for small H

$$\chi_{\text{singlet}} = 2\mu_B D(\varepsilon_F) \int \frac{\mathrm{d}\Omega}{4\pi} \int \mathrm{d}\varepsilon \frac{\beta}{4} \mathrm{sech}^2(\beta E_{\mathbf{k}0}/2). \tag{4.4.32}$$

However, of more interest is the Yosida function (see section 3.9 for an introduction), $Y(T)$. To calculate the Yosida function we must first calculate the normal state susceptibility. The normal state energy in a magnetic field is given by

$$\varepsilon_{\mathbf{k}\sigma} = \varepsilon_{\mathbf{k}} - \mu_B \sigma H. \tag{4.4.33}$$

Hence,

$$\begin{aligned} M &= \frac{\partial \Omega}{\partial H} = -\frac{1}{\beta} \sum_{\mathbf{k}\sigma} \frac{\partial}{\partial H} \ln\left(1 + e^{-\beta(\varepsilon_{\mathbf{k}\sigma} - \mu)}\right). & (4.4.34)\\ &= -\frac{\mu_B V}{(2\pi)^3} \sum_{\sigma} \sigma \int \mathrm{d}^3\mathbf{k} \frac{1}{1 + e^{\beta(\varepsilon_{\mathbf{k}\sigma} - \mu)}}. & (4.4.35) \end{aligned}$$

At low temperatures we therefore have

$$\begin{aligned} M &= -\frac{\mu_B V}{2\pi^2} \sum_{\sigma} \sigma \int_0^{k_{F\sigma}} \mathrm{d}k\, k^2 & (4.4.36)\\ &= -\frac{\mu_B V}{2\pi^2} \sum_{\sigma} \sigma \frac{k_{F\sigma}^3}{3}. & (4.4.37) \end{aligned}$$

But

$$N_\sigma = \sum_{\mathbf{k}} n_{\mathbf{k}\sigma} = \frac{V}{(2\pi)^3} \int \mathrm{d}^3\mathbf{k} \Theta(|\mathbf{k}| - k_F) = \frac{V}{\pi^2} \frac{k_F^3}{6}. \tag{4.4.38}$$

So

$$\begin{aligned} M &= -\mu_B \sum_{\sigma} \sigma N_\sigma & (4.4.39)\\ &= -\frac{1}{2}\mu_B \left(\int_0^{\varepsilon_{F\uparrow}} D(\varepsilon)\mathrm{d}\varepsilon - \int_0^{\varepsilon_{F\downarrow}} D(\varepsilon)\mathrm{d}\varepsilon \right) & (4.4.40)\\ &\simeq -\frac{1}{2}\mu_B D(\varepsilon_F) \int_{\varepsilon_{F\downarrow}}^{\varepsilon_{F\uparrow}} \mathrm{d}\varepsilon & (4.4.41)\\ &\simeq \mu_B^2 H D(\varepsilon_F). & (4.4.42) \end{aligned}$$

Clearly then

$$\chi_N \simeq \mu_B^2 D(\varepsilon_F). \tag{4.4.43}$$

Hence the Yosida function for a singlet superconductor in a weak magnetic field is

$$Y(T) = \int \frac{\mathrm{d}\Omega}{4\pi} \int \mathrm{d}\varepsilon \frac{\beta}{4} \mathrm{sech}^2(\beta E_{\mathbf{k}0}/2). \tag{4.4.44}$$

Free energy

The most important thermodynamic quantity to be able to evaluate is the free energy. Once this is known all other thermodynamic quantities can be calculated by taking (numerical[7]) derivatives with respect to the appropriate variable. To evaluate the free energy we must first calculate the expectation value of the Hamiltonian. To facilitate this we express the Hamiltonian (4.3.5) as

$$\hat{\mathcal{H}} = \hat{\mathcal{H}}_0 + \hat{\mathcal{H}}_{int} + \hat{\mathcal{H}}_H. \tag{4.4.45}$$

Where

$$\hat{\mathcal{H}}_0 = \sum_{ij\sigma} t_{ij} \hat{c}^\dagger_{i\sigma} \hat{c}_{j\sigma}, \tag{4.4.46}$$

$$\hat{\mathcal{H}}_{int} = \frac{1}{2} \sum_{ij\sigma\sigma'} U_{ij\sigma\sigma'} \hat{n}_{i\sigma} \hat{n}_{j\sigma'}, \tag{4.4.47}$$

$$\hat{\mathcal{H}}_H = \mu_B \sum_{i\sigma\sigma'} \hat{c}^\dagger_{i\sigma} (\sigma_{\sigma\sigma'} \cdot \mathbf{H}) \hat{c}_{i\sigma}. \tag{4.4.48}$$

Which immediately gives

[7] In practice taking numerical derivative is a poor way to calculate thermodynamic variables as it is computationally expensive and notoriously inaccurate.

$$
\begin{aligned}
F &= \langle\hat{\mathcal{H}}_0\rangle + \langle\hat{\mathcal{H}}_{int}\rangle + \langle\hat{\mathcal{H}}_H\rangle - TS && (4.4.49)\\
&= \sum_{\mathbf{k}\alpha\sigma}\varepsilon_{\mathbf{k}}\Big(u^*_{\alpha\sigma}(-\mathbf{k})u_{\alpha\sigma}(-\mathbf{k})f_{\mathbf{k}\sigma} + v_{\alpha\sigma}(\mathbf{k})v^*_{\alpha\sigma}(\mathbf{k})\big(1-f_{\mathbf{k}\sigma}\big)\Big)\\
&\quad -\frac{1}{2}\sum_{\mathbf{k}\mathbf{k}'\alpha\beta\sigma\sigma'}U(\mathbf{k}-\mathbf{k}')\Big[u^*_{\alpha\sigma}(-\mathbf{k})v_{\beta\sigma}(\mathbf{k})f_{\mathbf{k}\sigma} + v_{\alpha\sigma}(-\mathbf{k})u^*_{\beta\sigma}(\mathbf{k})\big(1-f_{\mathbf{k}\sigma}\big)\Big]\\
&\qquad\qquad \times\Big[u_{\alpha\sigma'}(-\mathbf{k}')v^*_{\beta\sigma'}(\mathbf{k}')f_{\mathbf{k}'\sigma'} + v^*_{\alpha\sigma'}(-\mathbf{k}')u_{\beta\sigma'}(\mathbf{k}')\big(1-f_{\mathbf{k}'\sigma'}\big)\Big]\\
&\quad +\sum_{\mathbf{k}\alpha\beta\sigma}\big(\sigma_{\alpha\beta}\cdot\mathbf{H}\big)\Big(u^*_{\alpha\sigma}(\mathbf{k})u_{\beta\sigma}(\mathbf{k})f_{\mathbf{k}\sigma} + v_{\alpha\sigma}(\mathbf{k})v^*_{\alpha\sigma}(\mathbf{k})\big(1-f_{\mathbf{k}\sigma}\big)\Big)\\
&\quad -k_BT\sum_{\mathbf{k}\sigma}\Big[f_{\mathbf{k}\sigma}\ln f_{\mathbf{k}\sigma} + \big(1-f_{\mathbf{k}\sigma}\big)\ln\big(1-f_{\mathbf{k}\sigma}\big)\Big] && (4.4.50)
\end{aligned}
$$

4.5 Numerical solution of the singlet Bogoliubov–de Gennes equations for a singlet superconductor in an exchange field

We now solve the spin-generalised BdG equations self consistently with a on site potential. The self consistency condition demands that all solutions have even parity, that is that only singlet solutions exist (and indeed only singlet solutions were found numerically). This means that we could solve the special case of the singlet BdG (4.4.3, 4.4.4) (or indeed the singlet gap equation (4.4.10)). However, we choose instead to solve the full spin-generalised BdG equations (4.3.25) self consistently (4.3.30) as this allows us to check that the code, which we will make extensive use of throughout this thesis, correctly reproduces the well tested results of BCS theory for $\mathbf{H} = 0$. The results in a finite exchange field are less well known so we report the results both in the zero temperature and finite temperature cases.

4.5.1 The special case of zero field: comparison of self-consistent solution of the spin-generalised BdG equations with the solution of the gap equation using the Bessel function method

We calculated the zero field gap as a function of temperature using both the density of states obtained by the Bessel function method given in appendix A.1 and by solving the spin generalised BdG equations self consistently. The results from both calculations are shown in figure 4.2. The two calculations are in excellent agreement and both reproduce the well known [108] result of BCS theory that

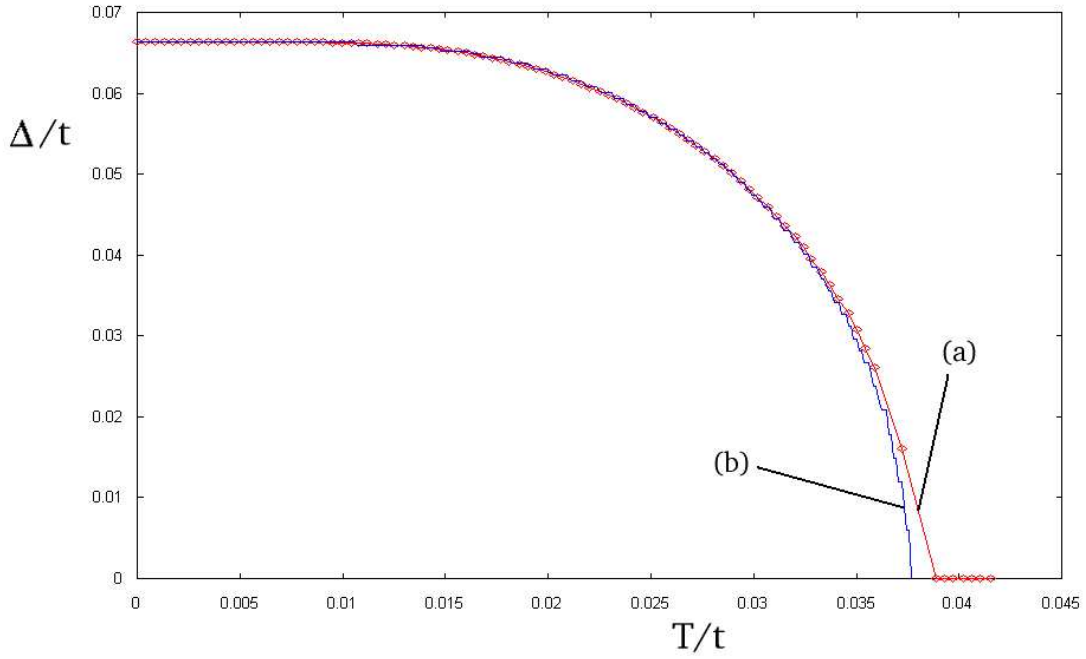

Figure 4.2: The gap of an s-wave superconductor in zero field as a function of temperature calculated (a) by solving the spin generalised BdG equations self consistently and (b) using the DOS found from the Bessel function method.

$$\frac{|\Delta(0)|}{k_B T} = 1.76 \tag{4.5.1}$$

where $|\Delta(0)|$ is the magnitude of the gap at zero temperature. Figure 4.3 shows the calculated heat capacity, as a function of temperature. This shows the expected (see table 3.1) $\sim e^{\frac{-|\Delta(0)|}{k_B T}}$ temperature dependence at low temperatures.

Near T_C the order parameter and hence the gap, becomes small. This means that the solution of the BdG equations takes much longer to converge, the accuracy of the numerical solution is also somewhat questionable as the (relative) importance of numerical noise increases. The standard BCS result for the specific heat anomaly,

$$\frac{C_V^{SC} - C_V^N}{C_V^N} = 1.43, \tag{4.5.2}$$

can only be obtained by fitting the gap near T_C to the behaviour of the gap over the whole range of temperature.

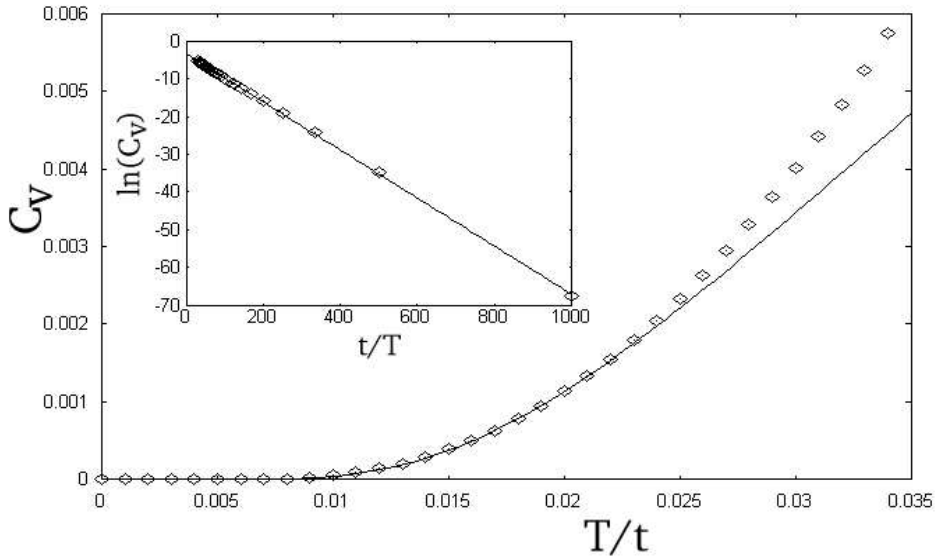

Figure 4.3: Low temperature heat capacity of a s-wave superconductor in zero field as a function of temperature. Inset: logarithmic plot of the same data. The line shown, in both plots, is $C_V = 1.06e^{-\Delta(0)/T}$.

4.5.2 The special case of zero temperature: comparison of numerical results with analytical results

The gap is plotted as a function of magnetic field strength in figure 4.4. We note that the zero temperature gap is independent of magnetic field strength as was predicted in section 4.4.1. In fact the order parameter does not go to zero when the Clogston–Chandrasekhar limiting field ($|\mathbf{H}| > \frac{|\Delta(0)|}{\sqrt{2}}$, see section 4.4.1 for details) is exceed. However, at the Clogston–Chandrasekhar limiting field the normal state free energy becomes lower than the superconducting free energy.

4.5.3 Finite fields and finite temperatures

We plot the gap over the full range of temperatures and fields for which it is finite and the ground state solution (figure 4.4). We note that in a finite field the superconducting transition is first order where as it is a second order phase transition in zero field. This means that we cannot fit the low temperature gap in small fields (where the phase transition is only weakly first order) and so we cannot calculate the specific heat anomaly accurately in a finite field. In figure 4.5 we plot the transition temperature as a function of magnetic field.

In 4.6, 4.7 and 4.8 we show the low temperature behaviour of specific heat, magnetisation

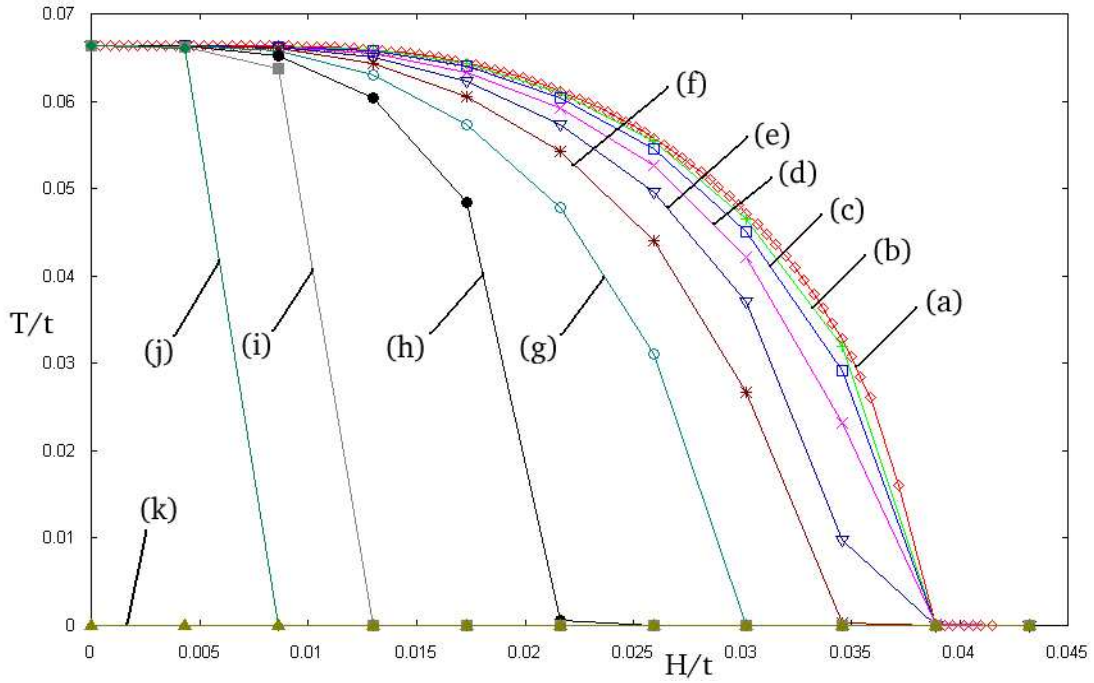

Figure 4.4: The gap as a function of magnetic field strength and temperature calculated by solving the spin generalised BdG equations self consistently. The field strengths are (a) $H = 0$, (b) $H = 0.005t$, (c) $H = 0.01t$, (d) $H = 0.015t$, (e) $H = 0.02t$, (f) $H = 0.025t$, (g) $H = 0.03t$, (h) $H = 0.035t$, (i) $H = 0.04t$, (j) $H = 0.045t$, (k) $H = 0.05t$.

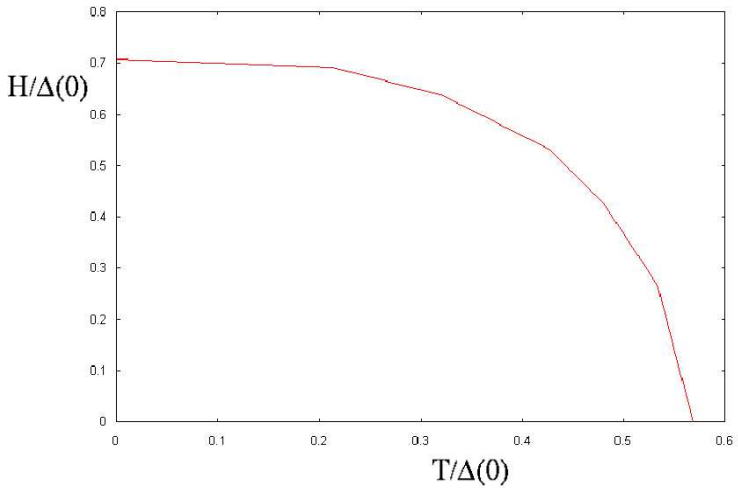

Figure 4.5: The phase diagram of an s-wave superconductor in a magnetic field calculated by solving the spin generalised BdG equations self consistently.

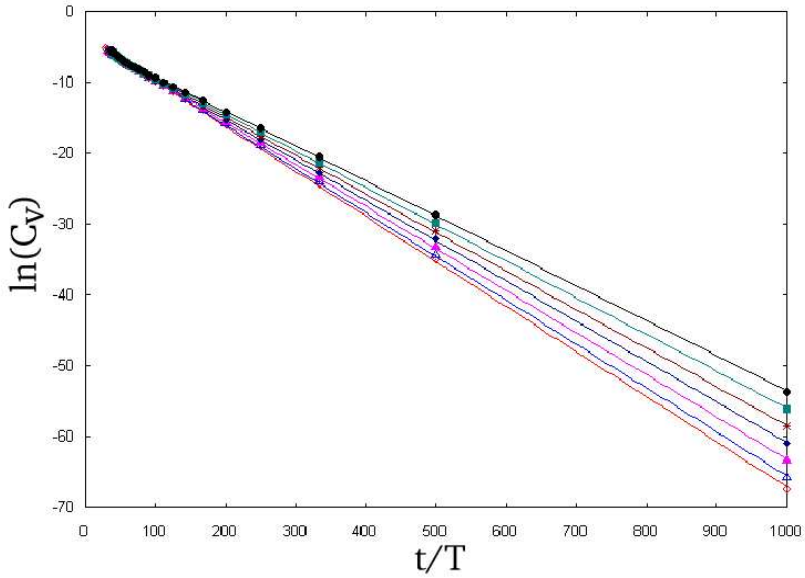

Figure 4.6: Logarithmic plot of the low temperature specific heat of an s-wave superconductor in a magnetic field as a function of magnetic field strength. From bottom up the magnetic field strengths are: 0, $0.0025t$, $0.005t$, $0.0075t$, $0.01t$ and $0.0125t$, $0.015t$. The lines are fits to the data.

and magnetic susceptibility as functions of temperature and field. By fitting each of these to the form

$$\{C_V, M, \chi\} \sim e^{\frac{-\Delta_{eff}}{k_B T}} \tag{4.5.3}$$

thus we are able to plot the effective gap, Δ_{eff}, as a function of magnetic field strength in figure 4.9. Thus we see that the *effective gap* 'seen' by thermodynamic functions of a s-wave superconductor is given by

$$\Delta_{eff} = \Delta(0) - \mu_B |H|. \tag{4.5.4}$$

Finally we note that these results are independent of the direction of the magnetic field as expected.

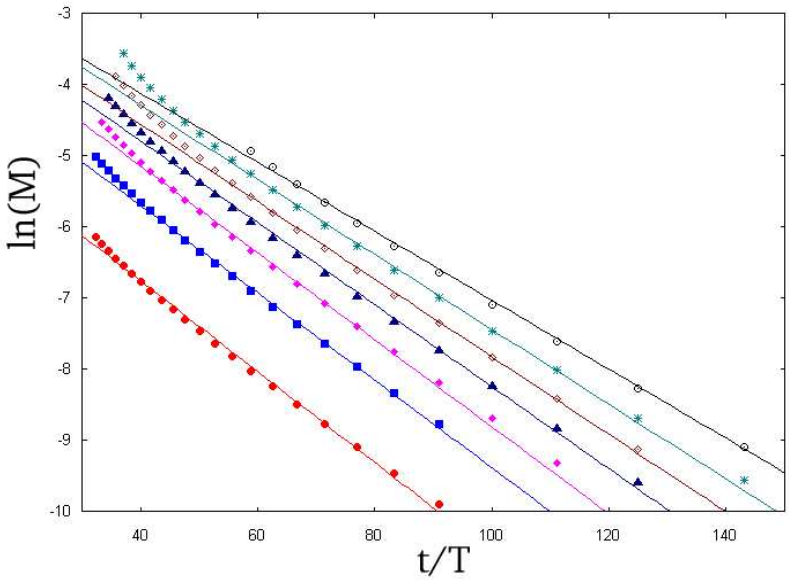

Figure 4.7: Logarithmic plot of the low temperature magnetisation of an s-wave superconductor in a magnetic field as a function of magnetic field strength. From bottom up the magnetic field strengths are: $0.00125t$, $0.00375t$, $0.00625t$, $0.0875t$, $0.01125t$, $0.01375t$ and 0.01625t. The lines are fits to the data.

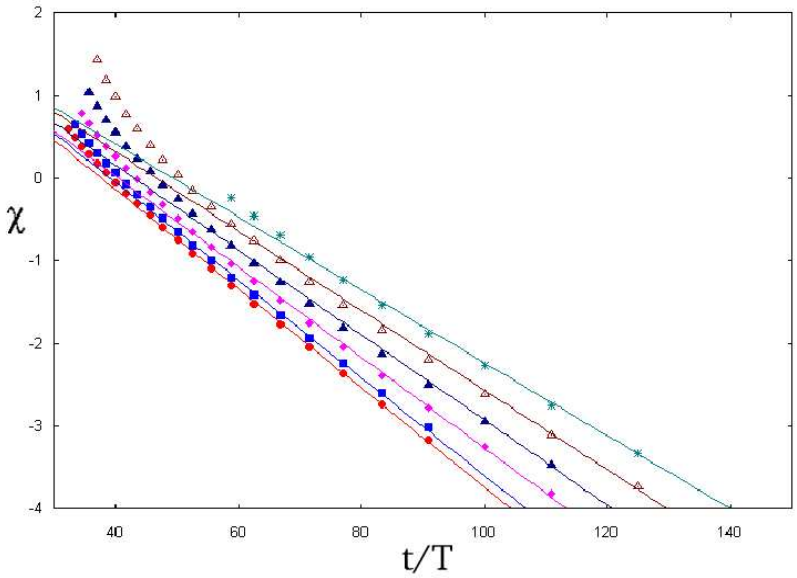

Figure 4.8: Logarithmic plot of the low temperature magnetic susceptibility of an s-wave superconductor in a magnetic field as a function of magnetic field strength. From bottom up the magnetic field strengths are: $0.0025t$, $0.005t$, $0.0075t$, $0.01t$ and $0.0125t$, $0.015t$. The lines are fits to the data.

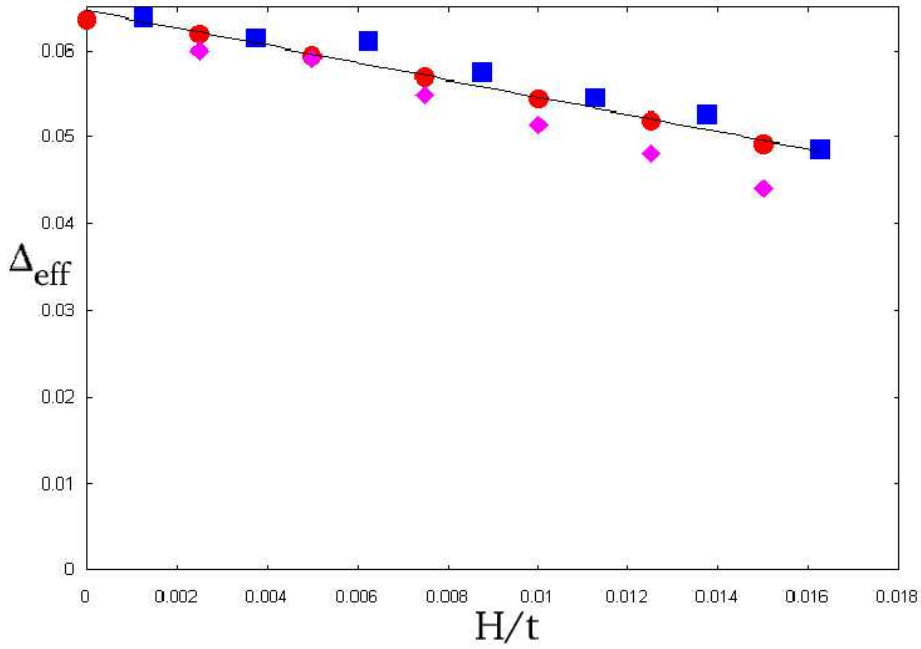

Figure 4.9: The effective gap of an s-wave superconductor as a function of magnetic field. As calculated from specific heat (●), magnetisation (■), and magnetic susceptibility (⧫).

4.6 A microscopic model for a triplet superconductor in a magnetic field

We will now consider the properties of a triplet superconductor in a magnetic field. We are able to derive many of the quantities that we have derived for a singlet superconductor.

4.6.1 The generalisation of a theorem concerning eigenstates which correspond to negative eigenvalues

Before we begin we will generalise a useful theorem due to de Gennes [56]. For a singlet superconductor in zero field the BdG equations are

$$\begin{pmatrix} \varepsilon_{\mathbf{k}} & d_0(\mathbf{k}) \\ d_0^*(\mathbf{k}) & -\varepsilon_{\mathbf{k}} \end{pmatrix} \begin{pmatrix} u(\mathbf{k}) \\ v(\mathbf{k}) \end{pmatrix} = E(\mathbf{k}) \begin{pmatrix} u(\mathbf{k}) \\ v(\mathbf{k}) \end{pmatrix}. \tag{4.6.1}$$

De Gennes showed that if $\begin{pmatrix} u(\mathbf{k}) \\ v(\mathbf{k}) \end{pmatrix}$ is the eigenvector corresponding to the eigenvalue $E(\mathbf{k})$,

then $\begin{pmatrix} -v^*(\mathbf{k}) \\ u^*(\mathbf{k}) \end{pmatrix}$ is also an eigenvector and that the corresponding eigenvalue is $-E(\mathbf{k})$. Clearly these are then the only eigenstates of the BdG equations. This theorem is a direct consequence of the fact that the Hartree–Fock–Gorkov Hamiltonian is diagonalised via a unitary transformation.

We will now extend this theorem to the spin generalised BdG equations in a magnetic field. We begin by writing the BdG equations (4.3.25) in a pseudo-spinor notation:

$$\begin{pmatrix} \underline{\underline{\xi}}(\mathbf{k}) & \underline{\underline{\Delta}}_{\mathbf{k}} \\ -\underline{\underline{\Delta}}^*_{-\mathbf{k}} & -\underline{\underline{\xi}}^*(\mathbf{k}) \end{pmatrix} \begin{pmatrix} \underline{u}_\sigma(\mathbf{k}) \\ \underline{v}_\sigma(\mathbf{k}) \end{pmatrix} = E_\sigma(\mathbf{k}) \begin{pmatrix} \underline{u}_\sigma(\mathbf{k}) \\ \underline{v}_\sigma(\mathbf{k}) \end{pmatrix}. \tag{4.6.2}$$

Where

$$\underline{\underline{\xi}}(\mathbf{k}) = \begin{pmatrix} \varepsilon_{\mathbf{k}} + \mu_B H_3 & \mu_B(H_1 - \mathtt{i}H_2) \\ \mu_B(H_1 + \mathtt{i}H_2) & \varepsilon_{\mathbf{k}} - \mu_B H_3 \end{pmatrix}, \tag{4.6.3}$$

$$\underline{\underline{\Delta}}_{\mathbf{k}} = \begin{pmatrix} \Delta_{\uparrow\uparrow}(\mathbf{k}) & \Delta_{\uparrow\downarrow}(\mathbf{k}) \\ \Delta_{\downarrow\uparrow}(\mathbf{k}) & \Delta_{\downarrow\downarrow}(\mathbf{k}) \end{pmatrix}, \tag{4.6.4}$$

$$\underline{u}_\sigma(\mathbf{k}) = \begin{pmatrix} u_{\uparrow\sigma}(\mathbf{k}) \\ u_{\downarrow\sigma}(\mathbf{k}) \end{pmatrix}, \tag{4.6.5}$$

and

$$\underline{v}_\sigma(\mathbf{k}) = \begin{pmatrix} v_{\uparrow\sigma}(\mathbf{k}) \\ v_{\downarrow\sigma}(\mathbf{k}) \end{pmatrix}. \tag{4.6.6}$$

Multiplying by -1, taking the complex conjugate, parity inverting and exchanging the rows of equation 4.6.2 leads to

$$\begin{pmatrix} \underline{\underline{\xi}}(-\mathbf{k}) & \underline{\underline{\Delta}}(\mathbf{k}) \\ -\underline{\underline{\Delta}}^*(-\mathbf{k}) & -\underline{\underline{\xi}}^*(-\mathbf{k}) \end{pmatrix} \begin{pmatrix} \underline{u}^*_\sigma(-\mathbf{k}) \\ \underline{v}^*_\sigma(-\mathbf{k}) \end{pmatrix} = -E_\sigma(-\mathbf{k}) \begin{pmatrix} \underline{u}^*_\sigma(-\mathbf{k}) \\ \underline{v}^*_\sigma(-\mathbf{k}) \end{pmatrix}. \tag{4.6.7}$$

But, $E_\sigma(-\mathbf{k})$ and $\underline{\underline{\xi}}(-\mathbf{k})$ are both even under parity inversion. So we arrive at

$$\begin{pmatrix} \underline{\underline{\xi}}(\mathbf{k}) & \underline{\underline{\Delta}}(\mathbf{k}) \\ -\underline{\underline{\Delta}}^*(\mathbf{k}) & -\underline{\underline{\xi}}^*(-\mathbf{k}) \end{pmatrix} \begin{pmatrix} \underline{u}^*_\sigma(-\mathbf{k}) \\ \underline{v}^*_\sigma(-\mathbf{k}) \end{pmatrix} = -E_\sigma(\mathbf{k}) \begin{pmatrix} \underline{u}^*_\sigma(-\mathbf{k}) \\ \underline{v}^*_\sigma(-\mathbf{k}) \end{pmatrix}. \tag{4.6.8}$$

We have therefore shown that if $\begin{pmatrix} \underline{u}_\sigma(\mathbf{k}) \\ \underline{v}_\sigma(\mathbf{k}) \end{pmatrix}$ is an eigenvector of the spin-generalised BdG

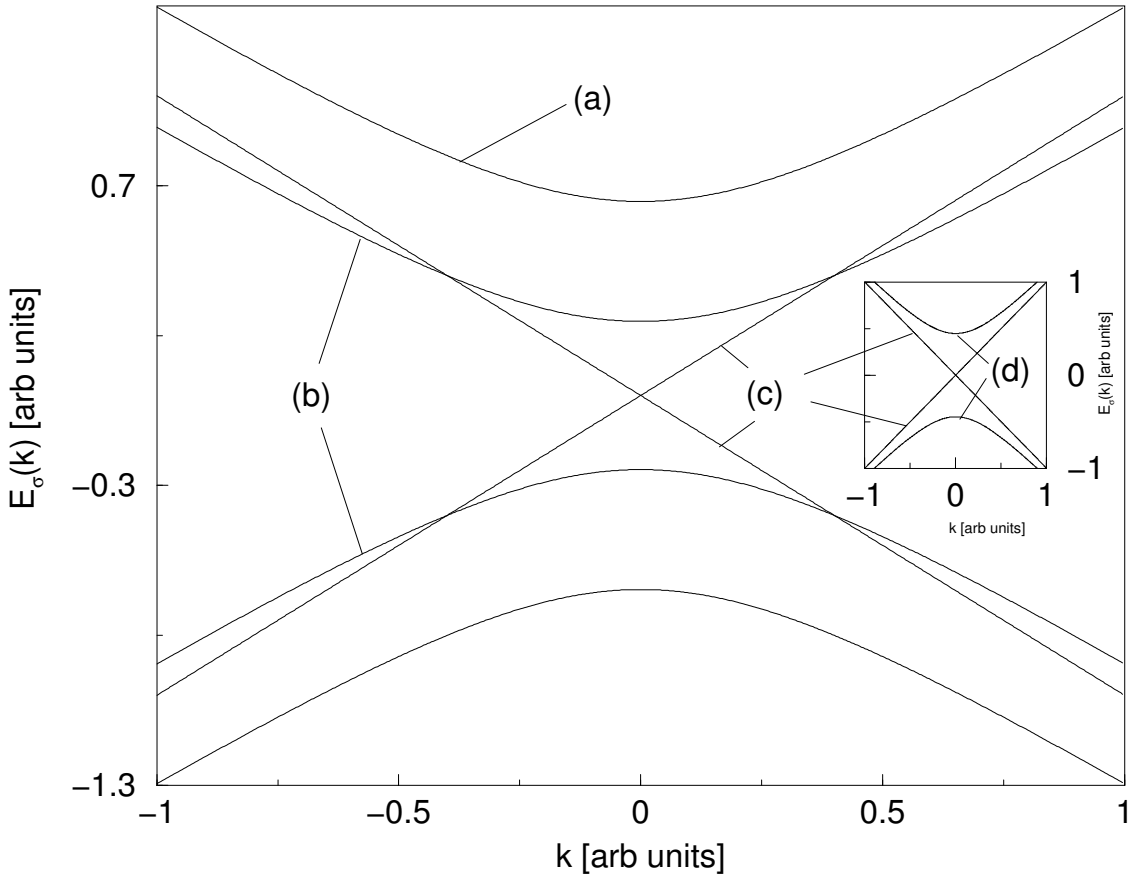

Figure 4.10: The four branches of the singlet spectrum in a magnetic field. Inset, the zero field limit where the two spin branches become degenerate. The branches are (a) the spectra for $\sigma = \uparrow$, (b) the spectra for $\sigma = \downarrow$, (c) the normal state spectra in zero field and (d) the singlet spectrum for $\mathbf{H} = 0$.

equations in a magnetic field, with the corresponding eigenvalue $E_\sigma(\mathbf{k})$ then, $\begin{pmatrix} \underline{u}^*_\sigma(-\mathbf{k}) \\ \underline{v}^*_\sigma(-\mathbf{k}) \end{pmatrix}$ is also an eigenvector and the corresponding eigenvalue is $-E_\sigma(\mathbf{k})$. As σ can take two values ($\uparrow$ or $\downarrow$) we have identified all of the eigenstates.

This analysis holds for both triplet and singlet states. (For a singlet state with $|\mathbf{H}| = 0$ it clearly reduces to the theorem of de Gennes.) For a singlet superconductor in a magnetic field the spectrum is given by (4.4.5). We plot the four branches of the singlet spectrum in figure 4.10 this result is in agreement with the theorem derived above.

4.6.2 The spectrum of a triplet superconductor in a magnetic field

By setting the singlet order parameter, $d_0(\mathbf{k})$, to zero we can write down the BdG equations for a triplet superconductor in magnetic field,

$$\begin{pmatrix} \varepsilon_{\mathbf{k}}+\mu_B H_3 & \mu_B(H_1-\mathtt{i}H_2) & -d_1(\mathbf{k})+\mathtt{i}d_2(\mathbf{k}) & d_3(\mathbf{k}) \\ \mu_B(H_1+\mathtt{i}H_2) & \varepsilon_{\mathbf{k}}-\mu_B H_3 & d_3(\mathbf{k}) & d_1(\mathbf{k})+\mathtt{i}d_2(\mathbf{k}) \\ -d_1^*(\mathbf{k})-\mathtt{i}d_2^*(\mathbf{k}) & d_3^*(\mathbf{k}) & -\varepsilon_{\mathbf{k}}-\mu_B H_3 & \mu_B(-H_1-\mathtt{i}H_2) \\ d_3^*(\mathbf{k}) & d_1^*(\mathbf{k})-\mathtt{i}d_2^*(\mathbf{k}) & \mu_B(-H_1+\mathtt{i}H_2) & -\varepsilon_{\mathbf{k}}+\mu_B H_3 \end{pmatrix} \begin{pmatrix} u_{\uparrow\sigma}(\mathbf{k}) \\ u_{\downarrow\sigma}(\mathbf{k}) \\ v_{\uparrow\sigma}(\mathbf{k}) \\ v_{\downarrow\sigma}(\mathbf{k}) \end{pmatrix} = E_\sigma(\mathbf{k}) \begin{pmatrix} u_{\uparrow\sigma}(\mathbf{k}) \\ u_{\downarrow\sigma}(\mathbf{k}) \\ v_{\uparrow\sigma}(\mathbf{k}) \\ v_{\downarrow\sigma}(\mathbf{k}) \end{pmatrix}. \quad (4.6.9)$$

The eigenvalues of the BdG equations are given by the solutions of the characteristic equation

$$\begin{aligned} &\Big(E_\sigma(\mathbf{k})^2+\mu_B^2|\mathbf{H}|^2-\varepsilon_{\mathbf{k}}\Big)^2-4\mu_B^2E_\sigma(\mathbf{k})|\mathbf{H}|^2 \\ -d_1(\mathbf{k})\Big\{&2d_1^*(\mathbf{k})\Big(\varepsilon_{\mathbf{k}}^2+H_3^2+E_\sigma^2(\mathbf{k})-H_1^2+H_2^2\Big) \\ &-2\mathtt{i}d_2^*(\mathbf{k})\Big(2H_3\varepsilon_{\mathbf{k}}-2\mathtt{i}H_1H_2\Big) \\ &+2d_1^*(\mathbf{k})\Big(-2H_1H_3+2\mathtt{i}H_2\varepsilon_{\mathbf{k}}\Big)\Big\} \\ +\mathtt{i}d_2(\mathbf{k})\Big\{&2d_3^*(\mathbf{k})\Big(2H_3\varepsilon_{\mathbf{k}}+2\mathtt{i}H_1H_2\Big) \\ &-2\mathtt{i}d_2^*(\mathbf{k})\Big(\varepsilon_{\mathbf{k}}^2+H_3^2-E_\sigma(\mathbf{k})+H_1^2+H_2^2\Big) \\ &+2d_3^*(\mathbf{k})\Big(-2H_1\varepsilon_{\mathbf{k}}+2\mathtt{i}H_2H_3\Big)\Big\} \\ -2d_3(\mathbf{k})\Big\{&d_1^*(\mathbf{k})\Big(-2H_1H_2-2\mathtt{i}H_2\varepsilon_{\mathbf{k}}\Big) \\ &-\mathtt{i}d_2^*(\mathbf{k})\Big(-2H_1\varepsilon_{\mathbf{k}}-2\mathtt{i}H_2H_3\Big) \\ &+d_3^*(\mathbf{k})\Big(\varepsilon_{\mathbf{k}}^2-E_\sigma^2(\mathbf{k})+H_1^2+H_2^2-H_3^2\Big)\Big\} \;&=\; 0. \end{aligned} \quad (4.6.10)$$

Upon 'spotting' the relevant vector terms we find that

$$\Big(E_\sigma(\mathbf{k})^2+\mu_B^2|\mathbf{H}|^2-\varepsilon_{\mathbf{k}}\Big)^2-4\mu_B^2E_\sigma(\mathbf{k})|\mathbf{H}|^2-2\Big\{|\mathbf{d}|^2\Big(\varepsilon_{\mathbf{k}}^2-E_\sigma^2(\mathbf{k})+|\mathbf{H}|^2\Big)$$
$$-2\mathrm{i}\varepsilon_{\mathbf{k}}\mathbf{H}\cdot\big(\mathbf{d}(\mathbf{k})\times\mathbf{d}^*(\mathbf{k})\big)-2\Big(\mathbf{H}\cdot\mathbf{d}(\mathbf{k})\Big)\Big(\mathbf{H}\cdot\mathbf{d}^*(\mathbf{k})\Big)\Big\} \;=\; 0. \tag{4.6.11}$$

On noting that $|\mathbf{d}(\mathbf{k})|^4-|\mathbf{d}(\mathbf{k})\cdot\mathbf{d}^*(\mathbf{k})|^2=|\mathbf{d}(\mathbf{k})\times\mathbf{d}^*(\mathbf{k})|^2$ we find that

$$\boxed{E_\sigma(\mathbf{k})=\sqrt{\varepsilon_{\mathbf{k}}^2+\mu_B^2|\mathbf{H}|^2+|\mathbf{d}(\mathbf{k})|^2+\sigma\sqrt{\Lambda(\mathbf{k})}}} \tag{4.6.12}$$

where

$$\boxed{\Lambda(\mathbf{k})=|\mathbf{d}(\mathbf{k})\times\mathbf{d}^*(\mathbf{k})|^2+4\varepsilon_{\mathbf{k}}^2\mu_B^2|\mathbf{H}|^2+4\mu_B^2|\mathbf{H}\cdot\mathbf{d}(\mathbf{k})|^2+4\mathrm{i}\varepsilon_{\mathbf{k}}\mu_B\mathbf{H}\cdot\mathbf{d}(\mathbf{k})\times\mathbf{d}^*(\mathbf{k}).} \tag{4.6.13}$$

It should be noted that this does not assume a unitary order parameter[8]. Also in zero field we clearly have the usual result for a triplet superconductor that

$$E_\sigma(\mathbf{k})=\sqrt{\varepsilon_{\mathbf{k}}^2+|\mathbf{d}(\mathbf{k})|^2+\sigma|\mathbf{d}(\mathbf{k})\times\mathbf{d}^*(\mathbf{k})|}. \tag{4.6.14}$$

4.6.3 Thermodynamic properties of a triplet superconductor in a magnetic field

As for the singlet case one can calculate thermodynamic properties for a triplet superconductor. Below we examine the same case which we considered for the singlet case.

Specific heat

For example the specific heat is given by

$$C_V = T\frac{\partial S}{\partial T} \tag{4.6.15}$$
$$= -k_BT\frac{\partial}{\partial T}\sum_{\mathbf{k}\sigma}(f_{\mathbf{k}\sigma}ln(f_{\mathbf{k}\sigma})+(1-f_{\mathbf{k}\sigma})ln(1-f_{\mathbf{k}\sigma})) \tag{4.6.16}$$
$$= \sum_{\mathbf{k}\sigma}f_{\mathbf{k}\sigma}(1-f_{\mathbf{k}\sigma})\left(\frac{E_\sigma(\mathbf{k})^2}{k_BT^2}+\frac{1}{k_BT}E_\sigma(\mathbf{k})\frac{\partial}{\partial T}E_\sigma(\mathbf{k})\right) \tag{4.6.17}$$

[8] A unitary state is any state for which $\mathbf{d}(\mathbf{k})\times\mathbf{d}^*(\mathbf{k})=0$. See section 3.9 for details.

From (4.6.12) we have

$$\sum_\sigma E_\sigma(\mathbf{k})\frac{\partial}{\partial T}E_\sigma(\mathbf{k}) = E_\sigma(\mathbf{k})\left(\frac{\partial \mathbf{d}(\mathbf{k})}{\partial T}\frac{\partial}{\partial \mathbf{d}(\mathbf{k})} + \frac{\partial \mathbf{d}^*(\mathbf{k})}{\partial T}\frac{\partial}{\partial \mathbf{d}^*(\mathbf{k})} + \frac{\partial \Lambda(\mathbf{k})}{\partial T}\frac{\partial}{\partial \Lambda(\mathbf{k})}\right)E_\sigma(\mathbf{k}) \tag{4.6.18}$$

$$= \sum_\sigma\left(\frac{\mathbf{d}^*(\mathbf{k})}{2}\frac{\partial \mathbf{d}(\mathbf{k})}{\partial T} + \frac{\mathbf{d}(\mathbf{k})}{2}\frac{\partial \mathbf{d}^*(\mathbf{k})}{\partial T} + \sigma\frac{\partial \Lambda(\mathbf{k})}{\partial T}\right) \tag{4.6.19}$$

$$= \frac{1}{2}\frac{\partial}{\partial T}|\mathbf{d}(\mathbf{k})|^2. \tag{4.6.20}$$

Hence

$$C_V = \sum_{\mathbf{k}\sigma}\frac{f_{\mathbf{k}\sigma}(1-f_{\mathbf{k}\sigma})}{k_B T^2}\left(E_\sigma(\mathbf{k})^2 - \frac{T}{2}\frac{d}{dT}|\mathbf{d}(\mathbf{k})|^2\right) \tag{4.6.21}$$

Magnetisation

The fact that the magnetic field only appears in the third term of the Hamiltonian greatly simplifies the calculation of the magnetisation.

$$\mathbf{M} = \frac{\partial F}{\partial \mathbf{H}} \tag{4.6.22}$$

$$= \frac{\partial\langle\hat{\mathcal{H}}_0\rangle}{\partial \mathbf{H}} + \frac{\partial\langle\hat{\mathcal{H}}_{int}\rangle}{\partial \mathbf{H}} + \frac{\partial\langle\hat{\mathcal{H}}_H\rangle}{\partial \mathbf{H}} + \frac{\partial S}{\partial \mathbf{H}} \tag{4.6.23}$$

$$= \frac{\partial\langle\hat{\mathcal{H}}_H\rangle}{\partial \mathbf{H}} + \frac{\partial S}{\partial \mathbf{H}} \tag{4.6.24}$$

Assuming $\frac{\partial S}{\partial H}$ is small we have

$$\mathbf{M} \simeq \mu_B\sum_{\mathbf{k}\alpha\beta}\langle\hat{c}^\dagger_{\mathbf{k}\alpha}\sigma_{\alpha\beta}\hat{c}_{\mathbf{k}\beta}\rangle \tag{4.6.25}$$

$$\begin{aligned} = \mu_B\sum_{\mathbf{k}}\Big(& u^*_{\uparrow\sigma}(\mathbf{k})u_{\downarrow\sigma}(\mathbf{k})f_{\mathbf{k}\sigma} + v_{\uparrow\sigma}(\mathbf{k})v^*_{\downarrow\sigma}(\mathbf{k})\big(1-f_{\mathbf{k}\sigma}\big) \\ &\quad + u^*_{\downarrow\sigma}(\mathbf{k})u_{\uparrow\sigma}(\mathbf{k})f_{\mathbf{k}\sigma} + v_{\downarrow\sigma}(\mathbf{k})v^*_{\uparrow\sigma}(\mathbf{k})\big(1-f_{\mathbf{k}\sigma}\big), \\ & -\mathtt{i}u^*_{\uparrow\sigma}(\mathbf{k})u_{\downarrow\sigma}(\mathbf{k})f_{\mathbf{k}\sigma} - \mathtt{i}v_{\uparrow\sigma}(\mathbf{k})v^*_{\downarrow\sigma}(\mathbf{k})\big(1-f_{\mathbf{k}\sigma}\big) \\ &\quad + \mathtt{i}u^*_{\downarrow\sigma}(\mathbf{k})u_{\uparrow\sigma}(\mathbf{k})f_{\mathbf{k}\sigma} + \mathtt{i}v_{\downarrow\sigma}(\mathbf{k})v^*_{\uparrow\sigma}(\mathbf{k})\big(1-f_{\mathbf{k}\sigma}\big), \\ & +u^*_{\uparrow\sigma}(\mathbf{k})u_{\uparrow\sigma}(\mathbf{k})f_{\mathbf{k}\sigma} + v_{\downarrow\sigma}(\mathbf{k})v^*_{\downarrow\sigma}(\mathbf{k})\big(1-f_{\mathbf{k}\sigma}\big) \\ &\quad - u^*_{\downarrow\sigma}(\mathbf{k})u_{\uparrow\sigma}(\mathbf{k})f_{\mathbf{k}\sigma} - v_{\downarrow\sigma}(\mathbf{k})v^*_{\uparrow\sigma}(\mathbf{k})\big(1-f_{\mathbf{k}\sigma}\big)\Big). \end{aligned} \tag{4.6.26}$$

Note that here we have calculated the magnetisation vector because in many triplet systems the direction of the applied field will often effect the magnetisation. Where as in the more isotropic singlet system we calculated $M = |\mathbf{M}|$.

Magnetic susceptibility

It is not clear how to calculate the susceptibility in the general case, as to take derivatives of the magnetisation (equation 4.6.26) one must know how the self-consistent solution of the BdG equations evolves with $\mathbf{H}$. This means that in numerical calculations the best strategy is to evaluate the susceptibility tensor (defined by $M_\alpha = \chi_{\alpha\beta} H_\beta$) by taking numerical derivatives of the magnetisation.

However, particularly for the inert phases, if one assumes a particular phase some analytical progress can be made. Such results are reported in section 3.9, while for detailed calculations the reader is referred to Leggett [123] or Mineev and Samokhin [154].

Free energy

The derivation of the free energy for a singlet superconductor (section 4.4.2) did not actually make any assumptions about the parity of the superconducting order parameter. Therefore equation 4.4.50 also holds for a triplet superconductor.

4.7 A few special cases

We conclude this chapter by examining a few special cases. We do this both because making a few assumptions can yield some surprising results and aid our understanding and because we can compare these exact results with our numerical calculations which will be presented in later chapters.

4.7.1 $\mathrm{d}(\mathrm{k})$ parallel to H

For a triplet superconductor with $\mathbf{H}$ parallel[9] to $\mathbf{d}(\mathbf{k})$ and $\mathbf{z}$ the BdG equations are

[9] As $\mathbf{d}(\mathbf{k})$ is a complex vector it is not immediately clear what saying $\mathbf{d}(\mathbf{k})$ is 'parallel to' or indeed 'perpendicular to' a real vector means. (On the other hand these notions are clearly well defined between two complex three-vectors in a six dimensional real space.) Rather than defining some complicated generalisation of parallel and perpendicular, in this thesis we will restrict ourselves to the following meaning, which will clearly satisfy any reasonable generalisations of parallel and perpendicular:

$$\begin{pmatrix} \varepsilon_{\mathbf{k}} + \mu_B H & 0 & 0 & d_3(\mathbf{k}) \\ 0 & \varepsilon_{\mathbf{k}} - \mu_B H & d_3(\mathbf{k}) & 0 \\ 0 & d_3^*(\mathbf{k}) & -\varepsilon_{-\mathbf{k}} - \mu_B H & 0 \\ d_3^*(\mathbf{k}) & 0 & 0 & -\varepsilon_{-\mathbf{k}} + \mu_B H \end{pmatrix} \begin{pmatrix} u_{\uparrow\sigma}(\mathbf{k}) \\ u_{\downarrow\sigma}(\mathbf{k}) \\ v_{\uparrow\sigma}(\mathbf{k}) \\ v_{\downarrow\sigma}(\mathbf{k}) \end{pmatrix}$$
$$= E_\sigma(\mathbf{k}) \begin{pmatrix} u_{\uparrow\sigma}(\mathbf{k}) \\ u_{\downarrow\sigma}(\mathbf{k}) \\ v_{\uparrow\sigma}(\mathbf{k}) \\ v_{\downarrow\sigma}(\mathbf{k}) \end{pmatrix}. \tag{4.7.1}$$

Hence, the eigenvalues are

$$E_\sigma(\mathbf{k}) = E_0(\mathbf{k}) + \sigma\mu_B H \tag{4.7.2}$$

where

$$E_0(\mathbf{k}) = \sqrt{\varepsilon_{\mathbf{k}} + |d_3(\mathbf{k})|^2}. \tag{4.7.3}$$

Which has the same form as the spectrum in zero field. The eigenvectors are

$$u_{\sigma\sigma}(\mathbf{k}) = \frac{d_3(\mathbf{k})}{\sqrt{(E_0(\mathbf{k}) - \varepsilon_{\mathbf{k}})^2 + |d_3(\mathbf{k})|^2}} \tag{4.7.4}$$

and

$$v_{\sigma-\sigma}(\mathbf{k}) = \frac{E_0(\mathbf{k}) - \varepsilon_{\mathbf{k}}}{\sqrt{(E_0(\mathbf{k}) - \varepsilon_{\mathbf{k}})^2 + |d_3(\mathbf{k})|^2}}. \tag{4.7.5}$$

Substituting these into the self-consistency condition (4.3.30) we find that the gap equation is

The complex vector $\mathbf{c}$ is parallel to the real vector $\mathbf{r}$ if and only if $\mathbf{c} \times \mathbf{r} = 0$. This means that we can only speak of a complex vector being parallel to a real vector if the complex vector can be written as the product of a real vector (which must be parallel or antiparallel to $\mathbf{r}$) and a complex phase. And hence we see that the notion of a complex vector being antiparallel to a real vector is not well defined. Further many complex vectors exist that are not be parallel to *any* real vector.

The complex vector $\mathbf{c}$ is perpendicular to the real vector $\mathbf{r}$ if and only if $\mathbf{c} \cdot \mathbf{r} = 0$. Thus it is possible to construct a complex vector which is perpendicular to only *one* distinct, non-trivial, real vector. (Where as all non-trivial real vectors are perpendicular to two distinct non-trivial real vectors.)

$$d_3(\mathbf{k}) = -\frac{1}{4}\sum_{\mathbf{k}\sigma} U_{\sigma-\sigma}(\mathbf{k})\frac{d_3(\mathbf{k})}{E_0(\mathbf{k})}\tanh\left(\frac{E_0(\mathbf{k})+\sigma\mu_B H}{2k_B T}\right) \tag{4.7.6}$$

At $T = 0$ this becomes

$$d_3(\mathbf{k}) = -\frac{1}{4}\sum_{\mathbf{k}\sigma} U_{\sigma-\sigma}(\mathbf{k})\frac{d_3(\mathbf{k})}{E_0(\mathbf{k})}. \tag{4.7.7}$$

which is independent of $\mathbf{H}$.

Hence we find that for this symmetry the zero temperature gap is independent of the magnetic field strength. We also note that the gap equation has the same form as the singlet gap equation (equation 4.4.10). This means that many of the features that are usually associated with singlet superconductivity may be observed. In particular we may expect to see a Clogston–Chandrasekhar limit. This makes qualitative sense as the we are considering the $S_z = 0$ projection, $\frac{1}{\sqrt{2}}(|\uparrow\downarrow\rangle + |\downarrow\uparrow\rangle)$. We now see that in a spin only magnetic field the important difference between pairing states, so far as many probes are concerned is not the difference between singlet and triplet pairing, but the difference between opposite spin pairing (OSP) states and equal spin pairing (ESP) states. An OSP state (e.g. a singlet state or the triplet state considered in this section) is destroyed by the magnetic field as it separates the ($|\mathbf{k},\uparrow\rangle$, $|-\mathbf{k},\downarrow\rangle$) states which are available for pairing in zero field. On the other hand ESP states are not destroyed as the relevant states here ($|\mathbf{k},\sigma\rangle$, $|-\mathbf{k},\sigma\rangle$) are not torn apart by the magnetic field. We will investigate this solution numerically in section 5.4.1.

4.7.2 $\mathbf{d}(\mathbf{k})$ parallel to $\hat{\mathbf{x}}$; $\mathbf{H}$ parallel to $\hat{\mathbf{z}}$

The BdG equations in this case are

$$\begin{pmatrix} \varepsilon_{\mathbf{k}}+\mu_B H & 0 & -d_1(\mathbf{k}) & 0 \\ 0 & \varepsilon_{\mathbf{k}}-\mu_B H & 0 & d_1(\mathbf{k}) \\ -d_1^*(\mathbf{k}) & 0 & -\varepsilon_{-\mathbf{k}}-\mu_B H & 0 \\ 0 & d_1^*(\mathbf{k}) & 0 & -\varepsilon_{-\mathbf{k}}+\mu_B H \end{pmatrix}\begin{pmatrix} u_{\uparrow\sigma}(\mathbf{k}) \\ u_{\downarrow\sigma}(\mathbf{k}) \\ v_{\uparrow\sigma}(\mathbf{k}) \\ v_{\downarrow\sigma}(\mathbf{k}) \end{pmatrix} = E_\sigma(\mathbf{k})\begin{pmatrix} u_{\uparrow\sigma}(\mathbf{k}) \\ u_{\downarrow\sigma}(\mathbf{k}) \\ v_{\uparrow\sigma}(\mathbf{k}) \\ v_{\downarrow\sigma}(\mathbf{k}) \end{pmatrix} \tag{4.7.8}$$

By separating into two 2×2 matrices we find that

$$
\begin{aligned}
E_\sigma(\mathbf{k}) &= \sqrt{(\varepsilon_{\mathbf{k}}+\sigma H)^2+|\mathbf{d}(\mathbf{k})|^2}, && (4.7.9)\\
u_{\sigma\sigma}(\mathbf{k}) &= \frac{-\sigma d_1(\mathbf{k})}{\sqrt{(E_\sigma(\mathbf{k})-\varepsilon_{\mathbf{k}}-\sigma H)^2+|\mathbf{d}(\mathbf{k})|^2}}, && (4.7.10)\\
v_{\sigma\sigma}(\mathbf{k}) &= \frac{E_\sigma(\mathbf{k})-\varepsilon_{\mathbf{k}}-\sigma H}{\sqrt{(E_\sigma(\mathbf{k})-\varepsilon_{\mathbf{k}}-\sigma H)^2+|\mathbf{d}(\mathbf{k})|^2}}, && (4.7.11)\\
u_{\sigma\sigma}(\mathbf{k}) &= v_{\sigma\sigma}(\mathbf{k})=0. && (4.7.12)
\end{aligned}
$$

So we find that both the eigenvectors and eigenvalues have an explicit field dependence, this means that the gap has a field dependence at *all* temperatures.

4.7.3 $\mathrm{d}(\mathrm{k})$ parallel to $\hat{\mathrm{z}}$; H antiparallel to $\hat{\mathrm{x}}$

We could evaluate this problem directly as we did for the two cases above. However, for this set of BdG equations this approach is rather difficult. It is simpler to simply rotate the solution above.

Following the procedure outlined in section 3.3 we find that,

$$
\begin{aligned}
E_\sigma(\mathbf{k}) &= \sqrt{(\varepsilon_{\mathbf{k}}+\sigma H)^2+|\mathbf{d}(\mathbf{k})|^2}, && (4.7.13)\\
u_{\uparrow\uparrow}(\mathbf{k}) &= -u_{\downarrow\uparrow}(\mathbf{k})=\frac{d_1(\mathbf{k})}{\sqrt{(E_\uparrow(\mathbf{k})-\varepsilon_{\mathbf{k}}-H)^2+|\mathbf{d}(\mathbf{k})|^2}}, && (4.7.14)\\
u_{\uparrow\downarrow}(\mathbf{k}) &= u_{\downarrow\downarrow}(\mathbf{k})=\frac{d_1(\mathbf{k})}{\sqrt{(E_\downarrow(\mathbf{k})-\varepsilon_{\mathbf{k}}+H)^2+|\mathbf{d}(\mathbf{k})|^2}}, && (4.7.15)\\
v_{\uparrow\uparrow}(\mathbf{k}) &= -v_{\downarrow\uparrow}(\mathbf{k})=\frac{E_\sigma(\mathbf{k})-\varepsilon_{\mathbf{k}}-H}{\sqrt{(E_\uparrow(\mathbf{k})-\varepsilon_{\mathbf{k}}-H)^2+|\mathbf{d}(\mathbf{k})|^2}}, && (4.7.16)\\
v_{\uparrow\downarrow}(\mathbf{k}) &= v_{\downarrow\downarrow}(\mathbf{k})=\frac{E_\sigma(\mathbf{k})-\varepsilon_{\mathbf{k}}+H}{\sqrt{(E_\uparrow(\mathbf{k})-\varepsilon_{\mathbf{k}}+H)^2+|\mathbf{d}(\mathbf{k})|^2}}. && (4.7.17)
\end{aligned}
$$

So, once again we find that the eigenvectors and hence the order parameter are field dependent at all temperatures. We therefore expect this type solution to strongly coupled to the magnetic field and that this type of solution ($S_z=\pm1$) will behave markedly differently from the $S_z=0$ solution in a magnetic field. We investigate this type of solution numerically in section 5.4.2.

Chapter 5

Triplet superconductivity in Sr_2RuO_4

In this chapter we use our extended Hubbard model (derived in the proceeding chapter) to study Sr_2RuO_4 - strontium ruthenate. We begin by reviewing the previous work on strontium ruthenate. We then derive a Ginzburg–Landau theory from our microscopic model. After making some reasonable assumptions about the nature of superconductivity in Sr_2RuO_4, we show that the Ginzburg–Landau analysis allows only axial (A, A_1 or A_2) (triplet) superconducting solutions. We then present numerical solutions of the microscopic model and explore the exchange field dependence of the order parameter and energy gap in a one-band model of Sr_2RuO_4. The numerical solutions show that the ground state is the A_2. However, we speculate that spin-orbit coupling may stabilise the A phase for fields aligned with the c-axis. We explore heat capacity as a function of temperature and field strength and find quantitatively different behaviours for the A and A_2 phases. We then discuss the Clogston–Chandrasekhar like behaviour of the A phase. Finally we speculate on the possibility of a bulk phase transition in Sr_2RuO_4 that is analogous to the Freedericksz transition. The Freedericksz transition has previously only been observed in superfluid ^{3}He and charged liquid crystals in both of these systems the Freedericksz transition is only observed in a confined geometry and a magnetic field.

Some of the results presented in this chapter have previously been published in reference [172].

5.1 Some experimental and theoretical properties of Sr_2RuO_4

Frank Lichtenberg and coworkers at the IBM research laboratory in Zürich first begin to study Sr_2RuO_4 (whose crystal structure is shown in figure 5.1) in the early nineties [216].

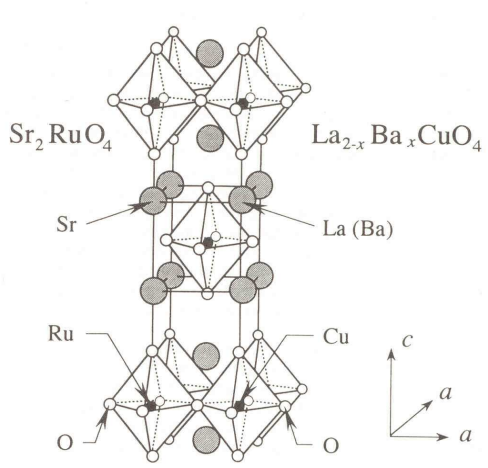

Figure 5.1: The crystal structure strontium ruthenate (Sr_2RuO_4) is of the same type as the prototypical perovskite K_2NiF_4. However, more importantly from out point of view Sr_2RuO_4 is isostructural to $La_{2-x}Ba_xCuO_4$, the parent compound of the high temperature cuprate superconductors. In fact, to date, Sr_2RuO_4 is the only known perovskite superconductor which does not contain copper. Taken from Maeno *et al*. [137].

Although other groups had previously studied Sr_2RuO_4, the IBM group where able to use the floating zone technique [127] to grow higher quality crystals than had previously been possible. Ostensibly this activity was motivated by the need for high quality substrates both for high temperature superconducting devices (such as SNS heterostructures - S = superconductor, N = normal metal) for the cuprate superconductor $YBa_2Cu_3O_{7-\delta}$ (which has an excellent lattice spacing match to Sr_2RuO_4) and as an alternative to Sr_2TiO_4 (which is a widely used substrate in both the microelectronics industry and in fundamental research).

Given the huge interest in the cuprate superconductors it was natural to search for superconductivity in Sr_2RuO_4, however the refrigerators at the IBM facility could not reach the very lowest temperatures. But, Yoshi Maeno, who was then at Hiroshima University, was able to cool Sr_2RuO_4 to well below 1K. At 0.93K a sudden drop in resistivity and a strong diamagnetic signal in the a.c. susceptibility were observed [137], the crystal had begun to superconduct. With the growth of better samples it soon became clear that the critical temperature of clean Sr_2RuO_4 is 1.5K [134].

5.1.1 Normal state properties of Sr_2RuO_4

Given the structural and chemical similarity of Sr_2RuO_4 to the cuprates it would be natural to assume that the nature of the many body problem in both systems would be broadly similar. However, this does not appear to be the case. In the cuprates the normal state[1] is not well understood [41, 42], but the normal state of Sr_2RuO_4 has proved to be much simpler. As any theory of superconductivity is greatly influenced by the normal state on which superconductivity is built we will begin by examining the normal state of Sr_2RuO_4.

Sr_2RuO_4 is well described by Landau–Fermi liquid theory [140]. For example the low temperature resistivity goes as T^2 in both the basal plane and along the c-axis [137] as is predicted by Landau–Fermi liquid theory [168]. However, the magnitude of the resistivity in the c-axis is about 550 times that in the basal plane [139] showing that we are dealing with a highly two dimensional Fermi liquid. The low temperature, normal state, specific heat is of the usual Fermi liquid form [140]

$$C_V = \gamma T + \beta T^3. \tag{5.1.1}$$

Another indication of the two dimensional nature of Sr_2RuO_4 is the Kadowaki–Woods ratio, A/γ^2, where A is the coefficient of the T^2 term of the resistivity. For most materials the Kadowaki–Woods ratio lies on one of two 'universality' lines: for heavy Fermion materials $A/\gamma^2 \simeq a_0 = 1.0 \times 10^{-5}$, while for materials without such large mass renormalisation (for example the transition metals) $A/\gamma^2 \simeq a_0/25$. For Sr_2RuO_4 the in plane Kadowaki–Woods ratio, $A_{ab}/\gamma^2 = 0.3 - 0.5a_0$, is somewhere between the two universality curves, where as, along the c-axis, the Kadowaki–Woods ratio, $A_c/\gamma^2 = 280 - 500a_0$, severely deviates from universality. The normal state magnetic susceptibility is high isotropic [140], suggesting that the Pauli term is dominant - in line the predictions Landau–Fermi liquid theory.

The availability of high quality single crystals allowed spectacularly detailed de Haas–van Alphen (dHvA) experiments to be performed on Sr_2RuO_4 [30, **?**]. The Fermi surface observed in the dHvA is in excellent agreement with (LDA) band structure calculations [147, 162]. The Fermi surface has also been probed by angle resolved photoemission spectroscopy (ARPES). Initially these experiments suggested that the γ sheet of the Fermi surface was an hole like sheet centred on the Γ point [130, 220]. (Conversely, both band structure and dHvA conclude that the γ sheet is electron like and centred on the X point.) However, later ARPES experiments appear to agree

[1] If it is really correct to call the non-superconducting state of the cuprates 'normal'.

with the conclusions drawn from the dHvA experiments and band structure calculations [54, 55]. The band structure and Fermiology of Sr_2RuO_4 is discussed in more detail in section 2.2.1.

There is ample evidence for strong correlations in Sr_2RuO_4. The mass enhancement (the ratio of the effective mass as measured by specific heat to the effective mass found in band structure calculations) is 3.6 [140]. This gives a measure of the mass renormalisation due to many body effects. From dHvA the mass enhancement on individual bands can be found [133] and is 3.4, 3.8 and 5.0 on the α, β and γ bands respectively. Renormalisation effects also give an large enhancement to the Pauli spin susceptibility. The Pauli spin susceptibility as measured by NMR is ~ 5.4 times the value found in band structure calculations [99]. The same experiments concluded that Sr_2RuO_4 is a Pauli paramagnet with an exchange enhancement factor ~ 0.82. It is useful to define the Wilson ratio,

$$R_W = \frac{1}{3}\left(\frac{\pi k_B}{\mu_B}\right)^2 \frac{\chi_0}{\gamma} \tag{5.1.2}$$

where χ_0 is the Pauli spin susceptibility and γ is the linear (electronic) component of the specific heat (see equation 5.1.1); the Wilson ratio is unity for the non-interacting Fermi gas. The Wilson ratio for Sr_2RuO_4 is 1.36, which indicates that the enhancements in χ and γ have the same origin [99].

It can therefore be seen from the experimental data that the normal state of Sr_2RuO_4 is a quasi-two dimensional Fermi liquid which is composed of electrons in narrow bands (arising from the Ru-4d_{xy}, -4d_{xz} and -4d_{yz} orbitals hybridised with O-2p orbitals) in which electron correlations play an important role.

5.1.2 The pairing symmetry of Sr_2RuO_4

The superconducting state of Sr_2RuO_4 is also very different from that of the cuprates. The superconducting transition temperature of Sr_2RuO_4 is a rather modest 1.5 K compared to the incredibly high transition temperatures (above 150 K in $HgBa_2CuO_{4+x}$ [41]) observed in the cuprates. It is well established that the order parameter in the cuprates is $d_{x^2-y^2}$ [14]. We will now review the constrains on the order parameter in Sr_2RuO_4.

In chapter 3 we noted that many anisotropic superconducting states, most notably the ABM and BW triplet states, were discussed in relation to ^{3}He before superfluidity had even been observed in ^{3}He. While theorist did not have this level of success in Sr_2RuO_4, Maurice Rice and Manfred Sigrist did make a startlingly accurate prediction of the symmetry of the

Γ	J, J_z	$\mathbf{d}(\mathbf{k})$
Γ_1^-	$0, 0$	$\mathbf{x}k_x + \mathbf{y}k_y$
Γ_2^-	$1, 0$	$\mathbf{x}k_y - \mathbf{y}k_x$
Γ_3^-	$2, \pm 2$	$\mathbf{x}k_x - \mathbf{y}k_y$
Γ_4^-	$2, \pm 2$	$\mathbf{x}k_y + \mathbf{y}k_x$
Γ_5^-	$1, \pm 1$	$\mathbf{z}(k_x \pm \mathtt{i}k_y)$

Table 5.1: The possible p-wave states on a two dimensional square lattice, C_{4v}, including splitting due to spin-orbit coupling.

superconducting state [178] in 1995, when relatively little was known about the superconducting state of Sr_2RuO_4 experimentally. On the basis of the normal state properties of Sr_2RuO_4 - in particular the strong correlations, but also because the similarities of the normal state of properties Sr_2RuO_4 of those of normal ^{3}He, they predicted that Sr_2RuO_4 is a triplet superconductor. Further support for this suggestion came from the large Hund's rule coupling [45] in Sr_2IrO_4 and the ferromagnetism [78] in $SrRuO_3$[2]. Rice and Sigrist analysed the superconducting state in Sr_2RuO_4 on the basis of a two dimensional lattice, in which case there are five distinct p-wave symmetry states which are detailed in table 5.1. In particular we note that Γ_1^- is the 2D analogue of the BW state and Γ_5^- is the 2D analogue of the ABM state. Any of the states in table 5.1 would be nodeless in Sr_2RuO_4 because of the cylindrical nature of the Fermi surfaces. In 1997 Daniel Agterberg along with Rice and Sigrist suggested that the A phase is the most likely state in Sr_2RuO_4 specifically they proposed the state

$$\mathbf{d}(\mathbf{k}) \approx \hat{\mathbf{z}}\Delta_0(k_x + \mathtt{i}k_y). \tag{5.1.3}$$

Early evidence for anisotropic pairing in Sr_2RuO_4 came from the strong suppression of the superconducting critical temperature by non-magnetic impurities [134]. Impurity scattering tends to average out the order parameter around the Fermi surface and therefore has a much weaker effect on the transition temperature of an isotropic superconductor. Further an anisotropic s-wave superconductor (i.e. an s-wave superconductor in which the magnitude of the gap varies around

[2] $SrRuO_3$ and Sr_2RuO_4 are respectively the $n = \infty$ and $n = 1$ members of Ruddlesden–Popper the series of strontium ruthenates, $Sr_{n+1}Ru_nO_{3n+1}$. The $n = 2$ member of the series, $Sr_3Ru_2O_7$, has also been synthesised and shows many interesting properties in particular it is thought to be a metamagnetic material with a quantum critical end point [84, 153, 163].

the Fermi surface) is much more weakly effected by this averaging than a gap in which the phase varies around the Fermi surface. Thus a large reduction in T_C due to non-magnetic impurities is indicative of a finite angular momentum pairing state.

The first direct evidence for triplet pairing in Sr_2RuO_4 came from muon spin relaxation (μSR). Luke *et al*. [131] observed the spontaneous appearance of an internal magnetic field, and hence the spontaneous breaking of time reversal symmetry (TRS) below T_C in Sr_2RuO_4. This internal field is suppressed by the application of a small field (50 G) parallel to the c-axis. This shows that the internal field is static on the microsecond timescale - as dynamic fields are only decoupled by much larger fields [36]. Hence, TRS is either broken by the superconducting state itself, or by a purely magnetic state which coincidentally appears at about 1.5K. To eliminate the latter possibility Luke *et al*. also studied samples with a lower transition temperature, in these samples the internal magnetic field appeared at the superconducting transition temperature, indicating that it is indeed the superconducting state which breaks TRS. Any superconducting state which breaks TRS must be twofold degenerate. Therefore the observation of broken TRS effectively rules singlet superconductivity in Sr_2RuO_4 as singlet states cannot be degenerate in the absence of multiple phase transitions, which are not observed in Sr_2RuO_4 (at least not in the relevant region of the phases diagram for these experiments). However, as we have seen there are degenerate triplet phases. Of the five possibilities detailed in table 5.1 the four 1D representations, Γ^-_{1-4}, do not break TRS. However, the 2D representation, Γ^-_5, is degenerate and hence does break TRS. This means that the only two dimensional p-wave states compatible with the μSR result are to the A, A_1 and A_2 phases.

Given this strong indication of ESP, it was important to measure the magnetic susceptibility in the superconducting state and hence the Yosida function (described in section 3.6). This was first measured by Ishida *et al*. [100] via the ^{17}O Knight shift and later by Duffy *et al*. [60] using the more direct probe of neutron scattering. Both groups found that, for fields in the basal plane, the spin susceptibility is unaltered by entering the superconducting state, i.e. that

$$Y_{ab}(T) = 1. \tag{5.1.4}$$

Neither group was able to measure the spin susceptibility for fields along the c-axis due to the small H_{C2} in this direction. This result implies that the superconducting state consists of only ESP states and in particular is consistent with either an A, A_1 or A_2 phase with $\mathbf{d}(\mathbf{k})$ parallel to the c-axis (in the sense of parallel defined in section 4.7.1).

So, the μSR and magnetic susceptibility collectively point to a ESP state that breaks TRS.

Experiment	Behaviour	Temperature range	Reference
Specific heat	$C_V \propto T^2$	$T \lesssim 0.55T_C$	[159]
Penetration depth	$\lambda(0) - \lambda(T) \propto T^2$	$T \lesssim 0.6T_C$	[32]
Thermal conductivity	$\kappa \propto T^2$	$T \lesssim 0.65T_C$	[202, 102]
NMR (Ru spin-lattice relaxation rate)	$1/T_1 \propto T^3$	$T \lesssim 0.28T_C$	[100]
Ultrasonic attenuation	$\alpha \propto T^3$	$T \lesssim 0.6T_C$	[146, 132]

Table 5.2: The low temperature behaviour of Sr_2RuO_4 as probed by various thermodynamic and transport measurements.

The strongest candidates are the A, A_1 and A_2 phases because the two dimensional nature of Sr_2RuO_4. Given the cylindrical nature of the Fermi surfaces (see section 2.2.1 and figure 2.2), the A, A_1 and A_2 phases are all nodeless. As we saw in section 3.5, we would therefore expect to see and exponential temperature dependence in many thermodynamic quantities at low T. The measured low temperature dependence of several quantities is shown in table 5.2. All of these experiments yield power laws which are consistent with line nodes and are hence inconsistent with the nodeless gap of the order parameter suggested by Agterberg, Rice and Sigrist (5.1.3).

Theorists were now faced with the challenge of reconciling the observation of line nodes with the requirement for ESP and broken TRS. However, for the cylindrical Fermi surface geometry of Sr_2RuO_4 a complete group theoretic analysis of symmetry distinct pairing states does not show any p-wave states which both break time-reversal symmetry and have line-nodes [13]. This led several groups to consider f-wave scenarios [90, 82, 141]. Another possible resolution to this dilemma has been developed in the orbital dependent pairing model of Zhitomirsky and Rice [224] and in a related model by Litak *et al*. [129]. For different reasons both groups proposed that the gap function is of the form

$$\mathbf{d}(\mathbf{k}) = \hat{\mathbf{z}}\Delta_\gamma(\sin k_x + \mathtt{i}\sin k_y). \tag{5.1.5}$$

on the dominant γ sheet of the Fermi surface, and of the form

$$\mathbf{d}(\mathbf{k}) = \hat{\mathbf{z}}\Delta_{\alpha\beta}\left[\sin\left(\frac{k_x}{2}\right)\cos\left(\frac{k_y}{2}\right) + \mathtt{i}\sin\left(\frac{k_y}{2}\right)\cos\left(\frac{k_x}{2}\right)\right]\cos\left(\frac{ck_z}{2}\right) \tag{5.1.6}$$

on the α and β sheets. Both of these functions possess the same E_u symmetry, but correspond to intra-plane and inter-plane pairing interactions respectively. This gap function has horizontal line

Parameter		In basal plane		Along c-axis
Superconducting critical temperature	T_C (K)		1.5	
Upper critical field	$\mu_0 H_{C2}(0)$ (T)	1.5		0.075
Clogston–Chandrasekhar limiting field	$\mu_0 H_P(0)$ (T)		0.0194	
Lower critical field	$\mu_0 H_{C1}(0)$ (T)	1.0×10^{-3}		5.0×10^{-3}
Ginzburg–Landau coherence length	$\xi(0)$ (Å)	660		33
London penetration depth	$\lambda(0)$ (Å)	1.8×10^3		3.7×10^4
Ginzburg–Landau parameter	$\kappa(0)$	55		2.7
Mean free path	$l(0)$ (Å)	2100		

Table 5.3: Superconducting properties of Sr_2RuO_4 after Akima, NishiZaki and Maeno [7].

nodes at $k_z = \pm\pi/c$ on the α and β sheets. These two scenarios can by sloganised as the choice between braces (f-wave nodes) or belts (horizontal line nodes on the α and β sheets). Comparison of the predictions of the belt and brace models with experiment reveals that the belt model provide at better fit to the specfic heat near T_C [159, 224, 129, 77], thermal conductivity [129, 77, 142] and the penetration depth measurements [129, 113].

In a magnetic field Sr_2RuO_4 shows a number of unusual features. Firstly the vortex lattice is square [180, 106] which agrees well with the predictions of a two-component E_u symmetry Ginzburg-Landau theory [6, 91]. Secondly there is an anomalous second feature close to H_{c2}, which only occurs when the field is aligned within 1^o of the a-b plane (see figure 5.2). At the present time the origin of this feature is uncertain. It may be a vortex lattice phase transition, or it may correspond to a change in pairing symmetry with field, perhaps analogous to the double superconducting transition in UPt_3 (see below).

We conclude this section by listing some of the key properties of Sr_2RuO_4 in table 5.3. Note that the upper critical field is larger than the Clogston–Chandrasekhar limit this is of course an indication of triplet pairing in general and equal spin pairing in particular and that the superconducting properties are highly anisotropic, as are the normal state properties.

5.1.3 Other triplet superconductors

In section 3.6 we discussed the prototypical triplet superfluid, ^{3}He. However, there is now evidence for triplet superconductivity in several other compounds. We will now briefly discuss the evidence for triplet pairing in the heavy Fermion compound UPt_3 and the organic

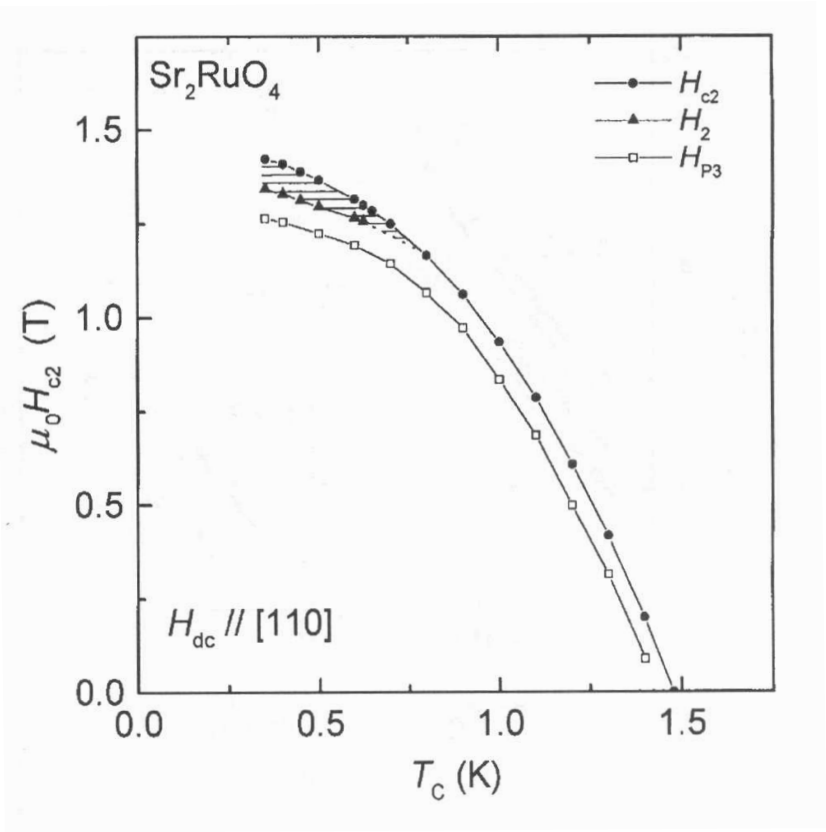

Figure 5.2: Evidence for a second superconducting phase transition in Sr_2RuO_4 taken from Mao *et al*. [143]. H_{c2} is the upper critical field, H_2 is the location of a second peak in the ac susceptibility which is taken as evidence for a phase transition. H_{P3} another peak in the observed ac susceptibility however, this is attributed to vortex synchronisation pinning [221]. The location of the H_2 is confirmed by specific heat measurements [159, 143].

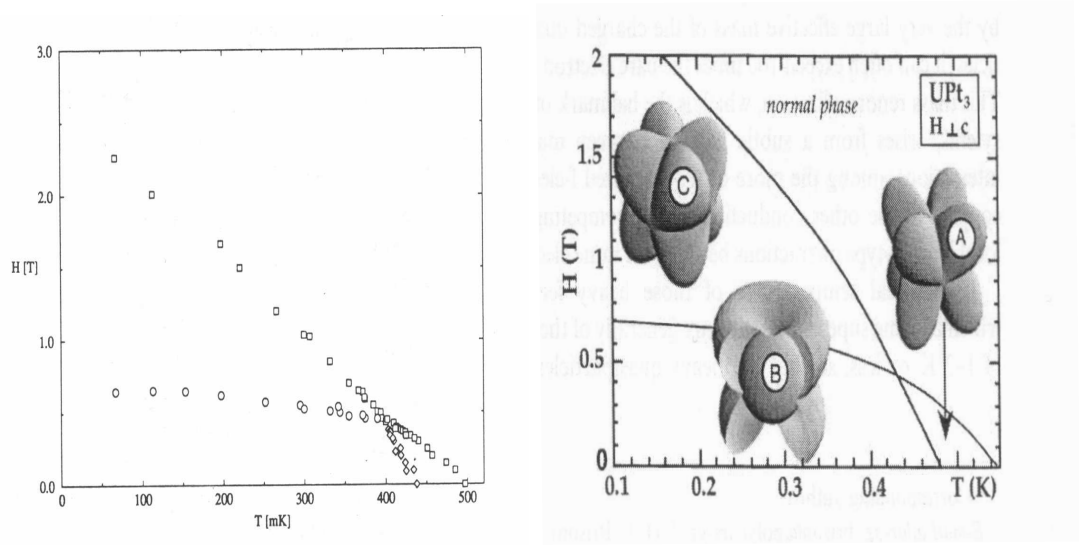

Figure 5.3: The superconducting phase diagram of UPt_3. Left the experimental phase diagram constructed from ultrasonic velocity measurements by Adenwalla *et al.* [5], right the theoretical phase diagram also showing the symmetry of the gap taken from Brison *et al.* [38].

superconductors.

Perhaps the best known of the heavy Fermion compounds is UPt_3. There is convincing evidence for the existence of triplet superconductivity in UPt_3 [38], not least of which is observation of multiple superconducting phases (see figure 5.3). The symmetry of the phases has been well characterised [185] within an E_{2u} model.

Evidence for triplet superconductivity has also been found in several quasi one dimensional organic superconductors. These belong to the Bechgaard salt family, $(TMTSF)_2X$ where X = PF_6 [49, 121], ClO_4 [122]. In these materials the triplet superconductivity may be reentrant, that is, when a magnetic field is applied the superconducting critical initially decreases, but as the field grows even larger T_C increases once again. This may be due to both triplet and singlet solutions existing in zero field, but the singlet state having the lower energy. Thus when the singlet state is suppressed by the magnetic field triplet superconductivity emerges rather than the usual paramagnetic state.

We will not discuss the ferromagnetic superconductors here as these materials will be discussed in some detail in chapter 6. But we do note here that there have been recent reports [101] of the coexistence of triplet superconductivity and antiferromagnetism in UNi_2Al_3.

5.1.4 The relevance of our model to Sr_2RuO_4

A spin triplet superconductor should show a number of interesting magnetic-field effects which are direct consequences of the magnetic moment of the Cooper pairs. In particular, for spin-triplet superconductors the Zeeman coupling between the quasiparticle spins an external magnetic field need not lead to Clogston–Chandrasekhar limiting, unlike the case of spin-singlet superconductors (see section 4.4.1). We may also expect possible phase transitions or symmetry changes of the order parameter in a magnetic field, which are analogous to the transitions seen in superfluid ^{3}He and UPt_3.

In this chapter we will focus specifically on the unique effects of the Cooper pair spin in a triplet superconductor. Therefore we neglect the effects of the vector potential on the quasiparticles, and instead focus solely on the Zeeman coupling of the quasiparticle spin to the magnetic field. We can further justify this model by appealing to the strong Stoner enhancement in Sr_2RuO_4 [147, 137], which means that the exchange field will be large in this material.

5.2 A Ginzburg–Landau theory of a quasi–two dimensional triplet superconductor in a magnetic field

Before considering numerical solutions of the self consistent Bogoliubov–de Gennes equations (derived in section 4.3), we will examine the possible results by deriving a Ginzburg–Landau theory from our microscopic theory.

Consider a quasi–two dimensional system with two orbital degrees of freedom (which we label x and y) and three spin degrees of freedom (henceforth labelled 1, 2 and 3.) Hence, instead of the familiar 3 by 3 order parameter of ^{3}He (described in section 3.8) this system is described by the complex 2 by 3 matrix A, which is related to the microscopic order parameter, $\mathbf{d}(\mathbf{k})$, by

$$\begin{pmatrix} d_1(\mathbf{k}) \\ d_2(\mathbf{k}) \\ d_3(\mathbf{k}) \end{pmatrix} = \begin{pmatrix} A_{1x}\sin k_x + A_{1y}\sin k_y \\ A_{2x}\sin k_x + A_{2y}\sin k_y \\ A_{3x}\sin k_x + A_{3y}\sin k_y \end{pmatrix} = \begin{pmatrix} \mathbf{A}_x & \mathbf{A}_y \end{pmatrix} \begin{pmatrix} \sin k_x \\ \sin k_y \end{pmatrix}. \tag{5.2.1}$$

We noted in chapter 3 that only five quartic terms ($\beta_1 - \beta_5$) are required to describe ^{3}He [26]. In a crystal two additional terms (β_6 and β_7) appear because the rotational symmetry of the crystal is discrete, where as rotational symmetry is continuous in a fluid. Gradient terms can also be

calculated [13, 6, 91], but we will not make use of these here. In zero field the condensation free energy for a tetragonal crystal is given by [13]

$$\begin{aligned} F_{SC}-F_N &= \alpha(T-T_c)(|\mathbf{A}_x|^2+|\mathbf{A}_y|^2)+\beta_1(|\mathbf{A}_x|^2+|\mathbf{A}_y|^2)^2+\beta_2|\mathbf{A}_x\cdot\mathbf{A}_x+\mathbf{A}_y\cdot\mathbf{A}_y|^2 \\ &+\beta_3((\mathbf{A}_x\cdot\mathbf{A}_y^*)^2+(\mathbf{A}_x^*\cdot\mathbf{A}_y)^2+(\mathbf{A}_x^*\cdot\mathbf{A}_x)^2+(\mathbf{A}_y^*\cdot\mathbf{A}_y)^2) \\ &+\beta_4(2|\mathbf{A}_x\cdot\mathbf{A}_y^*|^2+|\mathbf{A}_x|^4+|\mathbf{A}_y|^4) \\ &+\beta_5(2|\mathbf{A}_x\cdot\mathbf{A}_y|^2+|\mathbf{A}_x\cdot\mathbf{A}_x|^2+|\mathbf{A}_y\cdot\mathbf{A}_y|^2) \\ &+\beta_6(|\mathbf{A}_x\cdot\mathbf{A}_x|^2+|\mathbf{A}_y\cdot\mathbf{A}_y|^2)+\beta_7(|\mathbf{A}_x|^4+|\mathbf{A}_y|^4). \end{aligned} \tag{5.2.2}$$

In a finite magnetic field, to second order in A, the condensation free energy, $F_{\mathbf{H}}$, is

$$F_{\mathbf{H}}=\frac{1}{\beta}\sum_{\mathrm{i}\omega_n}\int \mathrm{d}\mathbf{k}\ \ tr\left(\underline{\underline{G}}_0(\mathbf{k},\mathrm{i}\omega_n)\underline{\underline{\Delta}}(\mathbf{k})\underline{\underline{G}}_0^*(-\mathbf{k},\mathrm{i}\omega_n)\underline{\underline{\Delta}}^\dagger(-\mathbf{k})\right), \tag{5.2.3}$$

where,

$$\underline{\underline{G}}_0(\mathbf{k},\mathrm{i}\omega_n)=(\mathrm{i}\omega_n+\varepsilon_{\mathbf{k}}-\mu+\mu_B\sigma\cdot\mathbf{H})^{-1} \tag{5.2.4}$$

and ω_n are the Matsubara frequencies.

Thus to all orders in $\mathbf{H}$

$$\begin{aligned} F_{\mathbf{H}} &= -\frac{1}{\beta}\sum_{\mathrm{i}\omega_n}\mathrm{tr}\int \mathrm{d}\mathbf{k}\ \frac{(\mathrm{i}\omega_n-\varepsilon_{\mathbf{k}}+\mu+\mu_B\sigma\cdot\mathbf{H})}{[(\mathrm{i}\omega_n-\varepsilon_{\mathbf{k}}+\mu)^2-|\mathbf{H}|^2]} \\ &\times(\sigma\cdot\mathbf{A}_x\sin k_x+\sigma\cdot\mathbf{A}_y\sin k_y)\sigma_2\frac{(\mathrm{i}\omega_n+\varepsilon_{\mathbf{k}}-\mu-\mu_B\sigma^*\cdot\mathbf{H})}{[(\mathrm{i}\omega_n+\varepsilon_{\mathbf{k}}-\mu)^2-|\mathbf{H}|^2]} \\ &\times(\sigma^*\cdot\mathbf{A}_x^*\sin k_x+\sigma^*\cdot\mathbf{A}_y^*\sin k_y)\sigma_2. \end{aligned} \tag{5.2.5}$$

Hence,

$$F_{\mathbf{H}}=\mathbf{A}_x\underline{\underline{\chi}}_{xx}\mathbf{A}_x^*+\mathbf{A}_x\underline{\underline{\chi}}_{xy}\mathbf{A}_y^*+\mathbf{A}_y\underline{\underline{\chi}}_{yx}\mathbf{A}_y^*+\mathbf{A}_y\underline{\underline{\chi}}_{yy}\mathbf{A}_y^*, \tag{5.2.6}$$

where,

$$\underline{\underline{\chi}}_{ij}=\begin{pmatrix}\chi_{ij}^{11} & \chi_{ij}^{21} & \chi_{ij}^{31}\\ \chi_{ij}^{12} & \chi_{ij}^{22} & \chi_{ij}^{32}\\ \chi_{ij}^{13} & \chi_{ij}^{23} & \chi_{ij}^{33}\end{pmatrix}, \tag{5.2.7}$$

and

$$\begin{aligned}\chi_{ij}^{\alpha\beta} &= -\frac{1}{\beta}\sum_{\mathtt{i}\omega_n}\int \mathrm{d}\mathbf{k}\sin k_i \sin k_j \\ &\times tr\left(\frac{(\mathtt{i}\omega_n - \varepsilon_{\mathbf{k}} + \mu + \mu_B\sigma\cdot\mathbf{H})\sigma_\alpha\sigma_2(\mathtt{i}\omega_n + \varepsilon_{\mathbf{k}} - \mu - \mu_B\sigma^*\cdot\mathbf{H})\sigma_\beta^*\sigma_2}{\left[(\mathtt{i}\omega_n - \varepsilon_{\mathbf{k}} + \mu)^2 - |\mathbf{H}|^2\right]\left[(\mathtt{i}\omega_n + \varepsilon_{\mathbf{k}} - \mu)^2 - |\mathbf{H}|^2\right]}\right).\end{aligned} \tag{5.2.8}$$

By x–y symmetry $\chi_{xy} = \chi_{yx} = 0$.

Some algebra then leads to

$$\begin{aligned}F_{\mathbf{H}} &= (\alpha_0 + \alpha_2|\mathbf{H}|^2)(|\mathbf{A}_x|^2 + |\mathbf{A}_y|^2) + \mathtt{i}\alpha_1\mathbf{H}\cdot(\mathbf{A}_x\times\mathbf{A}_x^* + \mathbf{A}_y\times\mathbf{A}_y^*) \\ &\quad -2\alpha_2(|\mathbf{H}\cdot\mathbf{A}_x|^2 + |\mathbf{H}\cdot\mathbf{A}_y|^2).\end{aligned} \tag{5.2.9}$$

Where,

$$\alpha_0 = \frac{2}{\beta}\sum_{\mathtt{i}\omega_n}\int \mathrm{d}\mathbf{k}\frac{\sin^2 k_x\left((\varepsilon_{\mathbf{k}}-\mu)^2 + \omega_n^2\right)}{\left[(\mathtt{i}\omega_n - \varepsilon_{\mathbf{k}} + \mu)^2 - \mu_B^2|\mathbf{H}|^2\right]\left[(\mathtt{i}\omega_n + \varepsilon_{\mathbf{k}} - \mu)^2 - \mu_B^2|\mathbf{H}|^2\right]}, \tag{5.2.10}$$

$$\alpha_1 = -\frac{4\mu_B}{\beta}\sum_{\mathtt{i}\omega_n}\int \mathrm{d}\mathbf{k}\frac{\sin^2 k_x(\varepsilon_{\mathbf{k}}-\mu)}{\left[(\mathtt{i}\omega_n - \varepsilon_{\mathbf{k}} + \mu)^2 - \mu_B^2|\mathbf{H}|^2\right]\left[(\mathtt{i}\omega_n + \varepsilon_{\mathbf{k}} - \mu)^2 - \mu_B^2|\mathbf{H}|^2\right]} \tag{5.2.11}$$

and

$$\alpha_2 = -\frac{2\mu_B^2}{\beta}\sum_{\mathtt{i}\omega_n}\int \mathrm{d}\mathbf{k}\frac{\sin^2 k_x}{\left[(\mathtt{i}\omega_n - \varepsilon_{\mathbf{k}} + \mu)^2 - \mu_B^2|\mathbf{H}|^2\right]\left[(\mathtt{i}\omega_n + \varepsilon_{\mathbf{k}} - \mu)^2 - \mu_B^2|\mathbf{H}|^2\right]}. \tag{5.2.12}$$

Clearly α_0 reduces to α (5.2.2) in zero magnetic field, but the α_1 and α_2 terms do not have analogues in the zero field Ginzburg–Landau expansion. It is reassuring to note the similarity between these extra terms and the Hartree–Fock–Gorkov quasiparticle spectrum in a magnetic field (equation 4.6.12). The fact that each term has an analogue in the other, independently derived, formalism is confirmation that both procedures have been carried out correctly. As we saw in chapter 3 the cross product of any complex vector with its complex conjugate is purely imaginary so the square root of minus one before the α_1 term in the expression for the free energy is to be expected.

As we have expanded in A, but not in $\mathbf{H}$, the above expression for the free energy is valid for small gaps at all field strengths. It is therefore valid close to H_c. But, note that, since we assumed an exchange-only magnetic field we do not consider the vortex lattice here. Agterberg and Heeb [6, 91] have discussed the vortex lattice using Ginzburg–Landau theory, but did not include the Zeeman terms of equation 5.2.9.

In the Ginzburg–Landau formalism the superconducting phase transition occurs when the quadratic terms go to zero. In a zero field this condition is simply

$$\alpha(T - T_C) = 0. \tag{5.2.13}$$

In a finite spin only magnetic field the equivalent condition is that the matrix

$$\underline{\underline{\alpha}} = \alpha_{ij} A_i A_j^* \tag{5.2.14}$$

has (at least) one zero eigenvalue, but no negative eigenvalues, where the indices i and j now run over both orbital and spin degrees of freedom. In this case

$$\underline{\underline{\alpha}} = \begin{pmatrix} \underline{\underline{\beta}} & 0 \\ 0 & \underline{\underline{\beta}} \end{pmatrix}, \tag{5.2.15}$$

where,

$$\underline{\underline{\beta}} = \begin{pmatrix} \alpha_0 + \alpha_2|\mathbf{H}|^2 - 2\alpha_2 H_1^2 & \mathtt{i}\alpha_1 H_3 & -\mathtt{i}\alpha_1 H_2 \\ -\mathtt{i}\alpha_1 H_3 & \alpha_0 + \alpha_2|\mathbf{H}|^2 - 2\alpha_2 H_2^2 & \mathtt{i}\alpha_1 H_1 \\ \mathtt{i}\alpha_1 H_2 & -\mathtt{i}\alpha_1 H_1 & \alpha_0 + \alpha_2|\mathbf{H}|^2 - 2\alpha_2 H_3^2 \end{pmatrix}. \tag{5.2.16}$$

Hence the condition for there being a zero eigenvalue of $\underline{\underline{\alpha}}$ is

$$\begin{aligned} &\left(\alpha_0 + \alpha_2|\mathbf{H}|^2 - 2\alpha_2 H_1^2\right)\left(\alpha_0 + \alpha_2|\mathbf{H}|^2 - 2\alpha_2 H_1^2\right)\left(\alpha_0 + \alpha_2|\mathbf{H}|^2 - 2\alpha_2 H_1^2\right) \\ &\quad - \left(\alpha_0 + \alpha_2|\mathbf{H}|^2 - 2\alpha_2 H_1^2\right)\alpha_1^2 H_1^2\left(\alpha_0 + \alpha_2|\mathbf{H}|^2 - 2\alpha_2 H_2^2\right)\alpha_1^2 H_2^2 \\ &\quad - \left(\alpha_0 + \alpha_2|\mathbf{H}|^2 - 2\alpha_2 H_3^2\right)\alpha_1^2 H_2^2 = 0. \end{aligned} \tag{5.2.17}$$

This expression can be greatly simplified by choosing our coordinate system so that $\mathbf{H}$ lies parallel to one of the axes. With, for example, $\mathbf{H} = (0, 0, H)$ we find

$$\underline{\underline{\beta}} = \begin{pmatrix} \alpha_0 + \alpha_2 H^2 & \mathtt{i}\alpha_1 H & 0 \\ -\mathtt{i}\alpha_1 H & \alpha_0 + \alpha_2 H^2 & 0 \\ 0 & 0 & \alpha_0 - \alpha_2 H^2 \end{pmatrix}. \tag{5.2.18}$$

Which has at least one zero eigenvalue when

$$\Big(\alpha_0 - \alpha_2 H^2\Big)\Big(\big(\alpha_0 + \alpha_2 H^2\big)^2 - \alpha_1^2 H^2\Big) = 0. \tag{5.2.19}$$

The eigenvectors of $\underline{\underline{\alpha}}$ are

$$\begin{pmatrix} A_{1x} \\ A_{2x} \\ A_{3x} \\ A_{1y} \\ A_{2y} \\ A_{3y} \end{pmatrix} = \begin{pmatrix} 0 \\ 0 \\ 1 \\ 0 \\ 0 \\ 0 \end{pmatrix}, \begin{pmatrix} 0 \\ 0 \\ 0 \\ 0 \\ 0 \\ 1 \end{pmatrix}, \begin{pmatrix} 1 \\ \mathtt{i}\kappa \\ 0 \\ 0 \\ 0 \\ 0 \end{pmatrix}, \begin{pmatrix} 0 \\ 0 \\ 0 \\ 1 \\ \mathtt{i}\kappa \\ 0 \end{pmatrix}, \begin{pmatrix} -\mathtt{i}\kappa \\ 1 \\ 0 \\ 0 \\ 0 \\ 0 \end{pmatrix} \text{ and } \begin{pmatrix} 0 \\ 0 \\ 0 \\ -\mathtt{i}\kappa \\ 1 \\ 0 \end{pmatrix}. \tag{5.2.20}$$

Where κ is real. To second order in A, κ is given by

$$\kappa = -\frac{\alpha_1 H}{\alpha_0 + \alpha_2 H^2} \tag{5.2.21}$$

Much recent work (see section 5.1.2) has suggested that Sr_2RuO_4 is likely to be in an state analogous to the A phase of ^{3}He. If the pairing interaction favours the A phase in zero magnetic field there are three possible solutions in a magnetic field.

$$\mathbf{A}_x = -\mathtt{i}\mathbf{A}_y = (0, 0, 1) \tag{5.2.22}$$

$$\mathbf{A}_x = -\mathtt{i}\mathbf{A}_y = (1, \mathtt{i}\kappa, 0) \tag{5.2.23}$$

$$\mathbf{A}_x = -\mathtt{i}\mathbf{A}_y = (-\mathtt{i}\kappa, 1, 0) \tag{5.2.24}$$

Equation 5.2.22 is the A phase with $\mathbf{d}(\mathbf{k})$ parallel to $\mathbf{H}$. Equations 5.2.23 and 5.2.24 both give an axial phase. In particular this axial phase is the A phase for $\kappa = 0$, A_2 phase for $0 < |\kappa| < 1$ and the A_1 phase for $|\kappa| = 1$. For all values of κ solutions (5.2.23) and (5.2.24) have $\mathbf{d}(\mathbf{k})$ perpendicular to $\mathbf{H}$.

5.3 Numerical methods

To progress further we must resort to solving the self consistent Bogoliubov–de Gennes equations numerically. That is we guess a $\underline{\underline{\Delta}}_{\mathbf{k}}$ and then find the eigenvalues, $E_\sigma(\mathbf{k})$, and

eigenvectors, $u_{\sigma'\sigma}(\mathbf{k})$ and $v_{\sigma'\sigma}(\mathbf{k})$, of the BdG equations. From these we then calculate $\underline{\underline{\Delta}}_{\mathbf{k}}$ via the self-consistency condition (equation 4.3.30). If the calculated $\underline{\underline{\Delta}}_{\mathbf{k}}$ is the same as the initial guess then we have a self-consistent solution, if not we take the calculated $\underline{\underline{\Delta}}_{\mathbf{k}}$ as the guess for the next iteration and repeat the process until self-consistency is achieved.

5.3.1 A method for improving the speed of convergence in the self consistent process

Self consistency can take many iterations to achieve. Therefore many schemes have be invented to decrease the number of iterations before self-consistency. One of the most widely used schemes involves guessing a mixture of the last two solutions, rather than simply the last solution.

In this work we employed the following method to increase the speed with which a self consistent solution is found: We define our measure of self consistency, $\mathcal{C}_{\alpha\beta}$, by

$$\mathcal{C}_{\alpha\beta} = \frac{1}{N}\sum_{\mathbf{k}}\left(1 - \frac{\left|\Delta_{\alpha\beta}^{(n-1)}(\mathbf{k})\right|}{\left|\Delta_{\alpha\beta}^{(n)}(\mathbf{k})\right|}\right), \tag{5.3.1}$$

where $\Delta_{\alpha\beta}^{(n)}(\mathbf{k})$ is the value of $\Delta_{\alpha\beta}(\mathbf{k})$ calculated from the n^{th} iteration and N is the number of k-space grid points. Clearly, $\mathcal{C}_{\alpha\beta}^{n} = 1 \,\forall\, \alpha, \beta$ implies that self consistency has been reached. For small $\mathcal{C}_{\alpha\beta}^{n}$, $\mathcal{C}_{\alpha\beta}^{n}$ is a linear function $\Delta_{\alpha\beta}(\mathbf{k})$ as is shown in figure 5.4. Therefore when $\mathcal{C}_{\alpha\beta}^{n}$ is sufficiently small we can easily extrapolate to find self consistent value of $\Delta_{\alpha\beta}(\mathbf{k})$. (Of course it is important to check that the extrapolated value of $\Delta_{\alpha\beta}(\mathbf{k})$ is indeed a self consistent value.) However, we also found that this extrapolation can be useful even for large values of $\mathcal{C}_{\alpha\beta}^{n}$, although it does not immediately yield the self consistent value of $\Delta_{\alpha\beta}(\mathbf{k})$, it can greatly decrease the number of iterations required to achieve self consistency. In practice we found the best method was calculate a few iterations from an informed initial guess and then perform an extrapolation. Thereafter the best strategy is to extrapolate after every second iteration. Of course, it is also important to start some calculations from a random point in phase space (so as to search for other solutions). In this case more integrations must be performed before the first extrapolation is performed.

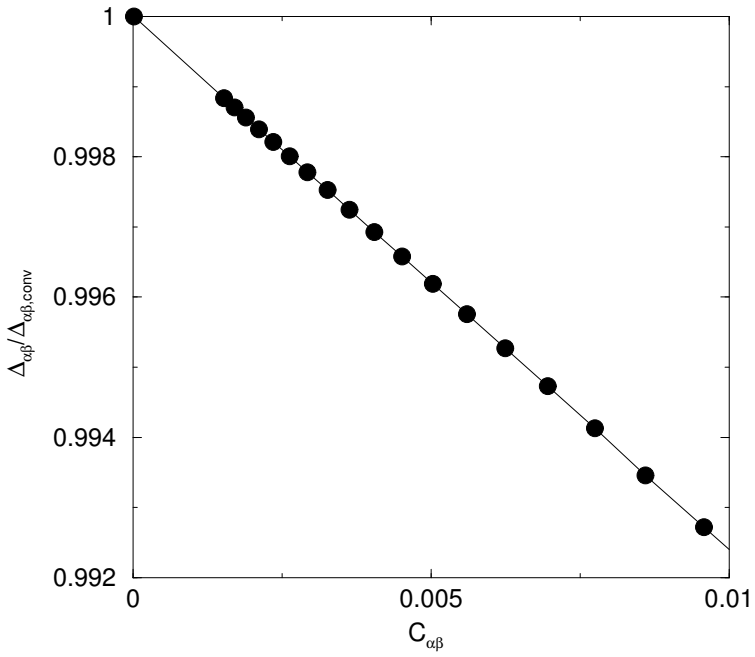

Figure 5.4: The behaviour of $\mathcal{C}_{\alpha\beta}$, a measure of self consistency, near self consistency.

5.3.2 An overview of parallel computing and MPI

As high speed computing is, by its very nature, a rapidly evolving subject, few traditional texts are available. Those that do exist [4] are usually written with the computer scientist in mind. I have found that for the physicist, who should be motivated primarily by the need for quick, reliable code, the best resources are web based [157, 149, 67]. Of course the longevity of these resources remains to be seen, but it seems reasonable to assume that they will be available for as long as the MPI (Message Passing Interface) routines retain their current popularity.

There are two common strategies for producing high speed computers. The first method is essentially brute force. By removing communication bottlenecks, increasing the clock speed, optimising the instruction set, miniaturising components so that they dissipate less heat and/or increasing the size of the processor cache so that memory has to be accessed less frequently, processor speed can be increased. This allows more instructions to be carried out per unit time, thence programs are executed more quickly.

A more modern approach is to use many computers to share the workload. This is known as parallel computing[3]. Parallel computing is attractive for many reasons. The main reason however is financial. Moore's law states that the speed of commercially available processors

[3] In contrast, computing on a single processor is known as serial computing.

doubles ever eighteen months, whilst, in the same time, the cost an equivalent processor halves[4]. This means that if one invests a large amount of money in buying a very fast serial computer within a few years it will be no faster than the average desktop. It is found that one can get the same speed, at least cost and crucially with greater ease of upgradability form a parallel computer.

An important factor with any computer program is portability of code. That is, the ability of the code to be compiled and run on many different machines. For this reason the MPI routines where devised. These routines consist of a set C functions, headers, types and so forth. (There is also a functionally equivalent and syntactically alike Fortran implementation of MPI.) The MPI routines handle the communications between processors in a uniform manor, thus insuring portability of code and freeing the programmer from concerns over the vagaries processor communication systems.

In the MPI model of parallel computing each processor or *node* is on an equal footing. (Although in practice it is often more convenient to work in a client-server paradigm.) The nodes can communicate with each other by *one to one* communication (for example the **SEND** or **RECEIVE** commands), *one to many* communication (for example the **SCATTER** command), *many to one* communication (for example the **GATHER** command) or *many to many* communication (an example of which is the **ALLGATHER** command).

Many of the numerical results presented in this thesis have been calculated using the 'Brunel' 'Beowulf'[5] machine which belongs to the LACMS [114] group of the University of Bristol mathematics department. This was done to increase speed with which the code executed as the program is extremely slow. The code executed slowly because it solves a self consistently a non-linear integral equation over a large number of reciprocal space points. The fact that the code allows for both triplet and singlet solutions means that four such self consistent numbers must be calculated. Also, as we are considering a large phase $(\mathbf{H}, T)$ space the code must be run for many different state variables. Therefore we parallelised our code by spreading the $\mathbf{k}$-space integration across several machines. The speed up is, to a good approximation, linear in the number of processors used (i.e. two process take about half the time to find a self consistent solution that it takes a single processor to perform the same task).

[4]Incidentally, in the same time the processor size halves, this means that Moore's law is likely to fail soon as it requires processers to be on the atomic scale by about 2020. Processors on this scale will be dominated by quantum effects, and thus 'classical' computing will cease to function. However, there is currently much effort being invested in inventing the 'quantum computer', which will (it is hoped) use these quantum effects to increase the speed with which many algorithms are executed.

[5]Beowulf machines are an *off the shelf* Linux implementation parallel computing [29].

5.4 Numerical results

We now present self consistent solutions of the BdG equations with parameters chosen to correspond to Sr_2RuO_4. To this end we fit the hopping integral and site energy to the experimentally determined Fermi surface of the γ-sheet of Sr_2RuO_4 (as is described in section 2.2.1). The interaction potential is restricted to include nearest neighbour terms only and chosen to give the experimentally observed critical temperature (1.5K).

5.4.1 $\mathrm{d}(\mathrm{k})$ parallel to H

We begin by studying the first solution of the Ginzburg–Landau theory (5.2.22), in which $\mathbf{d}(\mathbf{k})$ is parallel to $\mathbf{H}$. In zero field we find that the ground state of the model is a triplet state analogous to the A phase of ^{3}He, specifically the state is

$$\mathbf{d} = \Delta_0(\sin k_x + \mathrm{i} \sin k_y)\hat{\mathbf{e}}. \tag{5.4.1}$$

Here we have defined the vector order parameter to point in the $\hat{\mathbf{e}}$ direction. In zero field, all directions in spin space are degenerate if spin–orbit coupling is neglected. When an external field is applied the ground state has $\mathbf{d}(\mathbf{k})$ perpendicular to the field, as we will show below. However, in Sr_2RuO_4 the order parameter is thought to be aligned with the c-axis [138], by spin-orbit coupling [158]. Therefore despite the low critical field along the c-axis, Sr_2RuO_4 presents us with the possibility of studying a triplet superconductor with a magnetic field parallel to the order parameter. It is therefore interesting to predict what would be observed in such experiments. To do this we simply discard any axial solutions with $\mathbf{d}(\mathbf{k})$ not parallel to $\mathbf{H}$. We then consider the remaining self consistent solution of the BdG equation with the lowest free energy.

A field applied parallel to $\mathbf{d}(\mathbf{k})$ does not cause a change in the symmetry of the gap. It follows that at zero temperature the gap is independent of magnetic field strength (see section 4.7.1). At finite temperature, a field applied parallel to the order parameter causes a change in the magnitude of the gap (see figure 5.5.) It should be noted that the gap is nodeless but has minima at $k_x = 0$ and $k_y = 0$.

We calculate the heat capacity, magnetisation and magnetic susceptibility as functions of temperature and field strength. For an isotropic, nodeless gap in zero field it is well known [154]

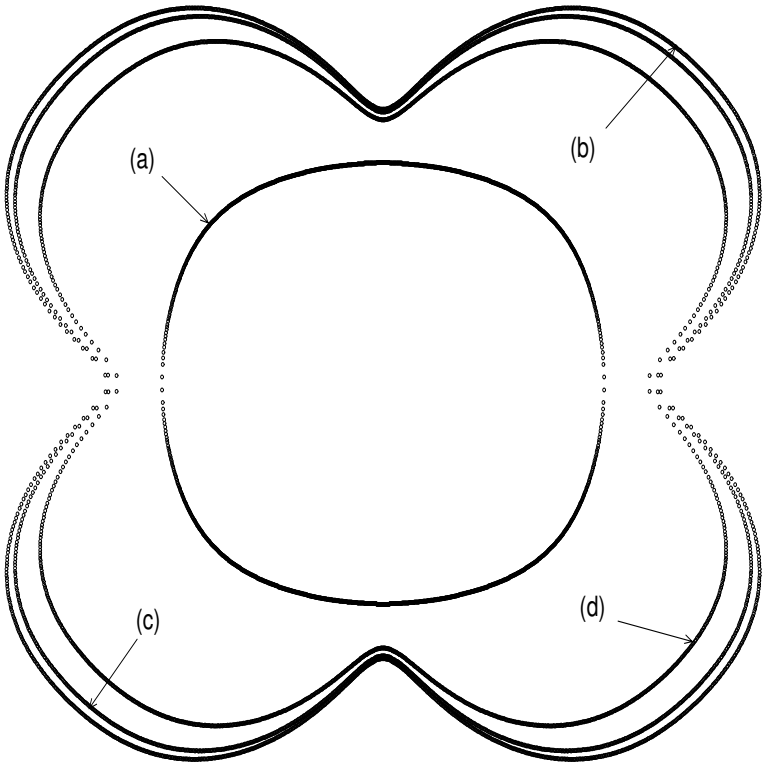

Figure 5.5: (a)The Fermi surface and the gap at $T/T_C = 0.5$ with (b) $\mu_B H/k_B T_C = 0$, (c) $\mu_B H/k_B T_C = 0.5$, (d) $\mu_B H/k_B T_C = 0.9$

that these properties behave as

$$C_v, M, \chi \sim \exp\left(-\frac{\Delta}{k_B T}\right). \tag{5.4.2}$$

We find that for an anisotropic, nodeless, p-wave gap the thermodynamics have the same form, even in the presence of a magnetic field (see inset figure 5.6) We therefore define the effective gap, Δ_{eff} 'seen' by the thermodynamic functions as

$$C_v, M, \chi \sim \exp\left(-\frac{\Delta_{eff}}{k_B T}\right). \tag{5.4.3}$$

We find that Δ_{eff} is the mean gap at the Fermi surface, $\overline{|\mathbf{d}(\mathbf{k_F})|}$ in zero field and that Δ_{eff} is a linear function of magnetic field strength (see figure 5.6.) That is to say that

$$\Delta_{eff} = \overline{|\mathbf{d}(\mathbf{k_F})|} - \mu_B |\mathbf{H}|. \tag{5.4.4}$$

With the field in this orientation a Clogston–Chandrasekhar limit is observed as the superconducting state vanishes when $\Delta_{eff} = 0$. (This is confirmation of our prediction in section 4.7.1). This is of course to be expected as we are considering spin one Cooper pairs in the $S_z = 0$ projection.

5.4.2 $\mathrm{d}(\mathrm{k})$ perpendicular to H

Recall that the ground state of the model in zero field is

$$\mathbf{d} = \Delta_0(\sin k_x + \mathrm{i} \sin k_y)\hat{\mathbf{e}} \tag{5.4.5}$$

(see figure 5.7a). We will now examine the numerical solutions of the full BdG equations corresponding to the second solution of the Ginzburg–Landau theory (5.2.23) and (5.2.24). We find this solution ($\mathbf{d}(\mathbf{k}) \cdot \mathbf{H} = 0$) to be the ground state of our model in a magnetic field. We also find that the symmetry of this state is A_2, that is

$$\mathbf{d} = \Delta_0(\sin k_x + \mathrm{i} \sin k_y)(1, \mathrm{i}\kappa, 0). \tag{5.4.6}$$

where κ is a real function of temperature and field strength (figure 5.7b,c). Physically this corresponds to a disparity in the number of the spin 1 Cooper pairs in the $S_z = 1$ and $S_z = -1$ projections, with no pairing in the $S_z = 0$ projection.

In ^{3}He as the field and temperature increase κ increases until $\kappa = 1$. This is the A_1 phase which is the ground state of ^{3}He near to T_C in finite fields. The A_1 phase has order parameter

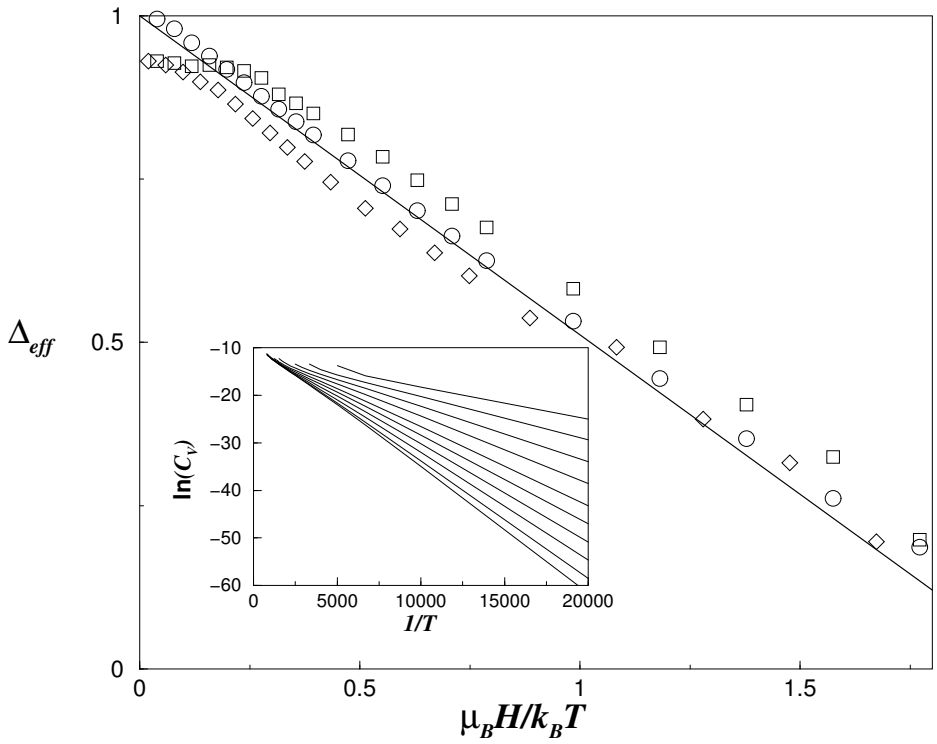

Figure 5.6: Δ_{eff} (normalised to $\overline{|\mathbf{d}(\mathbf{k_F})|}$ at $T = H = 0$) as a function of magnetic field parallel to $\mathbf{d}(\mathbf{k})$ extrapolated from heat capacity (circles), magnetisation (squares) and magnetic susceptibility (diamonds). The line is $\overline{|\mathbf{d}(\mathbf{k_F})|} - \mu_B H$. Inset - Logarithmic plot of heat capacity with inverse temperature at various fields. From the bottom up: $H = 0$ T, 0.28 T, 0.42 T, 0.71 T, 0.85 T, 1.13 T, 1.41 T, 1.76 T, 2.12 T, 2.47 T and 2.82 T.

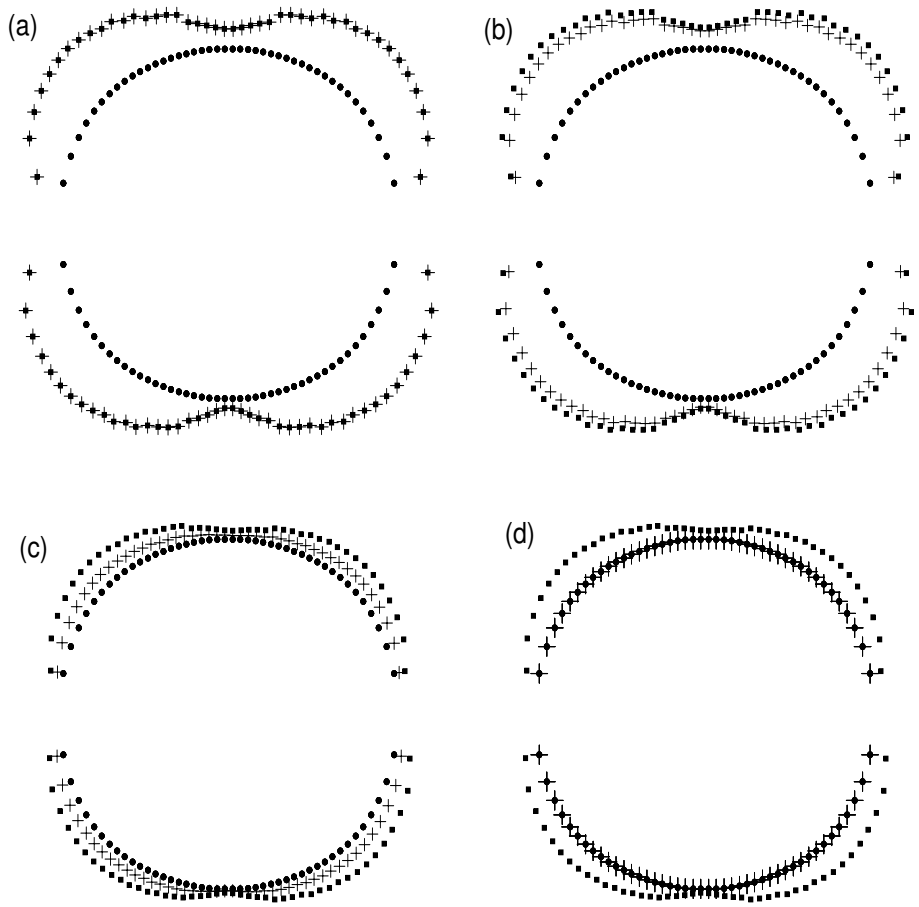

Figure 5.7: The Fermi surface (circles), spin up gap (crosses) and the spin down gap (squares). In the (a) A phase ($T = H = 0$), (b) the A_2 phase ($T = 0$, $H = 1.4$ T), (c) the A_2 phase with a larger κ ($T = 1.8$ K, $H = 1.4$ T) and (d) the A_1phase - not observed.

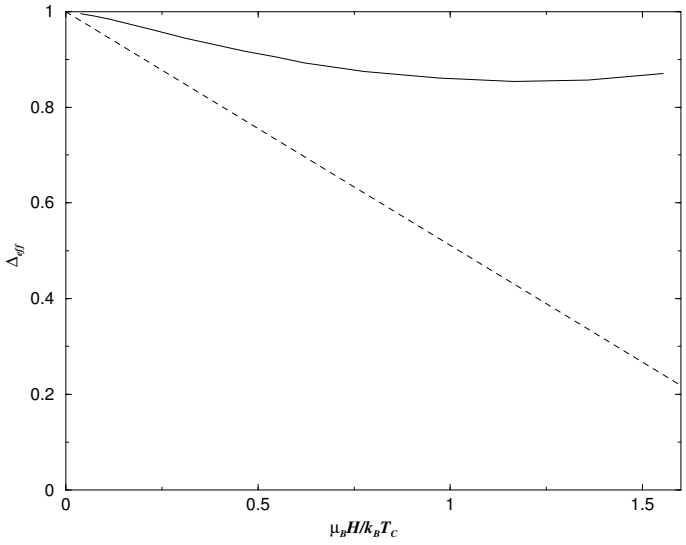

Figure 5.8: Δ_{eff} (normalised to $\overline{|\mathbf{d}(\mathbf{k_F})|}$ at $T = H = 0$)) as a function of $\mathbf{H}$ perpendicular to $\mathbf{d}(\mathbf{k})$ (solid line) extrapolated from heat capacity. For comparison we plot Δ_{eff} for $\mathbf{H}$ parallel to $\mathbf{d}(\mathbf{k})$ (dashed line).

$$\mathbf{d} = \Delta_0(\sin k_x + \mathtt{i} \sin k_y)(1, \mathtt{i}, 0) \tag{5.4.7}$$

and corresponds to all of the (ESP) Cooper pairs aligning themselves in a single direction either parallel or antiparallel to the magnetic field. (figure 5.7d). At no point in the range of fields and temperatures that we have examined do we find that the A_1 phase is the ground state of our model. (Although we cannot definitely rule the A_1 as we have not carried out an extensive search for it.) If such a transition does occur then it is certainly well above the experimentally observed upper critical field. This is in agreement with experiment as no A_1 phase has been observed to date.

Due to the nodeless gap in the A_2 phase the specific heat has an exponential temperature dependence. Hence we can calculate the effective gap for this field orientation (figure 5.8.) We find a linear field dependence in low fields but its dependence is much weaker than for $\mathbf{d}(\mathbf{k})$ parallel to $\mathbf{H}$ and there is an upturn in large fields. There is known to be a qualitative change in heat capacity in this field orientation (see figure 5.2 and section 5.1.2). It remains to be seen if these are related.

In this orientation the spin susceptibility does not drop to zero as temperature goes to zero because we are dealing with the $S_z = \pm 1$ projections of the spin one Cooper pairs (this is

explained in more detail in 3.9). The calculated Yosida function (defined as the ratio of susceptibility of the superconducting state to that of the normal state) is shown in figure 5.9. The most surprising feature of this calculation is the high temperature behaviour. At low temperatures the Yosida function tends to unity as expected. However, near the critical temperature the susceptibility changes from its low temperature value and hence the Yosida function in no longer unity. This may be an interesting, experimentally testable effect, but, it is also possible that it is attributable to numerical error. Near the critical temperature the gap is rather small. To calculate the susceptibility we must take numerical derivatives of the magnetisation, which depends of the magnitude of the gap. Thus the errors inherent to the process of taking numerical derivatives are likely to be most pronounced near the critical temperature.

We also note that the largest field considered in figure 5.9 is 2.82T, almost twice the upper critical temperature of Sr_2RuO_4 for field parallel to the c-axis (c.f. table 5.3). Of course, we did not expect to accurately predict the critical field of Sr_2RuO_4 as we have not included the effects of orbital currents (which determine H_{C2}). In figure 5.10 we plot the critical temperature for this configuration as a function of magnetic field strength. The increase in critical temperature is reminiscent of the behaviour of ^{3}He, however unlike ^{3}He we do not observe an A_1 phase. It should be noted that we have not carried out a systematic search for the A_1 phase and that near T_C numerical noise once again hamperers the correct identification of the phase. On the other hand it is quite simple to see that the only the A_1 phase is likely exist for very large fields as the normal state will be entirely spin polarised. The A_1 phase is indeed observed, even at zero temperature, in calculations for such unphysically large fields.

5.4.3 The Freedericksz transition

To understand the Freedericksz transition we must first take a brief detour into the world of liquid crystals.

Most organic molecules, particularly aromatic molecules, are diamagnetic. For example, a magnetic field applied perpendicular to the plane of a benzene ring causes a current flow around the ring. However, if the field is applied in the plane of the benzene molecule then no current is induced. A current flowing raises the total energy, therefore in a magnetic field benzene molecules tend to align themselves so that the magnetic field lies in the plane of the ring.

Many liquid crystals form nematic phases [57]. This can occur if the molecules have a rod-like or disk-like geometry. In the nematic phase the long axes of the molecules align themselves in some direction, this direction is known as the nematic director, $\mathbf{n}$. However, the

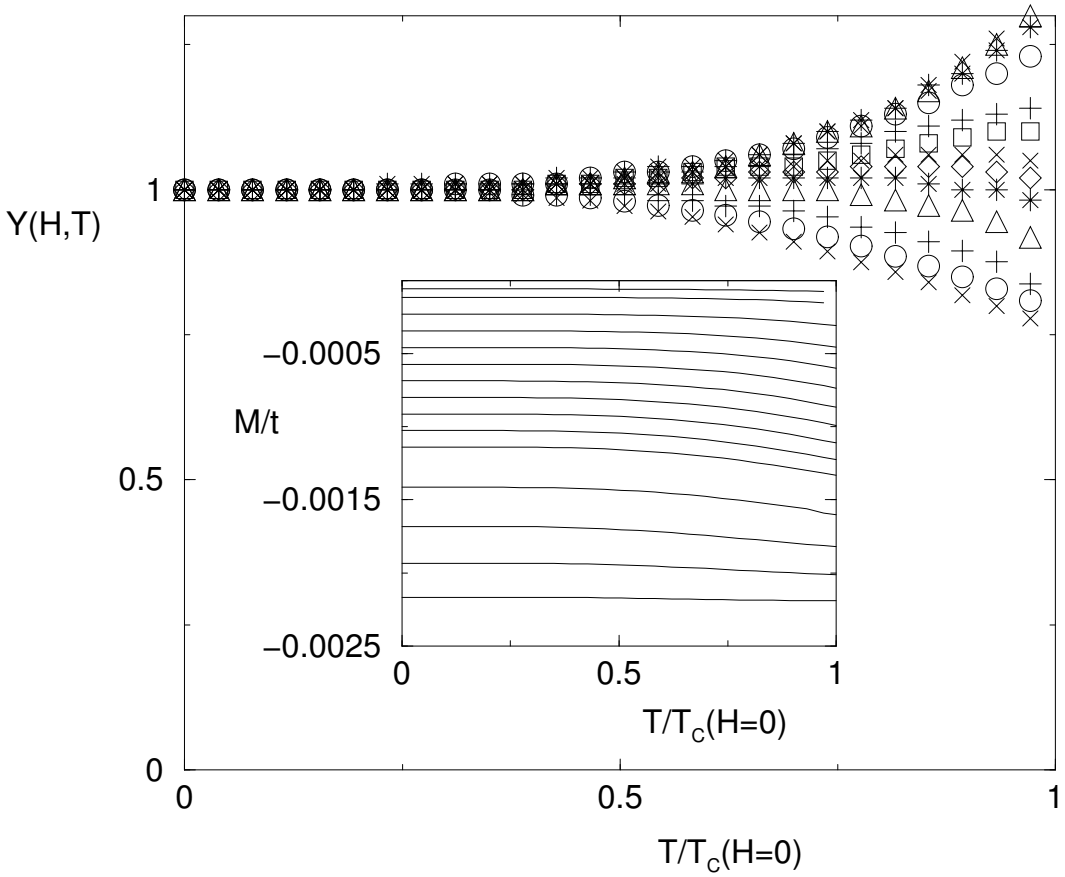

Figure 5.9: The Yosida function for $\mathbf{H}$ parallel to $\mathbf{d}(\mathbf{k})$ as a function of temperature and magnetic field strength. The curves correspond, from the top down, to the magnetic field strengths $H =$ 0.035 T, 0.18 T, 0.31 T, 0.49 T, 0.78 T, 0.91 T, 1.06 T, 1.19 T, 1.34 T, 1.59 T, 1.94 T, 2.29 T, and 2,64 T. Inset: the magnetisation of the superconducting state with $\mathbf{H}$ parallel to $\mathbf{d}(\mathbf{k})$ as a function of temperature and magnetic field strength. The curves correspond, from the top down, to the magnetic field strengths $H = 0$ T, 0.07 T, 0.14 T, 0.28 T, 0.42 T, 0.56 T, 0.71 T, 0.85 T, 0.99 T, 1.13 T, 1.27 T, 1.41 T, 1.76 T, 2.12 T, 2.48 T and 2.82 T.

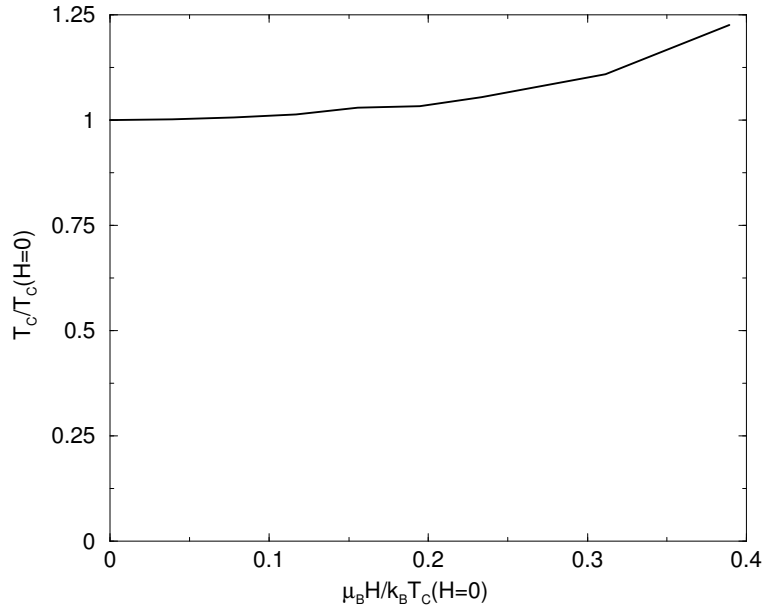

Figure 5.10: The superconducting critical temperature for $\mathbf{H}$ parallel to $\mathbf{d}(\mathbf{k})$ as a function of magnetic field strength.

centres of gravity of the molecules have no long range order in the nematic phase. In the bulk, the free energy is degenerate with respect to the direction of the nematic director. However, in a confined geometry the orientation of the nematic director is determined by guiding effects due to the walls of the container and thus an 'easy axis' is defined. (Whether the easy axis is parallel or antiparallel to the wall of the container depends on the fine details of the interaction between the molecules and the wall.)

Typical nematogenic molecules contain aromatic rings with the plane of the benzene ring along long axis of the molecule. Thus, in the nematic phase, $\mathbf{n}$, is parallel to the plane of the aromatic rings. This means that when a magnetic field, $\mathbf{H}$, is applied to the bulk nematic phase the rotational symmetry is broken and the liquid crystal aligns itself so the $\mathbf{n}$ is parallel to $\mathbf{H}$.

In a confined geometry if a magnetic field is applied parallel to the easy axis, then the term of the free energy caused by the interactions between the liquid crystals and the container and the diamagnetic term of the free energy are both minimised by the same orientation of $\mathbf{n}$. On the other hand, if the field is applied perpendicular to the easy axis, then there is a conflict as we cannot minimise both of the energy scales simultaneously whilst remaining in a bulk nematic phase. The simplest case to describe this effect in detail for is the slab geometry where the container consists of two infinite parallel planes and is thus described by a single parameter, L,

the separation of the planes. For large L the forces from the walls are small compared with the magnetic forces thence the nematic director aligns itself with the magnetic field (this clearly gives the correct behaviour as $L \to \infty$ and we regain the bulk case). For small L and small $|\mathbf{H}|$ the guiding effects of the container dominate and the nematic director aligns itself with the easy axis. For small L and large $|\mathbf{H}|$ the ground state is with $\mathbf{n}$ aligned with $\mathbf{H}$ in most of the sample but aligned with the easy axis in a thin layer near the walls. Thus the usual symmetry of the nematic phase is broken. Clearly at a certain field strength, H_F, (which is, in general, a function of L) there will be a phase transition between the small $|\mathbf{H}|$ phase and the large $|\mathbf{H}|$ configuration. This is known as the Freedericksz (also sometimes spelt Frederiks) transition. H_F can be calculated straightforwardly. This, and other aspects of the Freedericksz transition, are described in de Gennes and Prost's well known book on liquid crystals [57].

The Freedericksz transition in ^{3}He

A transition analogous to the Freedericksz transition (which, for brevities sake, we will also refer to as the Freedericksz transition) has been widely studied in ^{3}He.

In bulk ^{3}He in a magnetic field the ground state is with $\mathbf{d}(\mathbf{k})$ perpendicular to $\mathbf{H}$. However, in the axial (A, A_1 and A_2) phases, there is also a second vector quantity associated with the orbital ferromagnetism due to broken TRS. Taking the A phase as an example, we can write the order parameter as

$$\mathbf{d}(\mathbf{k}) = \Delta_0 \hat{\mathbf{d}}\big(\hat{\mathbf{k}} \cdot \hat{\mathbf{m}} + \mathtt{i}\hat{\mathbf{k}} \cdot \hat{\mathbf{n}}\big). \tag{5.4.8}$$

We can therefore define a vector, $\hat{\mathbf{l}}$, by

$$\hat{\mathbf{l}} = \hat{\mathbf{m}} \times \hat{\mathbf{n}}. \tag{5.4.9}$$

The orbital magnetic moment of the A phase is therefore in the direction $\hat{\mathbf{l}}$.

In the bulk the ground state is $\mathbf{d}(\mathbf{k})$ is parallel to $\hat{\mathbf{l}}$ due to dipole coupling. In a slab geometry the ground state is $\hat{\mathbf{l}}$ normal to the wall. This is easily understood semiclassically. If one visualises the ^{3}He Cooper pair as a diatomic molecule rotating about $\hat{\mathbf{l}}$ the orbital motion of the Cooper pair will be restricted by the wall unless $\hat{\mathbf{l}}$ is normal to the wall. In fact more rigourous arguments [213] reach the same conclusion. On the other hand we have already seen (section 3.6) that, in bulk, the ground state of the axial phases in a magnetic field is $\mathbf{d}(\mathbf{k})$

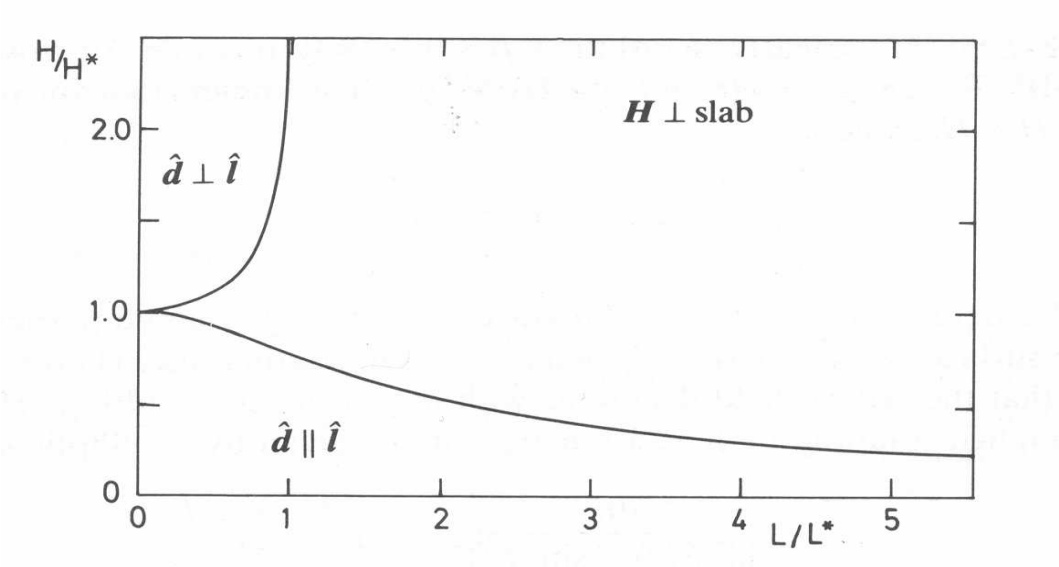

Figure 5.11: The phase diagram of ^{3}He confined in a slab geometry as a function of $\mathbf{H}$ and L, taken from Vollhardt and Wölfle [213].

perpendicular to $\mathbf{H}$. Thus in a slab geometry with a magnetic field normal to the walls we have three competing energy scales, only two of which can be minimised simultaneously.

For large L (and hence in the bulk) we have $\hat{\mathbf{l}} \parallel \mathbf{d}(\mathbf{k}) \parallel \mathbf{H}$ as the guiding forces of the walls are the weakest. For small L and small $|\mathbf{H}|$ we have $\hat{\mathbf{l}} \parallel \mathbf{d}(\mathbf{k}) \perp \mathbf{H}$ as the magnetic forces are weakest. While, for small L and large $|\mathbf{H}|$ we have $\hat{\mathbf{l}} \perp \mathbf{d}(\mathbf{k}) \parallel \mathbf{H}$ as dipole coupling is weaker than the other forces. Thus for small L at the field H_F, which clearly depends on L, we have a Freedericksz transition as we change from $\hat{\mathbf{l}} \parallel \mathbf{d}(\mathbf{k})$ to $\hat{\mathbf{l}} \perp \mathbf{d}(\mathbf{k})$ (see figure 5.11). The Freedericksz transition in ^{3}He is well reviewed in Vollhardt and Wölfle [213].

Is there a Freedericksz transition in Sr_2RuO_4?

In this chapter we investigated two triplet solutions. We saw that $\mathbf{d}(\mathbf{k})$ perpendicular to $\mathbf{H}$ had a lower energy than $\mathbf{d}(\mathbf{k})$ parallel to $\mathbf{H}$. However in Sr_2RuO_4 it is likely that spin-orbit coupling 'pins' $\mathbf{d}(\mathbf{k})$ to the crystallographic c-axis [138, 158]. Therefore, for fields applied along the c-axis, spin-orbit coupling would impose an energy penalty for $\mathbf{d}(\mathbf{k}) \perp \mathbf{H}$. This means that, at least for small fields, the ground state would be $\mathbf{d}(\mathbf{k}) \| \mathbf{H}$. If, for larger fields the ground state is $\mathbf{d}(\mathbf{k}) \perp \mathbf{H}$, then we would have a transition analogous to the Freedericksz transition. But, unlike perviously known examples, this transition is in a bulk material.

We have also noted (table 5.3) that H_{C2} is much smaller when the field when the field is

applied along the c-axis than when the field is in the basal plane. Clearly, much of this is due to the intrinsic anisotropy in Sr_2RuO_4 which is reflected in its normal state properties. The additional effect of spin-orbit coupling clearly cannot be calculated from the theory presented here, however one might speculate that spin-orbit coupling and the notable differences between the $\mathbf{d}(\mathbf{k})\|\mathbf{H}$ and $\mathbf{d}(\mathbf{k}) \perp \mathbf{H}$ states also contributes to this anisotropy.

Finally, we note that the differences in the thermodynamic properties in a magnetic field of the $\mathbf{d}(\mathbf{k})\|\mathbf{H}$ and $\mathbf{d}(\mathbf{k}) \perp \mathbf{H}$ states should allow for a clear experimental check of the suggestion that $\mathbf{d}(\mathbf{k})$ is 'pinned' to the c-axis. If this turns out to be the case Sr_2RuO_4 will provide us with a unique opportunity to study the $\mathbf{d}(\mathbf{k})\|\mathbf{H}$ in a bulk material.

5.5 Conclusions

We investigated the order parameter of Sr_2RuO_4 in an exchange-only magnetic field. A Ginzburg–Landau symmetry analysis implied two possibilities: either an axial (A, A_1 or A_2) phase with $\mathbf{d}(\mathbf{k})$ perpendicular to the magnetic field or an A phase with $\mathbf{d}(\mathbf{k})$ parallel to the magnetic field. We explored the exchange field dependence of the order parameter and energy gap in a one-band model of Sr_2RuO_4 via the self consistent solution of the BdG equations. These numerical solutions showed no A_1 phase for physically reasonable field strengths and also no A phase perpendicular to $\mathbf{H}$. Of the remaining possible phases (A with $\mathbf{d}(\mathbf{k}) \parallel \mathbf{H}$ and A_2 with $\mathbf{d}(\mathbf{k}) \perp \mathbf{H}$) the A_2 phase is lower in free energy. We investigated the behaviour of the heat capacity as a function of both field and temperature for both of these solutions. We have shown that the variation of the exponential cutoff below T_C as a function of $\mathbf{H}$ is quantitatively and qualitatively different for these two solutions. This makes heat capacity an excellent experimental probe of the symmetry state in a magnetic field.

We did not include the effect of spin-orbit coupling which could change the ground state for particular orientations of the magnetic field (particularly with $\mathbf{H}$ parallel to the c-axis of the crystal.) However, we did observe that the inclusion of such an effect (or indeed any effect which favours the alignment of $\mathbf{d}(\mathbf{k})$ with the crystallographic c-axis) could lead to a Freedericksz transition in strontium ruthenate.

Chapter 6

The ferromagnetic superconductor $ZrZn_2$

In this chapter we apply our extended Hubbard model (derived in chapter 4) to the ferromagnetic superconductor $ZrZn_2$. However, as will be seen from the brief review that begins this chapter rather little is known about the superconducting state of this material. Further, the superconducting transition temperature in the limit of no impurity scattering (the clean limit), T_{SC0}, is not known. We therefore attempt to extrapolate the transition temperature from the Abrikosov–Gorkov formula and both residual resistivity and de Haas-van Alphen experiments. We generalise our Ginzburg–Landau theory from two dimensions (chapter 5) to three dimensions. We then derive gap equations for arbitrary non-unitary states in zero exchange splitting and equal spin pairing (ESP) states (including non-unitary ESP states) in the presence of exchange splitting from our microscopic Hamiltonian. We show that these two formalisms are identical in the only limit in which the should be, that of zero exchange splitting and no opposite spin pairing (OSP). We then solve linearised versions of our gap equations for a tight binding fit chosen to give the DOS found in first principles electronic structure calculations for $ZrZn_2$ [183] and an effective, nearest neighbour, pairwise, attractive interaction chosen to give the clean transition temperature found in our analysis of the residual resistivity experiments. We include the effects of non-magnetic impurity scattering and compare our results with experiments performed on $ZrZn_2$.

6.1 Some experimental and theoretical properties of $ZrZn_2$

In the previous chapter we saw that there is an extensive literature of strontium ruthenate which was discovered to superconduct some eight years ago and has been the focus of much attention ever since. This is in no small part due to the availability of many high quality samples which allowed the unusual nature of the superconducting state to be studied in a wide variety of high quality experiments. Conversely, $ZrZn_2$ has not yet been studied so widely. Of course this is mainly because superconductivity was first observed in $ZrZn_2$ only last year [166]. However, there were predictions, discussed below, that superconductivity would be the ground state of $ZrZn_2$ - and several groups [53, 170] looked for superconductivity in $ZrZn_2$ many years before the phenomena was eventually observed. The fact that they did not observe superconductivity implies that superconductivity in $ZrZn_2$ is easily destroyed by disorder, this is, as we saw the previous chapter, strong evidence for unconventional superconductivity.

6.1.1 The normal state properties of $ZrZn_2$

$ZrZn_2$ crystalises in the C15 Laves phase crystal structure shown in figure 6.1. Bruno, Ginatempo and Staunton [40] showed that the density of states at the Fermi level, $D(\varepsilon_F)$, is dominated by the zirconium atoms with the contribution density of states due to the zinc atoms being about 0.6 Ry below the Fermi level. However, the presence of the zinc does substantially alter $D(\varepsilon_F)$ as they play the role of empty spheres which change the crystal structure of the zirconium. In fact, the density of states in the region of the Fermi level calculated for zirconium in a diamond structure with the appropriate lattice spacing for $ZrZn_2$ is remarkably similar to that of $ZrZn_2$ itself.

In the normal state, at ambient pressure, the resistivity of $ZrZn_2$ shows a T^2 temperature dependence [190]. This is consistent with the predictions of Fermi liquid theory. However, under pressure, but still in the normal state, this power law changes [85] to $T^{1.6}$ near P_C which has been attributed to the influence of spin waves. (The critical pressure, $P_C \sim 21$ kbar, above which ferromagnetism is not observed in any temperature range will be discussed further below.) (The ferromagnetic region also shows a $T^{1.6}$ behaviour, consistent with magnons.)

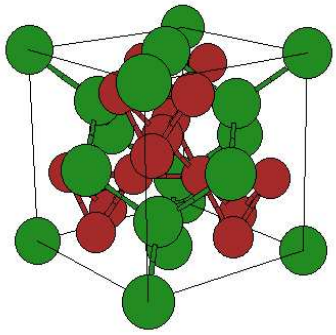

Figure 6.1: The C15 Laves phase crystal structure of $ZrZn_2$. The zirconium atoms (larger spheres) form a tetrahedrally coordinated diamond structure with the zinc atoms (smaller spheres) forming a network of interconnecting tetrahedra. Taken from the crystal lattice structure website [47].

6.1.2 The properties of $ZrZn_2$ in its ferromagnetic state

In ambient pressure $ZrZn_2$ is a ferromagnet with a Curie temperature[1] of 28.5 K [166, 208, 165]. The Curie temperature falls approximately linearly with applied pressure [208] and ferromagnetism is not observed a above the critical pressure, $P_C \approx 21$ kbar. Some authors [85] have claimed that $T_{FM} \propto (P_C - P)^{3/4}$, although other data does not seem to agree with this [166, 167, 215]. In any case the theory we present here is not strongly effected by either scenario and so we will, for simplicities sake assume $T_{FM} \propto P_C - P$ in what follows as the differences between the two behaviours is rather small except very close to P_C. The most unusual magnetic property of $ZrZn_2$ is that, although a field of 0.05 T is enough to form a single magnetic domain, the ordered moment is unsaturated up to 35 T [166, 211]. In contrast, the ordered moment of the prototypical ferromagnets iron, cobalt and nickel is only weakly effected by the application of a magnetic field once a single domain has been formed [19].

$ZrZn_2$ appears to be a rare example of a Stoner ferromagnet. The exchange splitting is clearly resolved in de Haas-van Alphen experiments [219] and band structure calculations (also presented in reference [219]) are in excellent agreement with these experiments. The calculated moment (0.18 μ_B) is also in excellent agreement with the observed moment (0.17 μ_B). Both the Curie temperature and low temperature magnetisation are linear functions of pressure [53]. Hence the low temperature magnetisation is a linear function of T_{FM}, in line with the predictions

[1] The fact that the Curie temperature and the superconducting critical temperature are both traditionally denoted T_C can, of course, lead to some confusion. Therefore in this chapter we will label the Curie temperature T_{FM} and the superconducting critical temperature T_{SC}.

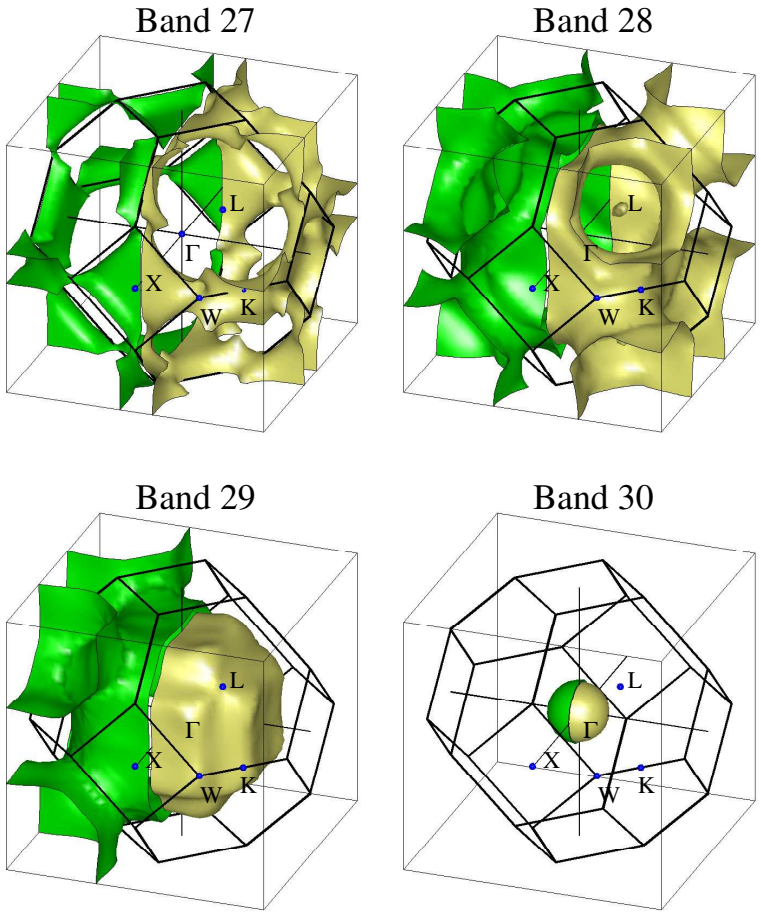

Figure 6.2: The Fermi surface of $ZrZn_2$ calculated from the LDA by Giles Santi and coworkers [219]. The left hand side of each figure shows the sheet for the majority spin state (↑) and the right hand side of each figure shows the fermi surface for the minority spin state (↓).

of the Stoner model.

The calculated Fermi surface (shown in figure 6.2) of $ZrZn_2$ shows four (spin split) sheets [194, 219]. The three smallest have been observed in dHvA experiments. The largest sheet (band 29 in the notation of reference [183] which we adopt throughout this chapter) of course has the biggest orbits and is thus the most difficult to resolve - but the calculations indicate that band 29 contributes $\sim 50\%$ of $D(\varepsilon_F)$ [183] so, unfortunately, the experimental determination of the Fermi surface of this system is incomplete.

6.1.3 Predictions of superconductivity in $ZrZn_2$

One reason that there has been long standing interest in $ZrZn_2$ is the prediction that superconductivity would be observed near the critical pressure.

In the 1970s several authors [120, 68, 126] considered the possibility of paramagnon induced p-wave pairing in nearly ferromagnetic metals. The scenario considered was that of a paramagnetic metal at very low temperatures which undergoes a transition to a ferromagnetic state as the strength of the exchange interaction is increased. It was found that as the exchange interaction is increased in such nearly ferromagnetic systems the superconducting transition temperature reaches a maximum and then drops to zero as the ferromagnetic transition is reached. Leggett pointed out [124] that for $P \geq P_C$ $ZrZn_2$ is an example of just such a nearly ferromagnetic metal. This led to much interest in the superconducting properties of $ZrZn_2$ [66, 69, 17, 53].

However, the prediction which sparked the most interest was that of Fay and Appel [70] in 1980 that paramagnons could also mediate superconductivity in the ferromagnetic state. Fay and Appel calculated the transition temperature of an ESP state (specifically the A_1 state) as a function of a Hubbard-type exchange interaction parameter, $\overline{I} = UD(\varepsilon_F)$, in for both a nearly ferromagnetic metal ($\overline{I} \lesssim 1$) and a weak ferromagnet ($\overline{I} \gtrsim 1$). They found that paramagnons can mediate superconductivity on *both* sides of the ferromagnetic transition. The superconducting transition temperature on the ferromagnetic side of transition increases as the exchange interaction is decreased until it reaches a maximum and then falls to zero when $\overline{I} = 1$ (at the transition to the paramagnetic state).

Fay and Appel performed calculations, assuming a spherical Fermi surface, for parameters suitable to $ZrZn_2$. On the basis of this model they predicted that $ZrZn_2$ would superconduct with $T_{SC} \sim 1$ K at ambient pressure. This transition would be near the maximum T_{SC}, so the transition temperature would then drop as $P \to P_C$. For $P > P_C$ Fay and Appel predicted that $T_{SC}(P)$ would rise to a maximum before falling again. They also speculated, on the basis of the superconductivity observed in elemental zirconium and zinc, that for $P \gg P_C$ a s-wave state would emerge because of the suppression of spin waves away from the ferromagnetic transition.[2]

[2] In fact Fay and Appel are rather confusing on where the maximum T_{SC} lies as a function of pressure. For example at one point in their paper they claim that 'the maximum of T_C^1 [that is T_{SC} in the p-wave channel] for $ZrZn_2$ seems to lie near zero external pressure.' While later on the predict that 'the progression of states that might be observed in clean $ZrZn_2$ at very low (probably < 0.5 K) temperature as the pressure is increased from zero to $P \gg P_C$ [is] itinerant ferromagnetism, itinerant ferromagnetism plus *p*-state pairing, paramagnetic *p*-wave pairing, and paramagnetic *s*-wave

The calculation of the superconducting critical temperature in the paramagnetic state from Fay and Appel's McMillan formalism is in reasonable agreement with numerical solutions of the Eliashberg equations [126] for this region, although the magnitude of T_{SC} is somewhat smaller in the McMillan formalism.

6.1.4 The properties of $ZrZn_2$ in its superconducting state

Very little is known about the superconducting state of $ZrZn_2$. Indeed to the best of our knowledge only two groups have reported of the observation of superconductivity in $ZrZn_2$ [166, 219]. Only Pfleiderer *et al.* [166] have studied the dependence of T_{SC} on pressure (see figure 6.3). They found that the transition temperature decreases linearly with applied pressure below 18 kbar and that the sample did not superconduct (they where able to go as cold as 15 mK) for $P = 22$ kbar $> P_C$. However, they did not report any results for pressures in the range 18 kbar $< P <$ 22 kbar. It should also be noted that the resistivity in the sample used did not fall all the way to zero (although a drop of $> 35\%$ was observed: see inset figure 6.3) this must call into doubt the quality of the sample. In particular one might question whether the entire sample or merely certain regions become superconducting. Clearer evidence for superconductivity was observed in both the imaginary and real parts of the a.c. susceptibility. The drops in resistivity and the real (reactive) part of the a.c. susceptibility and the increase in the imaginary (lossive) part of the a.c. susceptibility all begin at 0.3 K and consistently determine T_{SC}. However, the superconducting critical temperature has now been raised to 0.6 K [219]. In section 6.2 we will predict the further extent to which T_{SC} could be increased by growing cleaner crystals. Another puzzle is that to date no specific heat anomaly has been observed in $ZrZn_2$.

6.1.5 Theories of superconductivity in $ZrZn_2$: post experiment

Since the discovery of superconductivity in $ZrZn_2$ the calculations discussed in section 6.1.3 have been revisited. In particular several workers have revisited the calculations of Fay and Appel [70] to attempt to explain the fact that superconductivity has not been observed in the paramagnetic state.

Santi, Dugdale and Jarlborg [183] revisited Fay and Appel's calculations. However, Santi *et al.* began by performing *ab initio* band structure calculations for $ZrZn_2$. These band structure

pairing.' However, it is clear from the quoted numerical results and the discussion that the maximum in T_{SC} does actually lie near ambient pressure.

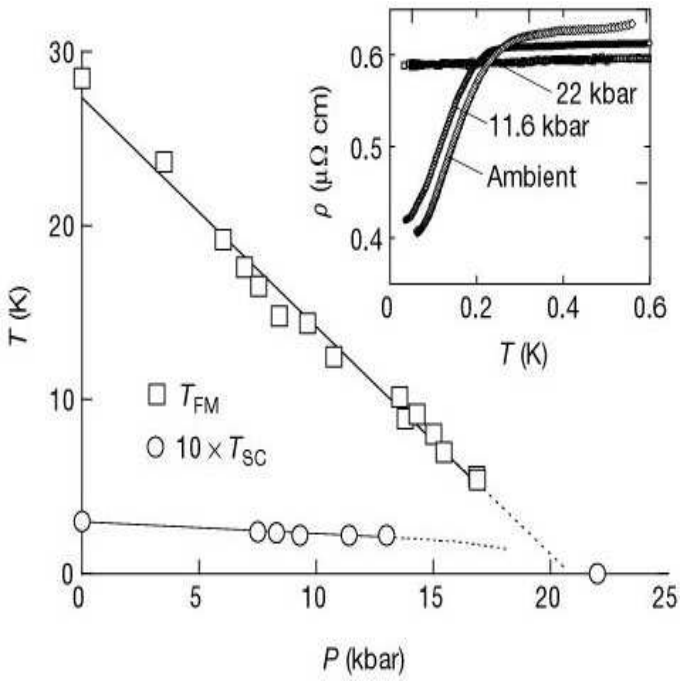

Figure 6.3: The phase diagram of $ZrZn_2$ taken from Pfleiderer *et al.* [166]. Inset: resistivity as a function of temperature, note that, in this sample, the resistivity does not drop to zero.

calculations where then used to calculate both the electron-phonon coupling constant, λ_{ph}, and the spin fluctuation coupling constant, $\lambda_{sf}^{L,T}$, for both longitudinal (L) and transverse (T) spin waves in both the s and p channels. On the basis of these calculations Santi *et al.* predicted ESP p-wave superconductivity in the ferromagnetic state with a critical temperature of order 1 K. However, they also predicted p-wave pairing in the paramagnetic state with a *higher* critical temperature. In light of previous speculation of s-wave pairing at very high pressures Santi *et al.* studied their coupling constants at a lattice spacing of $a = 13.17$ a.u. (equivalent to 160 kbar pressure) and found even at such extreme pressures the conditions would not be favourable for phonon mediated, s-wave superconductivity.

We have now seen that the model of Fay and Appel and Santi *et al.* gives a reasonable order of magnitude for the superconducting transition temperature in the ferromagnetic state. However, the description of superconductivity in the paramagnetic state from this model is clearly contradicted by the experimental facts. Kirkpatrick and coworkers [110, 109] attempted to resolve this problem by arguing that in the ferromagnetic state spin waves couple of the longitudinal susceptibility and thus contribute a mode-mode coupling term which has no analog in the paramagnetic phase. They showed that this can lead to a superconducting critical

temperature that is fifty times larger in the ferromagnetic state than it is in the paramagnetic state. However, they did not report the order of magnitude of the critical temperatures in their calculations and their model is based on the Heisenberg model which is not appropriate for $ZrZn_2$.

At this early stage in the study of $ZrZn_2$ phenomenological models are probably more useful solutions of exact Hamiltonians for (at least) two reasons: (i) The calculation of T_{SC} is notoriously difficult even for phonon mediated superconductivity, which is much better understood than the spin fluctuation mediated superconductivity which has been studied thus far. (ii) We do not yet have any understanding of the nature of the superconducting state in $ZrZn_2$. As we have seen in the case of Sr_2RuO_4 (chapter 5), the best way to interpret the results of the kind of experiments which can determine the nature of the superconducting state (see sections 3.5 and 5.1.2 for examples of such experiments) is via comparison with phenomenological models.

One such phenomenological model has been proposed by Walker and Samokhin [215] who studied a Landau theory for the magnetic state and a Ginzburg–Landau theory for the superconducting state simultaneously. This theory led them to conclude that the superconducting critical temperature, as a function of pressure, is given by

$$T_{SC}(P) = T_0 + T^{*\frac{1}{2}} \left(T_{FM}(P) - T_{SC}(P)\right)^{\frac{1}{2}} . \tag{6.1.1}$$

This theory then has the great virtue of making a clear, potentially falsifiable, prediction. However, it also requires that T_0, the superconducting critical temperature in the paramagnetic state, is very small and that the enhancement in T_{SC} by the exchange field is extremely large i.e. that $T^* \gg T_0$. It is rather hard to see how this condition might come about.

Samokhin and Walker [182] also conducted a group theoretic analysis of the possible superconducting states in the ferromagnetic phase of $ZrZn_2$. This led to the conclusion that if 'spin-orbit coupling is weak then superconductivity should appear only on one of the sheets of the Fermi surface.' (This also assumes that the effect interband scattering is weak, which is probably reasonable given the high sample purity required to observe superconductivity in the first place.) If this is the case then band 29 is the most likely candidate as it contributes $\sim 50\%$ of the density of states at the Fermi level [183]. The group theoretic analysis also shows that nodal structure depends on the strongly direction of the magnetisation density, $\mathbf{M}$. Combining this analysis with their Ginzburg–Landau theory Samokhin and Walker suggest that the for $\mathbf{M} \parallel [001]$ $ZrZn_2$ will have nodes along the line $k_x = k_y = 0$, while for $\mathbf{M} \parallel [111]$ $ZrZn_2$ will have nodes along the line $k_x = k_y = k_z$.

Singh and Mazin [194] have also raised the possibility of an FFLO state in $ZrZn_2$. (The FFLO state is discussed in a footnote in section 4.4.1.) However, this seems unlikely in view of the calculations of Santi *et al.* which indicate that OSP (opposite spin pairing) pairing is not favoured even a very high pressures. Further, the FFLO state is destroyed by fields only moderately larger than the Clogston–Chandrasekhar limiting field and therefore seems not to be the superconducting state found in $ZrZn_2$. Of course a third possibility also exists, namely that the superconducting states contains both ESP and OSP states, for example the B_2 phase, which after all is observed in ^{3}He in weak magnetic fields (see section 3.9). However, the B_2 phase is destroyed by fields larger than the Clogston–Chandrasekhar limiting field and would therefore appear to be ruled out in $ZrZn_2$.

6.1.6 Other ferromagnetic superconductors

The phrase 'magnetic superconductor' has been widely used in the history of physics. But in this chapter we are interested in only a small subset of the materials which have been called magnetic superconductors. Firstly we are interested in ferromagnetism, we will therefore not discuss at length the cuprates or heavy fermion materials like $CePd_2Si_2$ and $CeIn_3$ which are superconductors on the border of antiferromagnetism and are thought to be magnetically mediated [145]. It is interesting to note however, that for the two heavy Fermion superconductors the maximum in T_{SC} occurs at P_C (see figures 6.4 and 6.5), which is, of course the reverse of the situation in $ZrZn_2$. In the cuprates the control parameter is charge carrier concentration rather than pressure, rather than the usual chemical doping which has the side effect of distorting the lattice), further the strange pseudogap region lies between the superconducting and antiferromagnetic regions. Neither will we discuss at length materials where different electrons are involved in the magnetism and the superconductivity. Examples of this include the ruthenocuprates ($RuSr_2RECu_2O_8$, where RE = rare earth) in which it appears that electrons in the copper-oxygen planes superconduct, whilst the ferromagnetism arises from the ruthenium-oxygen planes [71] and borocarbines ($RENi_2B_2C$) in which antiferromagnetism arises in the RE-C sheets and superconductivity occurs in the separating slabs of Ni_2B_2 [44]. Ferromagnetism and superconductivity also occurs in non-layered systems such as $ErRh_4B_4$ [197] and $HoMo_6S_8$ [144]. In these systems superconductivity appears at the upper critical temperature T_{C1} but at then disappears at the (lower) critical temperature T_{C2}. Below T_{C2} a sinusoidally modulated ferromagnetic phase exists. The interested reader can find a nice (but in view of recent developments, slightly outdated) reviews of these other 'magnetic

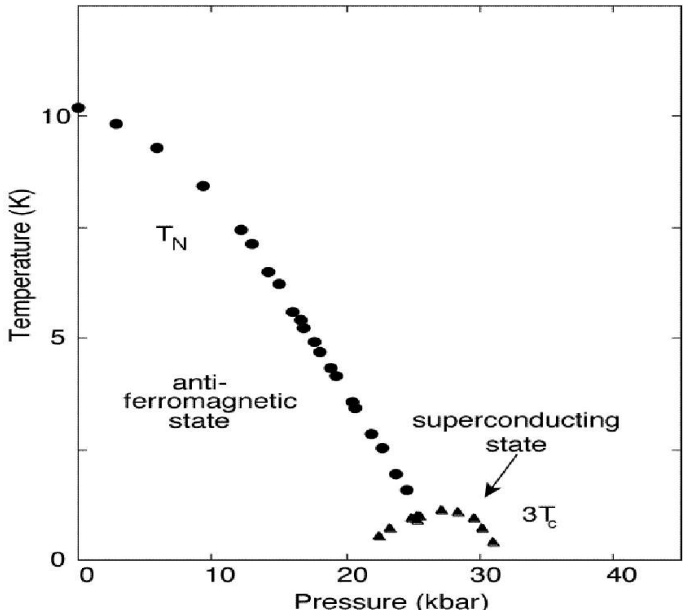

Figure 6.4: The phase diagram of $CePd_2Si_2$ taken from Mathur *et al.* [145]. Note that here the maximum in T_{SC} is at the critical pressure, unlike the situation in the ferromagnetic superconductors.

superconductors' in references [197, 144].

We now focus on systems in which the *same* electrons are *simultaneously* involved in both superconductivity and ferromagnetism. Other than $ZrZn_2$ only two examples of ferromagnetic superconductors in which the electrons are responsible for both superconductivity and ferromagnetism and both phenomena appear concurrently are currently known; they are UGe_2 and URhGe.

The phase diagram of UGe_2 (shown in figure 6.6) is not dissimilar to that of $ZrZn_2$. UGe_2 is a ferromagnet with a Curie temperature of 54 K at ambient pressure. With applied pressure the Curie temperature decreases (although not linearly as in $ZrZn_2$). Ferromagnetism is not observed above the critical pressure of 16 kbar. Further, muon spin relaxation experiments [218] show that the critical dynamics are consistent with the Heisenberg model.

Superconductivity is not observed at abient pressure in UGe_2, but appears at 10 kbar [98]. As a function of pressure, the superconducting critical temperature rises to a maximum at 12 kbar and then falls to zero again at approximately the critical pressure. Much interest [167] was provoked by the discovery of a second magnetic transition at the temperature $T_x \sim 24$ K which has now been observed by a number of probes including a.c. magnetic susceptibility [156],

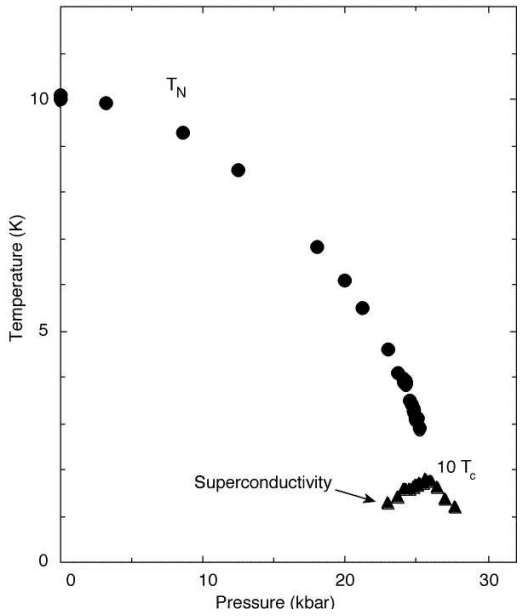

Figure 6.5: The phase diagram of $CeIn_3$ taken from Mathur *et al*. [145]. Note that the maximum in T_{SC} is at the critical pressure, as in $CePd_2Si_2$.

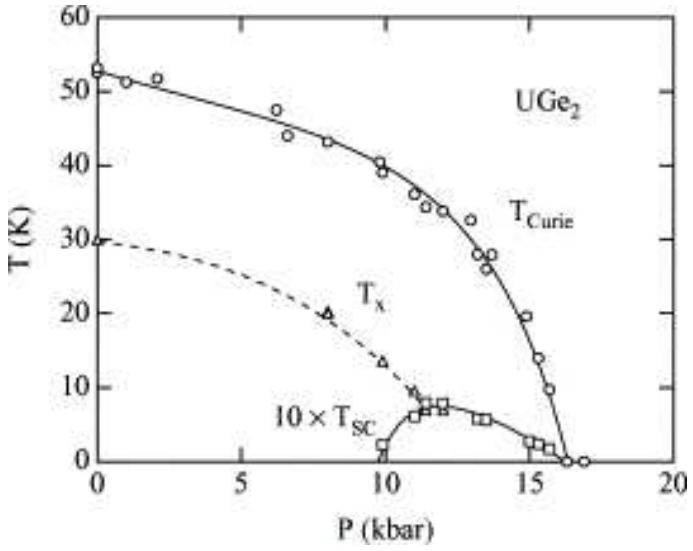

Figure 6.6: The phase diagram of UGe_2 taken from Aoki *et al*. [16].

thermal expansion [210], heat capacity [204] and magnetometery [164]. T_x falls with applied pressure and disappears at the pressure $P_x \sim 12.5$ kbar. The fact that P_x corresponds to maximum in T_{SC} led to speculation about the role of quantum critical points (QCPs). However, it was found that both magnetic transitions in UGe_2 are first order [164] which rules out the QCP scenarios as they require a second order transition [70, 110, 109]. The nature of the state below T_x is not known, although we should note that neutron scattering experiments found no evidence of modulated phases (e.g. charge density waves or spin density waves) below T_x [107]. De Haas–van Alphen experiments [205] indicate that a discontinuous change in the Fermi surface topology may occur in the region of P_C, which is consistent with the observation of a first order phase transition. The results of the de Haas–van Alphen experiments also suggest that T_x is unlikely to correspond to the formation of a modulated phase as no change in the nesting properties of the Fermi surface occur at the relevant pressure. On the other hand a new frequency is observed at 12.2 kbar ($\sim P_x$), which the authors (tentatively) attribute to a large hole surface shrinking and splitting in two. This seems to be the only clue about the origin of the 'x' transition at present.

In a magnetic field UGe_2 shows several unusual features. Near the pressure which gives the maximum T_{SC} the upper critical field, $H_{C2} \gtrsim 3$ T [98], is large in comparison to T_{SC}. If one assumes that UGe_2 is a weak coupling superconductor then this indicates that $H_{C2} > H_P$, the Clogston–Chandrasekhar limiting field. The pressure dependence of the upper critical field is high anisotropic and in certain field orientations UGe_2 shows reentrant superconductivity [191].

At ambient pressure URhGe is a ferromagnet with a Curie temperature of 9.5 K. In polycrystalline samples clear signs of a superconducting transition at $T_{SC} \sim 250$ mK are observed in resistivity, a.c. susceptibility, heat capacity (including an anomaly) and magnetisation [15]. The superconducting state is highly sensitive to disorder while the Curie temperature is relatively insensitive to impurities, indicating that the superconducting state is probably unconventional. At low temperatures $H_{C2} \gtrsim 0.71$ T $> H_P$, the (weak coupling) Clogston–Chandrasekhar limiting field [15], which indicates that the pairing state is probably triplet (although again FFLO states are not ruled out). It may be that rhodium effectively applies chemical pressure as the U-U bond length in URhGe (3.5 Å) is approximately the same as the bond length in UGe_2 under 12 kbar of pressure, where the maximum T_{SC} is observed.

6.1.7 The relevance of our model to $ZrZn_2$

In light of the fact that superconductivity has not been observed in the paramagnetic state of $ZrZn_2$ models other than variants of that proposed by Fay and Appel should be considered. Our extended Hubbard model (see chapter 4) is in fact probably more suited to $ZrZn_2$ than Sr_2RuO_4 as the Zeeman term is more important in a ferromagnet than it is for an external magnetic field. We make the substitution $\mathbf{E}_{xc} = -\mu_B \mathbf{H}$. We choose this sign convention so that $\uparrow$ electrons are the majority spin and thus avoid any potential confusion. We will use our model to consider the effect of the variation of pressure on the superconducting state via the pressure dependence of the exchange splitting. Thus we consider a effective, nearest neighbour, pairwise, attractive potential that is *independent* of pressure.

Our model is clearly not relevant to UGe_2 because it is a Heisenberg ferromagnet. (Of course the converse is true in that the Stoner ferromagnetism of $ZrZn_2$ rules out the model of Kirkpatrick *et al*. [110].)

6.2 The critical temperature of $ZrZn_2$ in the presence of disorder

Given that our formalism does not have the facility of handling disorder we need to know what the critical temperature of clean $ZrZn_2$ is. Unfortunately the lack of data makes this somewhat speculative at best. However, the order of magnitude of the calculation should at least be accurate.

6.2.1 The Abrikosov–Gorkov formula

Disorder will only have a pair breaking influence if it destroys the coherence of the condensate. In an s-wave superconductor magnetic impurities lower the critical temperature as they destroy the coherence of the OSP Cooper pairs. However, non-magnetic impurities have only a very weak effect on the critical temperature via the changes they cause in the density of states at the Fermi level, $D(\varepsilon_F)$.

In an unconventional superconductor (by which, in this context, we mean a superconductor in which the order parameter has any symmetry of than s-wave) the phase of order parameter varies around the Brillouin zone. Therefore scattering form non-magnetic impurities destroys the coherence of the orbital part of the pair wavefunction and thus lowers T_{SC}.

Abrikosov and Gorkov [2] derived an expression for the critical temperature of an s-wave

superconductor in the presence of magnetic impurities. This was then recast in the correct form for an unconventional superconductor in the presence of non-magnetic impurities by Larkin [118]. It turns out that both formalisms have the same mathematical form.

Larkin considered isotropic scattering from non-magnetic impurities in the Born approximation. In this case the normal part of the self-energy has the form [154]

$$\Sigma_{1,\alpha\beta}(\omega_n) = \Sigma(\omega_n)\delta_{\alpha\beta} = \frac{1}{2\pi D(\varepsilon_F)\tau_{tr}} \int \frac{\mathrm{d}\mathbf{k}}{(2\pi)^3} \mathcal{G}(\mathbf{k},\omega_n)\delta_{\alpha\beta}, \tag{6.2.1}$$

and the anomalous part of the self energy is given part

$$\Sigma_{2,\alpha\beta}(\omega_n) = \frac{1}{2\pi D(\varepsilon_F)\tau_{tr}} \int \frac{\mathrm{d}\mathbf{k}}{(2\pi)^3} \mathcal{F}_{\alpha\beta}(\mathbf{k},\omega_n), \tag{6.2.2}$$

where τ_{tr} is the quasiparticle lifetime (given by equation 6.2.33, we discuss why this particular lifetime is the relevant quantity is section 6.2.3). The Gorkov equations[3] are then

$$\left(\mathtt{i}\omega_n - \varepsilon(\mathbf{k}) - \Sigma(\omega_n)\right)\mathcal{G}(\mathbf{k},\omega_n)\delta_{\alpha\beta} + \Delta_{\alpha\gamma}(\mathbf{k})\mathcal{F}^{\dagger}_{\gamma\beta}(\mathbf{k},\omega_n) = \delta_{\alpha\beta} \tag{6.2.3}$$

$$\left(\mathtt{i}\omega_n + \varepsilon(\mathbf{k}) - \Sigma(\omega_n)\right)\mathcal{F}^{\dagger}_{\alpha\beta}(\mathbf{k},\omega_n) + \Delta^{\dagger}_{\alpha\beta}(\mathbf{k})\mathcal{G}(\mathbf{k},\omega_n) = 0 \tag{6.2.4}$$

$$\left(\mathtt{i}\omega_n - \varepsilon(\mathbf{k}) - \Sigma(\omega_n)\right)\mathcal{F}_{\alpha\beta}(\mathbf{k},\omega_n) + \Delta_{\alpha\beta}(\mathbf{k})\mathcal{G}(-\mathbf{k},-\omega_n) = 0 \tag{6.2.5}$$

Hence,

$$\mathcal{G}(\mathbf{k},\omega_n) = -\frac{\mathtt{i}\widetilde{\omega}_n + \varepsilon(\mathbf{k})}{\widetilde{\omega}_n^2 + \varepsilon(\mathbf{k})^2 + \Delta^2(\mathbf{k})} \tag{6.2.6}$$

$$\mathcal{F}_{\alpha\beta}(\mathbf{k},\omega_n) = -\frac{\Delta_{\alpha\beta}(\mathbf{k})}{\widetilde{\omega}_n^2 + \varepsilon(\mathbf{k})^2 + \Delta^2(\mathbf{k})}, \tag{6.2.7}$$

where,

$$\mathtt{i}\widetilde{\omega}_n = \mathtt{i}\omega_n - \Sigma(\omega_n), \tag{6.2.8}$$

$$\Delta^2(\mathbf{k}) = \begin{cases} \frac{1}{2}\mathrm{tr}\left(\underline{\underline{\Delta}}_{\mathbf{k}}\underline{\underline{\Delta}}_{\mathbf{k}}\right) & \text{unitary phases} \\ \underline{\underline{\Delta}}_{\mathbf{k}}\underline{\underline{\Delta}}_{\mathbf{k}}\left[\left(|\hat{\mathbf{d}}(\mathbf{k})|^2\underline{\underline{I}} + \mathtt{i}\left(\hat{\mathbf{d}}(\mathbf{k})\times\hat{\mathbf{d}}(\mathbf{k})\right)\cdot\underline{\underline{\sigma}}\right)\right]^{-1} & \text{non-unitary phases} \end{cases} \tag{6.2.9}$$

[3]The Gorkov equations are equivalent of BdG equations but written in Green's function notation. As we no not make extensive use of these in this work we refer the reader to references [154] and [193], both of which give excellent introductions to the Gorkov equations in the context of spin-generalised pairing. Also, note that in equations 6.2.3, 6.2.4 and 6.2.5 we use the Einstein summation notation for repeated spin indices.

and $\hat{\mathbf{d}}(\mathbf{k}) \equiv \frac{\mathbf{d}(\mathbf{k})}{|\mathbf{d}(\mathbf{k})|}$.

Assuming that there is symmetry between electrons and holes (6.2.1) and (6.2.6) give

$$\Sigma(\omega_n) = -\frac{\mathtt{i}\widetilde{\omega}_n}{2\tau_{tr}} \int \frac{\mathrm{d}\Omega}{4\pi} \frac{1}{\sqrt{\widetilde{\omega}_n^2 + \Delta^2(\mathbf{k})}}. \tag{6.2.10}$$

The self consistent solution of equations **??** and 6.2.10 depends on the symmetry of the gap however, regardless of the gap symmetry near T_{SC} $\Delta(\mathbf{k}) \to 0$ and we have

$$\Sigma(\omega_n) = -\frac{\mathtt{i}}{2\tau_{tr}} \mathrm{sgn}\,(\omega_n) \tag{6.2.11}$$

as one would expect for a normal metal.

Thus near T_{SC} the anomalous Green's functions are given by

$$\mathcal{F}_{\alpha\beta}(\mathbf{k}, \omega_n) = -\frac{\Delta_{\alpha\beta}(\mathbf{k})}{\left(\omega_n + \mathrm{sgn}(\omega_n)/2\tau_{tr}\right)^2 + \varepsilon(\mathbf{k})^2}. \tag{6.2.12}$$

In Green's function notation the self-consistency equation (4.3.30) is

$$\Delta_{\alpha\beta}(\mathbf{k}) = T \sum_n \sum_{\mathbf{k}'} U_{\alpha\beta}(\mathbf{k} - \mathbf{k}') \mathcal{F}_{\alpha\beta}(\mathbf{k} - \mathbf{k}', \omega_n). \tag{6.2.13}$$

Hence we find that

$$\Delta_{\alpha\beta}(\mathbf{k}) = \pi D(\varepsilon_F) T \sum_n \frac{\mathrm{sgn}(\omega_n)}{\omega_n + \mathrm{sgn}(\omega_n)/2\tau_{tr}} \int \frac{\mathrm{d}\Omega'}{4\pi} U_{\alpha\beta}(\mathbf{k} - \mathbf{k}') \Delta_{\alpha\beta}(\mathbf{k}'). \tag{6.2.14}$$

Taking

$$U_{\alpha\beta}(\mathbf{k} - \mathbf{k}') = \begin{cases} V\delta_{\alpha\beta} & \text{for } \varepsilon_F - \varepsilon_c \le \hbar|\mathbf{k}|^2/2m^*, \hbar|\mathbf{k}'|^2/2m^* \le \varepsilon_F + \varepsilon_c \\ 0 & \text{otherwise} \end{cases} \tag{6.2.15}$$

We find that

$$1 = \pi D(\varepsilon_F) V T \sum_n \frac{\mathrm{sgn}(\omega_n)}{\omega_n + \mathrm{sgn}(\omega_n)/2\tau_{tr}} \tag{6.2.16}$$

$$= 2\pi D(\varepsilon_F) V T \sum_{n \ge 0} \frac{1}{\omega_n} + 2\pi D(\varepsilon_F) V T \sum_{n \ge 0} \left(\frac{\mathrm{sgn}(\omega_n)}{\omega_n + \mathrm{sgn}(\omega_n)/2\tau_{tr}} - \frac{1}{\omega_n} \right). \tag{6.2.17}$$

The first term on the righthand side of equation 6.2.17 would diverge logarithmically but for the cutoff frequency ε_c. This term straightforwardly evaluated using the identity

$$\lim_{N\to\infty}\sum_{n\geq 0}^{N}\frac{1}{n+1/2}=\ln N+\ln 4\gamma, \tag{6.2.18}$$

and recalling that the critical temperature of a superconductor with the absence of impurity scattering, T_{SC0} is given by

$$T_{SC0}=\frac{2\gamma}{\pi}\varepsilon_c\exp\left(-\frac{1}{D(\varepsilon_F)V}\right), \tag{6.2.19}$$

where γ is Euler's constant $= 0.5772...$ [18], we find that

$$2\pi D(\varepsilon_F)VT\sum_{n\geq 0}\frac{1}{\omega_n}=1+D(\varepsilon_F)V\ln\left(\frac{T_{SC0}}{T}\right). \tag{6.2.20}$$

To evaluate the second term of the righthand side of equation 6.2.17 we note that [18]

$$\psi(z)=-\gamma-\sum_{n=1}^{\infty}\left(\frac{1}{z+n}-\frac{1}{n}\right) \tag{6.2.21}$$

and [1]

$$\psi(1+z)=\psi(z)+\frac{1}{z} \tag{6.2.22}$$

Therefore

$$2\pi D(\varepsilon_F)VT\sum_{n\geq 0}\left(\frac{\mathrm{sgn}(\omega_n)}{\omega_n+\mathrm{sgn}(\omega_n)/2\tau_{tr}}-\frac{1}{\omega_n}\right)=D(\varepsilon_F)V\left[\psi\left(\frac{1}{2}+\frac{1}{4\pi\tau_{tr}T}\right)-\psi\left(\frac{1}{2}\right)\right] \tag{6.2.23}$$

Equation 6.2.17 is clearly only valid at $T=T_{SC}$. Substituting (6.2.23) and (6.2.20) into (6.2.17) and setting $T=T_{SC}$ we arrive at the Abrikosov–Gorkov formula;

$$\ln\left(\frac{T_{SC0}}{T_{SC}}\right)=\psi\left(\frac{1}{2}+\frac{\hbar}{4\pi\tau_{tr}k_BT_{SC}}\right)-\psi\left(\frac{1}{2}\right). \tag{6.2.24}$$

The Baltensperger–Sarma equation [24, 184, 103] (which we will not derive here; details can be found in references [201, 200]),

$$\ln\left(\frac{T_{SC0}}{T_{SC}}\right) = \psi\left(\frac{1}{2} + \mathtt{i}\frac{E_{xc}}{4\pi k_B T_{SC}}\right) - \psi\left(\frac{1}{2}\right), \tag{6.2.25}$$

accounts for the reduction in the critical temperature of a superconductor due to exchange splitting but is only valid for OSP states. This would appear to complicate the analysis as this term would have to be included for OSP states, but not for ESP states. However, this term is not in fact relevant in the following analysis as all measurements are performed at ambient pressure and at extremely low temperatures ($T \lesssim 0.05 T_{FM}$), so the exchange splitting is constant throughout. However, if resistivity measurements where performed over a range of pressures, the Baltensperger–Sarma equation would be relevant (if the there is OSP) because of the variation of E_{xc} as a function of pressure.

6.2.2 The determination of the critical temperature of clean $ZrZn_2$ from residual resistivity experiments

The simplest approach to determine the critical temperature is to compare the residual resistivity of several samples with their superconducting transition temperatures.

In Fermi liquid theory the resistivity is given by

$$\rho(T) = \rho_0 + AT^2. \tag{6.2.26}$$

ρ_0 is known as the residual resistivity. Experimentally the residual resistivity can be measured by studying the limit of ρ as $T \to 0$ in the normal state. The residual resistivity is straightforward to compare to with the critical temperature as calculated from the Abrikosov–Gorkov formula because of the Drude formula for resistivity,

$$\rho_0 = \frac{m^*}{ne^2\tau_{tr}}. \tag{6.2.27}$$

For Sr_2RuO_4, the ratio m^*/n can be found straightforwardly from either band structure calculations or de Haas–van Alphen experiments. However, for $ZrZn_2$ this is not so straightforward so we treat m^*/n as a fitting parameter. (In the fit presented below the we take $\frac{m^*}{ne^2} = 3.4\ \mu\Omega$cmps.)

We are grateful to Stephen Hayden and Stephen Yates for providing us with the data to which we constructed the fit to the Abrikosov–Gorkov–Drude form shown in figure 6.7. On the basis of this fit we find that $\mathbf{T_{C0} = 1.15 \pm 0.15\ K}$. An additional point, from Pfleiderer *et al.* [166] is also shown in figure 6.7. We do not fit to this point as the resistivity does not fall to zero

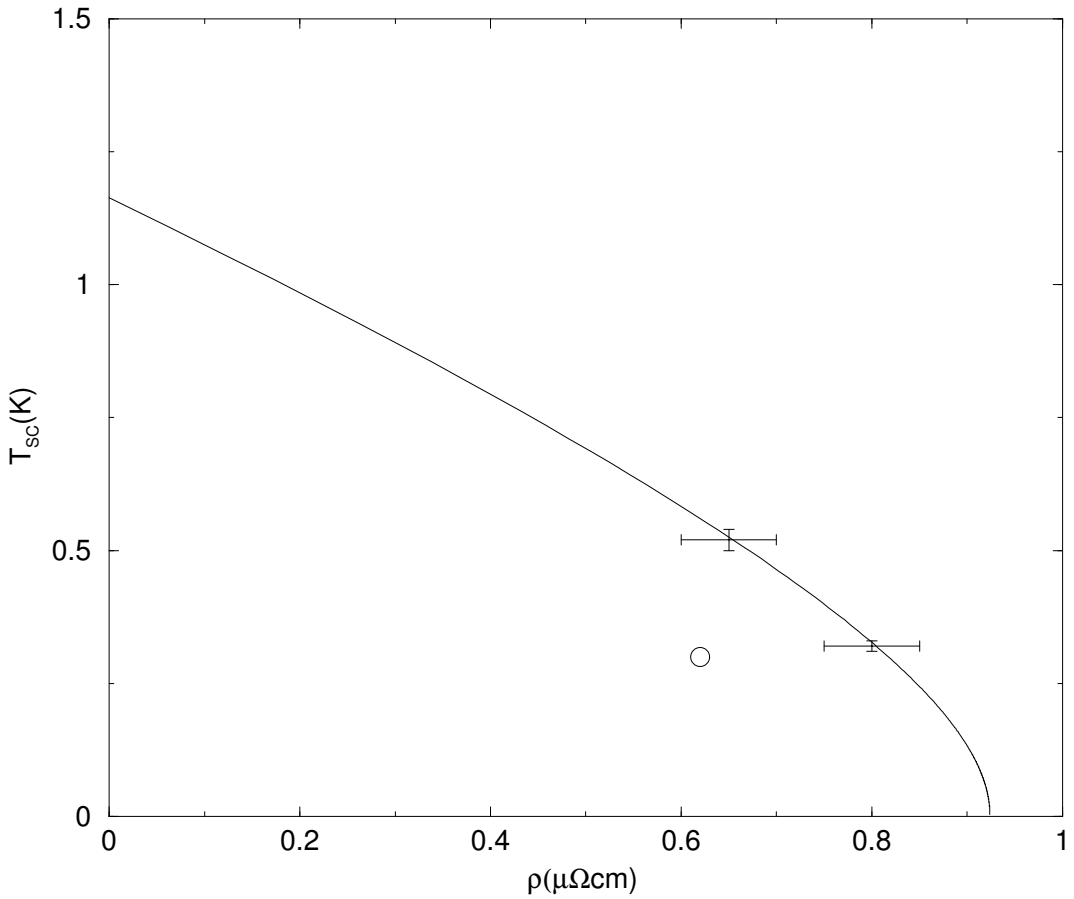

Figure 6.7: The superconducting critical temperature of $ZrZn_2$ as a function of residual resistivity. The data to which the fit is constructed was provided by Stephen Hayden and Stephen Yates (data shown with error bars). Another data point, taken from Pfleiderer *et al.* [166] is also shown (open circle) but was not fitted to - see the text for discussion.

in the superconducting state of this sample (see inset figure 6.3). The reason that the resistivity does not fall completely to zero is not well understood so the validity of the data point is questionable. However, the inclusion of this data point would only lower the clean transition temperature to $T_{C0} \sim 1$ K. Which is (just) within the quoted error. The quoted error is itself possibly a little optimistic on the basis of two data points.

6.2.3 The determination of the critical temperature of clean $ZrZn_2$ from de Haas van Alphen experiments

Given that we have only two ρ_0, T_{SC} data points to fit to, the validity of our fit is questionable. We have therefore investigated the possibility of finding T_{C0} from another experiment. De Haas-van Alphen provides a measurement of the quasiparticle lifetime. Yates *et al.* [219] measured the quasiparticle lifetime on three sheets of the sheets of the Fermi by this method. On each of the three sheets they reported $\tau \sim 0.3$ ps. On the basis of this quasiparticle lifetime, given that the sample in question has $T_{SC} \sim 0.6$ K, the Abrikosov–Gorkov formula gives $T_{SC0} \sim 14.5$ K.

Thus it would appear that the values of T_{SC0} extrapolated from residual resistivity and dHvA experiments are in strong disagreement. However, the extraction of the quasiparticle lifetime from dHvA experiments is a non trivial task which involves the calculation of the Dingle factor, R_D, from the amplitude of the dHvA oscillations[4]. The Dingle factor is given by

$$R_D = \exp\left(\frac{l\alpha m\hbar}{2\pi k_B H\tau}\right) \tag{6.2.28}$$

where l is the number of completed cyclotron orbits, α is a constant $= 14.69$ TK^{-1}. For free electrons, the introduction of electron-phonon effects (and similarly electron-magnon effects) renormalises the quasiparticle lifetime and the Fermi velocity, v_F, in the same ratio so that the product $v_F\tau$ (and hence the electrical conductivity) is unchanged. We therefore have

$$\frac{\tau^*}{\tau} = \frac{v_F}{v_F^*} = 1 + \lambda, \tag{6.2.29}$$

where λ is the electron-phonon (or electron-magnon) enhancement factor and an asterisk indicates a renormalised quantity. Recalling that

$$\frac{m^*}{m} = 1 + \lambda \tag{6.2.30}$$

we have

$$\frac{m^*}{\tau^*} = \frac{m}{\tau}. \tag{6.2.31}$$

Hence the Dingle factor (for free electrons at least) is unchanged. It is therefore traditional to calculate the unrenormalised quasiparticle lifetime from the Dingle factor. (Indeed this is the

[4]The following analysis summarises arguments presented by Poulsen, Randles and Springford [171].

lifetime calculated by Yates *et al.* [219].) However, as m^* enters the Drude formula we require τ^* and not τ. This renormalisation increases the lifetime by approximately a factor of five, the Abrikosov–Gorkov formula then gives $T_{SC0} = 3.1$ K, in far better agreement with the resistivity calculation.

One possible reason for the remaining difference in the two values of T_{SC0} is that the renormalised quasiparticle lifetime measured in dHvA experiments is not strictly the relevant factor in a transport experiment (e.g. resistivity). It can be shown that [3] in the Born approximation the quasiparticle lifetime measured in the dHvA experiments is given by

$$\frac{1}{\tau_{dHvA}} = \frac{nmk_F}{(2\pi)^2} \int |u(\theta)|^2 \mathrm{d}\Omega, \tag{6.2.32}$$

while the quasiparticle lifetime measured in transport experiments is

$$\frac{1}{\tau_{tr}} = \frac{nmk_F}{(2\pi)^2} \int |u(\theta)|^2 (1 - \cos\theta) \mathrm{d}\Omega. \tag{6.2.33}$$

In both of the above equations n is the number of impurity atoms per unity volume and $u(\theta)$ is the probability of an electron scattering through the angle θ. There is also factor of $(1 - \cos\theta)$ in the lifetime in the Abrikosov–Gorkov formula. Therefore the transport lifetime is (as stated in section 6.2.1) the appropriate lifetime to use in the Abrikosov–Gorkov formula. However, the factors of $(1 - \cos\theta)$ in the transport and Abrikosov–Gorkov lifetimes arise for very different physical reasons: The factor $(1 - \cos\theta)$ in the transport lifetime comes about because backscattering (that is scattering thorough $\sim 180^o$) is much more detrimental to transport than small angle scattering; where as, the $(1 - \cos\theta)$ factor in the Abrikosov–Gorkov formula is a direct consequence of the symmetry of the p-wave state. On the other hand any scattering destroys a cyclotron orbit, regardless of the direction of the scattering, and thus there is no $(1 - \cos\theta)$ factor in the dHvA lifetime.

Without a theory of normal state transport (that is without knowledge of $u(\theta)$) we cannot calculate the difference in this lifetimes. The two analyses give a ratio $\frac{\tau_{tr}}{\tau_{dHvA}} \sim 4$. The normal state scattering rate not would have to be extremely anisotropic to account for such a large ratio ($\frac{\tau_{tr}}{\tau_{dHvA}} = 1$ for isotropic scattering i.e. for $u(\theta) = u$). Note that the appropriate lifetime for the Abrikosov–Gorkov formula is τ_{tr} [118].

The remaining difference between the estimates of T_{SC0} obtained from residual resistivity and dHvA is then quite plausibly accounted for by anisotropic scattering. Such a difference in the quasiparticle lifetimes measured by transport and dHvA is by no means implausible, indeed in

some materials very large (i.e. order of magnitude) differences in the dHvA and transport lifetimes have been reported [89, 51].

The dHvA value of T_{C0} seems rather large but, more importantly, the quasiparticle lifetime has not been measured on band 29, which contributes $\sim 50\%$ of $D(\varepsilon_F)$. We therefore elect to use the value of the clean critical temperature found from the residual resistivity data in the following analysis.

6.3 The extension of our Ginzburg–Landau theory to three dimensions

The Ginzburg–Landau analysis presented in section 5.2 can straightforwardly be extended to three dimensions. For a cubic crystal we find that the condensation free energy in the presence of exchange splitting is given by

$$\begin{aligned} F_{\mathbf{E}_{xc}} &= (\alpha_0 + \alpha_2|\mathbf{E}_{xc}|^2)(|\mathbf{A}_x|^2 + |\mathbf{A}_y|^2 + |\mathbf{A}_z|^2) \\ &\quad + \mathrm{i}\alpha_1 \mathbf{E}_{xc} \cdot (\mathbf{A}_x \times \mathbf{A}_x^* + \mathbf{A}_y \times \mathbf{A}_y^* + \mathbf{A}_z \times \mathbf{A}_z^*) \\ &\quad - 2\alpha_2(|\mathbf{E}_{xc} \cdot \mathbf{A}_x|^2 + |\mathbf{E}_{xc} \cdot \mathbf{A}_y|^2 + |\mathbf{E}_{xc} \cdot \mathbf{A}_z|^2). \end{aligned} \tag{6.3.1}$$

Where,

$$\alpha_0 = \frac{2}{\beta} \sum_{\mathrm{i}\omega_n} \int \mathrm{d}\mathbf{k} \frac{\sin^2 k_x \left((\varepsilon_{\mathbf{k}} - \mu)^2 + \omega_n^2\right)}{\left[(\mathrm{i}\omega_n - \varepsilon_{\mathbf{k}} + \mu)^2 - |\mathbf{E}_{xc}|^2\right]\left[(\mathrm{i}\omega_n + \varepsilon_{\mathbf{k}} - \mu)^2 - |\mathbf{E}_{xc}|^2\right]}, \tag{6.3.2}$$

$$\alpha_1 = -\frac{4}{\beta} \sum_{\mathrm{i}\omega_n} \int \mathrm{d}\mathbf{k} \frac{\sin^2 k_x (\varepsilon_{\mathbf{k}} - \mu)}{\left[(\mathrm{i}\omega_n - \varepsilon_{\mathbf{k}} + \mu)^2 - |\mathbf{E}_{xc}|^2\right]\left[(\mathrm{i}\omega_n + \varepsilon_{\mathbf{k}} - \mu)^2 - |\mathbf{E}_{xc}|^2\right]} \tag{6.3.3}$$

and

$$\alpha_2 = -\frac{2}{\beta} \sum_{\mathrm{i}\omega_n} \int \mathrm{d}\mathbf{k} \frac{\sin^2 k_x}{\left[(\mathrm{i}\omega_n - \varepsilon_{\mathbf{k}} + \mu)^2 - |\mathbf{E}_{xc}|^2\right]\left[(\mathrm{i}\omega_n + \varepsilon_{\mathbf{k}} - \mu)^2 - |\mathbf{E}_{xc}|^2\right]}. \tag{6.3.4}$$

Hence, as in the two dimensional case, the critical temperature is determined by highest temperature solution of

$$\left(\alpha_0 - \alpha_2|\mathbf{E}_{xc}|^2\right)\left(\left(\alpha_0 + \alpha_2|\mathbf{E}_{xc}|^2\right)^2 - \alpha_1^2|\mathbf{E}_{xc}|^2\right) = 0. \tag{6.3.5}$$

If the microscopic variables are such that the A phase is the ground state in the absence of exchange splitting there are two possible states in the presence of exchange splitting. For $\mathbf{E}_{xc} = \big(0, 0, E_{xc}\big)$ these are

$$\mathbf{A}_i = \mathtt{i}\mathbf{A}_j = \big(0, 0, 1\big) \tag{6.3.6}$$

and

$$\mathbf{A}_i = \mathtt{i}\mathbf{A}_j = \big(1, \mathtt{i}\kappa, 0\big). \tag{6.3.7}$$

In this formalism the six states $ij = xy, yz, zx, yx, zy$ and xz are degenerate. However, spin orbit coupling would presumably mean that the states $ij = xy$ or yx are preferred.

6.3.1 Comparison of our Ginzburg–Landau theory with that proposed by Walker and Samokhin

We now compare and contrast the Ginzburg–Landau presented above with the theory presented by Walker and Samokhin [215] (hereafter WS).

The most obvious difference between the two formalisms is that the Ginzburg–Landau theory proposed by WS includes the ferromagnetism where as we must take the exchange splitting as an external parameter. However, as the behaviour of both the Curie temperature and zero temperature magnetisation as are well known as functions of pressure [53] this is not a significant problem. Further, our assertion that both T_{FM} and E_{xc} are linear functions of pressure which go smoothly to zero at P_C is in agreement with the Landau analysis of WS.

We now turn our attention to the Ginzburg–Landau part of the analysis. The WS Ginzburg–Landau free energy is

$$F_{SC} = \alpha\psi^* \cdot \psi - \mathtt{i}4\pi J\mathbf{M} \cdot (\psi^* \times \psi)\,. \tag{6.3.8}$$

where ψ is a 'three-component quantity... whose components transform under rotations like those of a three-dimensional polar vector' [215]. That is $\psi \propto \overline{\mathbf{d}(\mathbf{k})}$. Comparing this with equation 6.3.1 we find that WS do not include a term equivalent to the α_2 terms (note that α in equation 6.3.8 is independent of $\mathbf{M}$). Thus, given equation 6.3.1, we expect that the predictions of the two theories will be significantly different.

6.4 The gap equations for a ferromagnetic superconductor

It can be useful to write the spin-generalised BdG equations (4.3.25) in the form

$$\underline{\underline{\widetilde{E}}}_{\mathbf{k}} = \underline{\underline{U}}^{\dagger}_{\mathbf{k}} \, \underline{\underline{\xi}}_{\mathbf{k}} \, \underline{\underline{U}}_{\mathbf{k}}. \tag{6.4.1}$$

Where

$$\underline{\underline{\widetilde{E}}}_{\mathbf{k}} = \begin{pmatrix} \underline{\underline{E}}_{\mathbf{k}} & \underline{\underline{0}} \\ \underline{\underline{0}} & -\underline{\underline{E}}_{-\mathbf{k}} \end{pmatrix} = \begin{pmatrix} E_{\mathbf{k}\uparrow} & 0 & 0 & 0 \\ 0 & E_{\mathbf{k}\downarrow} & 0 & 0 \\ 0 & 0 & -E_{-\mathbf{k}\uparrow} & 0 \\ 0 & 0 & 0 & -E_{-\mathbf{k}\downarrow} \end{pmatrix}, \tag{6.4.2}$$

$$\underline{\underline{U}}_{\mathbf{k}} = \begin{pmatrix} \underline{\underline{u}}_{\mathbf{k}} & \underline{\underline{v}}^{*}_{-\mathbf{k}} \\ \underline{\underline{v}}_{\mathbf{k}} & \underline{\underline{u}}^{*}_{-\mathbf{k}} \end{pmatrix}, \tag{6.4.3}$$

$$\underline{\underline{u}}_{\mathbf{k}} = \begin{pmatrix} u_{\uparrow\uparrow}(\mathbf{k}) & u_{\uparrow\downarrow}(\mathbf{k}) \\ u_{\downarrow\uparrow}(\mathbf{k}) & u_{\downarrow\downarrow}(\mathbf{k}) \end{pmatrix}, \tag{6.4.4}$$

$$\underline{\underline{v}}_{\mathbf{k}} = \begin{pmatrix} v_{\uparrow\uparrow}(\mathbf{k}) & v_{\uparrow\downarrow}(\mathbf{k}) \\ v_{\downarrow\uparrow}(\mathbf{k}) & v_{\downarrow\downarrow}(\mathbf{k}) \end{pmatrix}, \tag{6.4.5}$$

$$\underline{\underline{\xi}}_{\mathbf{k}} = \begin{pmatrix} \underline{\underline{\varepsilon}}_{\mathbf{k}} & \underline{\underline{\Delta}}_{\mathbf{k}} \\ -\underline{\underline{\Delta}}^{\dagger}_{-\mathbf{k}} & -\underline{\underline{\varepsilon}}^{*}_{\mathbf{k}} \end{pmatrix} \tag{6.4.6}$$

and

$$\underline{\underline{\varepsilon}}_{\mathbf{k}} = \varepsilon_{\mathbf{k}} \underline{\underline{I}} + \underline{\underline{\sigma}} \cdot \mathbf{E}_{ex}. \tag{6.4.7}$$

For a singlet superconductor or a unitary triplet state

$$\underline{\underline{\Delta}}_{\mathbf{k}} \, \underline{\underline{\Delta}}^{\dagger}_{-\mathbf{k}} = \underline{\underline{I}} \, |\Delta(\mathbf{k})|^2 \tag{6.4.8}$$

where

$$\Delta(\mathbf{k}) \equiv \begin{cases} d_0(\mathbf{k}) & \text{for a singlet superconductor} \\ \mathbf{d}(\mathbf{k}) & \text{for a unitary triplet superconductor} \end{cases} \tag{6.4.9}$$

Recalling the self consistency condition (4.3.30) we quickly find that, in the absence of exchange splitting,

$$\Delta_{\alpha\beta}(\mathbf{k}) = \sum_{\mathbf{k}'} \frac{U_{\alpha\beta}(\mathbf{k}-\mathbf{k}')\Delta_{\alpha\beta}(\mathbf{k}')}{2E(\mathbf{k}')}(1-2f_{E(\mathbf{k}')}) \tag{6.4.10}$$

where

$$E(\mathbf{k}) = \sqrt{\varepsilon_{\mathbf{k}}^2 + |\Delta(\mathbf{k})|^2}. \tag{6.4.11}$$

for both singlet and unitary triplet superconductors.

6.4.1 Non-unitary states revisited: the definition of $\mathbf{q}(\mathbf{k})$

For a non-unitary state

$$\underline{\underline{\Delta}}_{\mathbf{k}}\underline{\underline{\Delta}}_{\mathbf{k}}^{\dagger} = \underline{\underline{I}}|\mathbf{d}(\mathbf{k})|^2 + \mathtt{i}\underline{\underline{\sigma}}\cdot(\mathbf{d}(\mathbf{k})\times\mathbf{d}(\mathbf{k})^*) \tag{6.4.12}$$

and, in the absence of exchange splitting,

$$E_\sigma(\mathbf{k}) = \sqrt{\varepsilon_{\mathbf{k}}^2 + |\mathbf{d}(\mathbf{k})|^2 + \sigma|\mathbf{d}(\mathbf{k})\times\mathbf{d}(\mathbf{k})^*|}. \tag{6.4.13}$$

where $\sigma = \pm 1$.

It is therefore useful to introduce the vector $\mathbf{q}(\mathbf{k})$ which is defined by

$$\mathbf{q}(\mathbf{k}) = \mathtt{i}\mathbf{d}(\mathbf{k})\times\mathbf{d}(\mathbf{k})^*. \tag{6.4.14}$$

It is clear from the arguments given in section 3.9 that $\mathbf{q}(\mathbf{k})$ is a *real* vector and that $\mathbf{q}(\mathbf{k}) = 0$ for a unitary state.

6.4.2 The gap equations for non-unitary states in the absence of exchange splitting

The derivation of the gap equations for non-unitary states is far more complicated than is the case for unitary states. The treatment given here follows the excellent review by Sigrist and Ueda [193], whose derivation unfortunately contains an erroneous numerical factor of $\sqrt{2}$, which we correct here.

In the absence of exchange splitting

$$\underline{\underline{\varepsilon}}_{\mathbf{k}} = \begin{pmatrix} \varepsilon_{\mathbf{k}} & 0 \\ 0 & \varepsilon_{\mathbf{k}} \end{pmatrix}. \tag{6.4.15}$$

Hence, writing the BdG equations (6.4.1) as two simultaneous 2×2 matrix equations gives

$$\underline{\underline{u}}_{\mathbf{k}}\left(\underline{\underline{E}}_{\mathbf{k}}-\varepsilon_{\mathbf{k}}\right) = -\underline{\underline{\Delta}}_{\mathbf{k}}\underline{\underline{v}}_{\mathbf{k}} \tag{6.4.16}$$

$$\underline{\underline{v}}_{\mathbf{k}}\left(\underline{\underline{E}}_{\mathbf{k}}+\varepsilon_{\mathbf{k}}\right) = -\underline{\underline{\Delta}}^{\dagger}_{\mathbf{k}}\underline{\underline{u}}_{\mathbf{k}}, \tag{6.4.17}$$

where,

$$E_{\sigma}(\mathbf{k})=\sqrt{\varepsilon_{\mathbf{k}}^{2}+|\mathbf{d}(\mathbf{k})|^{2}+\sigma|\mathbf{q}(\mathbf{k})|}. \tag{6.4.18}$$

Eliminating $\underline{\underline{v}}_{\mathbf{k}}$ from equations 6.4.16 and 6.4.17 we find that

$$\underline{\underline{u}}_{\mathbf{k}}\left(\underline{\underline{E}}_{\mathbf{k}}^{2}-\varepsilon_{\mathbf{k}}^{2}\right)=\underline{\underline{\Delta}}_{\mathbf{k}}\underline{\underline{\Delta}}^{\dagger}_{\mathbf{k}}\underline{\underline{u}}_{\mathbf{k}}. \tag{6.4.19}$$

But, from (6.4.18)

$$\underline{\underline{E}}_{\mathbf{k}}^{2}-\varepsilon_{\mathbf{k}}^{2}=\underline{\underline{\sigma_{0}}}|\mathbf{d}(\mathbf{k})|^{2}+\underline{\underline{\sigma_{z}}}|\mathbf{q}(\mathbf{k})| \tag{6.4.20}$$

and from (6.4.12) we find that

$$\underline{\underline{u}}_{\mathbf{k}}|\mathbf{q}(\mathbf{k})|\,\underline{\underline{\sigma_{z}}}=\underline{\underline{\sigma}}\cdot\mathbf{q}(\mathbf{k})\underline{\underline{u}}_{\mathbf{k}}. \tag{6.4.21}$$

Sigrist and Ueda solved this via the ansatz

$$\underline{\underline{u}}_{\mathbf{k}}=a\left(|\mathbf{q}(\mathbf{k})|\,\underline{\underline{\sigma_{z}}}+\underline{\underline{\sigma}}\cdot\mathbf{q}(\mathbf{k})\right)\left(\underline{\underline{\sigma_{0}}}+\underline{\underline{\sigma_{z}}}\right)+b\left(|\mathbf{q}(\mathbf{k})|\,\underline{\underline{\sigma_{z}}}-\underline{\underline{\sigma}}\cdot\mathbf{q}(\mathbf{k})\right)\left(\underline{\underline{\sigma_{0}}}-\underline{\underline{\sigma_{z}}}\right). \tag{6.4.22}$$

a and b can be chosen to be real without loss of generality.

From (6.4.17) we have

$$\underline{\underline{v}}_{\mathbf{k}}=\underline{\underline{\Delta}}_{\mathbf{k}}\underline{\underline{u}}_{\mathbf{k}}\left[\underline{\underline{E}}_{\mathbf{k}}-\varepsilon_{\mathbf{k}}\right]\left[\underline{\underline{E}}_{\mathbf{k}}^{2}-\varepsilon_{\mathbf{k}}^{2}\right]^{-1}. \tag{6.4.23}$$

The completeness relation (equation 4.3.14) can be rewritten,

$$\underline{\underline{u}}_{\mathbf{k}}\underline{\underline{u}}^{\dagger}_{\mathbf{k}}+\underline{\underline{v}}^{*}_{\mathbf{k}}\underline{\underline{v}}^{T}_{\mathbf{k}}=\underline{\underline{I}}. \tag{6.4.24}$$

Some rather tedious algebra leads to the simultaneous equations,

$$4|\mathbf{q}(\mathbf{k})|\left(|\mathbf{q}(\mathbf{k})|+\mathbf{q}_{z}(\mathbf{k})\right)\left(a^{2}\frac{2E_{\mathbf{k}\uparrow}}{E_{\mathbf{k}\uparrow}+\varepsilon_{\mathbf{k}}}+b^{2}\frac{2E_{\mathbf{k}\downarrow}}{E_{\mathbf{k}\downarrow}+\varepsilon_{\mathbf{k}}}\right)=1 \tag{6.4.25}$$

and

$$a^2 \frac{2E_{\mathbf{k}\uparrow}}{E_{\mathbf{k}\uparrow}+\varepsilon_{\mathbf{k}}} = b^2 \frac{2E_{\mathbf{k}\downarrow}}{E_{\mathbf{k}\downarrow}+\varepsilon_{\mathbf{k}}}, \tag{6.4.26}$$

which have the solutions

$$a^2 = \frac{E_{\mathbf{k}\uparrow}+\varepsilon_{\mathbf{k}}}{16E_{\mathbf{k}\uparrow}|\mathbf{q}(\mathbf{k})|\left(|\mathbf{q}(\mathbf{k})|+\mathbf{q}_z(\mathbf{k})\right)}, \tag{6.4.27}$$

$$b^2 = \frac{E_{\mathbf{k}\downarrow}+\varepsilon_{\mathbf{k}}}{16E_{\mathbf{k}\downarrow}|\mathbf{q}(\mathbf{k})|\left(|\mathbf{q}(\mathbf{k})|+\mathbf{q}_z(\mathbf{k})\right)}. \tag{6.4.28}$$

Hence the Bogoliubov transformation matrices for a non-unitary gap are

$$\underline{\underline{u}}_{\mathbf{k}} = \frac{1}{\sqrt{16|\mathbf{q}(\mathbf{k})|\left(|\mathbf{q}(\mathbf{k})|+\mathbf{q}_z(\mathbf{k})\right)}}\left[\sqrt{\frac{E_{\mathbf{k}\uparrow}+\varepsilon_{\mathbf{k}}}{E_{\mathbf{k}\uparrow}}}\left(|\mathbf{q}(\mathbf{k})|\,\underline{\underline{\sigma_0}}+\mathbf{q}(\mathbf{k})\cdot\underline{\underline{\sigma}}\right)\left(\underline{\underline{\sigma_0}}+\underline{\underline{\sigma_z}}\right)\right.$$
$$\left.+\sqrt{\frac{E_{\mathbf{k}\downarrow}\varepsilon_{\mathbf{k}}}{E_{\mathbf{k}\downarrow}}}\left(|\mathbf{q}(\mathbf{k})|\,\underline{\underline{\sigma_0}}-\mathbf{q}(\mathbf{k})\cdot\underline{\underline{\sigma}}\right)\left(\underline{\underline{\sigma_0}}-\underline{\underline{\sigma_z}}\right)\right], \tag{6.4.29}$$

$$\underline{\underline{v}}_{\mathbf{k}} = \frac{1}{\sqrt{16|\mathbf{q}(\mathbf{k})|\left(|\mathbf{q}(\mathbf{k})|+\mathbf{q}_z(\mathbf{k})\right)}}\left[\frac{\left(|\mathbf{q}(\mathbf{k})|\mathbf{d}(\mathbf{k})-\mathtt{i}\left(\mathbf{d}(\mathbf{k})\times\mathbf{q}(\mathbf{k})\right)\right)\cdot\underline{\underline{\sigma}}\sigma_y\left(\underline{\underline{\sigma_0}}+\underline{\underline{\sigma_z}}\right)}{\sqrt{E_{\mathbf{k}\uparrow}\left(E_{\mathbf{k}\uparrow}+\varepsilon_{\mathbf{k}}\right)}}\right.$$
$$\left.+\frac{\left(|\mathbf{q}(\mathbf{k})|\mathbf{d}(\mathbf{k})+\mathtt{i}\left(\mathbf{d}(\mathbf{k})\times\mathbf{q}(\mathbf{k})\right)\right)\cdot\underline{\underline{\sigma}}\sigma_y\left(\underline{\underline{\sigma_0}}+\underline{\underline{\sigma_z}}\right)}{\sqrt{E_{\mathbf{k}\uparrow}\left(E_{\mathbf{k}\uparrow}-\varepsilon_{\mathbf{k}}\right)}}\right], \tag{6.4.30}$$

and thus the gap equations for non-unitary states are

$$\Delta_{\alpha\beta}(\mathbf{k}) = \sum_{\mathbf{k}'} U_{\alpha\beta}(\mathbf{k}-\mathbf{k}')\left[\frac{1}{4E_{\mathbf{k}\uparrow}}\left(\mathbf{d}(\mathbf{k})+\mathtt{i}\frac{\mathbf{q}(\mathbf{k})\times\mathbf{d}(\mathbf{k})}{|\mathbf{q}(\mathbf{k})|}\tanh\left(\frac{\beta E_{\mathbf{k}\uparrow}}{2}\right)\right)\right.$$
$$\left.\frac{1}{4E_{\mathbf{k}\downarrow}}\left(\mathbf{d}(\mathbf{k})-\mathtt{i}\frac{\mathbf{q}(\mathbf{k})\times\mathbf{d}(\mathbf{k})}{|\mathbf{q}(\mathbf{k})|}\tanh\left(\frac{\beta E_{\mathbf{k}\downarrow}}{2}\right)\right)\right]. \tag{6.4.31}$$

6.4.3 The gap equations for a non-unitary state in the presence of exchange splitting

We now give two derivations of the gap equations for ESP states in the presence of exchanging splitting. The first derivation is a generalisation of the approach used above for the gap equations in the absence of exchange splitting. Unfortunately we find that this approach is not tractable in the presence of exchange splitting, but in closing one avenue, this derivation

opens another by naturally motivating the study of ESP states (particularly in light of the numerical results presented in the previous chapter and the Ginzburg–Landau theory presented in section 6.3). The second derivation begins by making several assumptions, which we will see are equivalent to those motivated by the first approach. This derivation is much more straightforward and gives a much clearer understanding of why the gap equations have the rather familiar form that we will discover. We recommend that the reader who only wishes to read one derivation follows the second.

Derivation via an ansatz

The simplest way to proceed is to *define* our coordinate system so that $\mathbf{E}_{ex} = \big(0, 0, -E_{ex}\big)$ direction. This means that to perform practical calculations we will have to rotate the crystal 'by hand' but this is a price well worth paying as it gives us

$$\underline{\underline{\varepsilon}}_{\mathbf{k}} = \underline{\underline{\varepsilon}}^{*}_{\mathbf{k}} = \begin{pmatrix} \varepsilon_{\mathbf{k}} - E_{ex} & 0 \\ 0 & \varepsilon_{\mathbf{k}} + E_{ex} \end{pmatrix}. \tag{6.4.32}$$

We can now write the BdG equations as

$$\underline{u}_{\mathbf{k}}\Big(\underline{\underline{E}}_{\mathbf{k}} - \underline{\underline{\varepsilon}}_{\mathbf{k}}\Big) = -\underline{\underline{\Delta}}_{\mathbf{k}}\underline{v}_{\mathbf{k}}, \tag{6.4.33}$$

$$\underline{v}_{\mathbf{k}}\Big(\underline{\underline{E}}_{\mathbf{k}} + \underline{\underline{\varepsilon}}_{\mathbf{k}}\Big) = -\underline{\underline{\Delta}}^{\dagger}_{\mathbf{k}}\underline{u}_{\mathbf{k}}. \tag{6.4.34}$$

Where we have used the fact that we are *only* dealing with the triplet case to note that $\underline{\underline{\Delta}}^{\dagger}_{\mathbf{k}} = -\underline{\underline{\Delta}}^{*}_{-\mathbf{k}}$. Eliminating $\underline{v}_{\mathbf{k}}$ gives

$$\underline{u}_{\mathbf{k}}\Big(\underline{\underline{E}}^{2}_{\mathbf{k}} - \underline{\underline{\varepsilon}}^{2}_{\mathbf{k}}\Big) = \underline{\underline{\Delta}}_{\mathbf{k}}\underline{\underline{\Delta}}^{\dagger}_{\mathbf{k}}\underline{u}_{\mathbf{k}} \tag{6.4.35}$$

Recall that in the presence of exchange splitting the spectrum of a triplet superconductor is given by

$$E_{\sigma}(\mathbf{k}) = \sqrt{\varepsilon^{2}_{\mathbf{k}} + |\mathbf{E}_{ex}|^{2} + |\mathbf{d}(\mathbf{k})|^{2} + \sigma\sqrt{\Lambda(\mathbf{k})}} \tag{6.4.36}$$

where

$$\Lambda(\mathbf{k}) = |\mathbf{q}(\mathbf{k})|^{2} + 4\varepsilon^{2}_{\mathbf{k}}|\mathbf{E}_{ex}|^{2} + 4|\mathbf{E}_{ex}\cdot\mathbf{d}(\mathbf{k})|^{2} - 4\varepsilon_{\mathbf{k}}\mathbf{E}_{ex}\cdot\mathbf{q}(\mathbf{k}). \tag{6.4.37}$$

Hence,

$$\underline{\underline{E}}^2_{\mathbf{k}} = \Big(\varepsilon^2_{\mathbf{k}} + E^2_{ex} + |\mathbf{d}(\mathbf{k})|^2\Big)\underline{\underline{\sigma}}_0 + \sqrt{\Lambda(\mathbf{k})}\underline{\underline{\sigma}}_3. \tag{6.4.38}$$

But,

$$\underline{\underline{\varepsilon}}^2_{\mathbf{k}} = \big(\varepsilon^2_{\mathbf{k}} + E^2_{ex}\big)\underline{\underline{\sigma}}_0 - 2\varepsilon_{\mathbf{k}} E_{ex}\underline{\underline{\sigma}}_3. \tag{6.4.39}$$

Equation 6.4.35 then becomes

$$\underline{\underline{u}}_{\mathbf{k}}\big(\sqrt{\Lambda(\mathbf{k})} + 2\varepsilon_{\mathbf{k}} E_{ex}\big)\underline{\underline{\sigma}}_3 = \mathbf{q}(\mathbf{k}) \cdot \underline{\underline{\sigma}}\ \underline{\underline{u}}_{\mathbf{k}} \tag{6.4.40}$$

This general case has thus far proved intractable. However, given the above Ginzburg–Landau analysis, the results of chapter 5 - which indicate that an ESP pairing state is the ground state of this model in two dimensions and that ESP phases (namely the A, A_1 and A_2 phases) are observed in bulk and, importantly, in three dimensions in ^{3}He we will now study the gap equations assuming that we have ESP states. Mathematically this is equivalent to the assumption that $\mathbf{d}(\mathbf{k}) \cdot \mathbf{E}_{ex} = 0$. Further this assumption is entirely pragmatic for this work as the state that we will propose below for $ZrZn_2$ is an ESP state and given that we do not know (despite some considerable effort) how to derive gap equations for non-unitary pairing in all spin states in the presence of exchange splitting. Further we have found that the numerical solution of the spin-generalised BdG equations takes an extremely long time (in the order of a month on a serial processor) to converge (for a single point in phase $(\mathbf{H}, T)$ space). (However, for the few points in phase space for which we have found the self-consistent solution we do find an ESP state and furthermore the same ESP we report below on the basis of the ESP gap equations.)

What follows, it must be stressed, is only valid for states in which $\mathbf{E}_{xc} \cdot \mathbf{d}(\mathbf{k}) = 0$, that is ESP states, therefore we cannot guarantee that we will find the ground state of the Hamiltonian.

If $\mathbf{d}(\mathbf{k})$ is perpendicular to $\mathbf{E}_{ex}$ (i.e. if $\mathbf{d}(\mathbf{k}) \cdot \mathbf{E}_{ex} = 0$ or equivalently for our choice of $\mathbf{E}_{ex}$ if $d_3(\mathbf{k}) = 0$) then

$$\mathbf{q}(\mathbf{k}) = \big(0, 0, q(\mathbf{k})\big) \tag{6.4.41}$$

and

$$\Lambda(\mathbf{k}) = \big(q(\mathbf{k}) - 2\varepsilon_{\mathbf{k}} E_{ex}\big)^2. \tag{6.4.42}$$

Hence

$$\big(\sqrt{\Lambda(\mathbf{k})} + 2\varepsilon_{\mathbf{k}} E_{ex}\big) = q(\mathbf{k}) \tag{6.4.43}$$

and

$$\underline{\underline{u}}_{\mathbf{k}} |\mathbf{q}(\mathbf{k})| \underline{\underline{\sigma}}_3 \quad = \mathbf{q}(\mathbf{k}) \cdot \underline{\underline{\sigma}}\ \underline{\underline{u}}_{\mathbf{k}} \tag{6.4.44}$$

This is solved by to Sigrist and Ueda's ansatz (equation 6.4.22). In our special case we have

$$\underline{\underline{u}}_{\mathbf{k}} = 4q(\mathbf{k}) \begin{pmatrix} a & 0 \\ 0 & b \end{pmatrix}, \tag{6.4.45}$$

and

$$\underline{\underline{v}}^*_{-\mathbf{k}} = \underline{\underline{\Delta}}_{\mathbf{k}} \underline{\underline{u}}^\dagger_{\mathbf{k}} \Big(\underline{\underline{E}}_{\mathbf{k}} - \underline{\underline{\varepsilon}}_{\mathbf{k}}\Big) \Big(\underline{\underline{E}}^2_{\mathbf{k}} - \underline{\underline{\varepsilon}}^2_{\mathbf{k}}\Big)^{-1}. \tag{6.4.46}$$

But, as $\underline{\underline{E}}_{\mathbf{k}}$ and $\underline{\underline{\varepsilon}}_{\mathbf{k}}$ are diagonal and real we have

$$\underline{\underline{v}}^T_{-\mathbf{k}} \quad = \quad \Big(\underline{\underline{E}}^2_{\mathbf{k}} - \underline{\underline{\varepsilon}}^2_{\mathbf{k}}\Big)^{-1} \Big(\underline{\underline{E}}_{\mathbf{k}} - \underline{\underline{\varepsilon}}_{\mathbf{k}}\Big) \underline{\underline{u}}_{\mathbf{k}} \underline{\underline{\Delta}}^\dagger_{\mathbf{k}} \tag{6.4.47}$$

Therefore

$$\underline{\underline{v}}^*_{-\mathbf{k}} \underline{\underline{v}}^T_{-\mathbf{k}} \quad = \quad \underline{\underline{\Delta}}_{\mathbf{k}} \underline{\underline{u}}^*_{\mathbf{k}} \Big(\underline{\underline{E}}_{\mathbf{k}} - \underline{\underline{\varepsilon}}_{\mathbf{k}}\Big) \Big(\underline{\underline{E}}^2_{\mathbf{k}} - \underline{\underline{\varepsilon}}^2_{\mathbf{k}}\Big)^{-2} \Big(\underline{\underline{E}}_{\mathbf{k}} - \underline{\underline{\varepsilon}}_{\mathbf{k}}\Big) \underline{\underline{u}}_{\mathbf{k}} \underline{\underline{\Delta}}^\dagger_{\mathbf{k}} \tag{6.4.48}$$

Using the fact that $d_3(\mathbf{k}) = 0$ and hence $\underline{\underline{\Delta}}_{\mathbf{k}}$ is diagonal we arrive at

$$\begin{aligned}
&\underline{\underline{u}}_{-\mathbf{k}}\underline{\underline{u}}^{\dagger}_{-\mathbf{k}} + \underline{\underline{v}}^{*}_{-\mathbf{k}}\underline{\underline{v}}^{T}_{-\mathbf{k}} \\
&\quad = 16q^2(\mathbf{k}) \begin{pmatrix} |a|^2\left(1+\frac{E_\uparrow(\mathbf{k})-\left(\varepsilon(\mathbf{k})-E_{ex}\right)}{E_\uparrow(\mathbf{k})+\left(\varepsilon(\mathbf{k})-E_{ex}\right)}\right) & 0 \\ 0 & |b|^2\left(1+\frac{E_\downarrow(\mathbf{k})-\left(\varepsilon(\mathbf{k}+E_{ex}\right)}{E_\downarrow(\mathbf{k})+\left(\varepsilon(\mathbf{k})+E_{ex}\right)}\right) \end{pmatrix} \qquad (6.4.49) \\
&\quad = \begin{pmatrix} 1 & 0 \\ 0 & 1 \end{pmatrix}, \qquad (6.4.50)
\end{aligned}$$

which is required to ensure that the Bogoliubov–Valatin transformation is unitary. Summing the diagonals gives

$$16q^2(\mathbf{k})\left(|a|^2\left(1+\frac{E_\uparrow(\mathbf{k})-\left(\varepsilon(\mathbf{k})-E_{ex}\right)}{E_\uparrow(\mathbf{k})+\left(\varepsilon(\mathbf{k})-E_{ex}\right)}\right)+|b|^2\left(1+\frac{E_\downarrow(\mathbf{k})-\left(\varepsilon(\mathbf{k}+E_{ex}\right)}{E_\downarrow(\mathbf{k})+\left(\varepsilon(\mathbf{k})+E_{ex}\right)}\right)\right)=2. \qquad (6.4.51)$$

But subtracting the diagonals gives

$$|a|^2\left(1+\frac{E_\uparrow(\mathbf{k})-\left(\varepsilon(\mathbf{k})-E_{ex}\right)}{E_\uparrow(\mathbf{k})+\left(\varepsilon(\mathbf{k})-E_{ex}\right)}\right)-|b|^2\left(1+\frac{E_\downarrow(\mathbf{k})-\left(\varepsilon(\mathbf{k}+E_{ex}\right)}{E_\downarrow(\mathbf{k})+\left(\varepsilon(\mathbf{k})+E_{ex}\right)}\right)=0. \qquad (6.4.52)$$

Solving these simultaneously we find that

$$\begin{aligned}
|a|^2 &= \frac{E_\uparrow(\mathbf{k})+\left(\varepsilon(\mathbf{k})-E_{ex}\right)}{32q(\mathbf{k})^2E_\uparrow(\mathbf{k})}, \qquad (6.4.53) \\
|b|^2 &= \frac{E_\downarrow(\mathbf{k})+\left(\varepsilon(\mathbf{k})+E_{ex}\right)}{32q(\mathbf{k})^2E_\downarrow(\mathbf{k})}. \qquad (6.4.54)
\end{aligned}$$

Therefore we have

$$\begin{aligned}
\underline{\underline{u}}_{\mathbf{k}} &= \begin{pmatrix} \sqrt{\frac{E_\uparrow(\mathbf{k})+\left(\varepsilon(\mathbf{k})-E_{ex}\right)}{2E_\uparrow(\mathbf{k})}} & 0 \\ 0 & \sqrt{\frac{E_\downarrow(\mathbf{k})+\left(\varepsilon(\mathbf{k})+E_{ex}\right)}{2E_\downarrow(\mathbf{k})}} \end{pmatrix} \qquad (6.4.55) \\
\underline{\underline{v}}^{*}_{-\mathbf{k}} &= \underline{\underline{\Delta}}_{\mathbf{k}} \begin{pmatrix} \frac{1}{\sqrt{2E_\uparrow(\mathbf{k}\left(E_\uparrow(\mathbf{k})+\left(\varepsilon(\mathbf{k})-E_{ex}\right)\right)}} & 0 \\ 0 & \frac{1}{\sqrt{2E_\downarrow(\mathbf{k})\left(E_\downarrow(\mathbf{k})+\left(\varepsilon(\mathbf{k})+E_{ex}\right)\right)}} \end{pmatrix}. \qquad (6.4.56)
\end{aligned}$$

Or in perhaps their simplest form;

$$u_{\sigma\sigma}(\mathbf{k}) = \sqrt{\frac{E_\sigma(\mathbf{k}) + \big(\varepsilon(\mathbf{k}) - \sigma E_{ex}\big)}{2E_\sigma(\mathbf{k})}} \tag{6.4.57}$$

$$v^*_{\sigma\sigma}(\mathbf{k}) = \frac{-\Delta_{\sigma\sigma}(\mathbf{k})}{\sqrt{2E_\sigma(\mathbf{k})\big(E_\sigma(\mathbf{k}) + \big(\varepsilon(\mathbf{k}) - \sigma E_{ex}\big)\big)}} \tag{6.4.58}$$

$$u_{\sigma\sigma}(\mathbf{k}) = v^*_{\sigma\sigma}(\mathbf{k}) = 0. \tag{6.4.59}$$

We can rewrite the self consistency equations (4.3.30) as

$$\Delta_{\alpha\alpha}(\mathbf{k}) = \sum_{\mathbf{k}'\sigma} U_{\alpha\alpha}(\mathbf{k}-\mathbf{k}')u_{\alpha\sigma}(\mathbf{k}')v^*_{\alpha\sigma}(\mathbf{k}')(1-2f_{E_{\mathbf{k}'\sigma}}) \tag{6.4.60}$$

and

$$\Delta_{\alpha\beta}(\mathbf{k}) = -\frac{1}{2}\sum_{\mathbf{k}'\sigma} U_{\alpha\beta}(\mathbf{k}-\mathbf{k}')\Big(u_{\alpha\sigma}(-\mathbf{k}')v^*_{\beta\sigma}(-\mathbf{k}') - v^*_{\alpha\sigma}(\mathbf{k}')u_{\beta\sigma}(\mathbf{k}')\Big)(1-2f_{E_{\mathbf{k}'\sigma}}) \tag{6.4.61}$$

where $\alpha \neq \beta$. We now arrive at the gap equations,

$$\boxed{\Delta_{\alpha\alpha}(\mathbf{k}) = -\sum_{\mathbf{k}'} \frac{U_{\alpha\alpha}(\mathbf{k}-\mathbf{k}')\Delta_{\alpha\alpha}(\mathbf{k}')}{2E_\alpha(\mathbf{k}')}(1-2f_{E_{\mathbf{k}'\alpha}})} \tag{6.4.62}$$

and

$$\Delta_{\alpha\beta}(\mathbf{k}) = 0. \tag{6.4.63}$$

It would of course be highly desirable to find a solution to equation 6.4.40 for $\mathbf{E}_{xc}\cdot\mathbf{d}(\mathbf{k}) \neq 0$, and this approach appears, at the present time to be the most likely way to derive such general gap equations. The most notable non-unitary state for which $\mathbf{E}_{xc}\cdot\mathbf{d}(\mathbf{k}) \neq 0$ is the B_2 phase.

It is particularly important to be able to write down the gap equations for non-unitary states in the presence of exchange splitting as, to date, non-unitary states have only been observed in the presence of exchange splitting. Indeed it can be argued that it is the exchange splitting which drives the formation of non-unitary states.

Derivation via a more direct route

Given that we were forced to derive a formalism valid for ESP states only above it is worth repeating the derivation in a rather more straightforward manner below as deeper insight can be gathered due to the greater simplicity of the derivation.

As we are now aware of the limitations we are prepared to accept in out theory we can study from the very begin the special case of $\mathbf{E}_{xc} \cdot \mathbf{d}(\mathbf{k}) = 0$. In this case, for $\mathbf{E}_{xc} = \big(0, 0, -E_{xc}\big)$, the spin triplet BdG equations are

$$\begin{pmatrix} \varepsilon_{\mathbf{k}} - E_{xc} & 0 & \Delta_{\uparrow\uparrow}(\mathbf{k}) & 0 \\ 0 & \varepsilon_{\mathbf{k}} + E_{xc} & 0 & \Delta_{\downarrow\downarrow}(\mathbf{k}) \\ -\Delta^*_{\uparrow\uparrow}(-\mathbf{k}) & 0 & -\varepsilon_{-\mathbf{k}} + E_{xc} & 0 \\ 0 & -\Delta^*_{\downarrow\downarrow}(-\mathbf{k}) & 0 & -\varepsilon_{-\mathbf{k}} - E_{xc} \end{pmatrix} \begin{pmatrix} u_{\uparrow\sigma}(\mathbf{k}) \\ u_{\downarrow\sigma}(\mathbf{k}) \\ v_{\uparrow\sigma}(\mathbf{k}) \\ v_{\downarrow\sigma}(\mathbf{k}) \end{pmatrix} = E_\sigma(\mathbf{k}) \begin{pmatrix} u_{\uparrow\sigma}(\mathbf{k}) \\ u_{\downarrow\sigma}(\mathbf{k}) \\ v_{\uparrow\sigma}(\mathbf{k}) \\ v_{\downarrow\sigma}(\mathbf{k}) \end{pmatrix}. \quad (6.4.64)$$

We can now easily separate the BdG equations into a pair of BdG equations for up electrons,

$$\begin{pmatrix} \varepsilon_{\mathbf{k}} - E_{xc} & \Delta_{\uparrow\uparrow}(\mathbf{k}) \\ -\Delta^*_{\uparrow\uparrow}(-\mathbf{k}) & -\varepsilon_{-\mathbf{k}} + E_{xc} \end{pmatrix} \begin{pmatrix} u_{\uparrow\sigma}(\mathbf{k}) \\ v_{\uparrow\sigma}(\mathbf{k}) \end{pmatrix} = E_\sigma(\mathbf{k}) \begin{pmatrix} u_{\uparrow\sigma}(\mathbf{k}) \\ v_{\uparrow\sigma}(\mathbf{k}) \end{pmatrix}. \quad (6.4.65)$$

and a set of BdG equations for down electrons,

$$\begin{pmatrix} \varepsilon_{\mathbf{k}} + E_{xc} & \Delta_{\downarrow\downarrow}(\mathbf{k}) \\ -\Delta^*_{\downarrow\downarrow}(-\mathbf{k}) & -\varepsilon_{-\mathbf{k}} - E_{xc} \end{pmatrix} \begin{pmatrix} u_{\downarrow\sigma}(\mathbf{k}) \\ v_{\downarrow\sigma}(\mathbf{k}) \end{pmatrix} = E_\sigma(\mathbf{k}) \begin{pmatrix} u_{\downarrow\sigma}(\mathbf{k}) \\ v_{\downarrow\sigma}(\mathbf{k}) \end{pmatrix}. \quad (6.4.66)$$

Using the self-consistency condition (6.4.60) we quickly find that the gap equations are

$$\boxed{\Delta_{\sigma\sigma}(\mathbf{k}) = -\sum_{\mathbf{k}'} \frac{U_{\sigma\sigma}(\mathbf{k}-\mathbf{k}')\Delta_{\sigma\sigma}(\mathbf{k}')}{2E_\sigma(\mathbf{k}')}(1 - 2f_{E_{\mathbf{k}'\sigma}}).} \quad (6.4.67)$$

with

$$E_{\mathbf{k}\sigma} = \sqrt{(\varepsilon_{\mathbf{k}} - \sigma E_{xc})^2 + |\Delta_{\sigma\sigma}(\mathbf{k})|^2} \tag{6.4.68}$$

It is now clear that in the presence of exchange splitting if there is no opposite spin pairing (i.e. if $\mathbf{d}_0(\mathbf{k}) = \mathbf{d}_3(\mathbf{k}) = 0$) then the two spin states are entirely separate systems. This means that the two gap equations can be solved independently *even in their linearised form!* This is particularly surprising as we, in general, do not expect the two gap equations to have the same transition temperature. This means that we will be able to use the linearised gap equations to accurately calculate the transition temperature of a second superconducting transition (e.g. between the A_1 and A_2 phases.)

6.4.4 Confirmation that the two formalisms are equivalent in the special case of equal spin pairing and no exchange splitting

As we now have two independently derived sets of gap equations (equation 6.4.31 and equations 6.4.62 and 6.4.63) which should be identical for ESP in the limit of $E_{xc} \to 0$, we can use this to check that both sets of gap equations are correct.

Clearly, for $E_{xc} = 0$ the mathematical form of equation 6.4.62 is unchanged but the spectrum of elementary excitations becomes

$$E_{\mathbf{k}\sigma} = \sqrt{\varepsilon_{\mathbf{k}}^2 + |\Delta_{\sigma\sigma}(\mathbf{k})|^2} \tag{6.4.69}$$

Rewriting equation 6.4.31 in this form is slightly more tricky. It is important to keep in mind that by considering ESP states only we are not insisting that $\mathbf{q}(\mathbf{k}) = 0$ for that would be equivalent to considering only unitary states.

However, we note that for ESP states

$$\mathbf{d}(\mathbf{k}) = \big(d_x, d_y, 0\big). \tag{6.4.70}$$

Therefore

$$\mathbf{q}(\mathbf{k}) = \mathtt{i}\big(0, 0, d_x d_y^* - d_y d_x^*\big) = \big(0, 0, q_z\big). \tag{6.4.71}$$

Which gives

$$\left(\mathbf{d}(\mathbf{k}) + \frac{\mathbf{d}(\mathbf{k}) \times \mathbf{q}(\mathbf{k})}{|\mathbf{q}(\mathbf{k})|}\right) \cdot \mathtt{i}\underline{\underline{\sigma}}\,\underline{\underline{\sigma}}_y = 2\begin{pmatrix} -d_x(\mathbf{k}) + \mathtt{i}d_y(\mathbf{k}) & 0 \\ 0 & 0 \end{pmatrix} \tag{6.4.72}$$

$$= 2\begin{pmatrix} \Delta_{\uparrow\uparrow}(\mathbf{k}) & 0 \\ 0 & 0 \end{pmatrix} \tag{6.4.73}$$

and

$$\left(\mathbf{d}(\mathbf{k}) - \frac{\mathbf{d}(\mathbf{k}) \times \mathbf{q}(\mathbf{k})}{|\mathbf{q}(\mathbf{k})|}\right) \cdot \mathtt{i}\underline{\underline{\sigma}}\,\underline{\underline{\sigma}}_y = 2\begin{pmatrix} 0 & 0 \\ 0 & d_x(\mathbf{k}) + \mathtt{i}d_y(\mathbf{k}) \end{pmatrix} \tag{6.4.74}$$

$$= 2\begin{pmatrix} 0 & 0 \\ 0 & \Delta_{\downarrow\downarrow}(\mathbf{k}) \end{pmatrix} \tag{6.4.75}$$

Substituting these identities into equation 6.4.31 gives

$$\underline{\underline{\Delta}}_{\mathbf{k}} = \sum_{\mathbf{k}'} \begin{pmatrix} \frac{\Delta_{\uparrow\uparrow}(\mathbf{k})}{2E_{\mathbf{k}\uparrow}}\left(1 - 2f_{E_{\mathbf{k}\uparrow}}\right) & 0 \\ 0 & \frac{\Delta_{\downarrow\downarrow}(\mathbf{k})}{2E_{\mathbf{k}\downarrow}}\left(1 - 2f_{E_{\mathbf{k}\downarrow}}\right) \end{pmatrix}. \tag{6.4.76}$$

Therefore the two formalisms agree in this, the only limit in which they should. This is, of course, confirmation of the numerical error in reference [193].

6.5 The linearised gap equation and calculation of the superconducting critical temperature of a ferromagnetic superconductor

As $T \to T_{SC}$ from below, $|\underline{\underline{\Delta}}_{\mathbf{k}}| \to 0$ and hence $E_\sigma(\mathbf{k}) \to \varepsilon(\mathbf{k}) + \sigma E_{xc}$. Therefore the gap equation becomes

$$\Delta_{\sigma\sigma}(\mathbf{k}) = \sum_{\mathbf{k}'} \frac{U_{\sigma\sigma}(\mathbf{k} - \mathbf{k}')}{2\big(\varepsilon(\mathbf{k}') - \sigma E_{xc}\big)} \tanh\left(\frac{\varepsilon(\mathbf{k}') - \sigma E_{xc}}{2k_B T}\right) \Delta_{\sigma\sigma}(\mathbf{k}'). \tag{6.5.1}$$

Thus, near T_{SC} the gap equation is linear. The eigenvalue problem is much easier solve numerically than the full gap equation which, like the full self-consistent solution of the BdG equations, converges rather slowly and is rather inaccurate near T_{SC}. If the eigenvalue is less than one then the full non-linear gap equation will converge to $\underline{\underline{\Delta}}_{\mathbf{k}} = \underline{\underline{0}}$. Hence, there is no

superconductivity in this channel. However, if the eigenvalue is greater than one then full non-linear gap equation will converge on a finite value of $\underline{\underline{\Delta}}_{\mathbf{k}}$ and hence there is superconductivity in the channel being considered. Therefore at T_{SC} the eigenvalue of the linearised gap equation in one. This allows T_{SC} to be determined very accurately. Further by comparing the transition temperatures of various symmetries one can find which has the highest transition temperature and hence which state occurs for $T \lesssim T_{SC}$.

Clearly, we cannot, in general, use the linearised gap equation to study transitions from one superconducting state to another as the gap equation can no longer be linearised below the first superconducting transition. The exception to this rule, as noted above, is the transition from an ESP state with only one type of pairing to an ESP state with both $\uparrow\uparrow$ and $\downarrow\downarrow$ pairing (an example of such a transition is the transition from the A_1 phase to the A_2 phase), because of the complete separation of the spin-up and spin-down subsystems in the presence of exchange splitting and the absence of opposite spin pairing or spin flip processes.

6.5.1 A tight binding fit to the LDA DOS

Before we can solve the linearised gap equations numerically we must first determine a band structure. *Ab initio* calculations have been performed by several groups, but using such detailed calculations would unnecessarily complicate matters and tie our results strongly to $ZrZn_2$, therefore we choose to use the tight binding approximation once again. However, we still require that our tight binding fit retains some of the important features of $ZrZn_2$.

The Fermi surface of $ZrZn_2$ [219] is far too complicated to be fit well by the tight binding approximation. However, it is well known [214, 70] that, in the weak coupling approximation the superconducting critical temperature is varies as

$$T_{SC} \sim \exp\left(-\frac{1}{UD(\varepsilon_F)}\right), \tag{6.5.2}$$

where $D(\varepsilon_F)$ is the density of states at the Fermi level. Therefore, as we are primarily interested in the variation of the superconducting critical temperature with exchange splitting, the important property of the material is the variation of the density of states with exchange splitting.

Giles Santi was kind enough to provide us with the results of his LDA band structure calculations [219]. We fitted a one band nearest neighbour tight binding model so that the relative DOS is correct over the range of exchange splitting found in the band structure calculations - which are in excellent agreement with de Haas-van Alphen experiments. The density of states

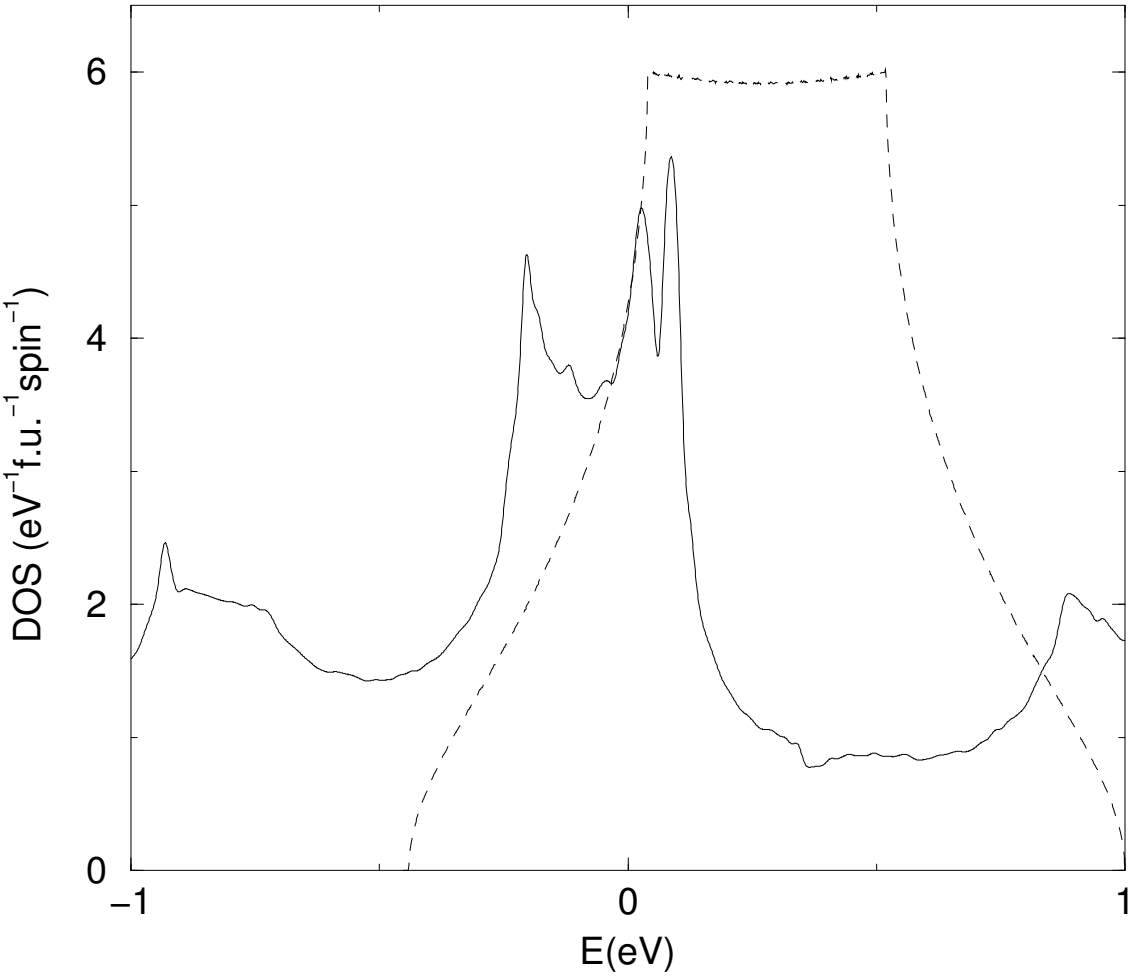

Figure 6.8: The density of states from the LDA calculations for $ZrZn_2$ (solid line) by Giles Santi and coworkers [219] and our tight binding fit to the LDA DOS (dashed line).

found in each calculation is shown in figures 6.8 with the relevant region of the DOS shown in detail in figure 6.9. The tight binding parameters of the our fit are given in table 6.1

6.5.2 The numerical solution of the linearised gap equations

We solved the linearised gap equations (6.5.1) numerically. To do this we used a k-space integration mesh of 10^9 points. We use such a large array for two reasons. A fine integration mesh is required to accurately the DOS. Our method (implicitly) requires an accurate calculation of the DOS. This is particularly important in our case as we are varying the exchange splitting and thus we are changing the DOS, so any errors in evaluating $D(\varepsilon)$ will lead to significant errors

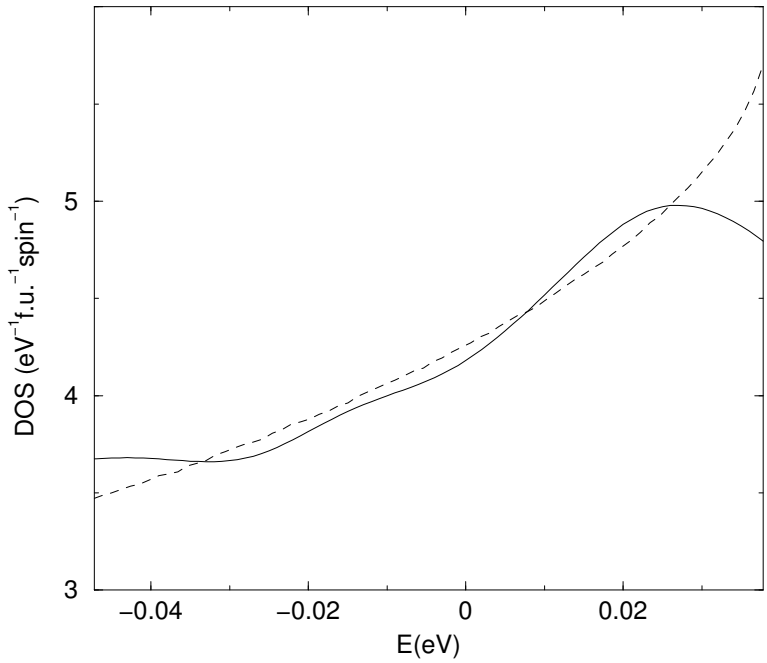

Figure 6.9: The density of states near the Fermi level from the LDA calculations for $ZrZn_2$ by Giles Santi and coworkers [219] (solid line) and our tight binding fit to the LDA DOS (dashed line).

t	0.12 eV
ε	$2.325t$
$E_{xc}^{\uparrow,max}$	$0.315t$
$E_{xc}^{\downarrow,max}$	$0.393t$

Table 6.1: Tight binding parameters fitted to the DOS found from LDA calculations for $ZrZn_2$.

in our calculation of the variation of T_{SC} with E_{xc}.

We show the results of our numerical calculations in figure 6.10. In these calculations we have used a simple cubic lattice. We have fitted our calculations by a cubic equation to account for numerical noise. The scale used on the x axis is not immediately obvious and so we will give a little explanation below. We have plotted the transition temperature for up, up pairing on the positive E_{xc} scale and the transition temperature for down, down paring on the negative E_{xc} scale. There are several good reasons for doing this.

(i) This is the behaviour of the up, up pairing state over a full range of exchange splitting as the majority (up) and minority (down) states are reversed under the transformation $E_{xc} \rightarrow -E_{xc}$.

(ii) By plotting our results in this fashion we see that the point $E_{xc} = 0$ in the transition temperature, exchange splitting curve is not a special case.

(iii) By using this choice of scale we have a larger range to fit over and thus increase the accuracy of the fit.

Zero exchange splitting is not a special point because in both the non-linear and linearised gap equations exchange splitting is mathematically equivalent to a chemical potential. Thus, by plotting the graph in figure 6.10 we have also found the critical temperature of the of the A phase as a function of the chemical potential in zero exchange splitting.

We now plot the critical temperature for both $|\uparrow\uparrow\rangle$ and $|\downarrow\downarrow\rangle$ pairing on the same graph (figure 6.11). This plot shows is then the (E_{xc}, T) superconducting phase diagram for our model in the absence of impurity scattering. (This, of course, assumes that no further phase transitions occur at low temperatures.) The higher transition temperature is the transition to the A_1 phase and the second transition is a transition to the A_2 phase. (Recall that we are able to calculate the lower transition temperature, even in the linearised approximation, because the exchange splitting makes the two spin states into separate subsystems.) In the paramagnetic state (the line $E_{xc} = 0$) the superconducting state is an A phase as the superconducting order parameter is the same for both the up, up and down, down pairing states. (Recall that the A_2 phase becomes the A phase via a cross over, rather than a phase transition - see section 3.9.6 for details.)

Note that the superconducting critical temperature for the majority spin state is higher than that of the minority spin state. This may seem rather intuitive but in fact this is fundamentally no more likely than minority state having the higher critical temperature. The fact that $\frac{\mathrm{d}D(E_{xc})}{\mathrm{d}E_{xc}}$ is positive for all E_{xc} leads to the higher superconducting critical temperature of the majority state (as increasing E_{xc} increases the DOS and hence increases T_{SC}). But the slope of $D(\varepsilon)$ is

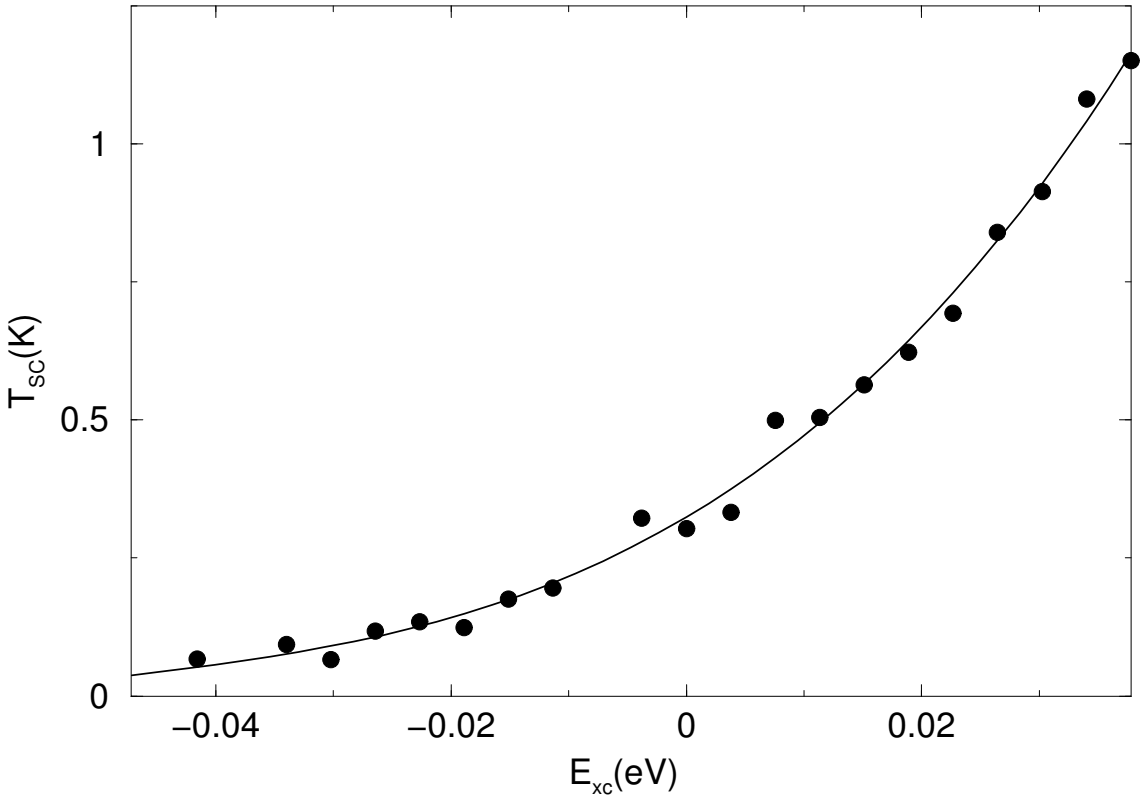

Figure 6.10: The results of our numerical solution of the linearised gap equations are shown by the points. The line is a fit to the calculated points by a cubic equation.

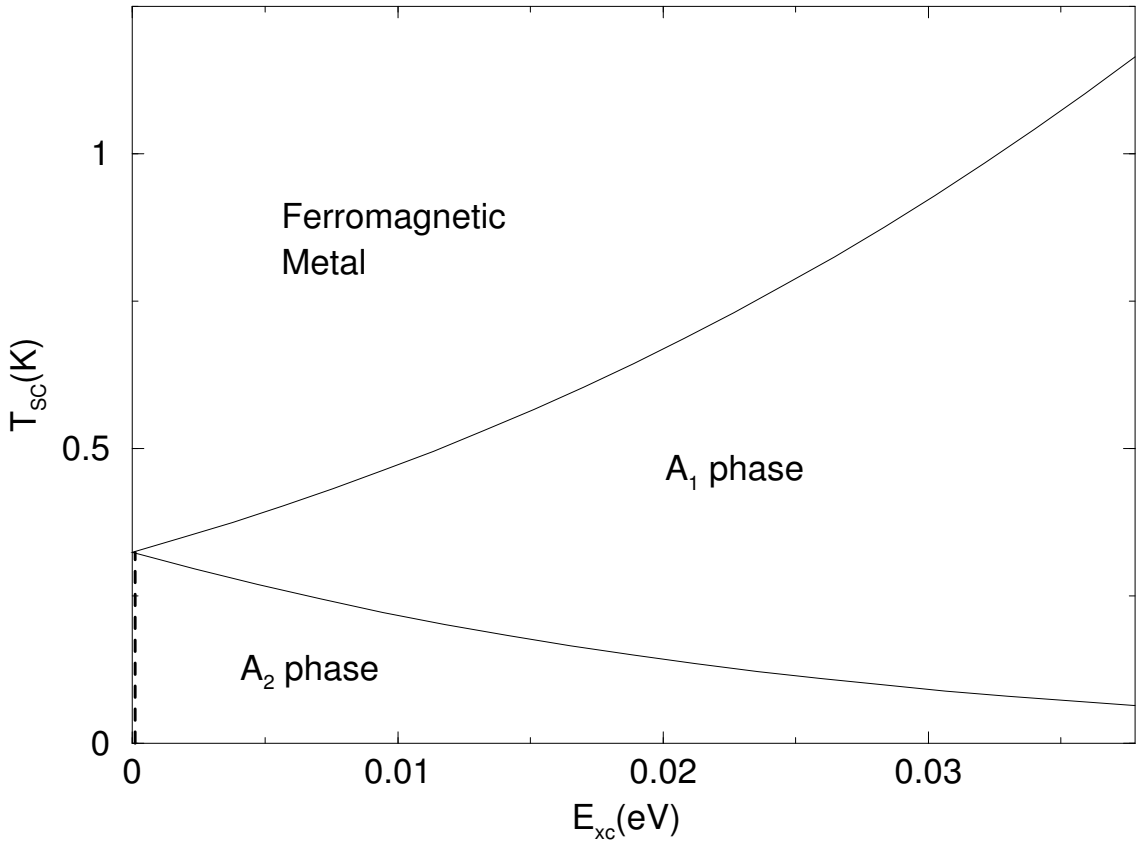

Figure 6.11: The phase diagram of our model. The critical temperature is shown for both A_1 and A_2 phases over a range of exchange splittings. The hatched area indictes the A phase, which is the ground state when $E_{xc} = 0$.

determined by our tight binding fit (figure 6.8). Thus if we were to change the chemical potential from $2.325t$ to, say, $-2.325t$ one would find that $\frac{\mathrm{d}D(E_{xc})}{\mathrm{d}E_{xc}} < 0$ for the same range of E_{xc} and hence that the minority spin state had the higher transition temperature. (In fact figure 6.13 would be rotated about the axis $E_{xc} = 0$ but figure 6.14 would look identical, but now the higher transition corresponds to down, down pairing, with the lower transition marking the onset of superconductivity in the majority spin state.

The phase diagram shown in figure 6.14 is clearly equivalent to the A_1-A_2 splitting of ^{3}He in a magnetic field. Experimental measurement of this phase transition in ^{3}He due to Remeijer *et al.* [175] are shown in figure 3.5. At first sight figures 6.14 and 3.5 look rather different, however the are in fact almost identical, as we will now show. The dimensionless measure of the exchange splitting for the Remijer *et al.* experiments is $\frac{\mu_n B}{k_B T_F}$, where T_F is the Fermi temperature, while for our calculation the dimensionless exchange splitting is given by $\frac{E_{xc}}{W}$. The experiments of Remijer *et al.* were not performed at constant pressure, which complicates the analysis somewhat, however they conclude that

$$\frac{T_{SC}^{A_1} - T_{SC}^{A_2}}{T_{SC}^{A}} = \widetilde{a}\left(\frac{\mu_n B}{k_B T_F}\right) + \widetilde{b}\left(\frac{\mu_n B}{k_B T_F}\right)^2 \tag{6.5.3}$$

where $\widetilde{a} = 36.3 \pm 0.91$ and $\widetilde{b} = 522 \pm 17$ in the range $0 \leq \frac{\mu_n B}{k_B T_F} \leq 0.01$ at an effective pressure of 3.4 MPa i.e the splitting is, to a very good approximation linear. The equivalent exchange splitting in our calculations is $E_{xc} = 0.01\, W = 0.01$ eV. It can clearly be seen from figure 6.14 that our calculations give an approximately linear splitting between the A_1 and A_2 phase transitions over the range of exchange splitting $0 \leq E_{xc} \leq 0.01$ eV. Hence our results are consistent with the what is known about ^{3}He. (Although, of course, we had no right to expect this agreement as our parameters where chosen for $ZrZn_2$ and not ^{3}He.) Further this illustrates the fact that ferromagnetic superconductors will provide an excellent laboratory in which to study the splitting of the A_1 and A_2 phase transitions (and the non-linear splitting in particular) over a far greater range of exchange splitting than is possible in ^{3}He.

6.6 Disorder, resistivity and the transition temperature

As we have seen in section 6.2, in terms of their superconducting properties, even the best, currently available, samples are not in the very clean limit. In the previous section we calculated the transition of the clean system for a variety of exchange splittings. Knowing the transition

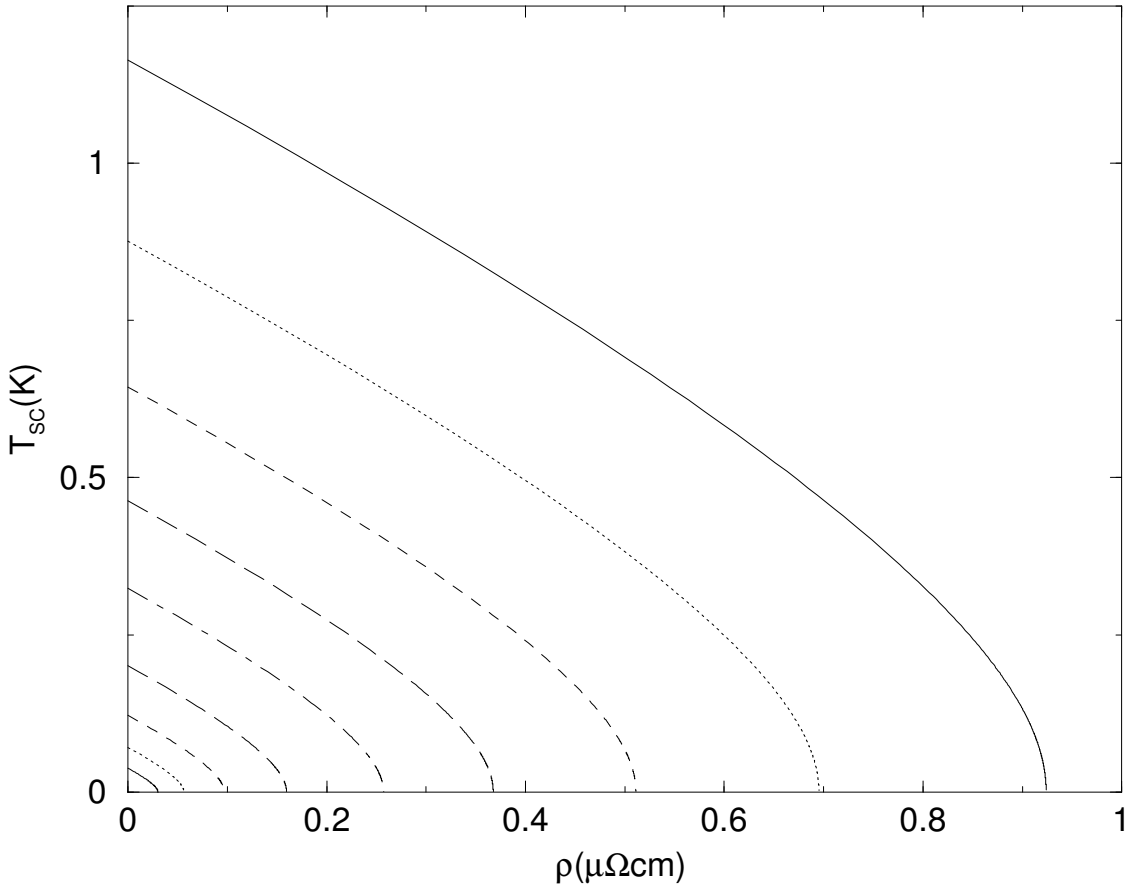

Figure 6.12: The superconducting critical temperature as a function of residual resistivity for a range of exchange splittings. The exchange splitting is, from the top down, 0.0378 eV, 0.02835 eV, 0.0189 eV, 0.0095 eV, -0.0188 eV, -0.0236 eV, -0.0354 eV, -0.0472 eV

temperature clean temperature we can calculate the transition temperature of the dirty systems from the Abrikosov–Gorkov formulism. We show the results of such calculations in figure 6.12.

In these calculations we assume that $\frac{m^*}{n}$ is independent of E_{xc} in the absence of experimental evidence to the contrary. The simplest way to plot these curves is to use $t = \frac{\hbar}{4\pi\tau_{tr}k_B T_{SC}}$ as a parametric variable. Hence, knowing $T_{SC0}(E_{xc})$, we calculate T_{SC} of t and thence ρ.

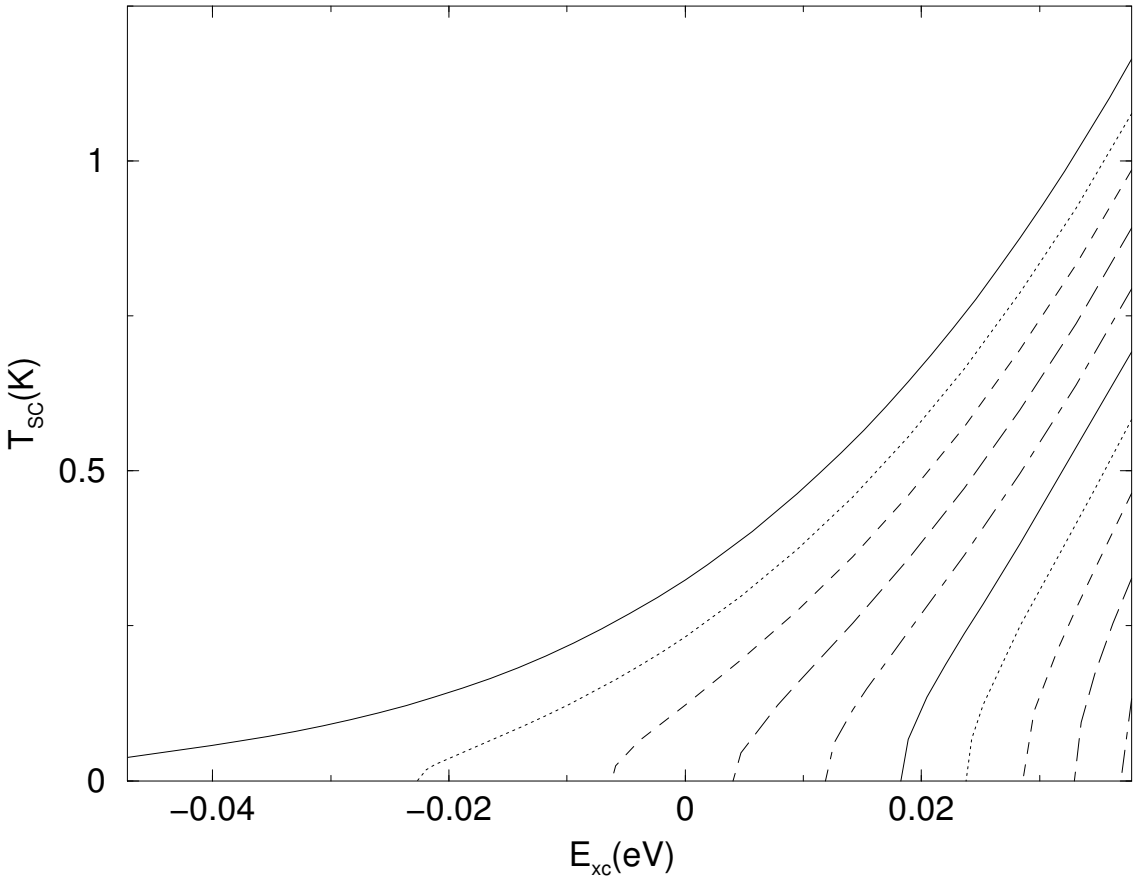

Figure 6.13: The critical temperature of a ESP p-wave superconductor as a function of exchange splitting (or equivalently chemical potential) in the presence of disorder. The curves correspond (from the top down) to ρ_{tr} = 0, 0.1 $\mu\Omega$cm, 0.2 $\mu\Omega$cm, 0.3 $\mu\Omega$cm, 0.4 $\mu\Omega$cm, 0.5 $\mu\Omega$cm, 0.6 $\mu\Omega$cm, 0.7 $\mu\Omega$cm, 0.8 $\mu\Omega$cm and 0.9 $\mu\Omega$cm.

6.6.1 The critical temperature of a dirty ferromagnetic superconductor as a function of exchange splitting

We now calculate the critical temperature as a function of exchange splitting for a variety different quasiparticle lifetimes, or more physically, for different residual resistivities. In figure 6.13 we show the superconducting critical temperature as a function of exchange splitting for both positive and negative exchange splitting, while is figure 6.14 we show the superconducting critical temperature and the temperature of the A_1-A_2 transition as a function of exchange splitting. Each figure shows plots for a range of quasiparticle lifetimes.

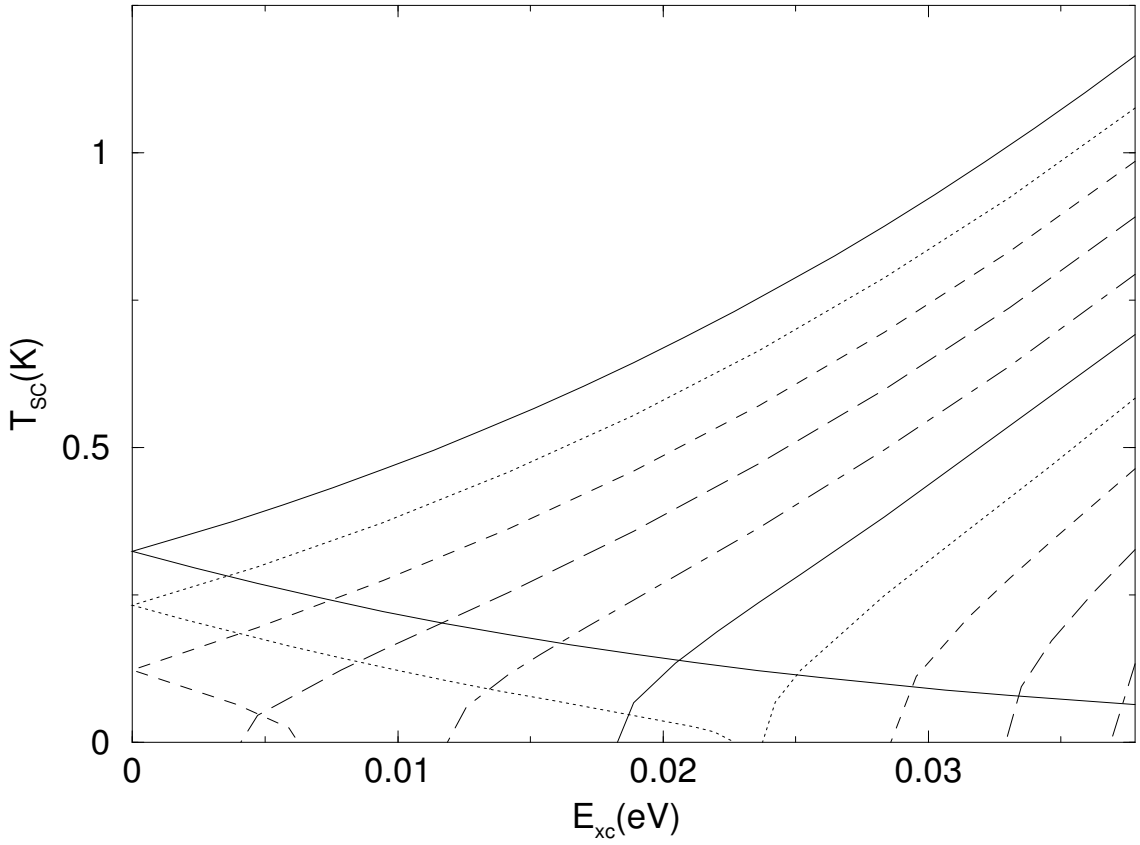

Figure 6.14: The critical temperature of a ESP p-wave superconductor and the temperature of the A_1-A_2 transition as a function of exchange splitting in the presence of disorder. The curves correspond (from the top down) to ρ_{tr} = 0, 0.1 $\mu\Omega$cm, 0.2 $\mu\Omega$cm, 0.3 $\mu\Omega$cm, 0.4 $\mu\Omega$cm, 0.5 $\mu\Omega$cm, 0.6 $\mu\Omega$cm, 0.7 $\mu\Omega$cm, 0.8 $\mu\Omega$cm and 0.9 $\mu\Omega$cm.

6.6.2 The critical temperature of $ZrZn_2$ as a function of pressure in the presence of non-magnetic impurities: comparison with experiment

To compare our results with experiment we must make contact with the 'control parameter', pressure. Fortunately, in $ZrZn_2$ this is not too difficult.

We begin by noting that experimentally the Curie temperature is, to within experimental error, a linear function of temperature [53, 166]. This is in agreement with the predictions of Walker and Samokhin's Landau theory [215]. Thus we have

$$T_{FM}(P) = T_{FM}(0)\left(1 - \frac{P}{P_C}\right). \tag{6.6.1}$$

Next we observe that the zero temperature magnetisation is also linear in pressure and thus proportional to T_{FM} (as is predicted by the Stoner model), giving

$$M(P, T = 0) = M(0, 0)\left(1 - \frac{P}{P_C}\right). \tag{6.6.2}$$

Finally, recall that for a Stoner ferromagnet, the magnetisation is linearly dependent on the exchange splitting and we have

$$E_{xc}(P, T = 0) = \begin{cases} E_{xc}(0,0)\left(1 - \frac{P}{P_C}\right) & P \leq P_C \\ 0 & P > P_C. \end{cases} \tag{6.6.3}$$

We now invoke the fact that $T_{FM} \gg T_{SC}$ which implies that

$$E_{xc}(P, T = T_{SC}) \sim E_{xc}(P, T = 0). \tag{6.6.4}$$

Thus we can map the results of $T_{SC}(E_{xc})$ (shown in figure 6.14) onto $T_{SC}(P)$ which we show in figure 6.15.

We see that our theory is not in quantitative agreement with experiment. For the sample studied in reference [166], which has a superconducting critical temperature of 0.3 K, our model predicts that, for such a large scattering, pressure destroys superconductivity rather quickly, where as Pfleiderer *et al.* observed superconductivity up to pressures of 13 kbar. However, our results are qualitatively in agreement with experiment. That is, for a moderate amount of

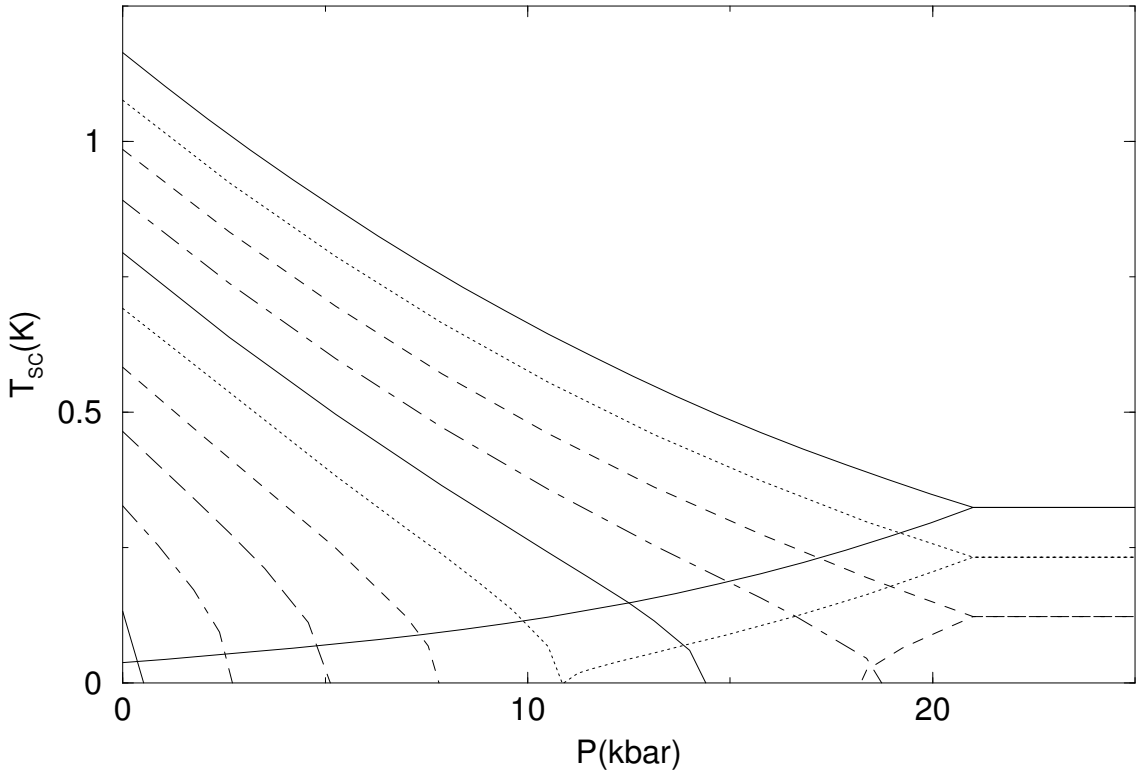

Figure 6.15: The critical temperature of a ESP p-wave superconductor and the temperature of the A_1-A_2 transition as a function of pressure in the presence of disorder. The curves correspond (from the top down) to ρ_{tr} = 0, 0.1 $\mu\Omega$cm, 0.2 $\mu\Omega$cm, 0.3 $\mu\Omega$cm, 0.4 $\mu\Omega$cm, 0.5 $\mu\Omega$cm, 0.6 $\mu\Omega$cm, 0.7 $\mu\Omega$cm, 0.8 $\mu\Omega$cm and 0.9 $\mu\Omega$cm.

disorder, we predict a approximately linear variation in T_{SC} with pressure, with a sudden drop (to zero) of T_{SC} near at P_C.

Our theory also makes a number of, potentially falsifiable predictions. Firstly, we predict that if the superconducting state of $ZrZn_2$ near T_{SC} is analogous to the A_1 phase of ^{3}He, that is the symmetry of the order parameter is

$$\mathbf{d}(\mathbf{k}) \sim (k_x + \mathtt{i}k_y)\,(1, \mathtt{i}, 0)\,, \tag{6.6.5}$$

where the z axis is defined such that $\mathbf{M} \parallel \hat{\mathbf{z}}$. We predict that if the quality of the samples is improved, i.e. if samples can be grown with a smaller residual resistivity then T_{SC} will increase across the full range of pressures that have been investigated experimentally. The relative increase in T_{SC} is predicted to be largest at large pressures (that is pressures in the region of P_C). Increasing the purity of samples will increase the maximum pressure at which superconductivity is observed. We predict that if the residual resistivity is less than $0.25\ \mu\Omega$cm then superconductivity will be observed in the paramagnetic state. Contrary to the predictions of Fay and Appel [70] and Santi *et al*. [183] we predict that the superconducting critical temperature in the paramagnetic state will be lower than the superconducting critical temperature in the ferromagnetic state. Further, samples with even lower residual resistivity we predict a second superconducting transition to the A_2, that is the order parameter becomes

$$\mathbf{d}(\mathbf{k}) \sim (k_x + \mathtt{i}k_y)\,(1, \mathtt{i}\kappa, 0)\,. \tag{6.6.6}$$

Initially this transition is only predicted to be observed near the critical pressure. But, as the purity of samples further increases the pressure required to observe the A_1, A_2 phase transition decreases. In the limit of no impurity scattering the second superconducting transition occurs even at ambient pressure with $\frac{T_{A_1-A_2}}{T_{SC}} = 0.0322$ or $T_{A_1-A_2} = 38$ mK. That $T_{A_1-A_2}$ is so small even in the ultra-clean limit means that it is unlikely that the second transition will ever be observed at ambient pressure. Above P_C, we enter the paramagnetic state and the order parameter crosses over to the A phase:

$$\mathbf{d}(\mathbf{k}) \sim (k_x + \mathtt{i}k_y)\,(1, 0, 0)\,. \tag{6.6.7}$$

One possible explanation for the lack of quantitative agreement between this theory and experiment is that this theory does not describe the essential physics of superconducting state in $ZrZn_2$. But there several, less drastic conclusions that appear worthy of investigation. T_{SC0}, one

of the initial inputs of this theory, is very badly known. Much more data is required to accurately determine the clean critical temperature, a large change in this would clearly have a rather drastic effect on our quantitative predictions. Our model is based on a simple cubic crystal structure. $ZrZn_2$ has a C15 Laves phase cubic lattice, this will clearly have some effect on the quantitative predictions of the model, although is unlikely to be large enough to account for the deviation from experiment. It has been suggested that only one sheet of the Fermi surface superconducts [215]. This would greatly effect the density of states and thus all of our predictions. If some experimental evidence emerges to suggest a particular sheet is solely responsible for superconductivity in $ZrZn_2$ it would be of great interest to see how this effects the superconducting transition temperature in this model. Finally of course performing these calculations with the actual LDA DOS rather than a tight binding approximation to the LDA DOS would probably alter the quantitative predictions if only slightly.

6.7 Conclusions

We have shown that a simple model in which the pairing potential is independent of pressure can qualitatively account for the variation in the superconducting critical temperature of $ZrZn_2$ with pressure. This shows that, at the very least, in the real material the pairing interaction is only very weakly dependent on pressure. We therefore conclude that the pressure dependence of the superconducting critical temperature in $ZrZn_2$ is due to the pressure dependence of the exchange splitting which in turn leads to a pressure dependence in the density of states. The superconducting critical temperature is dependent of the DOS which ensures that, in the absence of non-magnetic impurities, T_{SC} decreases as pressure is applied until it reaches a minimum in the paramagnetic state. (The superconducting critical temperature in the paramagnetic state is independent of pressure in this model.) Disorder has a very different effects on the superconductivity in the ferromagnetic and paramagnetic states because of the different magnitudes of the critical temperatures in the clean system. Only a very small number of non-magnetic impurities are required to completely suppress the unconventional superconductivity in the paramagnetic state, while in spite of its unconventional nature many more non-magnetic impurities are required to suppress the superconductivity in the ferromagnetic state (although in absolute terms still very moderate amounts of disorder destroy superconductivity in the ferromagnetic state). These two effects combine to give the illusion that the superconductivity disappears at P_C. Finally we predict that the order parameter goes to zero

on the line $k_x = k_y = 0$. As all of the sheets of the Fermi surface cross the line $k_x = k_y = 0$ this will lead to point nodes regardless of which sheets superconduct. Thus, this model has made a series of predictions that will, no doubt, either be confirmed or refuted as cleaner crystals become available and more experiments are performed.

We have also shown that for a ferromagnetic superconductor with ESP the linearised gap equations can be used to predict the temperature of a change of symmetry in the superconducting state. This is because the exchange splitting separates the two spin states in two subsystems, this is indicated by the fact that the spectrum of one spin state is entirely independent of the order parameter of the other spin state. Of course one may question the level to which, in a real material, spin flip processes invalidate this conclusion. However, as we have seen unconventional superconductivity is strongly suppressed by impurity scattering so in any system in which this model is valid such spin flip processes are likely to be extremely weak.

In fact a more serious concern to the validity of our conclusions is the possibility of OSP states (particularly the B_2 phase or the FFLO state for $P \lesssim P_C$ or the B phase in the paramagnetic region) as $E_{xc} \to 0$. However, the relevant area of the phase diagram is rather small and is certainly not accessible to experiment at present. Also we are unable to derive (linearised) gap equations which deal with all possible spin states and exchange splitting simultaneously. Until such equations are found this question will probably remain unanswered.

Chapter 7

Conclusions

So then, what progress have I made in the last three years? We have studied a the interplay of superconductivity and magnetism by considering a simple model which turned out to have a rather rich behaviour. The Hubbard model was extended to include nearest neighbour interactions and effects of the Zeeman term. We have neglected all effects due to the vector potential in this work.

We studied this model via several methods. In chapter 4 we attacked the model with the Hartree–Fock–Gorkov approximation and were thus able to derive the spin-generalised Bogoliubov–de Gennes equations for our model. Solving these equations numerically we able to show that our model reproduced well known results for s-wave superconductors. Studying the zero temperature limit we found, somewhat surprisingly, that the superconducting order parameter of an s-wave superconductor is independent of magnetic field strength. This is an interesting corollary to the Clogston–Chandrasekhar limit, the derivation of which assumes this without proof. Further we found that this surprising field independence is not confined only to singlet pairing states, but also found in $S_z = 0$ triplet states. Thus we predicted that for a triplet state with $\mathbf{d}(\mathbf{k}) \times \mathbf{H} = 0$ Clogston–Chandrasekhar limiting would occur.

In chapter 5 we studied our extended Hubbard model in two dimensions, applying our results to the triplet superconductor Sr_2RuO_4 in a magnetic field. We began by deriving a Ginzburg–Landau theory from our extended Hubbard model. The Ginzburg–Landau analysis showed that, assuming an A phase in zero field, there are two possible states in a magnetic field. The first is an A phase with a (vector) order parameter parallel to the magnetic field ($\mathbf{d}(\mathbf{k}) \times \mathbf{H} = 0$), the second phase is an equal spin pairing state with a (vector) order parameter perpendicular to the magnetic field ($\mathbf{d}(\mathbf{k}) \cdot \mathbf{H} = 0$) either an A, A_1 or A_2 state would be

consistent with the conclusions of Ginzburg–Landau theory.

We then numerically solved the Bogoliubov–de Gennes equations self-consistently. This showed that both the states predicted by Ginzburg–Landau theory are stable. (Indeed, our Ginzburg–Landau analysis is only sufficient to show that the two states are turning points in free-energy and not that they are minima.) The state with the order parameter perpendicular to $\mathbf{H}$ was found to be the ground state. Further, this state was found to be an A_2 phase. However, there has been speculation that in strontium ruthenate spin-orbit coupling pins the order parameter to the crystallographic c-axis. We therefore also studied the solution whose order parameter is parallel to the magnetic field. We found that the thermodynamic properties of the two solutions are very different, meaning that they should be straightforward to differentiate experimentally. Overall the state with the order parameter perpendicular to the magnetic field behaves in the way one expects of a state consisting wholly of equal spin pairs. However the state whose order parameter is parallel to the magnetic field contains only opposite spin pairs, its behaviour in an exchange field is therefore much more reminiscent of singlet pairing. Our prediction of a Clogston–Chandrasekhar limit for this state was confirmed. We were also predicted that spin-orbit coupling could lead to Freedericksz transition in strontium ruthenate.

In chapter 6 we studied our extended Hubbard model in three dimensions. These results were interpreted in the light of recent experiments on $ZrZn_2$. The Ginzburg–Landau theory is readily generalised to three dimensions, the results are not substantially changed. Given this, and given that the numerical solutions of the Bogoliubov–de Gennes equations are incredibly slow even with the aid of high speed computational techniques, we choose to make the reasonable assumption the ground state in $ZrZn_2$ only contains equal spin pairs. We were then able to derive the gap equations for equal spin pairing in a ferromagnetic superconductor. These gap equations have several remarkable qualities. Firstly, the exchange splitting plays only the role of a chemical potential. An alternative interpretation of this fact is that the exchange splitting only directly effects the normal state properties. (Of course changing the normal state properties has a dramatic effect on the superconducting state so the exchange splitting does influence the superconducting state, actually, as we saw, for the values of exchange splitting seen in ferromagnet the superconducting properties are drastically altered.) Secondly, the exchange splitting completely separates the spin degrees of freedom in the absence of spin flip processes (which are not accounted for in this theory). This means that linearised gap equations can be used, not only to predict the global superconducting critical temperature, but uniquely, to calculate the temperature at which a transition from one superconducting phase to another occurs

(in our case the A_1-A_2 transition).

We linearised our gap equations and solved them numerically. We fitted a tight binding model to the density of states found in band structure calculations so as to relate our results to $ZrZn_2$. We also estimated the superconducting transition temperature of $ZrZn_2$, in the absence of impurity scattering, from both residual resistivity and de Haas–van Alphen experiments. These estimations disagreed by a factor of 2-3. We concluded that the estimate from residual resistivity is the more reliable of the two and hence we assumed that the superconducting transition temperature of $ZrZn_2$ at ambient pressure and in the absence of impurity scattering is 1.15 K. This was used to fix the Hubbard interaction, U, which was assumed to be pressure independent. Our numerical solutions for the clean system showed that A phase superconductivity is found in the paramagnetic state. In the ferromagnetic state an A_1 is found immediately below the superconducting critical temperature. A second phase transition occurs at lower temperature, the state below the second phase transition is the A_2 phase. We then included the pair breaking effect of non-magnetic impurity scattering via the Abrikosov–Gorkov formula. We found only a very small number of impurities are required to suppress the second has transition. By the time there is enough impurity scattering to give rise to a residual resistivity of 0.25 $\mu\Omega$cm the second superconducting transition in the ferromagnetic state and all superconductivity in the paramagnetic state are completely suppressed. Assuming a linear dependence of exchange splitting on pressure we were able to calculate the pressure, temperature, disorder phase diagram for our model. This is in good qualitative agreement but poor quantitative agreement with experiments performed on $ZrZn_2$. We therefore concluded that the observed dependence of the superconducting critical temperature of $ZrZn_2$ on pressure is consistent with an (axial) ESP p-wave superconductivity mediated by a pressure independent potential in the presence of non-magnetic impurities.

The Hubbard model has provided rich pickings for theorists ever since it was first proposed forty years ago and it looks set to continue doing so well into this century. Even in this short work there have been many questions that we have not addressed. For example when considering strontium ruthenate we completely neglected the α and β sheets of the Fermi surface. We were even further from the real material when we discussed $ZrZn_2$, not only did we approximate the four sheets of the Fermi surface with an effective one band model, but we also assumed a simple cubic crystal structure while in actuality $ZrZn_2$ forms a cubic $C15$ Laves phase. This work could then clearly be usefully extended by the studying many band models and possibly more realistic models for the band structure of $ZrZn_2$ than the Hubbard model. Also, the study of the new

ferromagnetic superconductors would clearly be aided if the equal spin pairing gap equations for a ferromagnetic superconductor presented in this thesis could be generalised to include all spin states. But three years is, after all, only a short time....

Appendix A

Density of states calculations

It is often important to be able to calculate the density of states (DOS) accurately. In this appendix we present two methods for doing this. The first, the Bessel function method, which is a rather elegant mathematical technique that can be implemented with minimal computational effort, but is limited to one special case. The second method we consider is almost pure computational brute force. This computation requires an extremely fine k-space mesh, but given the number of points involved can be executed rather quickly. Further, the DOS need only be calculated once for any given model, thus speed is not a major concern. The density of states for the two dimensional nearest neighbour tight binding model as calculated by both of these methods is compared and contrasted in figure 2.7. The results from the second method are shown throughout this thesis.

A.1 The Bessel function method

In the special case of a tight binding model with nearest neighbour hopping only there is a particularly easy way to evaluate the DOS. In d dimensions the normal state spectrum of the linear/square/cubic/hypercubic lattice is

$$\varepsilon_{\mathbf{k}} = -2\sum_{i=1}^{d} t_i \cos(k_i). \tag{A.1.1}$$

In principle t_i may be different in each direction.

Recall that the DOS, $D(\varepsilon)$, is defined as

$$D(\varepsilon) = \frac{1}{N}\sum_{\mathbf{k}} \delta(\varepsilon - \varepsilon_{\mathbf{k}}) \tag{A.1.2}$$

for a lattice of N sites. For the above spectrum we therefore find that

$$\begin{aligned} D(\varepsilon) &= \int_{BZ} \frac{\mathrm{d}^d\mathbf{k}}{(2\pi)^d} \int_{-\infty}^{\infty} \frac{\mathrm{d}z}{2\pi} e^{\mathrm{i}z(\varepsilon + 2\sum_{i=1}^{d} t_i \cos k_i)} && \text{(A.1.3)} \\ &= \int_0^{\infty} \frac{\mathrm{d}^d\mathbf{k}}{(2\pi)^d} \cos\left(\frac{\varepsilon z}{2}\right) \prod_{i=1}^{d} J_0(t_i z), && \text{(A.1.4)} \end{aligned}$$

where the zeroth order Bessel function of the first kind is

$$J_0(x) = \int_{-\pi}^{\pi} \frac{\mathrm{d}\theta}{2\pi} \cos(x\cos\theta). \tag{A.1.5}$$

In principle this is straightforward to calculate numerically. However, in practice this converges rather slowly. One can easily sidestep this problem by calculating the asymptotic expansion analytically. It is well known [1] that the ν^{th} order Bessel function is given by

$$J_\nu(z) \sim \sqrt{\frac{2}{\pi z}} \left[\cos\left(z - \frac{1}{2}\nu\pi - \frac{\pi}{4}\right) + \mathcal{O}(|z|-1)\right] \tag{A.1.6}$$

So, for large V, we can write the density of states as

$$D(\varepsilon) = \int_0^V \frac{\mathrm{d}^d\mathbf{k}}{(2\pi)^d} \cos\left(\frac{\varepsilon z}{2}\right) \prod_{i=1}^{d} J_0(t_i z) + \int_V^{\infty} \frac{\mathrm{d}z}{2\pi} \cos\left(\frac{\varepsilon z}{2}\right) \prod_{i=1}^{d} \sqrt{\frac{2}{\pi t_i z}} \cos\left(t_i z - \frac{\pi}{4}\right). \tag{A.1.7}$$

The asymptotic expansion can be evaluated exactly in the case of $d = 1$

$$\begin{aligned} &\int_V^{\infty} \frac{\mathrm{d}z}{2\pi} \cos\left(\frac{\varepsilon z}{2}\right) \sqrt{\frac{2}{\pi t_i z}} \cos\left(t_i z - \frac{\pi}{4}\right) \\ &\quad = \frac{1}{2}\left[\sqrt{\frac{2t-\varepsilon}{\pi t}} + \sqrt{\frac{2t+\varepsilon}{\pi t}} - \sqrt{\frac{2t-\varepsilon}{\pi t}}\mathcal{S}\left(V\sqrt{\frac{2t+\varepsilon}{\pi t}}\right) - \sqrt{\frac{2t-\varepsilon}{\pi t}}\mathcal{C}\left(V\sqrt{\frac{2t+\varepsilon}{\pi t}}\right)\right. \\ &\qquad \left. -\sqrt{\frac{2t+\varepsilon}{\pi t}}\mathcal{S}\left(V\sqrt{\frac{2t-\varepsilon}{\pi t}}\right) - \sqrt{\frac{2t+\varepsilon}{\pi t}}\mathcal{C}\left(V\sqrt{\frac{2t-\varepsilon}{\pi t}}\right)\right]. \end{aligned} \tag{A.1.8}$$

The Fresnel sine and cosine integrals are defined by

$$\begin{aligned} \mathcal{S}(z) &= \int_0^z \sin\left(\frac{\pi}{2}t^2\right) \mathrm{d}t && \text{(A.1.9)} \\ \mathcal{C}(z) &= \int_0^z \cos\left(\frac{\pi}{2}t^2\right) \mathrm{d}t. && \text{(A.1.10)} \end{aligned}$$

While in two dimensions

$$\int_V^\infty \frac{\mathrm{d}z}{2\pi}\cos\left(\frac{\varepsilon z}{2}\right)\prod_{i=1}^{2}\sqrt{\frac{2}{\pi t_i z}}\cos\left(t_i z-\frac{\pi}{4}\right)$$
$$=\int_V^\infty \frac{\mathrm{d}z}{4\pi^2\sqrt{t_1t_2}}\frac{1}{z}\Bigg[\sin\left(\left(t_1+t_2+\frac{\varepsilon}{2}\right)z\right)+\sin\left(\left(t_1+t_2-\frac{\varepsilon}{2}\right)z\right)$$
$$+\cos\left(\left(t_1-t_2+\frac{\varepsilon}{2}\right)z\right)+\cos\left(\left(t_1-t_2-\frac{\varepsilon}{2}\right)z\right)\Bigg]$$

$$=\frac{1}{8\pi^2\sqrt{t_1t_2}}\Bigg[\pi\mathrm{sign}\left(t_1+t_2+\frac{\varepsilon}{2}\right)-\pi\mathrm{sign}\left(t_1+t_2-\frac{\varepsilon}{2}\right)-\pi\mathrm{sign}\left(t_1-t_2+\frac{\varepsilon}{2}\right)$$
$$+\pi\mathrm{sign}\left(t_1-t_2-\frac{\varepsilon}{2}\right)+4\ln 4-4\ln V-8\ln 2+2\pi-2\ln\left(2t_1-2t_2+\varepsilon\right)$$
$$+2\ln\left(V\left(2t_1+2t_2-\varepsilon\right)\right)+2\ln\left(V\left(2t_1-2t_2+\varepsilon\right)\right)-2\ln\left(2t_1+2t_2-\varepsilon\right)$$
$$-2\mathcal{S}i\left(V\sqrt{t_1+t_2+\frac{\varepsilon}{2}}\right)+2\mathcal{S}i\left(V\sqrt{-t_1+t_2+\frac{\varepsilon}{2}}\right)$$
$$-2\mathcal{C}i\left(V\sqrt{t_1-t_2+\frac{\varepsilon}{2}}\right)++2\mathcal{C}i\left(V\sqrt{t_1-t_2-\frac{\varepsilon}{2}}\right)\Bigg]. \tag{A.1.11}$$

We leave $d=3$ and higher dimensions as an exercise to the reader.

The ability to calculate the DOS simply and accurately is very useful as it allows us to rewrite any integral over $\mathbf{k}$-space,

$$I = \sum_{\mathbf{k}} F(\varepsilon_{\mathbf{k}}) \tag{A.1.12}$$
$$= \int_{BZ}\frac{\mathrm{d}^d\mathbf{k}}{(2\pi)^d}F(\varepsilon_{\mathbf{k}}), \tag{A.1.13}$$

where $F(\varepsilon_{\mathbf{k}})$ is an arbitrary function, as follows:

$$I = \sum_{\varepsilon} F(\varepsilon)\left(\sum_{\mathbf{k}}\delta(\varepsilon-\varepsilon_{\mathbf{k}})\right) \tag{A.1.14}$$
$$= \sum_{\varepsilon} F(\varepsilon)N(\varepsilon). \tag{A.1.15}$$

This is particularly useful as in most of the numerical computations considered in this thesis the vast majority of the CPU time is directed to performing the $\mathbf{k}$-space integration. For example the s-wave gap equation (4.4.10) with an on-site potential becomes

$$d_0 = -\frac{1}{4}\sum_{\varepsilon\sigma} N(\varepsilon)U\frac{d_0}{\sqrt{\varepsilon^2+|d_0|^2}}\tanh\left(\frac{\sqrt{\varepsilon^2+|d_0|^2}+\sigma\mu_B H}{2k_BT}\right). \tag{A.1.16}$$

In section 4.5 we solve this gap equation

A.2 Direct evaluation of the density of states

Unfortunately the Bessel function method is not easily generalised to next nearest neighbour hopping. It is therefore useful to be able to calculate the density of states without recourse to special cases. Rather than considering the general (d-dimensional) case, direct evaluation of the density of states is best understood by considering examples. We will therefore consider this method in both one and two dimensions. Higher dimensional cases are no more complicated to evaluate.

It is clear from equation A.1.2 that evaluating the density states numerically only involves numerically integrating over delta functions. At first sight, this does not appear particularly difficult, however matters are complicated by the fact that we are not dealing with isolated delta functions in general. We will therefore consider integrating an isolated delta function in one dimension and then discuss integrating over a line of delta functions in both one and two dimensions.

A.2.1 Isolated delta functions in one dimension

For numerical integration the important fact to recall about the Dirac delta function is that

$$\int_{-\infty}^{\infty}\delta(x)\mathrm{d}x = 1. \tag{A.2.1}$$

Any numerical calculation the continuum must be approximated by a mesh of discreet points. We can identify the zero(s) of $f(x)$ to within the accuracy of the mesh by looking for the mesh point(s) where the $f(x)$ changes sign[1]. We can therefore assign a 'delta function' to the mesh point closest to the zero. This must be done so that in such a way that (A.2.1) is satisfied. Therefore the area of the triangle (shown in figure A.1) must therefore be one, hence the height

[1]This of course assumes that f(x) does not go to zero in without changing sign, as for example $f(x) = x^2$ does. If this occurs (frequently enough to be seen above the numerical noise) then we must take care to account for these zeros. Also if the function, $f(x)$, is rapidly oscillating then we must ensure that the mesh is fine enough to 'catch' all of the zeros. However, neither of these problems are frequently encountered in DOS calculations.

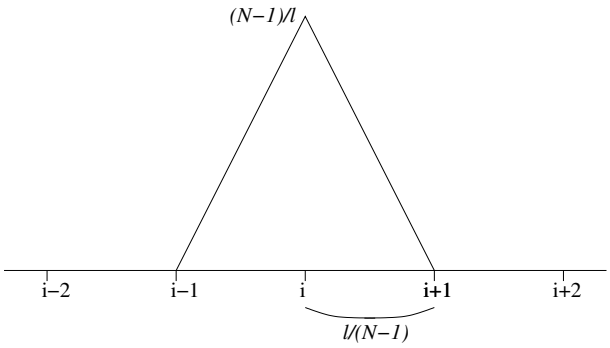

Figure A.1: Sketch of isolated 'numerical delta function' in 1D.

assigned of the to the kernel of the integral at the zero must be $\frac{N-1}{l}$ where l is the range of integration and N is the number of mesh points used for the calculation.

A.2.2 An line of delta function in one dimension

If we know consider a line of delta functions we must define the kernel of our integral so that

$$\int_a^{a+l} \delta(0) \mathrm{d}x = l. \tag{A.2.2}$$

is satisfied. Clearly along a line of delta functions in 1D all of the mesh points will lie on 'delta functions' (figure A.2) hence we are integrating over a constant kernel. Hence we have $N-1$ rectangles each of a width of $\frac{l}{N-1}$. To ensure that equation A.2.2 is satisfied the rectangles must have height 1. We have therefore seen that, in one dimension, the kernel for an isolated delta function is different from that for a line of delta functions. Fortunately the case of a d dimensional surface in d dimensions implies that energy is momentum independent. This means that we do not have to deal with the problem as it can always be transformed away.

A.2.3 An line of delta function in two dimensions

While isolated zeros of the spectrum are not impossible in two dimensions, they are rare and the arguments given in section A.2.1 are easily generalised, so we will not discuss this case here. The plane of zeros is also a rather trivial generalisation of the case considered in section A.2.2 and so we will not repeat that analysis. We have now considered a surface of dimension 0 and a d-dimensional surface in a d-dimensional space. The only remaining case to be considered is that of an n-dimensional surface in a d-dimensional space where $0 < n < d$. The simplest

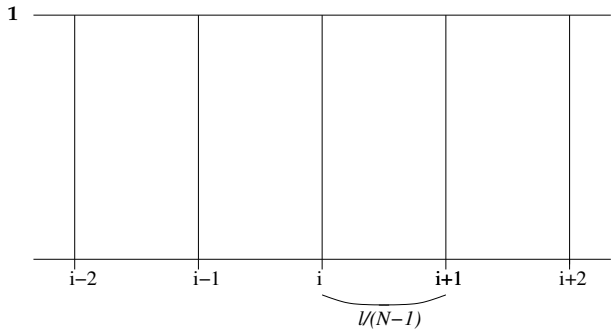

Figure A.2: Sketch of a line of 'numerical delta functions' in 1D.

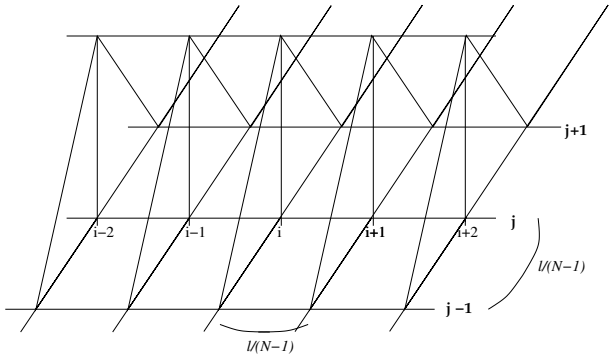

Figure A.3: Sketch of a line of 'numerical delta functions' in 2D.

example of that is a line of zeros in two dimensions. All other cases (for example a plane of zero in three dimensions) are straightforward generalisations of this case.

In this case we must satisfy

$$\int_b^{b+l} \mathrm{d}y \int_a^{a+l} \mathrm{d}x \delta(x) = l. \tag{A.2.3}$$

The geometrical situation is illustrated in figure A.3. This situation is greatly hampered by the fact that there are many paths the a curve may take through a given mesh box. Obviously, using a fine mesh ensures that a straight line is locally a good approximation to the path of the zeros. Thus we find that if our function takes the value $\frac{N-1}{2\pi}$ in any mesh point through which the line of delta functions passes, it will reduce to A.2.3 in the limit of an infinitesimally fine mesh. (In practice reasonable results can be obtained with mesh of $\sim 10^6$ points per k-axis.)

Bibliography

[1] M. Abramowitz and I.A. Segun, *Handbook of Mathematical Functions*, Dover, New York, 1965.

[2] A.A. Abrikosov and L.P. Gorkov, Sov. Phys. JETP **12**, 1243 (1961).

[3] A.A. Abrikosov, L.P. Gorkov, and I.E. Dzyaloshinski, *Methods of Quantum Field Theory in Statistical Physics*, Dover, New York, 1963.

[4] J-M. Adamo, *Multi-Threaded Object-Oriented MPI-Based Message Passing Interface*, Kluwer, Boston, 1998.

[5] S. Adenwalla, S.W. Lin, Q.Z. Ran, Z. Zhao, J.B. Ketterson, J.A. Sauls, L. Taillefer, D.G. Hinks, M. Levy, and B.K. Sarma, Phys. Rev. Lett. **65**, 2298 (1990).

[6] D.F. Agterberg, Phys. Rev. Lett. **80**, 5184 (1998).

[7] T. Akima, S. NishiZaki, and Y. Maeno, J. Phys. Soc. Japan **68**, 694 (1999).

[8] P.W. Anderson, Phys. Rev. **115**, 2 (1959).

[9] ———, *The Theory of Superconductivity in the High-T_C Cuperates*, Princeton University Press, Princeton, 1997.

[10] P.W. Anderson and W.F. Brinkman, Phys. Rev. Lett. **30**, 1108 (1973).

[11] ———, *The Physics of Liquid and Solid Helium Part II*, Wiley, New York, 1978.

[12] P.W. Anderson and P. Morel, Phys. Rev. **123**, 1911 (1961).

[13] J.F. Annett, Advances in Phys. **39**, 83 (1990).

[14] J.F. Annett, N.D. Goldenfeld, and S.R. Renn, *Physical Properties of High Temperature Superconductors II*, World Scientific, Singapore, 1990.

[15] D. Aoki, A. Huxley, E. Ressouche, D. Braithwaite, J. Flouquet, J-P. Brison, E. Lhotel, and C. Paulsen, Nature **413**, 613 (2001).

[16] D. Aoki, A. Huxley, E. Ressouche, I. Sheikin, J. Flouquet, J-P. Brison, and C. Paulsen, J. Phys. Chem. Sol. **63**, 1179 (2002).

[17] J. Appel and D. Fay, Solid State Commun. **28**, 157 (1978).

[18] G. Arfken, *Mathematical Methods for Physicists*, Academic Press, Orlando, 1985.

[19] N.W. Ashcroft and N.D. Mermin, *Solid State Physics*, Holt, Rinehart and Winston, New York, 1976.

[20] Asian Technology Information Program (ATIP), http://www.atip.or.jp/ATIP/public/atip.reports.97/atip97.015r.html.

[21] M. Ausloos and M. Houssa, Supercond. Sci. Tech. **12**, R103 (1999).

[22] H. Azizi, *Tight Binding and Resonance Schemes for d Bands*, Ph.D. thesis, Unversity of Bristol, 1975.

[23] R. Balian and N.R. Werthamer, Phys. Rev. **131**, 1553 (1963).

[24] W. Baltensperger, Physica **24**, S153 (1958).

[25] J. Bardeen, L.N. Cooper, and J.R. Schrieffer, Phys. Rev. **108**, 1175 (1957).

[26] G. Barton and M.A. Moore, J. Phys. C **7**, 2989 (1974).

[27] _____, J. Phys. C **7**, 4220 (1974).

[28] K.H. Benneman and J.B. Ketterson (editors), *The Physics of Liquid and Solid Helium*, Wiley, New York, 1978.

[29] The Beowulf Project, http://www.beowulf.org/.

[30] C. Bergemann, S.R. Julian, A.P. Mackenzie, S. NishiZaki, and Y. Maeno, Phys. Rev. Lett. **84**, 2662 (2000).

[31] N.F. Berk and J.R. Schrieffer, Phys. Rev. Lett. **17**, 433 (1966).

[32] I. Bonalde, B.D. Yanoff, M.B. Salamon, D.J. Van Harlingen, E.M.E. Chia, Z.Q. Mao, and Y. Maeno, Phys. Rev. Lett. **85**, 4775 (2000).

[33] M. Born and E. Wolf, *Principles of Optics*, Pergamon Press, Oxford, 1980.

[34] W. Brenig and H.J. Mikeska, Phys. Lett. **24A**, 332 (1967).

[35] W. Brenig, H.J. Mikeska, and E. Riedel, Z. Phys. **206**, 439 (1967).

[36] J.H. Brewer, *Encyclopedia of Applied Physics*, vol. 11, ch. 23, VCH, New York, 1994.

[37] W.F. Brinkman and S. Engelsberg, Phys. Rev. **169**, 417 (1968).

[38] J-P. Brison, L. Glémot, H. Suderow, A. Huxley, S. Kambe, and J. Flouquet, Physica B **280**, 165 (2000).

[39] K.A. Brueckner, T. Soda, P.W. Anderson, and P. Morel, Phys. Rev. **118**, 1442 (1960).

[40] E. Bruno, B. Ginatempo, and J.B. Staunton, Phys. Rev. B **65**, 092503 (2002).

[41] P. Brusov, *Mechanism of High Temperature Superconductivity*, vol. 1, Rostov State University Publishing, Rostov on Don, 1999.

[42] _____, *Mechanism of High Temperature Superconductivity*, vol. 2, Rostov State University Publishing, Rostov on Don, 1999.

[43] P. Brussaard and H.W. Capel, Physica A **265**, 370 (1999).

[44] P.C. Canfield, P.L. Gammel, and D.J. Bishop, Physics Today **51**, 40 (1998).

[45] G. Cao, J. Bolivar, S. McCall, J.E. Crow, and R.P. Guertin, Phys. Rev. B **57**, R11039 (1998).

[46] E. Cartan, *The Theory of Spinors*, M.I.T. Press, Cambridge, Massachusetts, 1966.

[47] Center for Computational Materials Science, *Crystal Lattice Structures*, http://cst-www.nrl.navy.mil/lattice/struk/c15.html.

[48] B.S. Chandrasekhar, Appl. Phys. Lett. **1**, 7 (1962).

[49] E.I. Chashechkina, I.J. Lee, S.E. Brown, D.S. Chow, W.G. Clark, M.J. Naughton, and P.M. Chaikin, Synthetic Metals **119**, 13 (2001).

[50] A.M. Clogston, Phys. Rev. Lett. **9**, 266 (1962).

[51] P.T. Colridge, R. Stoner, and R. Fletcher, Phys. Rev. B **39**, 1120 (1989).

[52] L.N. Cooper, Phys. Rev. **104**, 1189 (1956).

[53] H.G. Cordes, K. Fischer, and F. Pobell, Physica B **107**, 531 (1981).

[54] A. Damascelli, D.H. Lu, K.M. Shen, N.P. Armitage, F. Ronning, D.L. Feng, C. Kim, Z.X. Shen, T. Kimura, Y. Tokura, Z.Q. Mao, and Y. Maeno, Phys. Rev. Lett. **85**, 5194 (2000).

[55] A. Damascelli, K.M. Shen, D.H. Lu, N.P. Armitage, F. Ronning, D.L. Feng, C. Kim, Z.X. Shen, T. Kimura, Y. Tokura, Z.Q. Mao, and Y. Maeno, J. Elect. Spect. Rel. Phen. **114**, 641 (2001).

[56] P.G. de Gennes, *Superconductivity of Metals and Alloys*, W.A. Benjamin, New York, 1966.

[57] P.G. de Gennes and J. Prost, *The Physics of Liquid Crystals*, Clarendon Press, Oxford, 1993.

[58] E.R. Dobbs, *Helium Three*, Oxford University Press, Oxford, 2000.

[59] S. Doniach and S. Engelsberg, Phys. Rev. Lett. **17**, 750 (1966).

[60] J.A. Duffy, S.M. Hayden, Y. Maeno, Z. Mao, J. Kulda, and G.J. McIntyre, Phys. Rev. Lett **85**, 5412 (2000).

[61] A. Einstein, Sitz. Berlin Preuss. Akad. Wiss., 3 (1925).

[62] G.M. Eliashberg, JETP **38**, 966 (1960).

[63] ———, JETP **39**, 1437 (1960).

[64] V.J. Emery, Ann. Phys. **28**, 1 (1964).

[65] V.J. Emery and A.M. Sessler, Phys. Rev. **119**, 43 (1960).

[66] C.P. Enz and B.T. Matthias, Z. Phys. B **33**, 129 (1979).

[67] EPCC, *The Edinburgh Parallel Computing Centre*, http://www.epcc.ed.ac.uk/computing/training/document_archive/index.php.

[68] D. Fay and J. Appel, Phys. Rev. B **16**, 2325 (1977).

[69] ———, Phys. Rev. B **20**, 3705 (1979).

[70] ———, Phys. Rev. B **22**, 3173 (1980).

[71] I. Felner, U. Asaf Y. Levi, and O. Millo, Phys. Rev. B **55**, R3374 (1997).

[72] A.L. Fetter and J.D. Walecka, *Quantum Theory of Many-Particle Systems*, McGraw-Hill, London, 1971.

[73] R.P. Feynman, Physica **24**, S18 (1958).

[74] H. Frölich, Phys. Rev. **79**, 845 (1950).

[75] P. Fulde and R.A. Ferrell, Phys. Rev. **135**, A550 (1964).

[76] P. Gegenwart, M. Deppe, M. Köppen, F. Kromer, M. Lang, R. Modler, M. Weiden, C. Geibel, F. Steglich, T. Fukase, and N. Toyota, Annalen der Physik **5**, 307 (1996).

[77] A. Ghosh, J. Superconductivity **15**, 129 (2002).

[78] T.C. Gibb, R. Greatrex, N.N. Greenwood, J.J. Krajewski, W.F. Peck, and L.W. Rupp, J. Solid State Chem. **51**, 17184 (1974).

[79] V.L. Ginzburg and L.D. Landau, Zh. Eksp. Teor. Fiz **20**, 1064 (1960).

[80] K. Gloos, R. Modler, H. Schmanski, C.D. Bredl, C. Geibel, F. Steglich, A.I. Buzdin, N. Sato, and T. Komatsubara, Phys. Rev. Lett. **70**, 501 (1993).

[81] L.P. Gorkov, Sov. Phys. JETP **9**, 1364 (1959).

[82] M.J. Graf and A.V. Balatsky, Phys. Rev. B **62**, 9697 (2000).

[83] W. Greiner and J. Reinhardt, *Field Quantisation*, Springer–Verlag, Berlin, 1996.

[84] S.A. Grigera, R.S. Perry, A.J. Schofield, M. Chiao, S.R. Julian, G.G. Lonzarich S.I. Ikeda, Y. Maeno, A.J. Millis, and A.P. Mackenzie, Science **294**, 329 (2001).

[85] F.M. Grosche, C. Pfleiderer, G.J. McMullan, G.G. Lonzarich, and N.R. Bernhoeft, Physica B **206-207**, 20 (1995).

[86] M.C. Gutzwiller, Phys. Rev. Lett. **10**, 159 (1963).

[87] B.L. Györffy, J.B. Staunton, and G.M. Stocks, Phys. Rev. B **44**, 5190 (1991).

[88] W.R. Hamilton, Transactions of the Royal Irish Academy **21**, 199 (1848).

[89] J.P. Harrang, R.J. Higgins, R.K. Goodall, P.R. Jay, M. Laviron, and P. Delescluse, Phys. Rev. B **32**, 8126 (1985).

[90] Y. Hasegawa, K. Machida, and M. Ozaki, J. Phys. Soc. Japan **69**, 336 (2000).

[91] R. Heeb and D.F. Agterberg, Phys. Rev. B **59**, 7076 (1999).

[92] J. Hubbard, Proc. R. Soc. London A **276**, 238 (1963).

[93] _____, Proc. R. Soc. London A **277**, 237 (1964).

[94] _____, Proc. R. Soc. London A **281**, 401 (1964).

[95] _____, Proc. R. Soc. London A **285**, 1403 (1965).

[96] _____, Proc. R. Soc. London A **296**, 82 (1967).

[97] _____, Proc. R. Soc. London A **296**, 100 (1967).

[98] A. Huxley, I. Sheiken, E. Ressouche, N. Kernavanois, D. Braithwaite, R. Calemczuk, and J. Flouquet, Phys. Rev. B **63**, 144519 (2001).

[99] K. Ishida, Y. Kitaoka, K. Asayama, S. Ikeda, S. NishiZaki, Y. Maeno, K. Yoshida, and F. Fujita, Phys. Rev. B **56**, R505 (1997).

[100] K. Ishida, H. Mukuda, Y. Kitaoka, K. Asayama, Z.Q. Mao, Y. Mori, and Y. Maeno, Nature (London) **396**, 658 (1998).

[101] K. Ishida, D. Ozaki, T. Kamatsuka, H. Tou, M. Kyogaku, Y. Kitaoka, N. Tateiwa, N.K. Sato, N. Aso, C.Geibel, and F. Steglich, Phys. Rev. Lett. **89**, 037002 (2002).

[102] K. Izawa, H. Takahashi, H. Yamaguchi, Y. Matsuda, M. Suzuki, T. Sasaki, T. Fukase, Y. Yoshida, R. Settai, and Y. Onuki, Phys. Rev. Lett. **86**, 2653 (2001).

[103] Yu.A. Izymov, Yu.N. Proshin, and M.G. Khusainov, Phys. Uspekhi **25**, 109 (2002).

[104] M.Yu. Kagan, P. Brussaard, and H.W. Capel, Phys. Lett. A **221**, 407 (1996).

[105] J. Kanamori, Prog. Theor. Phys. **30**, 275 (1963).

[106] P.G. Kealey, T.M. Riseman, E.M. Forgan, L.M. Galvin, A.P. Mackenzie, S.L. Lee, D.McK. Paul, R. Cubitt, D.F. Agterberg, R. Heeb, Z.Q. Mao, and Y. Maeno, Phys. Rev. Lett. **84**, 6094 (2000).

[107] N. Kernavanois, B. Grenier, A. Huxley, E. Ressouche, J.P. Sanchez, and J. Flouquet, Phys. Rev. Lett. **64**, 174509 (2001).

[108] J.B. Ketterson and S.N. Song, *Superconductivity*, Cambridge University Press, Cambridge, 1999.

[109] T.R. Kirkpatrick and D. Belitz, cond-mat/0204440.

[110] T.R. Kirpartrick, D. Belitz, T. Vojta, and R. Narayanan, Phys. Rev. Lett. **87**, 127003 (2001).

[111] E.B. Kolomeisky and J.P. Straley, Rev. Mod. Phys. **68**, 175 (1996).

[112] M. Krawiec, B.L. Györffy, and K.I. Wysokiński, cond-mat/0203184.

[113] H. Kusunose and M. Sigrist, cond-mat/0205050.

[114] Laboratory for Advanced Computation in the Mathematical Sciences (LACMS), http://lacms.maths.bris.ac.uk/.

[115] L.D. Landau, Sov. Phys. JETP **3**, 920 (1956).

[116] _____, Sov. Phys. JETP **5**, 101 (1957).

[117] L.D. Landau and E.M. Lifshitz, *Statistical Physics*, Pergamon Press, Oxford, 1959.

[118] A.I. Larkin, JETP Lett. **2**, 130 (1965).

[119] A.I. Larkin and Yu.N. Ovchinnikov, Sov. Phys. JETP **20**, 762 (1965).

[120] A. Layzer and D. Fay, Int. J. Magn. **1**, 135 (1971).

[121] I.J. Lee, S.E. Brown, W.G. Clark, M.J. Strouse, M.J. Naughton, W. Kang, and M.J. Chaikin, Phys. Rev. Lett. **88**, 017004 (2002).

[122] I.J. Lee, A.P. Hope, M.J. Leone, and M.J. Naughton, Synthetic Metals **70**, 747 (1995).

[123] A.J. Leggett, Rev. Mod. Phys. **47**, 331 (1975).

[124] _____, J. Phys. (Paris) **39**, C6–1264 (1978).

[125] _____, *Physical Phenomena at High Magnetic Fields*, Addison–Wesley, Redwood City, California, 1991.

[126] K. Levin and O.T. Valls, Phys. Rev. B **17**, 191 (1978).

[127] F. Lichtenburg, A. Cantana, J. Mannhart, and D.G. Schlom, Appl. Phys. Lett. **60**, 1138 (1992).

[128] E.H. Lieb and F.Y. Wu, Phys. Rev. Lett. **20**, 1445 (1968).

[129] G. Litak, J.F. Annett, B.L. Györffy, and K.I. Wysokinski, cond-mat/0105376.

[130] D.H. Lu, M. Schmidt, T.R. Cummins, S. Schuppler, F. Lichtenberg, and J.G. Bednorz, Phys. Rev. Lett. **76**, 4845 (1996).

[131] G.M. Luke, Y. Fudamoto, K.M. Kojima, M.I. Larkin, J. Merrin, B. Nachumi, Y.J. Uemura, Y. Maeno, Z.Q. Mao, Y. Mori, H. Nakamura, and M. Sigrist, Nature (London) **394**, 558 (1998).

[132] C. Lupein, W.A. MacFarlane, C. Proust, L. Taillefer, Z.Q. Mao, and Y. Maeno, Phys. Rev. Lett. **86**, 5986 (2001).

[133] A.P. Mackenzie, J. Supercond. **12**, 543 (1999).

[134] A.P. Mackenzie, R.K.W. Haselwimmer, A.W. Tyler, G.G. Lonzarich, Y. Mori, S. NishZaki, and Y. Maeno, Phys. Rev. Lett. **80**, 161 (1998).

[135] A.P. Mackenzie, S. Ikeda, Y. Maeno, T. Fujita, S.R. Julian, and G.G. Lonzarich, J. Phys. Soc. Japan **67**, 385 (1998).

[136] A.P. Mackenzie, S.R. Julian, A.J. Diver, G.J. McMullan, M.P. Ray, G.G. Lonzarich, Y. Maeno, S. NishZaki, and T. Fujita, Phys. Rev. Lett. **76**, 3786 (1996).

[137] Y. Maeno, H. Hashimoto, K. Yoshida, S. Nishizaki, T. Fujita, J.G. Bednorz, and F. Lichtenberg, Nature (London) **372**, 532 (1994).

[138] Y. Maeno, T.M. Rice, and M. Sigrist, Physics Today **54**, 42 (2002).

[139] Y. Maeno and K. Yoshida, Czechoslovak J. Phys. **46**, no. Suppl. S6, 3097 (1996).

[140] Y. Maeno, K. Yoshida, H. Hashimoto, S. Nishizaki, S. Ikeda, M. Nohara, T. Fujita, A.P. Mackenzie, N.E. Hussey, J.G. Bednorz, and F. Lichtenberg, J. Phys. Soc. Japan **66**, 1405 (1997).

[141] K. Maki and S. Haas, Phys. Rev. B **62**, R11969 (2000).

[142] K. Maki, G.L. Yang, and H. Won, Physica C **341**, 1647 (2000).

[143] Z.Q. Mao, Y. Maeno, S. NishiZaki, T. Akima, and T. Ishiguro, Phys. Rev. Lett. **84**, 991 (2000).

[144] M.B. Maple, Physica B **215**, 110 (1995).

[145] N.D. Mathur, F.M. Grosche, S.R. Julian, I.R. Walker, D.M. Freye, R.K.W. Haselwimmer, and G.G Lonzarich, Nature **394**, 39 (1998).

[146] H. Matsui, Y. Yoshida, A. Mukai, R. Settai, Y. Ōnuki, H. Takei, N. Kimura, H. Akoi, and N. Toyota, Phys. Rev. B **63**, 60505 (2001).

[147] I.I. Mazin and D.J. Singh, Phys. Rev. Lett. **79**, 733 (1997).

[148] N.D. Mermin and C. Stare, Phys. Rev. Lett. **30**, 1135 (1973).

[149] Message Passing Interface Forum, http://www.mpi-forum.org/docs/mpi-11-html/mpi-report.html.

[150] R. Micnas, J. Ranninger, and S. Robaszkiewicz, Rev. Mod. Phys. **62**, 113 (1990).

[151] P. Miller, *De Haas–van Alphen Oscillations in the Vortex State*, Ph.D. thesis, Unversity of Bristol, 1994.

[152] P. Miller and B.L. Gyöffy, J. Phys. Cond. Matt. **7**, 5579 (1995).

[153] A.J. Millis, A.J. Schofield, G.G. Lonzarich, and S.A. Grigera, Phys. Rev. Lett. **88**, 217204 (2002).

[154] V.P. Mineev and K.V. Samokhin, *Introduction to Unconventional Superconductivity*, Gordan and Breach, Amsterdam, 1999.

[155] R. Modler, P. Gegenwart, M. Lang, M. Deppe, M. Weiden, T. Lühmann, C. Geibel, F. Steglich, C. Paulsen, J.L. Tholence, N. Sato, T. Komatsubara, Y. Ōnuki, M. Tachiki, and S. Takahashi, Phys. Rev. Lett. **76**, 1292 (1996).

[156] G. Motoyama, S. Nakamura, H. Kadoya, T. Nishioka, and N.K. Sato, Phys. Rev. B **65**, 20510 (2002).

[157] NCSA, *Introduction to MPI*, http://foxtrot.ncsa.uiuc.edu:8900/public/MPI/.

[158] K.K. Ng and M. Sigrist, Europhys. Lett. **49**, 473 (2000).

[159] S. NishiZaki, Y. Maeno, and Z. Mao, J. Phys. Soc. Japan **69**, 572 (2000).

[160] P. Nozières, *Bose–Einstein Condensation*, Cambridge University Press, Cambridge, 1995.

[161] R.A. Ogg Jr., Phys. Rev. **69**, 243 (1946).

[162] T. Oguchi, Phys. Rev. B **51**, 1385 (1995).

[163] R.S. Perry, L.M. Galvin, S.A. Grigera, L. Capogna, A.J. Schofield, A.P. Mackenzie, M. Chiao, S.R. Julian, S.I. Ikeda, S. Nakatsuji, Y. Maeno, and C. Pfleiderer, Phys. Rev. Lett. **86**, 2661 (2001).

[164] C. Pfleiderer and A.D. Huxley, Phys. Rev. Lett. **89**, 147005 (2002).

[165] C. Pfleiderer, A. Faißt, H. von Löhneysen, S.M. Hayden, and G.G. Lonzarich, J. Mag. Mag. Mat. **226-230**, 258 (2001).

[166] C. Pfleiderer, M. Uhlarz, S.M. Hayden, R. Vollmer, H. von Löhneysen, N.R. Bernhoeft, and G.G. Lonzarich, Nature (London) **412**, 58 (2001).

[167] C. Pfleiderer and H. von Löhneysen, J. Low Temp. Phys. **126**, 933 (2002).

[168] D. Pines and P. Nozieres, *The Theory of Quantum Liquids*, vol. 1, Benjamin, New York, 1966.

[169] L.P. Pitaevskii, Sov. Phys. JETP **10**, 1267 (1960).

[170] F. Pobell, Physica B **109-110**, 1485 (1982).

[171] R.G. Poulsen, D.L. Randles, and M. Springford, J. Phys. F. **4**, 981 (1974).

[172] B.J. Powell, James F. Annett, and B.L. Györffy, *Ruthenate and Rutheno-cuprate Materials: Theory and Experiments*, LNP Series, Springer Verlag, Berlin, 2002, preprint:cond-mat/0203087.

[173] P. Preuss, *Pointing the way to Granular Superconductivity in BSSCO*, http://www.lbl.gov/Science-Articles/Archive/MSD-granular-Orenstein.html.

[174] L.E. Reichl, *A Modern Course in Statistical Physics*, Wiley, New York, 1998.

[175] P. Remeijer, L.P. Roobol, S.C. Steel, R. Jochemsen, and G. Frossati, J. Low Temp. Phys. **111**, 119 (1998).

[176] M.J. Rice, Phys. Rev. **159**, 153 (1967).

[177] ———, Phys. Rev. **162**, 189 (1967).

[178] T.M. Rice and M. Sigrist, J. Phys. Cond. Matt. **7**, L643 (1995).

[179] E. Riedel, Z. Phys. **210**, 403 (1968).

[180] T.M. Riseman, P.G. Kealey, E.M. Forgan, A.P. Mackenzie, L.M. Galvin, A.W. Tyler, S.L. Lee, C. Ager, D.McK. Paul, C.M. Aegerter, R. Cubitt, Z.Q. Mao, T. Akima, and Y. Maeno, Nature (London) **396**, 242 (1998).

[181] D. Saint-James, G. Sarma, and E.J. Thomas, *Type II Superconductivity*, Pergamon Press, Oxford, 1969.

[182] K.V. Samokhin and M.B. Walker, Phys. Rev. B **66**, 024512 (2002).

[183] G. Santi, S.B. Dugdale, and T. Jarlborg, Phys. Rev. Lett. **87**, 247004 (2001).

[184] G. Sarma, J. Phys. Chem. Solids **24**, 1029 (1963).

[185] J.A. Sauls, Adv. Phys. **43**, 114 (1994).

[186] J.A. Sauls and J.W. Serene, Phys. Rev. B **24**, 183 (1981).

[187] S. Schmitt-Rink, K. Miyake, and C.M. Varma, Phys. Rev. Lett. **57**, 2575 (1986).

[188] M.R. Schrafroth, Phys. Rev. **100**, 463 (1955).

[189] ———, Phys. Rev. **100**, 502 (1955).

[190] L.W.M. Schreurs, H.M. Weijers, A.P.J. van Deursen, and A.R. Vroomen, Mat. Res. Bull. **24**, 1141 (1989).

[191] I. Sheikin, A. Huxley, D. Braithwaite, J.P. Brison, S. Watanabe, K. Miyake, and J. Flouquet, Phys. Rev. B **64**, 220503 (2001).

[192] H. Shimahara and S. Hata, Phys. Rev. B **62**, 14541 (2000).

[193] M. Sigrist and K. Ueda, Rev. Mod. Phys. **63**, 239 (1991).

[194] D.J. Singh and I.I. Mazin, Phys. Rev. Lett. **88**, 187004 (2002).

[195] J. Singleton and C. Mielke, Contemporary Physics **43**, 63 (2002).

[196] J. Singleton, J.A. Symington, M-S. Nam, A. Ardavan, M. Kurmoo, and P. Day, J. Phys. Cond. Matt. **12**, L641 (2000).

[197] K.P. Sinha and S.I. Kakani, *Magnetic superconductors*, Nova Science Publishers, New York, 1989.

[198] J. Spalek, Phys. Rev. B **63**, 104513 (2001).

[199] A. Stein and J. Mitton, *Pluto and Charon*, Wiley, New York, 1999.

[200] S. Takada, Prog. Theo. Phys. **43**, 27 (1970).

[201] S. Takada and T. Izuyama, Prog. Theo. Phys. **41**, 635 (1969).

[202] M.A. Tanatar, S. Nagai, Z.Q. Mao, Y. Maeno, and T. Ishiguro, Phys. Rev. B **63**, 064505 (2001).

[203] M.A. Tantar, T. Ishiguro, H. Tanaka, and H. Kobayashi, cond-mat/0205239.

[204] N. Tateiwa, T.C. Kobayashi, K. Amaya, R. Settai, and Y. Ōnuki, Physica B **312**, 109 (2002).

[205] T. Terashima, T. Matsumoto, C. Terakura, S. Uji, N. Kimura, M. Endo, T. Komatsubara, H. Akoi, and K. Maezawa, Phys. Rev. B **65**, 174501 (2002).

[206] D.J. Thouless, Ann. Phys. **10**, 1960 (1960).

[207] M. Tinkham, *Group Theory and Quantum Mechanics*, McGraw Hill, New York, 1964.

[208] M. Uhlarz, C. Pfleiderer, H. von Löhneysen, S.M. Hayden, and G.G. Lonzarich, Physica B **312-313**, 487 (2002).

[209] S. Uji, H. Shinagawa, T. Terashima, T. Yakabe, Y. Terai, M. Tokumoto, A. Kobayashi, H. Tanaka, and H. Kobayashi, Nature **410**, 908 (2001).

[210] Y. Ushida, H. Nakane, T. Nishioka, G. Motoyama, S. Nakamura, and N.K. Sato, *Thermal Expansion Measurement Under Pressure of UGe_2*, To appear in the proceedings of the 23rd international conference of low temperature physics, Physica B.

[211] A.P.J. van Deursen, L.W.M. Schreurs, C.B. Admiraal, F.R. de Boer, and A.R. de Vroomen, J. Magn. Mater **54-57**, 1113 (1986).

[212] D. Vollhardt, Rev. Mod. Phys. **56**, 99 (1984).

[213] D. Vollhardt and P. Wölfe, *The Superfluid Phases of Helium 3*, Taylor and Francis, London, 1990.

[214] S.V. Vonsovsky, Yu.A. Izyumov, and E.Z. Kurmaev, *Superconductivity of Transition Metals*, Springer–Verlag, Berlin, 1982.

[215] M.B. Walker and K.V. Samokhin, Phys. Rev. Lett. **88**, 207001 (2002).

[216] L. Walz and F. Lichtenburg, Acta Cryst. C **49**, 1268 (1993).

[217] J.C. Wheatley, Rev. Mod. Phys. **47**, 415 (1975).

[218] A. Yaouanc, P. Dalmas de Réotier, P.C.M. Gubbens, C.T. Kaiser, A.A. Menovsky, M. Mihalik, and S.P. Cottrell, Phys. Rev. Lett. **89**, 147001 (2002).

[219] S.J.C. Yates, G. Santi, S.M. Hayden, P.J. Meeson, and S.B. Dugdale, cond-mat/0207285.

[220] T. Yokoya, A. Chainani, T. Takahashi, H. Ding, J.C. Campuzano, H. Katayama-Yoshida, M. Kasai, and Y. Tokura, Phys. Rev. B **54**, 13311 (1996).

[221] K. Yoshida, Y. Maeno, S. NishiZaki, and T. Fujita, J. Phys. Soc. Japan **65**, 2220 (1996).

[222] K. Yosida, Phys. Rev. **110**, 769 (1958).

[223] F.C. Zhang and T.M. Rice, Phys. Rev. B **37**, 3759 (1988).

[224] M.E. Zhitomirsky and T.M. Rice, Phys. Rev. Lett. **87**, 57001 (2001).

[225] J.M. Ziman, *Electrons and Phonons*, Clarendon Press, Oxford, 1960.